Energy Analysis of Photovoltaic Thermal System Integrated with Roof

and

HVAC System

Sasa Pantic

A Thesis

in

The Department

Of

Building, Civil and Environmental Engineering

Presented in Partial Fulfillment of the Requirements
for the Degree of Master of Applied Science (Building Engineering) at
Concordia University
Montreal, Quebec, Canada

March 2007

Your file Votre référence
ISBN: 978-0-494-28890-0
Our file Notre référence
ISBN: 978-0-494-28890-0

ABSTRACT

Energy Analysis of Photovoltaic Thermal System Integrated into Roof and HVAC System

Sasa Pantic

Integration of a photovoltaic-thermal system with housing roofs can replace shingles while generating electricity and heat. This thesis is focused on energy performance of different configurations of building integrated photovoltaic-thermal (BIPV/T) and HVAC system that utilize recovered heat.

A dynamic model for Concordia solar house which included an open loop air-cooled BIPV/T roof system was developed. The thermal network approach with explicit finite difference method was used to simulate the thermal behaviour of the house. The system studied included an air-water heat exchanger for preheating domestic hot water (DHW), water tank and rockbed storage.

Predicted temperatures of the preheated air in the BIPV/T systems, PV panels and DHW were obtained and verified with data collected from the solar house. Results showed the dependence of thermo-electrical performance of the BIPV/T roof on the ambient conditions, air velocity, length and PV cavity depth. For the unglazed BIPV/T system, the heated air is suitable to be used as a preheated air in the HVAC system; for the same reason, thermal rockbed storage is not beneficial for extreme winter conditions with unglazed BIPV/T open loop air system. The BIPV/T system considered is suitable for DHW preheating. By adding 1.5m of vertical glazed solar air collector (SAC) at the end of the unglazed BIPV/T section, significant air temperature increase at the outlet of the PV cavity can be achieved in winter and it is suitable for combination with the rockbed storage. With passing the air behind the absorber of the SAC and placing a low-emissivity coating on a glass cover, higher exiting air temperatures can be achieved. Appropriate air velocities in the PV cavity that limit the PV panel temperature of the glazed BIPV/T roof were determined.

To my mother

ACKNOWLEDGEMENTS

I would like to express my gratitude to my supervisor Dr. A.K. Athienitis for his expert guidance, encouragement and support during my studies.

I would also like to thank my family for their love and support.

Special thanks and appreciation go to Dr. R. Zmeureanu for his patience, understanding and encouragement.

The useful advices from Mr. Meli Stylianou are greatly appreciated.

Many thanks go to my friends and colleagues on their friendship and assistance Mark, Danielle, Luis, Miljana, Xiang and Remi. Working at the solar house would have been much less fun without you two guys, Jose and Brendan.

Financial support of this work was provided by NSERC through the Solar Buildings Research Network and by Natural Resources Canada through the Innovative Research Initiative and the Technology and Innovation Program as part of the Climate Change Plan for Canada.

TABLE OF CONTENTS

CHAPTER 3: SIMULATION TOOL DEVELOPMENT AND EXPERIMENTS

CHAPTER 4: RESULTS AND DISCUSSION

LIST OF FIGURES

LIST OF TABLES

NOMENCLATURE

A	Area (m^2)
abs	Absorber
ACH	Air change per hour
AHU	Air handling unit
AWHE	Air-water heat exchanger
b	bottom
BIPV/T	Building integrated photovoltaic/thermal
c	Cold fluid
conv	Convection
C_c	Capacity rate of fluid on cold side
C_h	Capacity rate of fluid on hot side
CFD	Computational fluid dynamics
CHP	Combined heat and power
CHTC	Convective heat transfer coefficient
COP	Coefficient of performance
C_i	Thermal capacitance of the layer i ($J/^oC$)
c_p	Specific heat capacity ($J/kg\ ^oC$)
D	Distance (m)
D_H	Hydraulic diameter (m)
DHW	Domestic hot water
ext	Exterior

ERV	Energy recovery unit
f	Friction factor
$F^{'}$	Collector efficiency factor
F_R	Heat removal factor
$F_{i,j}$	View factors between surfaces i,j
$F_{\varepsilon i,j}$	Emissivity factor for surfaces i,j
Gr	Grashoff number
H	Height (m)
$\overline{H}$	Dimensionless height
h	Hot fluid
h_{eq}	Equivalent heat transfer coefficient ($W/m^2\,^oC$)
hc	Convective heat transfer coefficient ($W/m^2\,^oC$)
$h_{r,i,j}$	Radiation heat exchange between surfaces i,j ($W/m^2\,^oC$)
HVAC	Heating, ventilation and air-conditioning
h_w	Convective heat transfer coefficient due to wind ($W/m^2\,^oC$)
i	Interior, element
k_i	Thermal conductivity of i ($W/^oC$)
L	Characteristic length (m)
$\dot{m}_{air}$	Mass flow rate (kg/s)
mc	Mono-crystalline silicon
Nu	Nusselt number
o	Outdoor
pc	Poly-crystalline silicon

Pr	Prandtl number
P_{el}	Generated electricity (W,kWh)
P	Perimeter (m)
PCM	Phase change material
PV	Photovoltaic
Q	Heat (W,kWh)
r	Rockbed
rad	Radiation
Ra	Rayleigh number
Re	Reynolds number
$R_{i,j}$	Thermal resistance between nodes i, j (°C/W)
S	Solar irradiation (W/m^2)
SAC	Solar air collector
t	Top, time
T_i	Temperature of the element i (°C)
TRNSYS	Transient energy system
U	Overall heat transfer coefficient (W/°C)
U_{inf}	Infiltration conductance (W/°C)
V_{air}	Air speed in the PV cavity (m/s)
Vol	Volume (m^3)
V_w	Wind speed (m/s)
V_{10}	Wind speed at the height above 10m (m/s)
W	Width (m)

X	Thickness (m)
ZESH	Zero energy solar homes
α_i	Absorptance of the element i
β	Tilt angle (^{o})
ε_{HE}	Effectiveness of the heat exchanger
ε_i	Emissivity of the surface i
η	Efficiency
μ_i	Dynamic viscosity of element i (kg/ms)
ρ_i	Density of element i (kg/m^3)
σ	Stefan Boltzmann's constant $\sigma = 5.67\ 10^{-8}$ ($W/m^2\ ^oC$)

CHAPTER 1

INTRODUCTION

1.1 Introduction

Buildings are one of the major fossil fuel energy consumers. Buildings consumed about 30% of the secondary energy in Canada and contributed about 135 MT equivalent CO_2 emissions in 2001 (Natural Resources Canada, 2004). Nowadays, when environmental issues are becoming important, interest in renewable energy sources and its applications in buildings is rising. Solar energy systems can significantly decrease building energy consumption (Wang, et al., 2006). Homes that employ solar thermal and photovoltaic technologies to generate as much energy as they yearly consume are defined as net zero energy solar homes (ZESH), (Charron et al., 2005).Photovoltaic (PV) panels convert 5 to 20% of sunlight into electricity. The reminder is partly reflected and turned into heat (Helden, et al., 2004). Unless that heat is not captured appropriately, it is usually lost by convection and infrared radiation to the outdoor environment. The heat can be harvested similarly as in the solar-air or solar-water collectors. The PV panels that are part of the building envelope and recover released heat are called building integrated photovoltaic- thermal (BIPV/T) systems. Therefore, the PV panels can be integrated into building envelope, either façade or the roof, to cover the building's energy demand in heating and power. When PV arrays are integrated into roof, more solar radiation is incident upon them than in case of façade installations. Consequently, more heat and electricity is generated.

Presently, the main disadvantage of the PV panels is the high cost for watt of electricity generated. However, when considering the economic aspect of the BIPV/T system, several factors must be taken into account. Firstly, the high price of PV panels will drop due to the development of the PV technology and mass production (Charron, 2004). Costa et al (2000) concluded that cost effectiveness of the BIPV/T system is increased when providing multiple functions. By substituting the conventional construction elements such as shingles and façade elements and besides behaving as electrical and thermal generator, the PV panels can serve as a rain screen, sun shading device and visually attractive cladding of the building. Finally, it is most likely that the BIPV/T heating systems will become competitive due to anticipated energy crises and carbon emission taxes (Claessens and DeHerde, 2006).

Although, the specific heat capacity of the air is four times lower than that of the water, several advantages are identified over convential solar water systems:

- The simple and cheap way of installation during the construction phase (Bazilian and Prasad, 2002)
- Low thermal inertia of the system
- BIPV/T system can create a warm envelope for the buildings reducing the heat loads
- No corrosion, leak and frost problems (IEA 2000).

Today, many photovoltaic roof systems have been being built around the world as long-term, clean and safe energy sources of thermal and electrical energy to meet the needs of the occupants.

1.2 Motivation

Many researchers are concerned with designing active solar space heating systems for residencies. Various solar air collector types and their interaction with HVAC system were being investigated. However, very little research has been done on energy performance of the various BIPV/T roof configurations connected with HVAC system to develop general design guidelines to optimize the system energy performance. This thesis is focused on studying how much electricity can be generated from the BIPV/T roof, how much heat can be recovered from the BIPV/T roof and what to do with it afterwards *e.g.* will it be used immediately for space heating or stored in thermal storage for later use or for heating domestic hot water (DHW).

Some researchers have studied the performance of the PV applications integrated into facade but few reports were found on the building integrated PV panels into roofs of the houses. Furthermore, these studies were focused only on specific parameters *i.e.* the tilt angle and orientation effects on the PV roof performance, the effects of inlet and outlet conditions, finding suitable heat transfer coefficients *etc.* with little research being done to develop general design guidelines to be used by designers to optimize the performance of BIPV/T systems and integration with HVAC system.

Most of commercial building energy simulation programs are often black-box software or require advanced programming skills to build or modify new components. In contrast, innovative designs require flexibility in simulation and; therefore, developed simulation programs have to be user friendly *i.e.* with an unrestricted access to the source codes to create new or change existing components (Stec, Paassen, 2005).

1.3. Objectives

The objectives of this thesis are as follows:

- To develop one-dimensional transient simulation model to study the thermal behaviour of a house with different roof configurations of BIPV/T system
- To study the performance of BIPV/T roof
- To analyze energy interaction of the several BIPV/T roof configurations and HVAC system components (thermal rockbed, water storage and air-to-water heat exchanger) under various climate conditions
- To find appropriate air speeds in a PV cavity to maintain the PV temperature below 75°C

1.4. Thesis layout

Chapter 2 reviews the related literature. Chapter 3 presents developed simulation tool and experimental setup at the solar house. The most important results and discussion are summarized in the Chapter 4. The conclusions and recommendations for future work of this innovative technology in sustainable building design are presented in Chapter 5.

CHAPTER 2

LITERATURE REVIEW

2.1 Introduction

In Chapter 2, a discussion about various BIPV/T and Photovoltaic/Thermal concepts is presented followed by parameters that affect both thermal and electrical performance of the PV panels. Moreover, the basic concepts of the control strategies and convection heat transfer coefficients are analyzed. This chapter includes overview of the HVAC components used in air solar system applications. Finally, a comparison among the most commonly used existing solar system and building simulation software is presented.

2.2 BIPV/T Applications Overview

Various researchers and designers around the world designed and analyzed the BIPV/T system concept. However, only few BIPV/T applications have been implemented in Canada according to the author's knowledge. Recently assembled research facilities at the roof of the BE building of Concordia University, Montreal, Canada were used for thermo-electrical BIPV/T research studies. Two configurations of the PV panels integrated into façade are depicted by Figure 2.1. While Configuration 1 has a PV panel attached to the outer glazing of the PV cavity, Configuration 2 has a PV panel sandwiched between the outer glazing and inner side of the façade.

Extensive experimental and simulation work was done for predicting the PV electrical performance and thermal behavior of the air in the PV cavity under different ambient conditions. One and two-dimensional thermo-fluid models were developed for both configurations. The results showed that combined thermo-electrical efficiency of 70% can be achieved (Charron, 2004). In another study, Liao (2005) has developed relationships for forced convective heat transfer coefficients in the cavity.

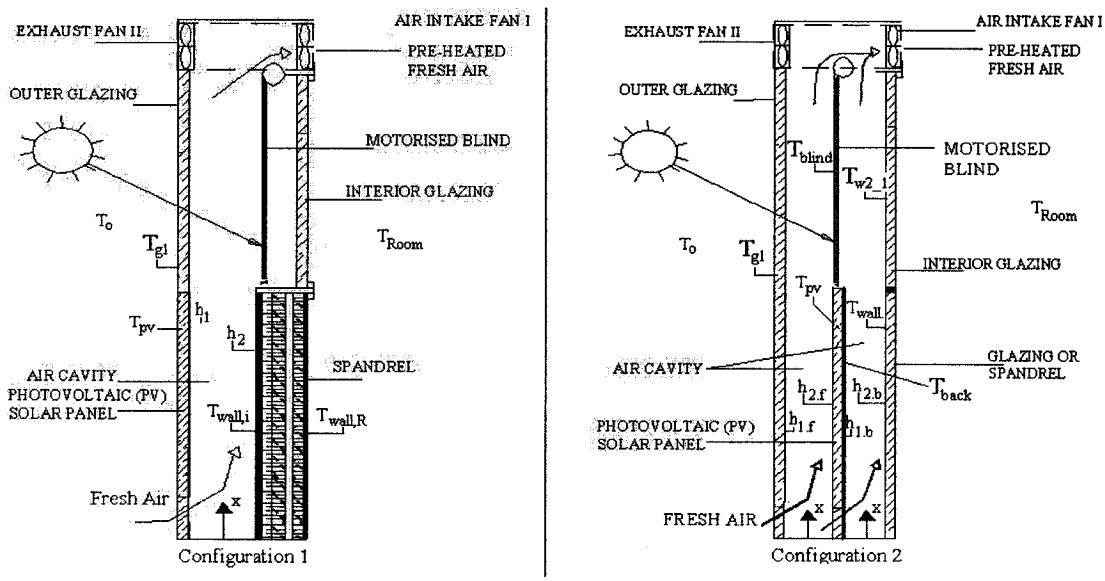

Figure 2.1: Configuration 1 and 2 of the BIPV/T facade (Charron, 2004)

On a commercial scale, the retrofit of the William Farrel Building in Vancouver, Canada is a good example of implementing the BIPV/T technology. Figure 2.2 presents the exterior appearance of the building and the system configuration. The semi-transparent PV arrays consisted of polycrystalline silicon panels that were incorporated into the northwest and southwest double façade glazed 48 meters high curtain wall.

Thus, several objectives are achieved. The arrangement of the cells allows some of the incident solar radiation to pass through the PV cells and double glazed windows. Moreover, while a natural ventilation intake for a double façade cavity in winter reduces heating losses, the forced ventilation strategy is used in the summer to cool the PV panels and reduce the cooling loads. Consequently, the PV efficiency is increased. However, not all BIPV/T system potential is utilized. The ambient air is just used to ventilate the double façade to reduce cooling loads and useful hot air is rejected outside when it could be used for example to prepare DHW.

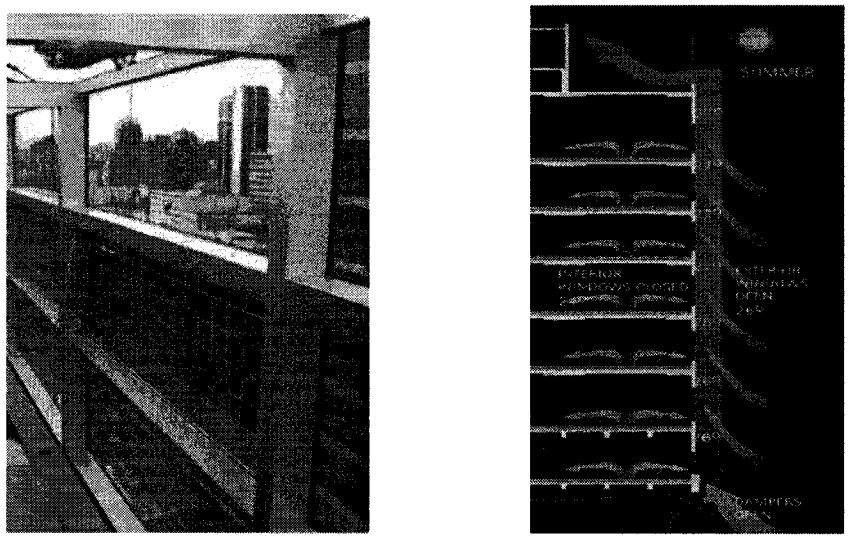

Figure 2.2: Exterior appearance and system layout of the William Farrel building (Natural Resources Canada, 2004)

A similar concept was used for Mataro Library, Spain. A rectangular building with the south façade area of 225 m^2 includes 6.5m high PV section. While previously mentioned researchers considered only the BIPV/T as a single system, the study reported by Mei and Infield (2003) investigated the interaction of the Mataro Library south façade with the thermal zone. A BIPV/T mathematical component was written in Delphi and

incorporated into TRNSYS building simulation environment. It was found that the influence of the BIPV/T system on heating load depends upon location and cooling loads are slightly higher with the PV façade.

Some applications for houses were also performed. A solar roof system named SOLARWALL system developed by Conserval Engineering utilizes waste heat from PV panels mounted on a perforated panel on the roof of a house. The perforated panel is used to balance air flow passed beneath the PV panels. The general concept for both summer and winter scenarios is presented in Figure 2.3.

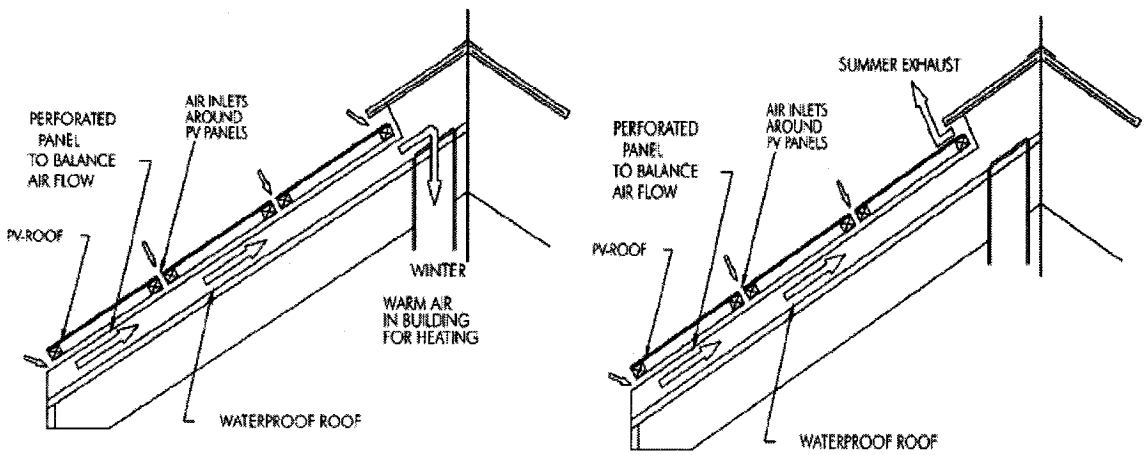

Figure 2.3: Cross section of Solarwall system for winter and summer (IEA, 2000)

The advantages of presented open air loop solar system are:

- Low initial cost
- Thermal efficiency of 50% to 60% can be reached
- Improved electrical conversion efficiency
- Reduced cooling loads
- Improved indoor air quality

Another application was successfully developed by researchers from Concordia University, Montreal, Canada. As a Canadian entry into Solar Decathlon Competition held in 2005 in Washington D.C., USA, both active and passive solar systems were fully implemented into typical Canadian house. The Concordia's award-winning solar house combines BIPV/T system, motorized blinds and smart control techniques. A 7 kW PV system mounted on the roof consists of 40 unglazed monocrystalline PV panels of 175W power. The PV panels embodied into the roof slightly overlap to form a waterproof rain screen allowing to act as a roofing material. Large double-glazed low-emissivity windows are placed on the south wall to transmit large amount of sunlight into the zone. In order to maximize the thermal comfort, motorized blinds with smart control system operates according to the amount of transmitted solar radiation into the space. Moreover, the solar house is heavily insulated due to Canadian harsh climate. The walls have total resistance value of approximately of RSI 5.6. The ceiling has RSI 9. The floor has resistance value of RSI 7.2. Distinguishing feature of mechanical system is flexibility that permits several operation modes for cooling and heating scenario. This thesis is focused on solar house's energy performance of the active solar system, BIPV/T roof, and its interaction with HVAC system. Collected data from the BIPV/T and HVAC system installed at the solar house were used to verify developed model.

Figure 2.4: Solar house - "Northern Light" (Pasini and Athienitis, 2006)

Finally, the above mentioned systems considered only open air systems. A very interesting technology that combines heat and power (CHP) was developed by Dawn Solar Systems Inc. depicted in Figure 2.5. The CHP system consists of steel roofing material and incorporates PV panels. The solar energy is used for generating electricity but is also absorbed and transferred to the liquid flowing in tubes beneath the metal roof. It is capable of providing heating and pre-heating of domestic hot water, radiant heating or process water heating to temperatures as high as 65°C.

Figure 2.5: Combined heat and power application developed by Dawn Solar System Inc. (www.dawnsolar.com)

2.3 Photovoltaic / Thermal Collectors

Another very promising technology in achieving zero energy house target is development of a hybrid photovoltaic / thermal (PV/T) collector. A PV/T collector is a combination of photovoltaic cells embodied into thermal absorber and is not part of the building envelope as opposed to BIPV/T system.

Zondag (2002) discussed the main advantages of such systems such as higher overall conversion efficiency, reduced energy payback and improved aesthetics. Their results indicated that 2 m^2 of PV/T collector would yield 700kWh thermal and 132 kWh electrical energy annually, whereas separate $1m^2$ components would yield 520 kWh thermal and 72 kWh electrical energy yearly.

Helden et al. (2004) concluded that different demands require different PV/T concepts. They investigated performance of two PV/T concepts linked with HVAC system. When PV/T system is used as a source for a heat pump, a solar fraction of 100% can be achieved. Therefore, heat for both room heating and hot water and electricity for the heat pump is provided. The International Energy Agency (IEA) is currently investigating under task 35 various energy transfer models in the PV/T systems in order to define, model and predict energy performance of the system separately and in a whole building context.

2.4 Overview of Other Parameters that Affect the BIPV/T Performance

As mentioned earlier, the main disadvantage of the PV technologies is high initial cost, small electric output and wasted useful heat unless captured in a proper manner. The main types of PV cells available on the market are crystalline and amorphous silicon PV cells.

Crystalline silicon PV panels are widely used in building integrated systems. The crystalline cell family includes both mono-crystalline and poly-crystalline cells (Natural Resources Canada, 2004). Despite the high manufacturing cost, the mono-crystalline PV panels have the highest electrical efficiency *e.g.* around 15%. In contrast, the poly-

crystalline PV panels have lower electrical efficiencies around 12% but they are generally cheaper. For crystalline technologies, the power generation drops with temperature rise from 0.2 to 0.5%/°C (Charron, 2004).

Although amorphous silicon cells are not sensitive to high temperatures and the cheapest cells found on the current market, they are less efficient than crystalline cells with average electrical efficiency of around 6% to 8%. Therefore, they require more surface area to achieve the same electrical output as mc-PV and pc-PV and are recommended for milder climates. It should be noted that electrical efficiencies are calculated under standard test conditions (STC) at 1000 W/m^2 incident solar radiation, PV temperature of 25 °C and air mass of 1.5. Therefore, the actual electrical efficiency is lower than indicated above.

Another feature that affects the PV performance is transparency. Semi-transparent BIPV/T systems are suitable for both roof and façade integration. The spacing between PV cells must be carefully selected to determine the amount of daylight entering the zone and produced electrical power. Semi-transparent BIPV/T system behaves as a passive solar component reducing heating and cooling loads. Obviously, as compared to the opaque BIPV/T system, a trade–off is lower efficiency per meter square. Electrical efficiency is strongly influenced by the type of solar cell. Clarke et al. (1996) showed that mono-crystalline semi-transparent PV panels can recover 27.5% heat and have 11.7% electrical efficiency during typical UK winter. Furthermore, ambient conditions have significant impact on PV thermal and electrical efficiency. A few published papers included outdoor conditions such as wind speed, ambient temperature and solar radiation; *e.g.* Jones and Underwood (2001) predicted the impact of the solar irradiation and wind

speed on the PV panel temperature. The conclusions indicated that the temperature of the PV panels significantly decrease with the higher wind speeds and lower levels of incident solar radiation.

Finally, there are other factors that reduce the performance of the PV panel such as dirt, shadow, air leakage, connections and orientation. These factors will not be investigated in this thesis.

2.5 Heat Transfer in the BIPV/T Systems

Heat transfer in cavities generally includes longwave radiation exchange and convection heat transfer. Undoubtedly, the most critical factor in evaluating thermal behaviour of air in the PV cavity and BIPV/T system performance is the convective heat transfer coefficient (CHTC). Outdoor CHTC and that in the PV cavity have a big impact on the overall energy performance of the entire BIPV/T system.

2.5.1 Outdoor CHTC

Various researchers have been studying the wind heat transfer mechanisms over inclined surfaces and flat solar collectors. It is generally accepted that the problem is quite complex and depends upon various factors. Wind speed has significant effect on the value of CHTC and exterior surface heat losses. One of the first studies done in this area was suggested by McAdams (1954):

$$h_w = 5.7 + 3.8 \cdot V_w \tag{2.1}$$

Where, V_w is the wind speed (m/s).

Although this equation is applicable for lengths not higher than 0.5m and $V_w \leq 0.5m/s$ (Duffie and Beckman,1980), it is being widely used. Wastmuff et al. (1977) noticed that equation 2.1 gives overestimated values for h_w due to included radiation effects and proposed the following correlation for $V_w \leq 0.5m/s$:

$$h_w = 2.8 + 3.0 \cdot V_w \tag{2.2}$$

Furthermore, Sharples and Charlesworth (1998) concluded that CHTC depend upon the wind direction. The CHTC is higher on the windward side than on the leeward side. Sharples (1984) proposed correlations for the windward and leeward surface. However, he considered vertical but not tilted surfaces.

$$V_w = 1.8 \cdot V_{10} + 0.2 \quad \text{Windward surface} \tag{2.3}$$

$$V_w = 0.2 \cdot V_{10} + 1.7 \quad \text{Leeward surface} \tag{2.4}$$

$$h_w = 1.7 \cdot V_w + 5.1 \quad \text{Either surface} \tag{2.5}$$

Where, V_{10} is the wind speed (m/s) measured height above 10m.

Ernari (2006) compared several correlations found from the literature with those derived from the boundary layer theory to find the most accurate equation of the CHTC for the forced convection over the inclined plane surface. He stated that the heat transfer rate between the surface and air greatly depends whether the flow is laminar, transient or turbulent. Even relatively low turbulence can increase the heat transfer rates and hence the heat losses from the BIPV/T roof. Furthermore the following parameters can alter the flow and therefore; CHTC: length, shape, surface roughness, air velocity *etc.*

The suggested equations that depend upon the length of the BIPV/T roof *L(m)* are as follows:

$$h_w = 3.83 \cdot V_w^{0.5} \cdot L^{-0.5} \quad \text{Laminar flow} \quad (2.6)$$

$$h_w = 3.83 \cdot V_w^{0.5} \cdot L^{-0.2} \quad \text{Fully Turbulent flow} \quad (2.7)$$

$$h_w = 5.74 \cdot V_w^{0.8} \cdot L^{-0.5} - 16.46 \cdot L^{-1} \quad \text{Mixed flow} \quad (2.8)$$

As can be seen many correlations have been developed but no consensus has been reached for the best correlations as they are strongly applicable to the particular experimental conditions at the test site (Sharples and Charlesworth, 1998).

2.5.2 CHTC in the PV Cavity

CHTC in the PV cavity are also subject to uncertainty. As in the case of outdoor CHTC, the results vary from one researcher to another. While investigating the empirical relations to determine the Nusselt number, Ong (1995) concluded that results can vary in the range from ± 50%. Similar conclusion can be drawn as in the case of outdoor CHTC *i.e.* derived empirical correlations can be applied only for the experimental setup. Charron and Athienitis (2006) extensively investigated the available correlations for determining the CHTC in the cavity of a BIPV/T system and concluded that the problem is quite complex and many flow scenarios can be created *i.e.* laminar, turbulent, transition and either developing or fully developed. Charron et al. (2005) considered an algorithm that investigates which of the CHTC should be used for natural, forced and mixed convection.

The assessment criteria is based on Grashoff *(Gr)* and Prandtl *(Pr)* number ratio:

$Gr/\mathrm{Re}^2 > 4$	Free convection	(2.9)
$Gr/\mathrm{Re}^2 < 0.25$	Forced convection	(2.10)
$0.25 \leq Gr/\mathrm{Re}^2 \leq 4$	Mixed convection	(2.11)

Moreover, whether to use the channel or separate flow approximation is a subject of argument among research community. If the distance between the plates is narrow, boundary layers developed on both plate sides will merge into one single profile at a certain distance. In contrast, if the gap is too wide, two separate boundary layers will develop on each plate. The selection criterion is the distance between the plates *(D)* and height ratio *(H)*. Mei et al. (2003) stated that for the D/H = 0.14/2.5 separate flow approximation should be used. In contrast, Charron et al. (2005) suggested plate flow approximation should be applied for D/H = 0.3/2.5 ratio. However, no information was found in the literature regarding inclined surfaces and all these values were developed for the vertical double facades.

The nature of the flow at the entrance is strongly influenced by smoothness and geometry (Incropera and DeWitt, 1985). If the there is no abrupt change of flow direction and the surface is smooth, laminar flow will occur at the entrance followed by transition region and finally becomes turbulent. Equations 2.12-2.14 present expressions that were developed for the solar air collectors but not for the BIPV/T applications.

$$h_i = \frac{k_{air}}{D_h}\left[5.4 + \frac{0.00190\cdot(\mathrm{Re}\cdot\mathrm{Pr}\cdot\frac{D_H}{L})^{1.71}}{1+0.00563\cdot(\mathrm{Re}\cdot\mathrm{Pr}\cdot\frac{D_H}{L})^{1.17}}\right] \qquad \mathrm{Re}<2300 \qquad (2.12)$$

$$h_i = \frac{k_{air}}{D_h}\left[0.116\cdot(\mathrm{Re}^{2/3}-125)\cdot\mathrm{Pr}^{1/3}\cdot(1+(\frac{D_H}{L})^{2/3})\cdot\left(\frac{\mu}{\mu_w}\right)^{0.14}\right] \quad 2300<\mathrm{Re}<6000 \qquad (2.13)$$

$$h_i = \frac{k_{air}}{D_h}\cdot\left[0.036\cdot\mathrm{Re}^{0.8}\cdot\mathrm{Pr}^{1/3}\cdot\left(\frac{D_h}{L}\right)^{0.055}\right] \qquad \mathrm{Re}>6000 \qquad (2.14)$$

Recently, Liao (2005) developed local values of the forced CHTC for two configurations depicted in Figure 2.1 and presented below. The investigation was carried out using two-dimensional k-ε turbulent computational fluid dynamics (CFD) model neglecting the heat transfer through the insulation side. For Configuration 1 depicted in Figure 2.1, equation 2.15 represents local CHTC on the PV side and 2.16 represents on local CHTC on insulation side.

$$h_i = \frac{k_{air}}{W}\cdot\left[(0.11\cdot\mathrm{Re}+62.856)\cdot e^{-0.475\bar{H}} + 2.766\cdot10^{-3}\cdot\mathrm{Re}+5.58\right] \qquad (2.15)$$

$$h_i = \frac{k_{air}}{W}\cdot\left[(0.109\cdot\mathrm{Re}-124.344)\cdot e^{(-1.635\cdot10^{-5}\cdot\mathrm{Re}-0.593)\bar{H}} + 4.098\cdot10^{-3}\cdot\mathrm{Re}+3.896\right] \qquad (2.16)$$

$$\mathrm{Re} = \frac{V_{air}\cdot L}{\nu_{air}} \qquad (2.17)$$

Where, W is cavity width (m), $\bar{H}$ is dimensionless channel height (m), $\bar{H} = \frac{H}{W}$, Re is Reynolds number, V_{air} *is* air speed in the cavity (m/s) ν_{air} is kinematic viscosity of air (m^2/s). Similarly, the local CHTC were derived for Configuration 2.

For the PV panel side at the inner cavity the following expression was derived:

$$h_i = \frac{k_{air}}{W} \cdot \left[(79.356) \cdot e^{-0.475\bar{H}} + 9.729 \right] \tag{2.18}$$

Local value of CHTC at insulating side in the inner cavity is shown below:

$$h_i = \frac{k_{air}}{W} \cdot \left[(39.156) \cdot e^{(-0.61753)\bar{H}} + 10.043 \right] \tag{2.19}$$

The following relation was found at the glazing side of the outer cavity:

$$h_i = \frac{k_{air}}{W} \cdot \left[(69.456) \cdot e^{-0.475\bar{H}} + 7.24 \right] \tag{2.20}$$

The equation represented below was determined at the PV side of the outer cavity:

$$h_i = \frac{k_{air}}{W} \cdot \left[(-58.9) \cdot e^{-0.603\bar{H}} + 6.355 \right] \tag{2.21}$$

The average CHTC for all cases can be obtained by integrating h_i over entire height, y = 0 to $\bar{H}$ as presented by the equation below:

$$\overline{h_i} = \frac{1}{\bar{H}} \cdot \int_0^{\bar{H}} h_i \cdot dy \tag{2.22}$$

Major assumption in this investigation was to use a turbulent model in CFD software, FLUENT. The assumption was justified by the fact that flow becomes turbulent at the inlet due to abrupt turn of 90°. The turbulent flow stays in developing region not becoming fully developed due to small height of 1m. It was found that for Configuration 1, average CHTC is 5.8 W/m^{2}K and 8.6 W/m^{2}K for the PV and insulation side,

respectively. The results are valid for the air velocity range of 0.3 m/s to 0.6 m/s and ambient temperature from -10°C to 10°C, respectively. Liao (2005) used his results as an input to 1D model for Configuration 1 developed by Charron (2005) to calculate PV panel and insulation temperatures. A good agreement was found with experimental results (±2°C).

Mei (2003) suggested that for air flow velocities lower than 0.5 m/s buoyancy effect may be significant and CHTC expressions for mixed convection should be used. The well-known expression for inclined asymmetrically heated parallel plates found by Hollands cited in Duffie and Beckman (1980) is often used:

$$h_i = \frac{k_{air}}{D_h}\left[1+1.44\cdot\left[1-\frac{1708\cdot(\sin 1.8\beta)^{1.6}}{Ra\cdot\cos\beta}\right]\cdot\left[1-\frac{1708}{Ra\cdot\cos\beta}\right]^{+}+\left[\frac{(Ra\cdot\cos\beta)^{1/3}}{5830}-1\right]^{+}\right] \quad (2.23)$$

Where, sign $[\ ]^{+}$ denotes if the expression in the brackets is negative; it should be set equal to zero. The equation is applicable for tilt angles (β) from 0° to 75° and Rayleigh number *(Ra)* in ranges from 0 to 10^5.

Some researchers neglected the affect of radiation heat exchange between the surfaces of naturally ventilated and inclined channels. Lin and Harrison (2003) experimentally investigated the heat transfer in an asymmetrically heated, inclined channel including the radiation heat exchange. They developed local and average Nusselt numbers for inclination angle of 18° and surface emissivities of 0.95. The results showed that with low emissivity surface, channel space and tilt angle do not have big impact on heat transfer.

2.6 Fan Control Strategies and Airflow

Regarding the fact that BIPV/T applications can deliver preheated air into the HVAC system, proper fan control strategy must be employed to achieve maximum possible energy efficiency both thermal and electrical. By increasing the velocity, the mass flow rate will be also increased and more air is available to transport energy. Consequently, the heat transfer is enhanced leading to higher rates of recovered heat and higher thermal efficiencies. The temperature of the PV panels is decreased leading to higher electrical efficiency. However, there are some disadvantages to this approach. The trade off is lower outlet air temperatures delivered than those in case of lower air velocities in the BIPV/T cavity. Furthermore, fan energy consumption is increased. Finally, the total mass flow rate of air should not exceed the occupants' requirements (Charron, 2004). If the flow rate exceeds this requirement some additional heating of the preheated air might be required due to low air outlet temperature. Charron (2004) concluded that higher flow rates are preferable in cooling season when ventilated air is rejected outside.

Kreider and Kreith (1981) suggested that two types of fan control strategies are to be employed for building scale applications *i.e.* on/off and proportional. While on/off fan controller operates fan according to the specified condition such as temperature, solar radiation, time, the proportional controller varies the fan speed to maintain a certain air temperature at the outlet of PV cavity. IEA (2000) compared performance of the open air

loop system with integrated SAC with above mentioned fan control strategies under various weather conditions. He concluded that time control has the highest efficiency, almost the same as for the always running strategy. The system performance decreases with later start and earlier stop and therefore; other fan strategies were less efficient. However, if the comfort is an issue, the temperature control strategy is preferred. Finally, the level of solar radiation intensity affects the efficiency of the solar driven fan. Higher efficiencies are achieved with higher levels of solar radiation intensity and vice-versa.

As discussed previously, another useful strategy is to maintain the certain level of temperature at the outlet of the air gap. For this purpose a variable fan or mixing dumper can be used. Abbud et al. (2005) argued that such control strategy is advantageous when hot air at constant temperature is supplied to the thermal rockbed storage. Better thermal stratification in the pebble bed is achieved and lower fan energy consumption as opposed to cases with constant flow rates.

2.7 Thermal storage

In solar air heating, the heated air can immediately be delivered to the zone to cover the heating loads or stored in thermal storage for later use. Thermal energy storage consists of various storage media. The type of storage media depends on the nature of the process. The heat can be stored as sensible or latent heat. In this thesis only sensible heat storage will be considered. Sensible heat storage, on the basis of the heat storage media is classified as:

- Solid media storage
- Liquid media storage

- Combination of the previous two

2.7.1 Rockbed Thermal Storage

If the hot air is used for heating purposes, a possible choice would be to use a rockbed thermal storage. Unless otherwise defined, the fixed rockbed, pebble, thermal storage is further considered. Kreider and Frank (1981) compared various thermal storage and concluded that technically and economically the most advantageous thermal storage systems are pebble beds. Tiwari (2002) stated the advantages of the rockbed system over other thermal storages:

- Rocks are easy to handle, non-toxic, non-flammable and abundant
- High storage temperatures and high degree of thermal stratification are possible
- No heat exchanger is needed
- No freezing or corrosion problems

On the other hand, there are some disadvantages:

- Large storage volumes, taking a lot of space in the basement
- High pressure drops
- Simultaneous heat charging and discharging is not possible
- Possibility of mold and fungi growth

There are many parameters that influence the performance of the rockbed thermal storage. The rate and direction of the air flow are some of them. Higher flow rates increase the BIPV/T system efficiency but deliver lower air temperatures to the rockbed.

Larsen cited in (IEA, 2000) concluded that vertical rockbed as opposed to horizontal rockbed is advisable due to higher heat exchange rate *i.e.* hot air does not accumulate in the upper parts during charging and in lower parts during discharging of the rockbed.

The rockbed storage may yield the highest pressured drop in the HVAC system and significantly increase the fan energy consumption. Chandra and Willits (1981) concluded that pressure drop besides the air flow rate and length of the rockbed, depend upon the type of the solar air system, rock porosity and rock diameter. While low pressure drop saves the fan energy, the high pressure drop contributes to uniform temperature distribution in the rockbed storage (IEA, 2000). Open air loop solar systems may have higher pressure drop than that of the closed air loop solar systems (IEA, 2000). Moreover, with higher values of rock porosity, the pressure drop is decreased. Finally, stone size defines thermo-physical properties of the rockbed. While small stones produce a high pressure drop, they also provide a larger contact area for heat transfer between the air and rocks and shorter air flow length for heat convection. On the other hand, in case of solar air heating system with a heat pump, the large sized storage materials *i.e.* bricks, concrete blocks have the same overall thermal performance as small sized rocks (Sagara and Nakahara, 1991). This is due to the fact that reduced collected heat for large materials is compensated by low fan energy consumption as the pressure drop is small over large sized heat storage materials.

2.7.2 Water Thermal Storage

Water tanks are usually used to store the heat in liquid-based solar heating systems. However, they can be used in solar air heating applications by introducing an air to water heat exchanger. Ward et al. (1977) discussed the performance of the various thermal storage systems.

They concluded that a water tank has three times lower tank volume capacity than pebble bed for the same amount of the stored heat. Furthermore, the heat can be added and removed simultaneously (Kreider and Kreith, 1981). The same researchers concluded that liquid thermal storage is expensive. Water tank requires a heat exchanger to deliver the heat to the storage, valves and pumps.

Various researchers investigated the phenomenon of thermal stratification in water tanks as a main research area in this field. They can operate with significant degree of thermal stratification. Therefore, many stratified models have been developed. The most common used is multi-node approach where a tank is divided into N nodes with energy balances written for each section of the tank.

2.8 Building Simulation Software Overview

Building designers need to predict the long-term energy performance of the HVAC system and thermal behaviour of the building. Simulations are fast, easy to handle and inexpensive tools to deliver such outputs. When considering the BIPV/T system modeling, Charron, et al. (2005) concluded that it is more demanding than modeling a typical house due to integration of the active solar technologies. Klein, et al. (1976) suggested that solar process simulations can serve three purposes:

- To investigate long-term energy performance of the system under various weather data and control strategies,
- To develop a design tool for a specific application of interest,
- To determine the correlations among the system performance, design parameters and weather.

The design tool developed in this thesis serves all three above mentioned objectives.

The use of simulations in solar applications and building thermal analysis has started relatively recently with the development of computers. These advancements have allowed the development of sophisticated building performance simulation tools that can accurately model transient heat transfer and other aspects relevant to the building modeling (Charron et al., 2005). Since Sheridan et al. (1967) simulated the operation of solar water heaters, various researchers developed many different solar simulation programs. Detailed history development of the programs especially designed for solar processes applications can be found in Duffie and Beckman (1980). Crawley et al. (2005) provided a detailed comparison of the capabilities of twenty building simulations programs including eQUEST, DOE-2.1E, HAP, EnergyPlus, IDA, ESP-r and TRNSYS. The assessment was made by comparing the programs' features in the categories ranging from the general modeling features, building envelope, daylighting and solar, green building components, HVAC systems to results reporting. However, only major capabilities and properties of EnergyPlus, ESP-r and TRNSYS have been extracted from the report and presented in this thesis. The selection criteria were made based on the fact that these programs are the most often used and tested in building energy analysis

community. A brief description of each selected energy calculation tool and its capabilities is presented below.

2.8.1 EnergyPlus

EnergyPlus is an energy analysis and building thermal load simulation program developed by the U.S. Department of Energy in 2001. It is a stand-alone program that allows simultaneous simulation of the building and HVAC system at time steps less than an hour. It is based on a heat balance method with transient heat conduction through the building envelope calculated by conduction transfer functions. Anisotropic sky model is used for improved calculation of a diffuse solar radiation on tilted surfaces. HVAC components are defined as an open source code. Good FORTRAN 90 knowledge is required to make desired modifications. Building integrated photovoltaic system that accounts for heat removed from surfaces layers which have defined electrical characteristics is also included. The software does not have a user-friendly graphical interface. Inputs and outputs are only text files. Moreover, graphical interpretation of the variables of interest during the simulation is not possible (DOE, 2006).

2.8.2 ESP-r

ESP-r has been under development by research team from the University of Stratchlyde, UK for over 25 years. It is the energy modeling tool that utilizes thermal network method with finite difference approach to calculate the transient conduction heat transfer through the walls. It has a graphical user interface and in addition to the

advanced features listed for EnegyPlus, it supports one-dimensional (1D), two-dimensional (2D) and three-dimensional (3D) conduction heat transfer, computational fluid dynamics (CFD) and indoor air quality analysis *etc.* (DOE, 2006).

The outputs can be represented through graphs and text files. McQuiston (2005) concluded that it is more powerful and flexible than EnergyPlus.

2.8.3 TRNSYS

Another building simulation software was developed by the University of Wisconsin – Madison Solar Energy Lab and the University of Colorado Solar Energy Applications Lab in 1970s. TRaNsient energy SYStem is transient simulation software with a modular structure where a system is broken into series of components: TRNSYS simulation studio – graphical interface to select mechanical components to define the input files, TRNBuild – building input data visual interface and TRNEdit – editor used to create stand-alone applications define TRNSYS. It utilizes conduction transfer functions for calculating the heat flow through the building envelope. It has an extensive library of HVAC, BIPV/T components, solar thermal and PV/Thermal collectors that can be easily modified. One of the advantages of the TRNSYS is the very user-friendly graphical interface with drag-and-drop components for creating input files. Any component can be plotted during the simulation and exported into many various software packages *e.g.* MATLAB, Excel, Contam *etc.* The capabilities of these programs relevant to designers of ZESHs and objectives of this thesis are summarized in Table 2.1.

Although system modeling is cheap, fast and easy-to-use tool for design purposes, some limitations must be taken into account (Duffie and Beckman, 1980). Firstly, how realistic the simulation will be, greatly depends upon assumptions. Moreover, the accuracy of the results is greatly influenced by the extent of details included in the simulation. However, not all details can be considered *e.g.* leaks, poor installation of the equipment *etc.* that affect the thermal performance of the system. It can be concluded, that the best way to verify the results obtained by the simulations is to compare with those of experimental work. Model verification with experimental data is presented in Chapter 4.

Table 2.1. Contrasted capabilities of building energy performance simulation programs (Crawley et al., 2005)

Features	EnergyPlus	ESP-r	TRNSYS
Conduction solution method			
• Transfer functions	X		X
• Finite difference		X	
Solar analysis			
• Distribution of solar radiation through the glazing computed at each time step	X		X (EI)
Sky model			
• Isotropic		X	X
• Anisotropic	X	X	X
Convective & Radiative Calculations			
• Inside radiation view factors	X	X	
• Radiation-to-air component separate from detailed exterior convection	X	X	X
Surface Conduction			
• 1D	X	X	X
• 2D and 3D	X	X(RI)	
BIPV, electrical side and thermal interaction with the building	X	X	X (E)
Solar thermal collectors	-Glazed flat plate -Unglazed transpired	-Glazed flat plate - Unglazed flat plate	- All types
HVAC components			
• Heat exchangers(user defined effectiveness)		X	X
• Rockbed thermal storage		X	X
• Stratified water heat tank		X (R)	X
• User defined control strategy			X
Results reporting			
• Graphs			X
• Plot of variables during the simulation		X	X

Note: R- capability that is intended for research use
E – capability that requires considerable knowledge
I – capability that requires data that can be difficult to obtained

CHAPTER 3

SIMULATION TOOL DEVELOPMENT AND EXPERIMENTS

3.1 Introduction

Building designers are faced with many challenges in designing solar-optimized houses. Integration of the PV panels into the roof is more than simply connecting mechanical and building envelope components. The PV panels should be integrated appropriately to maximize the use of solar energy and cost effectiveness. The major questions to be answered in designing the BIPV/T systems are: how much electricity can be generated, how much heat can be recovered, what type of the BIPV/T roof configuration will yield the highest efficiency? Four different BIPV/T roof configurations have been investigated in this thesis. To achieve net zero energy target for houses in cold zones, not only active but passive solar systems should be used such as heavy thermal mass, fenestration, overhangs and motorized blinds. For example, a lot of energy is available but is typically not needed for immediate use due to the fact that passive solar gains through south windows could satisfy daytime heating load. This excess heat obtained from the roof can be utilized for different purposes *e.g.* to be stored in the thermal heat storage for later use or for heating DHW with air-water heat exchanger. Therefore, to approach net zero energy goal, thermal interaction between BIPV/T and HVAC system such as rockbed storage and air-water heat exchanger have been examined. The following sections present the methodology used for the analysis of this innovative building envelope.

3.2 System Description

In this thesis, energy analysis of four different BIPV/T system configurations linked to HVAC components and thermal behaviour of the solar house have been investigated. As mentioned previously, only open air loop systems were considered to keep the temperature of the PV panels as low as possible. The open-loop air solar system configurations are shown in Figures 3.1-3.4. The unglazed BIPV/T roof (Configuration 1) is the same as that installed at the solar house. The experimental verification of the developed model will be presented in Chapter 4. Significant increase in outlet air temperatures can be achieved with some modifications of the Configuration 1. Therefore, Configuration 2 presents a modified case of the Configuration 1 where 1.5m long flat plate solar air collector (SAC) is added vertically to the outlet of the unglazed BIPV/T roof section. Glazed BIPV/T roof (Configuration 3) resembles a SAC where the PV panels are used as absorbers. Finally, Configuration 4 presents improved model of Configuration 2 where a low emissivity coating has been added to the inner side of the glazing and air is passed behind the absorber of the SAC. Operation of the combined BIPV/T and HVAC system is similar to that of the solar air heating systems. When immediate space heating is required, outdoor air is heated by recovered heat from the BIPV/T system, supplied to the air handling unit (AHU) for additional heating or delivered directly into the zone. In case when solar heat gains through the south windows could satisfy daytime heating load, the recovered heat is stored in the rockbed storage for later use. A fan control strategy with constant airflow supply was considered in that case. During cold winter nights, the stored heat is withdrawn by the fan from the rockbed storage and delivered to the zone to reduce the heating load. The air-water heat exchanger

(AWHE) in winter is by-passed. In summer, total airflow through the PV gap is circulated through the AWHE. The hot water from the AWHE is used to heat water in the water tank. The heated water can be used as a DHW. The air is then exhausted outdoors. Finally, air speeds in the PV cavity that limit the PV panel temperature to be no higher than 75°C was investigated. Although PV manufacturers suggest critical temperatures to be between 80°C and 85°C, a temperature of 75°C was chosen as a safety factor.

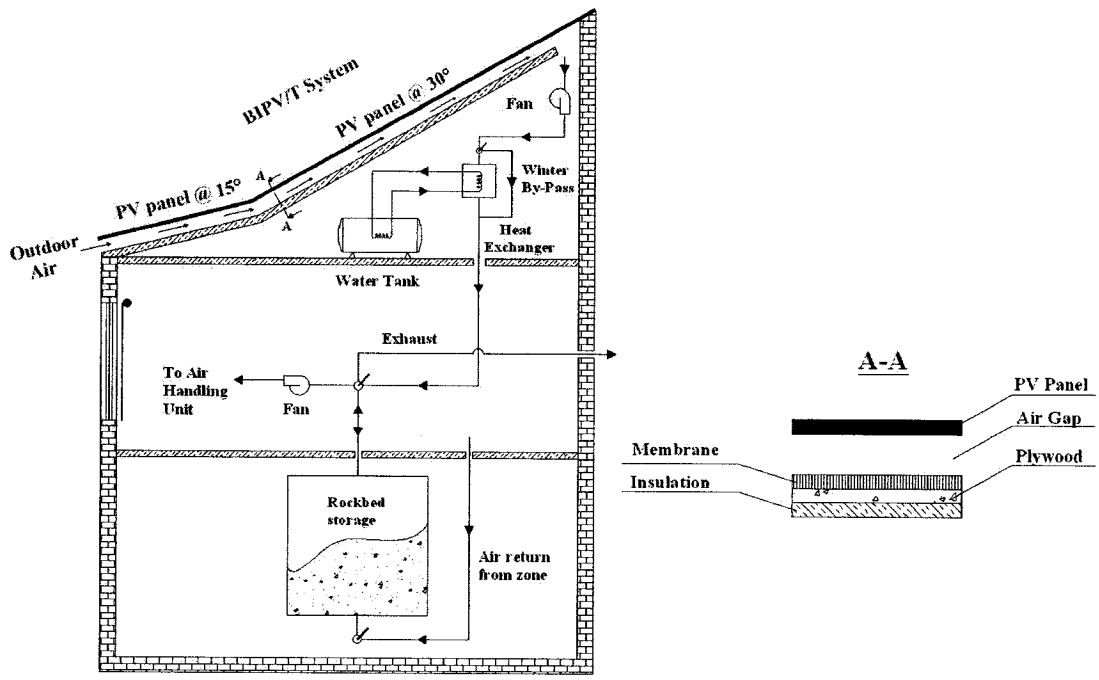

Figure 3.1: Schematic of Configuration 1

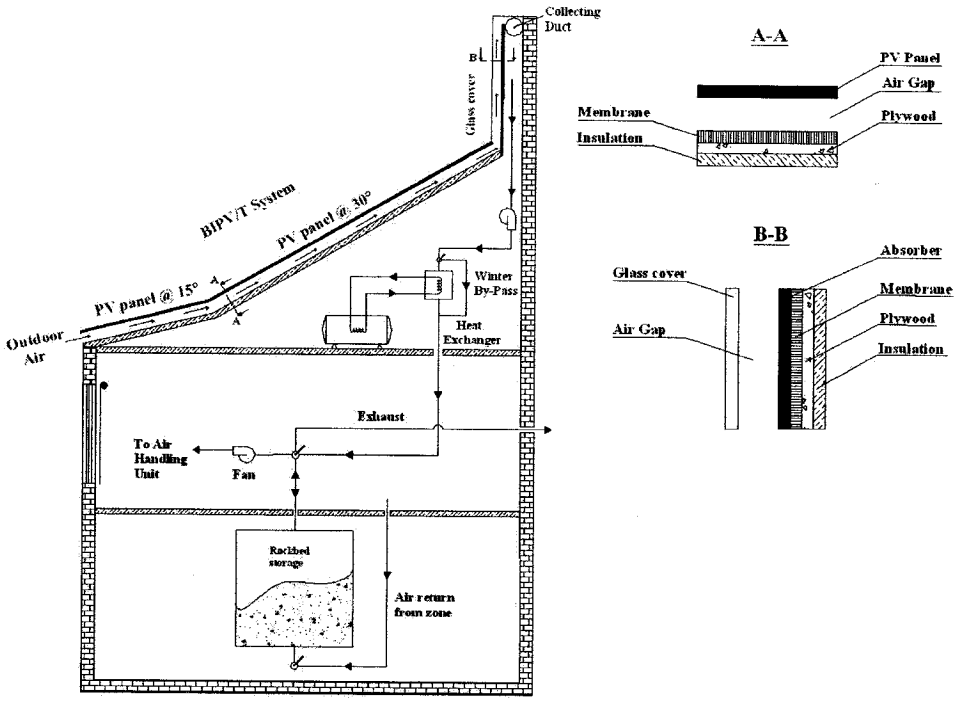

Figure 3.2: Schematic of Configuration 2

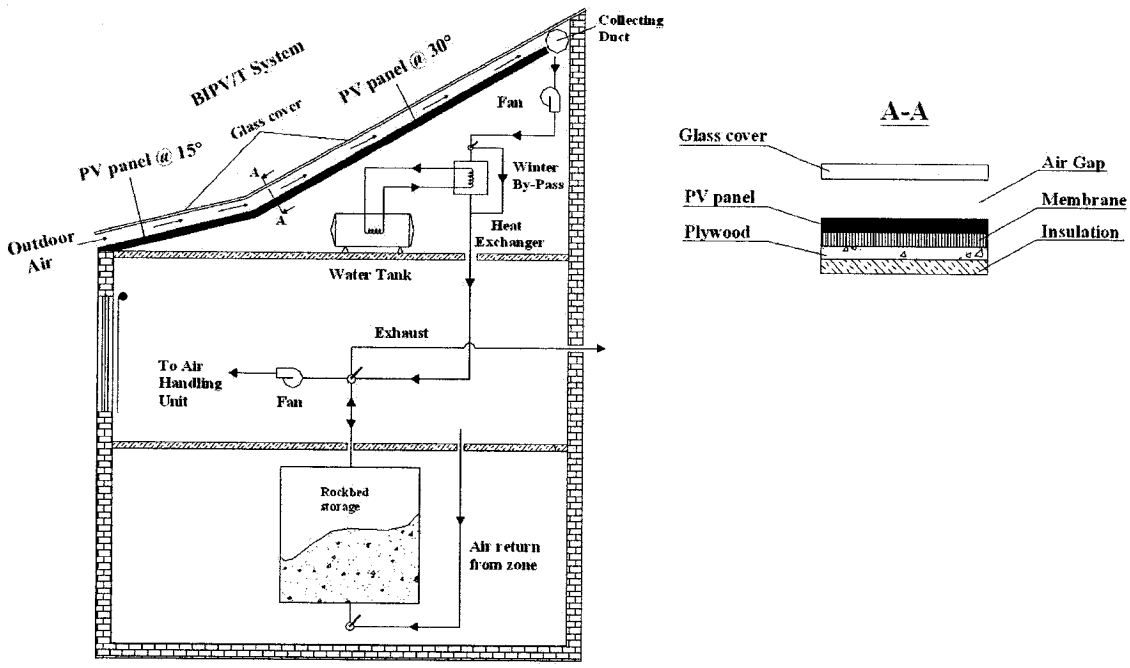

Figure 3.3: Schematic of Configuration 3

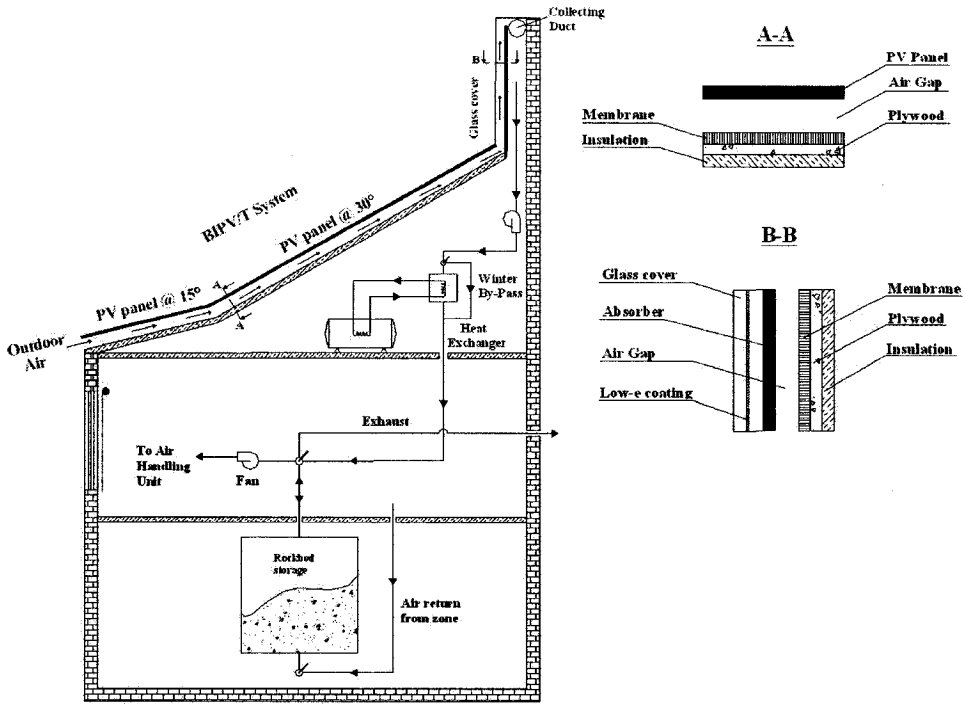

Figure 3.4: Schematic of Configuration 4

3.3 General Model Description

Mathematical model describing thermal response of the house with BIPV/T roof was implemented in MathCad 2001i software. The thermal network model approach was used to simulate transient thermal behaviour of the house. In this approach, each wall layer was divided into a network of nodes with interconnecting paths through which energy flows. This technique presents improved heat balance method, have the most flexibility and huge potential for achieving high accuracy (ASHRAE, 2005). Thermal network approach can successfully model control strategies and non-linearities such as convection and radiation.

Moreover, thermal network includes heat balance at each node to determine the temperature and energy flow between interconnecting nodes at regular time steps. Therefore, a set of algebraic equations was solved simultaneously in a matrix. However, the main disadvantage was that initial conditions were unknown; thus, they were assumed and simulation was repeated until steady state periodic response was obtained usually after the third day for a single day analysis. Energy flow included all heat transfer mechanisms *i.e.* conduction, convection and radiation and were represented as resistances between surrounding nodes. The heat transfer mechanisms were modelled according to the equations found in the literature (Athienitis, 1993; McClellan and Pedersen, 2005).

One dimensional conduction heat transfer was assumed. There are many developed techniques to accurately calculate transient conduction heat transfer through the walls due to transient nature of solar radiation and outdoor temperature as well as thermal capacitance of the layers. Thermal capacitance was calculated as:

$$C = c_p \cdot \rho \cdot V \tag{3.1}$$

Where, c_p(J/kg°C) is the specific heat capacity, ρ (kg/m^3) is the layer density and V (m^3) is the volume of the mass element. The explicit finite difference method was chosen between response factor and frequency domain techniques for calculating conduction through the walls as it can accurately model the system non-linearities. When all thermal resistances and thermal capacitances were calculated, a simulation time step was selected based on numerical stability criteria.

The general form of the explicit finite difference method (Athienitis and Santamouris, 2002):

$$T(i,t+1) = (\frac{\Delta t}{C_i})\left[q_i + \sum_j \frac{T(j,t) - T(i,t)}{R(i,j)} \right] + T(i,t) \tag{3.2}$$

where, $t+1$ indicates next time step, j all nodes connected to node i, $R(i,j)$ is the thermal resistance between nodes i and j, C_i is the thermal capacitance of node i, Δt is time step and q_i is a heat sources at node i.

Convection can be modeled in different degrees of detail pending on desired accuracy. Indoor convection heat transfer between the room surfaces and indoor air was modeled as follows (Athienitis, 1993):

$$h_c = 0.59 \cdot (\frac{T_S - T_{ai}}{L})^{0.25} \quad \text{For heat flow downwards} \tag{3.3}$$

$$h_c = 1.52 \cdot (T_S - T_{ai})^{1/3} \quad \text{For heat flow upwards} \tag{3.4}$$

$$h_c = 1.31 \cdot (T_S - T_{ai})^{1/3} \quad \text{For vertical surfaces} \tag{3.5}$$

Both outdoor and PV gap convective heat transfer coefficients are analyzed in detail in upcoming sections as they have a strong effect on thermo-fluid behaviour of the air stream in the PV cavity. Radiation heat transfer between all interior and exterior surfaces was modeled in detail using the radiosity method. Radiation heat exchange between all interior surfaces was presented with non-linear heat transfer coefficients as follows:

$$hr_{i,j} = \frac{\sigma \cdot (T_i^4 - T_j^4) \cdot F_{\varepsilon i,j} \cdot F_{i,j}}{T_i - T_j} \tag{3.6}$$

Where,

$T_{i,j}$ ($^{\circ}C$) - temperature of the interior surfaces i, j

$F_{i,j}$ - view factors between interior surfaces

$F_{\varepsilon i,j}$ - emissivity factor between surfaces i, j

Radiation heat exchange between inner and outer glass of a double glazed windows with low emissivity coating was calculated by linearized radiative heat transfer coefficient

$$h_{ro} = \frac{4 \cdot \sigma \cdot T_m^3}{(\frac{1}{\varepsilon_1} + \frac{1}{\varepsilon_2} - 1)} \tag{3.7}$$

Where ε_1/ ε_2 are the emissivities of the exterior/interior glass surface, taken to be 0.1/0.9, respectively and T_m (^{o}C) is the mean temperature of glazed surfaces. Assuming standard spacing between glazing of 13 mm, the CHTC in a window cavity was taken to be 2 W/m^2 ^{o}C (Athienitis and Santamouris, 2002). Computation time can be increased without significantly affecting the accuracy by disregarding the multiple reflections and considering room surfaces to be black (Hutcheon and Handegord, 1995). Therefore, $F_{ri,j}$ is simplified and reduced to emissivity of a room surface that was taken to be 0.9. Calculation of the view factors by correlations taken from Incropera and Howell (2006) is presented in Appendix D. Radiaton heat transfer between exterior house surfaces and sky, ground is combined with expressions for exterior CHTC and presented later.

The incident solar radiation on a surface was calculated according to correlations found in Athienitis and Santamouris (2002) using Hottel's model for the clear sky. The calculation procedure is included in Appendix B. Periodic solar radiation and outdoor temperatures were modeled by Fourier discrete series.

In order to simplify calculations of the absorbed solar radiation transmitted through windows, it was assumed that 70% was absorbed by the floor and the rest by other surfaces. The amount of absorbed heat in glazing and that of released to the room air was calculated. Calculation of optical properties of the windows is presented in Appendix B.

Internal heat gains from lights, people and appliances were also modeled on hourly basis. Infiltration through the cracks and openings was determined for the ventilated attic and zone. The following equation was used:

$$U_{\inf} = \frac{ACH \cdot Vol}{3600} \rho_{air} \cdot c_p \tag{3.8}$$

Where, U_{inf} (W/°C) is the infiltration conductance, ACH is air changes per hour and Vol (m^3) is the volume of the zone/ attic. The value of ACH was assumed to be 0.5 (Athienitis, 1998). The entire house was modeled as a single zone. North, east and west walls and windows were lumped into two nodes and connected in parallel as their window-wall ratio is not high compared to that of south façade. Although the interior room height is not the same in all rooms, the average value of 2.5m was used in simulations to simplify view factor calculations. Set point temperature of 22°C without a night setback was assumed.

Once all thermal resistances were calculated, a simulation time step was selected based on numerical stability criterion:

$$\Delta t_{critical} = \min\left(\frac{C_i}{\sum_j \frac{1}{R_{i,j}}}\right) \tag{3.9}$$

A simulation time step of 5 min was chosen for calculations as it was found suitable for adequate degree of desired accuracy and minimum computational time. As energy balance was applied on each node, a system of linear and non-linear equations was solved simultaneously in a matrix. Complete thermal network and energy balances on each node for presented Configurations are included in Appendix C and Appendix E.

Air to water heat exchanger, water tank and rockbed thermal storage mathematical models were developed using equations found in the literature and are presented later in this thesis.

The following major assumptions were made for developing simulation model:

- One dimensional heat transfer
- Neglected thermal capacitance of the PV panel
- BIPV/T roof is divided into 3 sections, where inlet to one section is outlet of the pervious one
- Isothermal surfaces of the PV channel for each segment
- Neglected edge effects of the surface and air cavity
- No leakage in the PV cavity
- PV efficiency is a function of temperature only
- Uniform solar radiation on the exterior surface
- Air steam temperature vary linearly along the BIPV/T roof for short lengths
- CHTC values for upper and lower channel of the PV cavity are equal (Ong, 1995; Wang et al., 2006; TRNSYS 16, 2005)
- The PV cells operate at their maximum power point condition

3.4 Features of the Solar House

Concordia's award-winning solar house "Northern Light" of 75 m^2 floor area depicted in Figure 2.4 was used as a case study for model development and verification. Combined passive and active solar technologies were employed to achieve a zero energy target. Detailed house layout is included in Appendix A. The walls have total resistance value of approximately of RSI 5.6 m^2C/W. The ceiling has 180 mm of spray-foam insulation directly applied to the wood decking of the roof achieving RSI 9 m^2C/W. The floor has resistance value of RSI 7.2 m^2C/W. Thermal properties of the building envelope are included in Appendix E. Large double-glazed and triple glazed low-emissivity argon windows are placed on the south wall to transmit large amount of sunlight into the zone. They occupy about 35% of the south wall. Overhangs and controlled motorized blinds are employed to reduce solar heat gains and cooling load. A 7 kW PV system mounted on the roof was consists of 40 unglazed monocrystaline PV panels of 175W power. Technical details of the PV panel can be found in Appendix G. The PV panels cover 70% of total roof area with surface of approximately 50 m^2. Solar panels are connected in pairs producing twenty strings linked with five charge controllers. Four charge controllers were Xantrex C40 and one was a Sky Boost 3048 charge controller with maximum power point tracking system. The PV panels are embodied on the south roof creating a 4 cm high PV cavity through which the ambient air is withdrawn by a 250W variable speed fan. The roof has two sections - one at slope of 15^o connecting to a second section at 30^0. The first section at 15^o slope is consisted of 2 rows with 6 PV panels having total dimension of 9.5m x 1.6m. The 30^o roof slope has 4 rows with 7 PV panels having total dimension of 11.1m x 3.2m.

Electricity generated by the PV panels is used to run electrical appliances in the house or stored in the batteries for later use over 3-day period. Two evacuated tube solar water collectors are placed on the east side of the roof mainly to serve for DHW purposes. Their interaction with other HVAC components was excluded from the analysis in this thesis. The solar house has a thermal storage system designed to store heat for one day. Hollow clay bricks are soaked into the phase change material (PCM) mixture (48% butyl stearate, 50% propyl palmitate and 2% fat acid) and put into the floor cavity. In this thesis, vertical thermal rockbed storage is analyzed instead of the horizontal PCM thermal storage. Preheated ambient air is collected at the top of the roof and passed through 12" (Ø30mm) air collecting duct and mechanical room. The mechanical system installed in the solar house is flexible that allows different modes of operation for both summer and winter. Schematics of the mechanical system, both water and air side, installed in the solar house is depicted in Figures 3.5 and 3.6. In winter mode, the ambient air heated by recovered heat from the BIPV/T system is used as a preheated air in the AHU for zone heating. Before passed through the AHU, the preheated air is by-passing the AWHE by positioning dumpers D3 to D8, mixed in the mixing box with return air from the zone, preheated fresh air from the energy recovery unit (ERV) and warm air heated by the floor thermal storage. During the cold winter nights, the stored heat can be taken from the thermal storage and supplied to the AHU. In summer mode, hot air is used for heating the water in AWHE and exhausted outside by the fan. The hot water can be used for heating the water in the 151 liter water tank covering DHW needs or as a source to the heat pump increasing its coefficient of performance (COP).

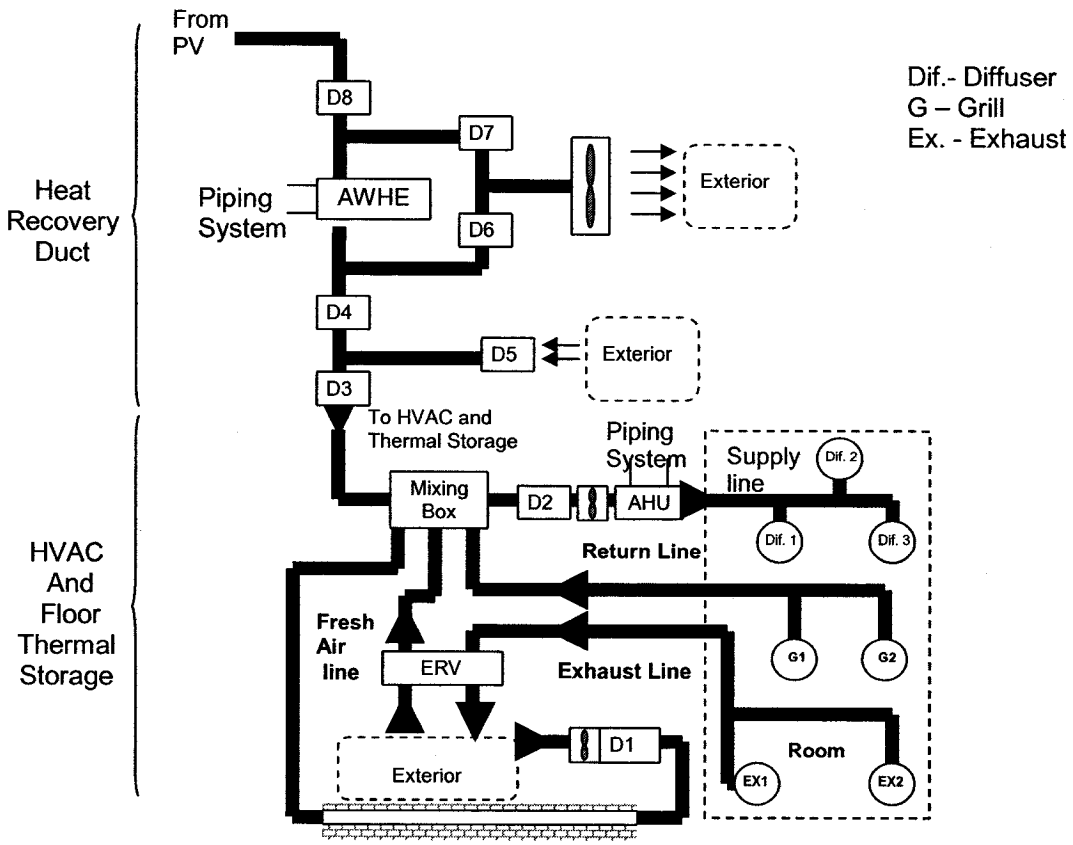

Figure 3.5: Schematic of the ducting system at the solar house (Candanedo J., et al, 2006)

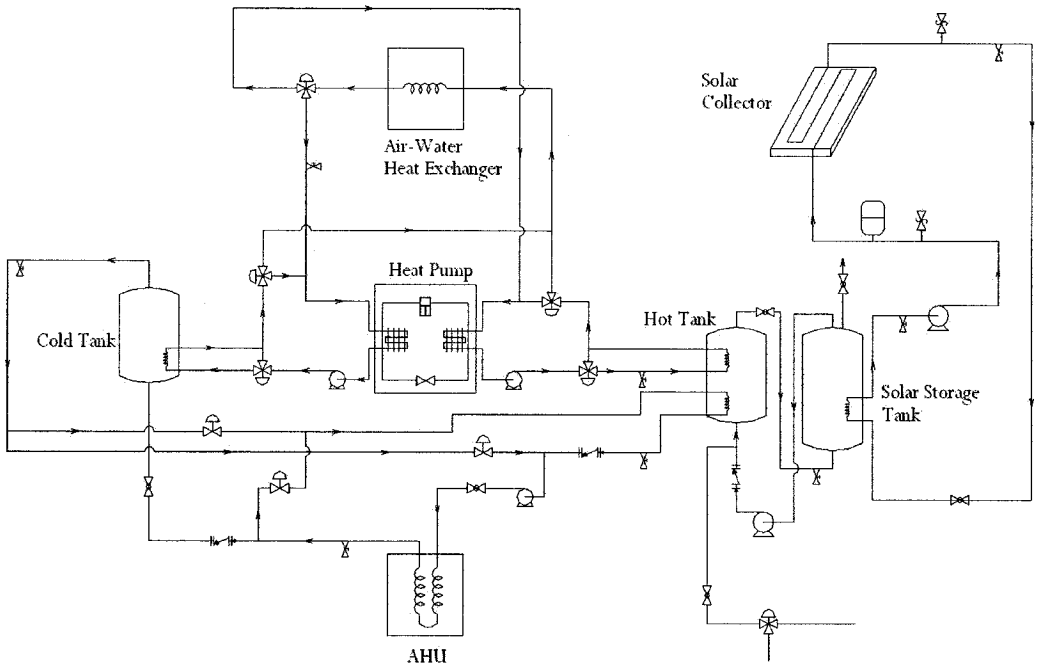

Figure 3.6: Schematic of the piping system at the solar house (Candanedo J., et al., 2006)

3.5 BIPV/T Roof Model

The mathematical model of the BIPV/T roof involves many aspects of heat and mass transfer. In order to better simulate the air temperature profile in the PV gap, the BIPV/T roof was divided into short sections. The BIPV/T roof was split into three sections with length of 1.6m each, one at 15° slope and two at 30° slope, as it was found suitable for adequate degree of desired accuracy and minimum computational time. The sections were linked such that exiting air temperature of one section was used as the input value to a next one. Theoretical solution procedure for finding temperatures of the BIPV/T roof elements and exiting air is briefly explained below. The energy balance was applied on each BIPV/T roof component. Channel walls and mean air temperatures of the first section were initially guessed. The initial CHTC were calculated according to the guessed temperature values and used to find air outlet temperature. An iterative procedure was created to find the air outlet and surface temperatures. The calculated values were compared with those of initially guessed. The iterative procedure was repeated until temperature difference was less than 0.1°C. The same procedure was repeated for other two sections. For the case of unglazed BIPV/T roof (Configuration 1) depicted in Figure 3.1, equations 3.10-3.13 were used to calculate the node temperatures.

Exterior PV surface node (3.10)

$$(T_{pv,ext} - T_o)\cdot U_t + (T_{pv,ext} - T_{pv,\text{int}})\cdot U_{pv} - (\alpha_{pv} S - P_{el}) = 0$$

Interior PV surface node (3.11)

$$(T_{pv,\text{int}} - T_{roof,ext})\cdot U_{rad} + (T_{pv,\text{int}} - T_{pv,ext})\cdot U_{pv} + (T_{pv,\text{int}} - T_{air})\cdot U_{hi} = 0$$

Exterior roof node (3.12)

$$(T_{roof,ext} - T_{pv,\text{int}})\cdot U_{rad} + (T_{roof,ext} - T_{roof,\text{int}})\cdot U_{roof} + (T_{roof,ext} - T_{air})\cdot U_{hi} = 0$$

Interior roof node (3.13)

$$(T_{roof,\text{int}} - T_{roof,ext})\cdot U_{roof} + (T_{roof,\text{int}} - T_{attic})\cdot U_{attic} = 0$$

Saelens (2002) concluded that the temperature profile in the ventilated façade is exponential. In the model, the change in enthalpy of air in the control volume is equal to the energy transferred to the air by convection. The energy balance on the air:

$$W\cdot h_c (T_{pv,\text{int}} - T_{air}) + W\cdot h_c (T_{roof,ext} - T_{air}) = mc_p \frac{dT_{air}}{dy} \quad (3.14)$$

Solution of equation 3.14 is presented by the following equation:

$$T_{air}(y) = e^{-(\frac{h_c + h_c}{\dot{m}\cdot c_p})\cdot W\cdot y} + (1 - e^{(\frac{h_c + h_c}{\dot{m}\cdot c_p})\cdot W\cdot y})\cdot(\frac{h_c\cdot T_{pv,\text{int}} + h_c\cdot T_{roof,ext}}{h_c + h_c}) \quad (3.15)$$

The mean air temperature was obtained by integrating T_{air} from y=0 to L with initial condition that inlet air temperature was equal to the ambient temperature

$$\overline{T_{air}} = \frac{1}{L}\int_0^L T_{air}(y)dy \quad (3.16)$$

Collected heat, heat losses, reflected solar radiation and generated electricity can be written in the equations below:

$$Q_{heat} = \dot{m}_{air} \cdot c_p \cdot (T_{air,out} - T_o) \quad (3.17)$$

$$Q_{loss,top} = A_{pv} \cdot h_{eq} \cdot (T_{pv,ext} - T_o) \quad (3.18)$$

$$Q_{loss,bottom} = U_{roof} \cdot (T_{roof,ext} - T_{roof,\text{int}}) \quad (3.19)$$

$$S_{refl} = (1 - \alpha_{pv}) \cdot A_{pv} \cdot S \quad (3.20)$$

$$P_{el} = \alpha_{pv} \cdot \eta_{pv} \cdot A_{pv} \cdot S \quad (3.21)$$

With these definitions, energy balance for the unglazed BIPV/T roof can be written as:

$$A_{pv} \cdot S = Q_{heat} + Q_{loss,top} + Q_{loss,bottom} + P_{el} + S_{refl} \quad (3.22)$$

Satisfactory tolerance for achieving desired level of accuracy has been selected to be ± 5%.

For the case of BIPV/T-SAC system (Configuration 2) depicted in Figure 3.2, equations 3.23-3.25 were used to calculate the node temperatures using the same algorithm as previously described. As mentioned previously, a 1.5 m SAC is linked to the unglazed BIPV/T section to increase air outlet temperature keeping the channel height at 4 cm. The optical properties of the SAC are a function of the angle of incidence, the glass thickness, refractive index and the extinction coefficient. The procedure for calculating these properties is given in detail in Athienitis and Santamouris (2002). The values for conductivity (k_{sac}) of 0.04 W/m°C, thickness (x_{sac}) of 0.025m and absorptance of 0.95 (α_{abs}) the absorber were assumed. Thermal capacitance of the glass cover was neglected. Energy balance on the SAC was performed as follows:

Glass cover node (3.23)

$$(T_{glass} - T_o)\cdot U_t + (T_{glass} - T_{air})\cdot U_{hi} + (T_{glass} - T_{abs})\cdot U_{rad} - \alpha_{glass} S = 0$$

Absorber node (3.24)

$$(T_{abs} - T_{glass})\cdot U_{rad} + (T_{abs} - T_{air})\cdot U_{hi} + (T_{abs} - T_o)\cdot U_b - \tau_{glass}\cdot\alpha_{abs} S = 0$$

Energy balance of the air (3.25)

$$W\cdot h_c(T_{glass} - T_{air}) + W\cdot h_c(T_{abs} - T_{air}) = mc_p \frac{dT_{air}}{dy}$$

The BIPV/T roof (Configuration 3) shown in Figure 3.3 was modeled according to equations 3.23-3.25 but with PV panel absorptivity of 0.9 instead. The energy balance on the BIPV/T system can be expressed as:

$$Q_{heat} = \dot{m}_{air}\cdot c_p\cdot(T_{air,out} - T_o) \quad (3.26)$$

$$Q_{loss,top} = A\cdot h_{eq}\cdot(T_{glass,ext} - T_o) \quad (3.27)$$

$$Q_{loss,bottom} = U_{pv}\cdot(T_{pv,ext} - T_{pv,\text{int}}) \quad (3.28)$$

$$S_{refl} = \rho_{glass}\cdot A\cdot S \quad (3.29)$$

$$P_{el} = \alpha_{pv}\cdot\eta_{pv}\cdot A\cdot\tau_{glass}\cdot S \quad (3.30)$$

$$A\cdot S = Q_{heat} + Q_{loss,top} + Q_{loss,bottom} + P_{el} + S_{refl} \quad (3.31)$$

Again, satisfactory tolerance for achieving desired level of accuracy has been selected to be ± 5%.

Finally, mathematical model of the BIPV/T roof (Configuration 4) depicted in Figure 3.4 is explained by expressions 3.32-3.36.

Glass cover node (3.32)

$$(T_{glass} - T_o)\cdot U_t + (T_{glass} - T_{abs,ext})\cdot U_{rad,conv} - \alpha_{glass} S = 0$$

Exterior absorber node (3.33)

$$(T_{abs,ext} - T_{glass})\cdot U_{rad,conv} + (T_{abs,ext} - T_{abs,\text{int}})\cdot U_{abs} - \tau_{glass}\cdot\alpha_{abs} S = 0$$

Interior absorber node (3.34)

$$(T_{abs,\text{int}} - T_{air})\cdot U_{conv} + (T_{abs,\text{int}} - T_{ins,ext})\cdot U_{rad} + (T_{abs,\text{int}} - T_{abs,ext})\cdot U_{abs} = 0$$

Exterior insulation node (3.35)

$$(T_{ins,ext} - T_{air})\cdot U_{conv} + (T_{ins,ext} - T_{abs,\text{int}})\cdot U_{rad} + (T_{ins,ext} - T_o)\cdot U_b = 0$$

Energy balance of the air (3.36)

$$W\cdot h_c(T_{abs,ext} - T_{air}) + W\cdot h_c(T_{abs,\text{int}} - T_{air}) = mc_p\frac{dT_{air}}{dy}$$

3.6 Convection Heat Transfer

Outdoor CHTC has a major impact on the convective heat losses and should be modeled with care. In this thesis, the total exterior CHTC was calculated as the sum of convective and radiation part:

$$h_o = h_{co} + h_{ro} \quad (3.37)$$

As shown in Chapter 2, none of presented equations included combined effect of wind speed, surface roughness and orientation. The combination of MoWitt and DOE-2 convection models in McClellan and Pedersen (2005) considered above mentioned parameters and was used in this model. The exterior CHTC was calculated as the sum of free and forced convective coefficients. The natural convection was calculated as follows:

$$h_n = 1.81 \frac{\sqrt[3]{T_S - T_O}}{1.382 + \cos \beta_{wall}} \tag{3.38}$$

Where, T_S (°C) is surface temperature, T_o (°C) is ambient temperature and β_{wall} (°) is tilt angle. Finally, exterior CHTC is equal to:

$$h_{c,glass} = \sqrt{h_n^2 + (a \cdot V_{wind}^b)^2} \qquad \text{For glass (PV) surfaces} \tag{3.39}$$

$$h_{co} = h_n + R_f \cdot (h_{c,glass} - h_n) \qquad \text{For rough (wall) surfaces} \tag{3.40}$$

Where, V_{wind} (m/s)is the wind speed at standard conditions, R_f is surface roughness coefficient (1.13 for clear pine) and a,b are MoWitt coefficients:

a=2.38, b=0.89 For a windward side

a=2.86, b=0.617 For a leeward side

In this thesis, all surfaces were assumed to be leeward but south wall and roof. Unless otherwise stated, the wind speed of 3.0 m/s will be used in simulations.

Radiation heat exchange between exterior walls, ground and sky, with respect to the view factors, was combined with convective CHTC to yield total exterior CHTC. Linearized radiative heat transfer coefficient in this case was applied for simplicity:

$$h_{ro} = 4 \cdot \sigma \cdot \varepsilon_s \cdot T_m^3 \tag{3.41}$$

Where ε_s is the emissivity of the exterior surface, taken to be 0.9 for building materials including the PV panels, and T_m (^oC) is the mean temperature of the sky, ground and surface temperature. Sky temperature was calculated (McClellan and Pedersen, 2005):

$$T_{ground} = T_o \tag{3.42}$$

$$T_{sky} = T_o - 6K \tag{3.43}$$

CHTC in the PV cavity is as important parameter as outdoor CHTC and influenced by many factors as described in Chapter 2. Although Liao (2005) found forced convective correlations for the ventilated BIPV/T facades, his findings were not used in this model for several reasons. Firstly, in his model, air flow becomes turbulent at the inlet and stays turbulent due to the abrupt inlet of 90°. In case of the solar house, the inlet of the BIPV/T roof is tilted at 15° and; therefore, the flow may start as laminar flow. Secondly, the correlations were derived for small length of 1m and flow does not become fully developed but stays in developing region. In contrast, the length of the BIPV/T roof is 4.8m and it is very likely possible that the air flow will become fully developed. In this thesis, it was assumed that flow may start as laminar in the inlet section due to smooth entrance and no abrupt change in the direction. Moreover, it was assumed that both temperature and velocity profiles develop simultaneously in the entry region due to absence of an unheated starting length. Incropera and DeWitt (1985) derived correlations for laminar flow in the entrance region for developing and fully developed flow when Re<2300 and following equations were used for forced flow:

$$h_i = \frac{k_{air}}{D_h}\left[1.86 \cdot \left(\frac{\mathrm{Re}\,\mathrm{Pr}\,D_h}{L}\right)^{1/3} \cdot \left(\frac{\mu}{\mu_s}\right)^{0.14}\right] \qquad \text{For developing flow} \tag{3.44}$$

Where, μ_s was calculated for the air mean temperature. The equation is valid when surface temperature T_s is constant, 0.48<Pr<16700 and 0.0044<(μ/μ_s)<9.75. Furthermore, the equation is recommended for the values of $(\frac{\mathrm{Re}\,\mathrm{Pr}\,D_h}{L})^{1/3}\cdot(\frac{\mu}{\mu_s})^{0.14}\geq 2$.

Below this limitation, the fully developed flow occurs.

$$h_i=\frac{7.54\cdot k_{air}}{D_h} \qquad \text{For fully developed flow} \tag{3.45}$$

This equation is valid for two flat plate surfaces and T_s=const. Hydraulic diameter D_h was calculated as twice the separation distance between the plates. Based on Ong's (1995) discussion for finding appropriate equations for his solar air collector model, the following equation was used for transient flow region suggested by Hausen cited by Ong (1995).

$$h_i=\frac{k_{air}}{D_h}\left[0.116\cdot(\mathrm{Re}^{2/3}-125)\cdot\mathrm{Pr}^{1/3}\cdot(1+(\frac{D_h}{L})^{2/3})\cdot(\frac{\mu}{\mu_w})^{0.14}\right] \tag{3.46}$$

The correlation is valid for 2300< Re < 6000.

For turbulent flow region relationship where 6000<Re<10^6, correlation developed by Gnielinski (1983) was used.

$$h_i=\frac{k_{air}}{D_h}\left[\frac{\left(\frac{f}{8}\cdot(\mathrm{Re}-1000)\cdot\mathrm{Pr}\right)}{1+12.7\cdot\sqrt{\frac{f}{8}}\cdot(\mathrm{Pr}^{2/3}-1)}\cdot(1+(\frac{D_h}{L})^{2/3})\right] \tag{3.47}$$

Where the friction factor f is calculated as follows f = $(1.82\log\mathrm{Re}-1.64)^{-0.5}$. The equation is valid for 0<D_h/L<1 and 0.6<Pr<2000.

Above mentioned equations were used for forced flow. The equation for natural convection is presented below (Tang, et al., 2001)

$$h_i = \frac{k_{air}}{D_h}\left[(\frac{h_{pv}}{L}) \cdot Ra \cdot \sin\beta\right]^{0.25} \tag{3.48}$$

3.7 Physical Properties of Air

The BIPV/T roof deals with low temperature ranges and physical properties are assumed to vary linearly with temperature (Ong, 1995).

Specific heat:

$$c_p = 1.0057 + 0.000066 \cdot (T - 27) \tag{3.49}$$

Density:

$$\rho = 1.1774 - 0.00359 \cdot (T - 27) \tag{3.50}$$

Viscosity:

$$\mu = \left[1.983 + 0.00184 \cdot (T - 27)\right] \cdot 10^{-5} \tag{3.51}$$

Thermal conductivity:

$$k = 0.02624 + 0.0000758 \cdot (T - 27) \tag{3.52}$$

Kinematic viscosity:

$$\nu = \frac{\mu}{\rho} \tag{3.53}$$

Thermal diffusivity:

$$\alpha = \frac{k}{\rho \cdot c} \tag{3.54}$$

The coefficient of volumetric thermal expansion (assuming ideal gas)

$$\beta = \frac{1}{T} \tag{3.55}$$

The Prandtl number compares momentum with the thermal diffusivity and links the temperature to the velocity boundary layer.

$$\mathrm{Pr} = \frac{\nu}{\alpha} \tag{3.56}$$

When flow is dominated by natural convection, the Grashof number *(Gr)* replaces Reynolds number.

$$Gr = \frac{\beta \cdot g \cdot L^3 \cdot \Delta T}{\gamma^2} \tag{3.57}$$

Where g is the gravitational acceleration (9.81 m/s^2) and ΔT is the difference between surface temperature and air.

3.8 Heat Removal Factor

Two expressions associated in assessing the efficiency of SAC have been used and can be applied on BIPV/T systems. These are collector efficiency factor (F') and heat removal factor (F_R). F' is the ratio of actual useful energy gain to the gain that would occur if the plate temperature equaled the flow temperature. F_R corresponds to the effectiveness of the heat exchanger and is defined as the ratio of actual heat transfer to the maximum possible heat transfer where absorbing plate is at inlet fluid temperature.

These factors are very useful as they show the influence of known physical parameters on the system efficiency. They can be calculated according to equations provided in (Duffie and Beckman, 1980).

For Configuration 3 (glazed BIPV/T roof), collector efficiency factor (F') and overall heat loss coefficient (U_L) can be calculated in the same way as for the solar air collector depicted in Figure 3.7.

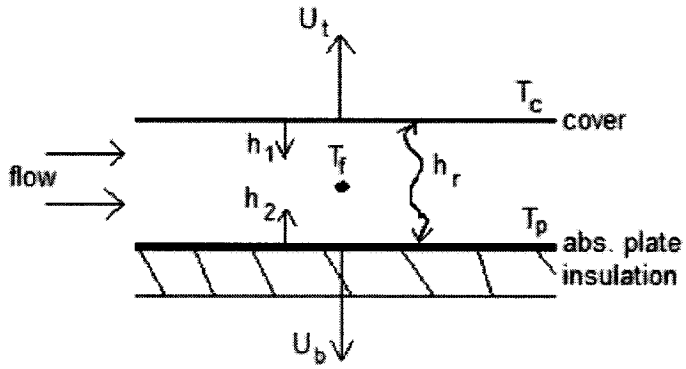

Figure 3.7: Solar air collector (Charron, 2004)

$$U_L = \frac{(U_b + U_t)\cdot(h_1h_2 + h_1h_r + h_2h_r) + U_bU_t(h_1 + h_2)}{h_1h_r + h_2U_t + h_2h_r + h_1h_2} \tag{3.58}$$

$$F' = \frac{h_1h_r + h_2U_t + h_2h_r + h_1h_2}{(U_t + h_r + h_1)(U_b + h_2 + h_r) - h_r^2} \tag{3.59}$$

$$h_r = \frac{\sigma(T_1^2 + T_2^2)(T_1 + T_2)}{\frac{1}{\varepsilon_1} + \frac{1}{\varepsilon_2} - 1} \tag{3.60}$$

For a SAC with low emissivity coating and where the air is passed behind the absorber, F' and U_L were calculated as follows (Duffie and Beckman, 1980):

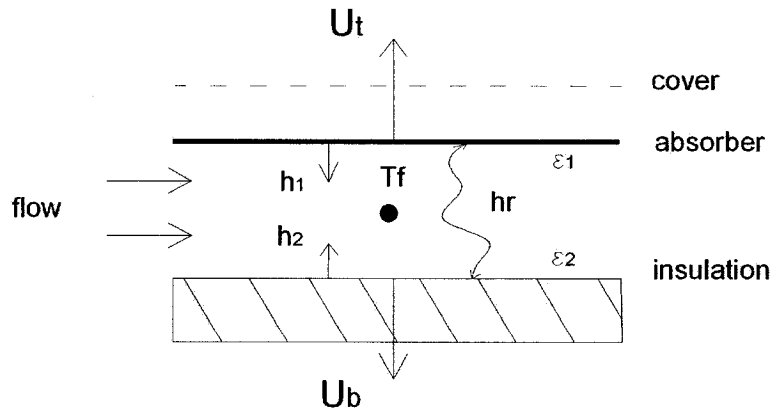

Figure 3.8: Solar air collector with passing air behind absorber

$$U_L = U_b + U_t \tag{3.61}$$

$$F' = \frac{1}{1 + \dfrac{U_L}{h_1 + \dfrac{1}{\dfrac{1}{h_2} + \dfrac{1}{h_r}}}} \tag{3.62}$$

$$h_r = \frac{\sigma(T_1^2 + T_2^2)(T_1 + T_2)}{\dfrac{1}{\varepsilon_1} + \dfrac{1}{\varepsilon_2} - 1} \tag{3.63}$$

Heat removal factor for both cases can be calculated as:

$$F_R = \frac{\dot{m}_{air} \cdot c_p}{A \cdot U_L}\left[1 - e^{-\left(\frac{A\,U_L F_p'}{\dot{m}_{air} c_p}\right)}\right] \tag{3.64}$$

3.9 Air –Water Heat Exchanger

An unmixed counter flow fluid heat exchanger with constant heat effectiveness was modeled. The maximum possible sensible heat transfer was based on a minimum capacity rate of the fluids entering the AWHE. The mathematical model that follows is explained in detail in Incropera and DeWitt (1985).

$$C_c = \dot{m}_c \cdot c_{pc} \tag{3.65}$$

$$C_h = \dot{m}_h \cdot c_{ph} \tag{3.66}$$

$$C_{\min} = C_h, Q_{\max} = C_h \cdot (T_{hi} - T_{ci}) \tag{3.67}$$

$$C_{\min} = C_c, Q_{\max} = C_c \cdot (T_{hi} - T_{ci}) \tag{3.68}$$

Total heat transfer rate across the heat exchanger (Q_T) is calculated as:

$$Q_T = \varepsilon_{HE} \cdot Q_{\max} \tag{3.69}$$

Finally, heat exchanger outlet conditions are calculated as:

$$T_{ho} = T_{hi} - Q_T \tag{3.70}$$

$$T_{co} = T_{ci} + Q_T \tag{3.71}$$

3.10 Water Tank

Mathematical model of the cylindrical horizontal water tank with a heating coil developed by Duffie and Beckman (1980) was used for analysis and briefly described below. It was assumed that there was no heat loss from pipe connections of the AWHE to the water tank and to the surroundings. Thermal non-stratified water tank was assumed. Therefore, thermal energy balance for a 151 liter water tank with RSI 2.5 m^2C/W installed at the solar house can be written as follows:

$$m_w \cdot c_{pw} \cdot \frac{dT_w(t)}{dt} = Q_s(t) - U_L[T_w(t) - Ta(t)] \tag{3.72}$$

Where,

U_L – Overal Heat Loss Coefficient (W/m^2C)

T_a – Ambient Temperature (C)

$Q_s(t)$ – Energy exchanged in the air to water heat exchanger (W)

$Q_L(t)$ – Heat losses from the tank to the ambient (W)

Equation 3.72 can be solved under reasonable assumption that $Q_s(t)$ is constant over the small time step *e.g.* 5 min.

3.11 Thermal Rockbed Storage

In order to model vertical thermal rockbed storage, the following assumptions were made according to data taken from Abbud et al. (1995), Chandra and Willits (1981) and presented in Table 3.1.

Table 3.1: Rockbed design data

Parameter		Value
Rock diameter	(m)	$20 \cdot 10^{-3}$
Rock porosity		0.4
Rock density	(kg/m^3)	1533
Rock conductivity	(W/m^oC)	0.125
Rock specific heat	(J/kg^oC)	880
Change in rockbed temperature	(^oC)	30
Days of required heat storage		1
Rockbed height	(m)	2
U_r value of the rockbed	(W/m^2C)	1.8
Initial temperature of the segments 1-5	(^oC)	20-16°C

The square cross-section rockbed was sized based on the following model (IEA, 2000).

$$C_{storage} = Q_T \cdot n \tag{3.73}$$

$$V_r = \frac{C_{storage}}{c_r \rho_r \Delta T} \tag{3.74}$$

$$A_r = \frac{V_r}{h_r} \tag{3.75}$$

Where, $C_{storage}$ (Wh) is storage capacity, V_r(m^3) is rockbed volume, A_r (m^2) is rockbed face area and n is number of days required for thermal storage. It was assumed that heat recovered from the BIPV/T roof (Q_T) was delivered directly to the top of the thermal rockbed storage. Thermal rockbed storage model was described by equations found in Hughes et al. (1976).

Based on their findings the following assumptions were made in this model:

- Temperature gradients within each rock were neglected
- Uniform flow distribution of air through the rockbed
- Rockbed storage was divided into five isothermal sections to decrease the computation time with satisfactory accuracy *i.e.* 0.2 m was the length of each section
- Infinite NTU model
- No axial conduction

The following partial differential equation that describes air and rock temperatures as a function of distance *(x)*and time *(t)* was solved numerically by explicit finite difference method for each segment with a time step of 5 min.

$$-A_r \rho_r c_r \frac{\partial T_r(t)}{\partial t} = \dot{m} c_p \frac{\partial T_r(x)}{\partial x} + U_r P(T_r - T_{amb}) \tag{3.76}$$

The first expression of the equation 3.76 presents rockbed temperature distribution over time, the second presents rockbed temperature distribution over length and the last one presents heat losses to the ambient.

The rate of energy supplied by the rockbed to the zone *(Q_{supply})* to cover a heating load of the zone, when air enters from the bottom and leaves from the top of the rockbed storage is:

$$Q_{\sup ply} = \dot{m}_{air} \cdot c_{p,air} \cdot (T_{top} - T_{in}) \tag{3.77}$$

Where, T_{top} and T_{in} are temperatures of the top layer and air entering the rockbed (°C), respectively.

3.12 Experimental Setup

Experimental verification of the modeled BIPV/T roof performance was provided by the data collected from various instruments installed at the solar house. The list of instruments and their technical specifications that measure wind speed, wind direction, solar radiation, outdoor temperature and PV panel temperature is presented in Table 3.2. All instruments have a digital output signal that was being recorded by Agilent 34970A Data Acquisition System. The time step for collecting the data was set to be 5 minutes. The VEE Pro Software algorithm was used to display measured results and control the fan controller. The fan was operated at maximum speed of 60Hz from sunrise to sunset as it was controlled to switch on/off when pyranometer sensed incident solar radiation to be higher/lower than 10 W/m^2 at 30^o slope, respectively.

Table 3.2: List of instruments installed on the roof of the solar house

Instrument	Purpose of use	Manufacturer	Model	Accuracy
Pyranometer	Total incident solar radiation	LI-COR	LI-200	± 5%
Wind Monitor	Wind speed and direction	Campbell Scientific Inc.	05103	Speed: ±0.3 m/s Direction: ±3 %
Thermocouple	Temperature	n/a	T-type	±2 %
Data Acquisition System	Collecting Data	Agilent	34970A	n/a

The PV panel temperatures were measured by thermocouples installed in two columns on each PV panel of the unglazed BIPV/T roof and properly shielded to avoid the impact of the solar radiation. The experimental setup is presented in Figure 3.9.

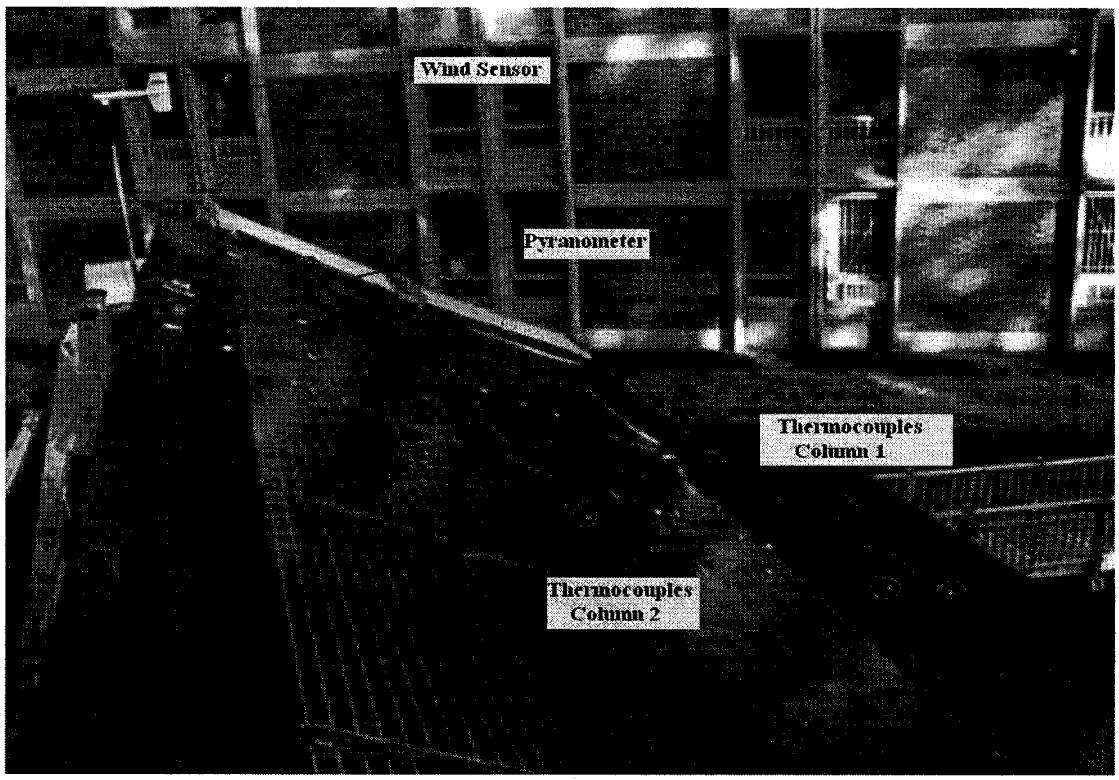

Figure 3.9: Photo of the solar house test facility

In the mechanical room, depicted in Figure 3.10, a custom made three row AWHE with effectiveness of 0.8 was installed. T-type thermocouples were used for temperature measurements and attached at the inlet and outlet of the AWHE, both water and air side. A F-1000 Polardwater electronic flow meter with ±2% accuracy was mounted at the water outlet of the AWHE. The air speed in the 12"(Ø30mm) PV air collecting duct and inlet/outlet ducts was measured at five positions by TSI's Velocity Meter Model 8386A with ±3% accuracy. The average value was taken as an input data into simulations. The PV duct is continued into a rectangular 400x400mm duct at the inlet of the AWHE. The schematic of the duct arrangement is depicted in Figure 3.5.

Moreover, for outdoor and indoor air temperature two T-type thermocouples were mounted at upper deck and in the hallway of the solar house. Collected data from the mechanical room as well as the weather data were used as an input to simulations.

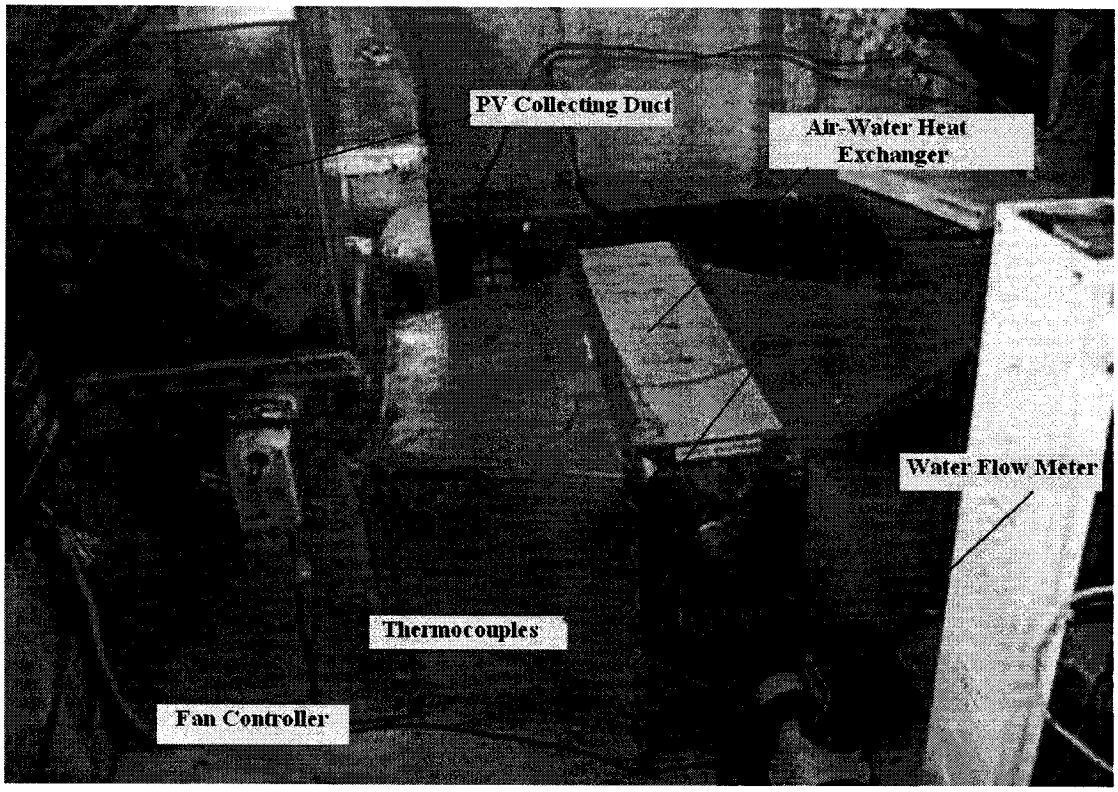

Figure 3.10: Photo of the mechanical room

Finally, thermographic technique is a powerful tool for qualitative assessments of the system and was employed for detecting non-uniformities in the airflow beneath the BIPV/T roof as such surfaces tend to be hotter than the others. The FLIR Thermacam PM595 camera was used for this kind of investigation (Flir Systems, 2006).

CHAPTER 4

RESULTS AND DISCUSSION

4.1 Introduction

This chapter presents simulation results and experimental verification for the developed model in seven sections. The first section presents thermographic analysis of the solar house. The second section compares results between simulated and experimental results of the developed BIPV/T roof in *MathCad 2001i* software. Thermo-electrical performance of the unglazed BIPV/T roof (Configuration 1) under various climate conditions, air velocities in the PV cavity, PV gap depth and different A_{pv}/A_{roof} ratios are shown. Energy performance of Configuration 4 BIPV/T roof is presented. Variation of the heat removal factor with varying air velocity and PV cavity depth is also presented. The next part looks at temperature distribution in the rockbed storage with constant air flow supply and effects of delivering stored heat to the zone on the zone air temperature. Relationship between rockbed volume and unglazed BIPV/T-SAC (Configuration 2) roof area is established. The effect of rock diameter, rock porosity and face velocity on air pressure drop across the rockbed storage is presented. Moreover, comparison between simulation and experimental results between exiting air temperature of the unglazed BIPV/T roof (Configuration 1) and air - water heat exchanger interaction is presented. Additionally, time needed for heating the water in a 40 gallon (151 liter) water tank by recovered heat from Configurations 1 and 3 are shown. Finally, these findings are followed by yearly system performance simulations of Configurations 1 and 2 and air velocity in the PV cavity that limits the temperature of the glazed BIPV/T roof (Configuration 3) below 75°C.

4.2 Thermographic Analysis

A thermographic image of the solar house was taken to detect non-uniformities in the airflow beneath the BIPV/T roof as such surfaces are hotter than the others. The measurements were performed on July 17th, 2006 at 12:42 pm with ambient temperature of 32°C and solar irradiation at 30° slope of 916 W/m^2. It is evident from Figure 4.1 that the first and half of the second column on the right side of the roof can be excluded from the analysis as no heat can be recovered. The airflow beneath that part of the BIPV/T roof is blocked reducing the cooling rate increasing the temperature of the PV panels. Thus, the total PV roof area employed for calculations was 39 m^2. The dimensions of the BIPV/T roof used for investigation are presented in Table 4.1.

Table 4.1: Dimensions of the BIPV/T roof of the solar house used for calculations

Parameter	**Value**	
Slope (°)	15	30
Width (m)	7.1	8.7
Length (m)	1.6	3.2

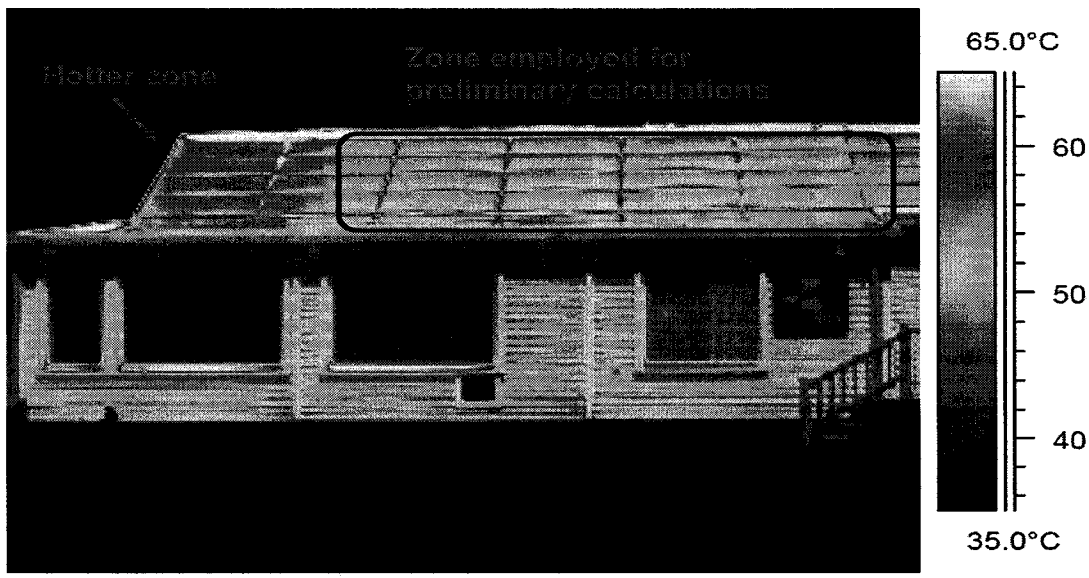

Figure 4.1: Thermographic image of the solar house (Candanedo J., et al., 2006)

4.3 Model Verification

Simulated results of the developed building design tool for a single zone house with unglazed PV panels integrated into roof have been compared with experimental data from the solar house. Measured data such as PV panels and outlet air temperature are used to verify the model. Experimental setup was explained in detail in Chapter 3. The model is verified for both summer and winter conditions. Table 4.2 summarizes the parameters used in the simulations.

Table 4.2: Parameters used in simulations

Parameter	**Value**	
	Summer	Winter
Maximum outdoor temperature (^{o}C)	25	4.5
Average wind speed (m/s)	2.8	2.0
Maximum solar irradiation at 30^{o} slope (W/m^{2})	985	785
Fan control strategy	Operate Sunrise to sunset	
Air speed in the PV cavity with max. fan power (m/s)	0.40	0.55
Heat exchanger bypassed	No	Yes

Figures 4.2 and 4.3 present experimental and simulation results for summer and winter conditions.

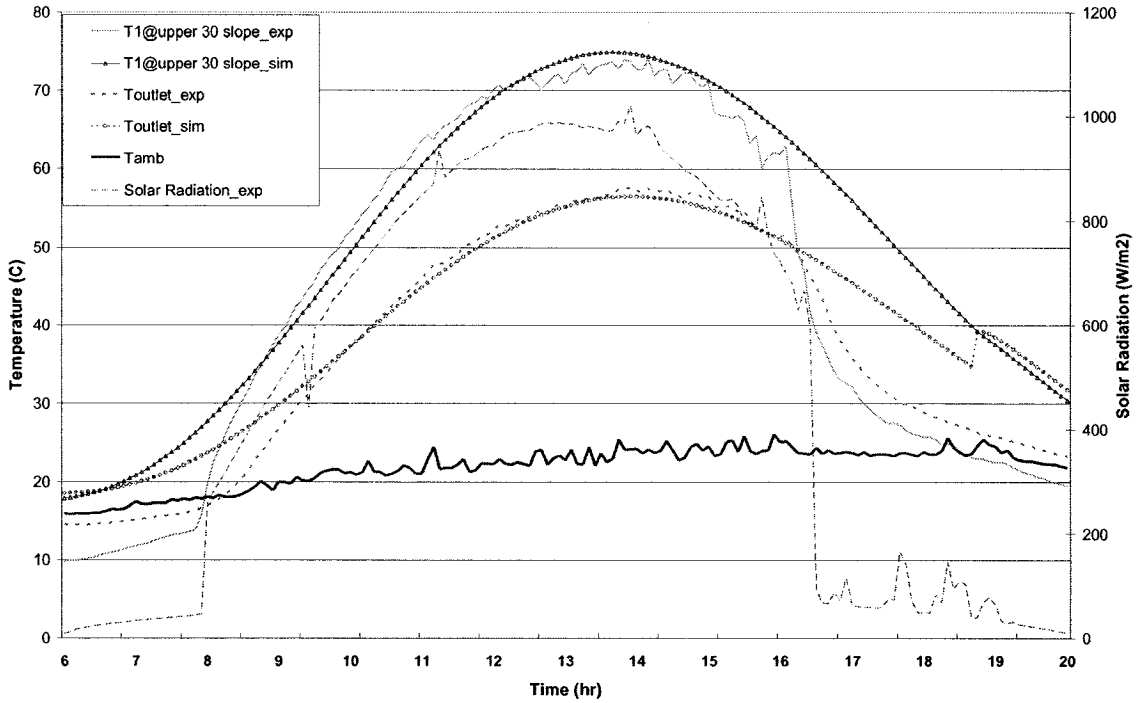

Figure 4.2: Comparison between measured and simulation temperatures of the PV surface and air outlet on 08/05/2006; S_{max} = 985 W/m^2, To_{max}=25°C, V_{wind} =2.8 m/s

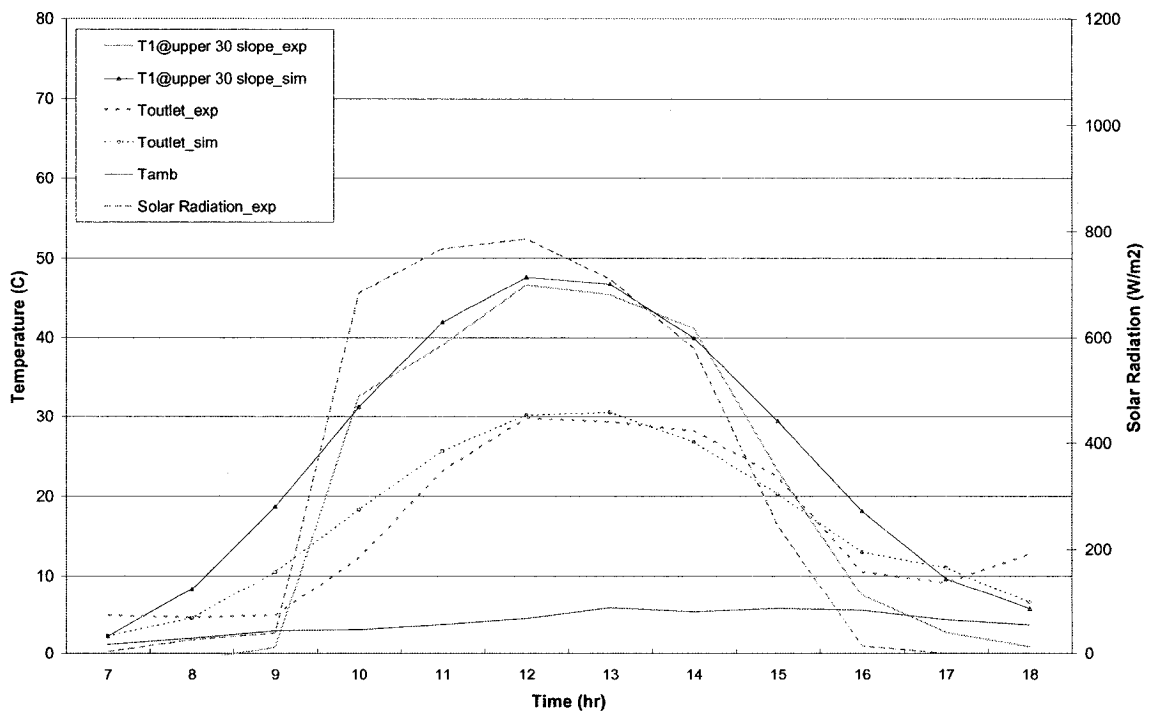

Figure 4.3: Comparison between experimental and simulation temperatures of the PV surface and air outlet on 11/24/2006; S_{max} = 785 W/m^2, To_{max}=4.5°C, V_{wind}=2.0 m/s

From Figures 4.2 and 4.3 it can be seen that simulation and experimental results for a single zone house with unglazed BIPV/T roof are in good agreement. Both PV surface and air outlet temperatures are strongly influenced by intensity of solar irradiation and follow the sun pattern. The thermal inertia of the system generates a time delay between solar radiation and temperatures. The time delay is found to be about one hour and fifteen minutes. While the maximum simulated PV temperature is about 72°C in summer, PV surface heats up to 46°C in winter. Exiting air temperature of the PV cavity is about 56°C in summer and 30°C in winter on clear sunny days. The air temperature rise over 4.8 m unglazed BIPV/T roof is around 25°C to 30°C. A sudden drop in solar irradiation, air outlet and PV panel temperatures shown in Figure 4.2 is explained by the fact that after 16:00 roof has been shaded. Analysis presented later in this thesis will show correlation of the air and PV surface temperatures as a function of length, air speed and ambient conditions. In summer, exiting air of the PV cavity can be utilized in air-water heat exchanger for making DHW. In winter period, exiting air of the PV cavity can be delivered directly to the zone for heating as air temperature between 11:00 and 15:00 is above 22°C. A zone temperature of 22°C is usually selected to be the set point temperature. In other cases, exiting air of the PV cavity can be used as a preheated fresh air in the HVAC system of the house for heating purposes.

4.4 Energy Performance of the Unglazed BIPV/T Roof

For fast and practical design guidelines with solar air heating systems, it is desirable to establish simple correlations among key design parameters and outputs. Important parameters such as air velocity, outdoor temperature, geometrical properties of the PV gap, levels of solar radiation intensity and wind speed have a significant impact on thermo - electrical performance of the unglazed BIPV/T roof. These relationships are presented in the following sections. The correlations between the outputs such as recovered heat, generated electricity and air outlet temperature, as a function of the unglazed BIPV/T roof per total roof area are presented. Unless otherwise stated, all simulations were done for the PV cavity depth of 4 cm.

4.4.1 PV Surface and Air Outlet Temperature

Figures 4.4 and 4.5 show the effect of different air velocities and wind speeds on the PV surface and air outlet temperature. It can be seen that with higher air and wind speeds in the PV cavity, both PV surface and air outlet temperature are decreasing. The cooling effect on the PV panels is stronger for higher wind speeds as they lead to higher convection heat losses. For the same air speed in the PV cavity and with wind speed increase from 2 m/s to 3 m/s, temperature decrease of the PV surface is about 5°C. Temperature of the air in the PV cavity is less affected by the wind and temperature decrease is around 3°C. Moreover, by increasing the ventilating air speed from 0.5 m/s to 1.5 m/s, both PV panel and exiting air temperature are reduced by about 8°C.

Lower PV surface temperatures result in higher electrical efficiencies and prolong operating life expectancy of the PV panel. High air speeds result in higher pressure drops, noise problems and increased fan energy consumption. Other than being able to accurately predict the PV surface temperature, other important concerns must be taken into account. The air speed in the cavity should be carefully selected. As previously mentioned, high air speeds in the PV cavity lead to higher efficiencies but ventilating air might be preheated at temperature below the room set point temperature. Thus, auxiliary heater might be needed to warm the fresh air to the desired temperature.

Table 4.3. summarizes results obtained from Configuration 4 on a clear sunny day in February with average outdoor temperature of -9.5 °C and air gap depth of 2 cm.. The maximum air temperature at the outlet of the SAC cavity is found to be 41 °C. For the same outdoor conditions, Configuration 4 has higher exiting air temperature for about 50% as opposed to that of Configuration 2. This is due to fact that air is passed behind the absorber reducing the heat losses. Moreover, the air gap between the absorber and glazing behaves as insulation. The energy performance of Configuration 2 is presented in the forthcoming sections. The energy performance of Configuration 4 can be significantly increased by adding a low emissivity coating on inner side of glazing cover. As can be seen from Table 4.3, radiation heat transfer coefficient is reduced by 87% resulting in increased exiting air temperature of 56 °C. The heat removal factor is found to be 85%.

Table 4.3. Energy performance of Configuration 4, S_{max}=815W/m^2,V_{wind}=2.2 m/s, V_{air}=1.0 m/s

Parameter		**Value**	
Low emissivity coating		Yes	No
Radiation heat transfer coefficient	(W/m^2 °C)	0.6	4.6
Max. air outlet temperature	(°C)	56.0	41.0
Heat removal factor-FR	(/)	0.85	0.81

Air temperature and air speed in the PV gap can have a significant impact on heating and cooling loads. Every degree in temperature increase can reduce the heating load of the house by making its envelope warmer. In summer, higher air speeds in the PV cavity cool the envelope and decrease the cooling load (Yang, et al., 2001). However, the trade-off is in increased fan energy consumption.

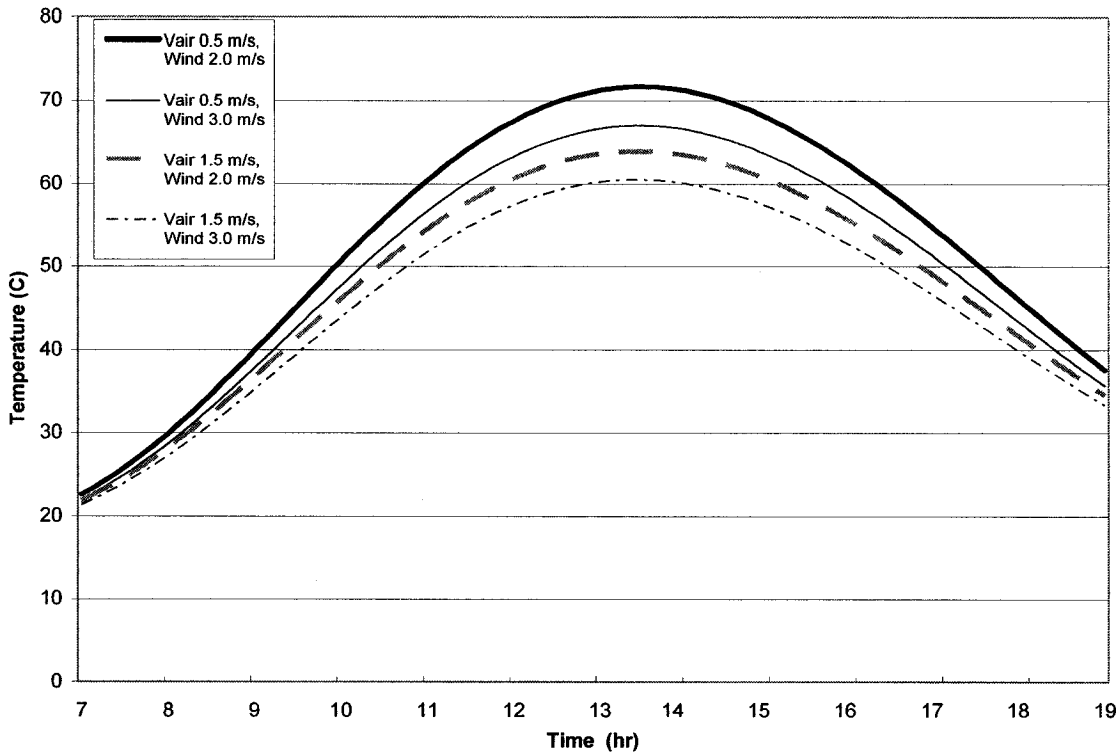

Figure 4.4: Simulated PV surface temperatures for different air flow velocities and wind speeds; S_{max}=915W/m^2, To_{max}=25°C

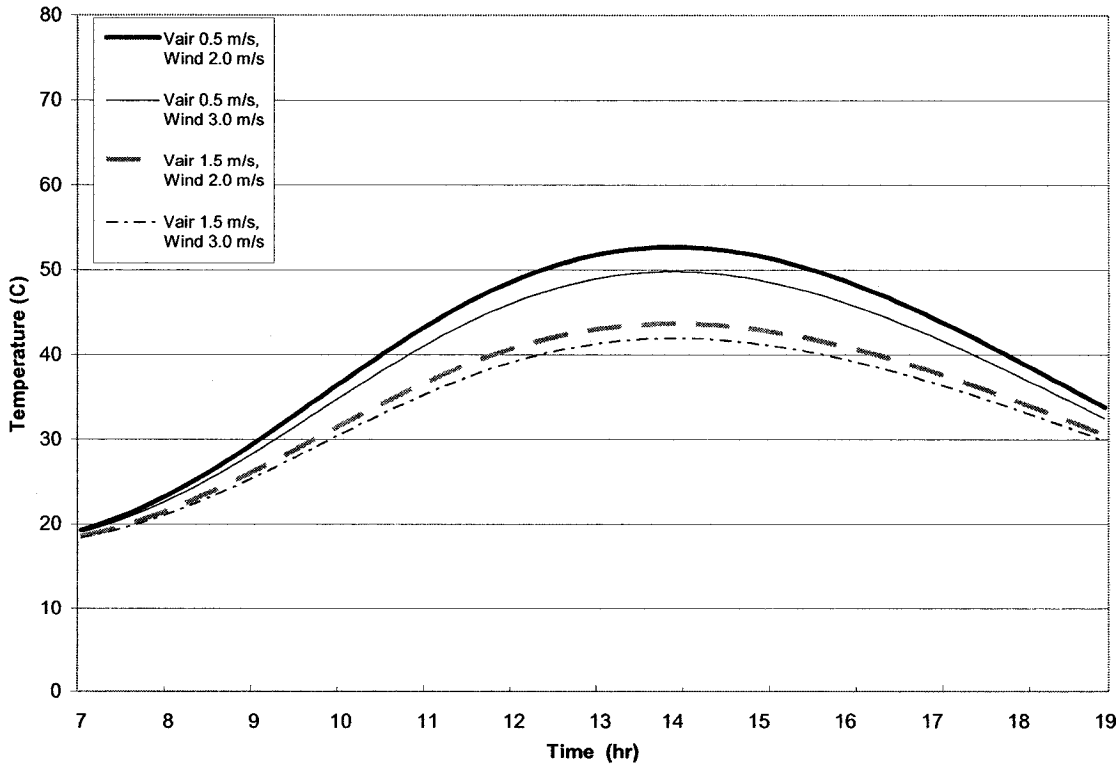

Figure 4.5: Simulated outlet air temperatures for different air flow velocities and wind speeds; S_{max}=915 W/m^2, To_{max}=25°C

4.4.2 Air Temperature vs. Channel Depth

Figure 4.6 shows the effect of PV gap depth on the air temperature at the outlet of the PV cavity. The level of air temperature change is strongly influenced by channel depth. As the PV cavity depth decreases, higher air outlet temperatures are observed. The difference in outlet air temperatures between 0.05m and 0.2m can be up to 35%. Decrease in outlet air temperature is about 10°C when the gap thickness increases from 0.05m to 0.1m as more air is passed through the PV cavity.

Figure 4.7 depicts the effect of the PV gap depth and air speed in the PV cavity on the maximum air temperature at the outlet of the PV cavity. The air outlet temperature decreases in exponential fashion with increasing PV gap depth. With varying the PV gap from 0.05m to 0.2m, the maximum air outlet temperature decreases for about 17°C. These results can be used for developing fan control strategies to achieve desired air temperature at the outlet of the PV cavity.

Figure 4.8 shows how heat removal factor (F_R) depends on air velocity in the PV cavity and PV cavity depth in the case of the BIPV/T roof of the Configuration 3. As the air flow speed increases in the PV cavity, the F_R is also increased. This is explained by the fact that higher air velocities lead to lower air temperature rise through the PV cavity. Consequently, the average PV surface temperature is decreased leading to lower heat losses and increase in the useful energy gain and F_R. The same result is obtained with the increase of the PV cavity depth as more air is transported to remove heat.

Besides selecting appropriate gap height based on desired air temperature to be achieved, other considerations must be taken into account. If the cavity is too small, air pressure drops can be increased and fan energy consumption is increased. Moreover, the problems with noise and maintenance might arise. Finally, gap widths that are very small could be often difficult to clean.

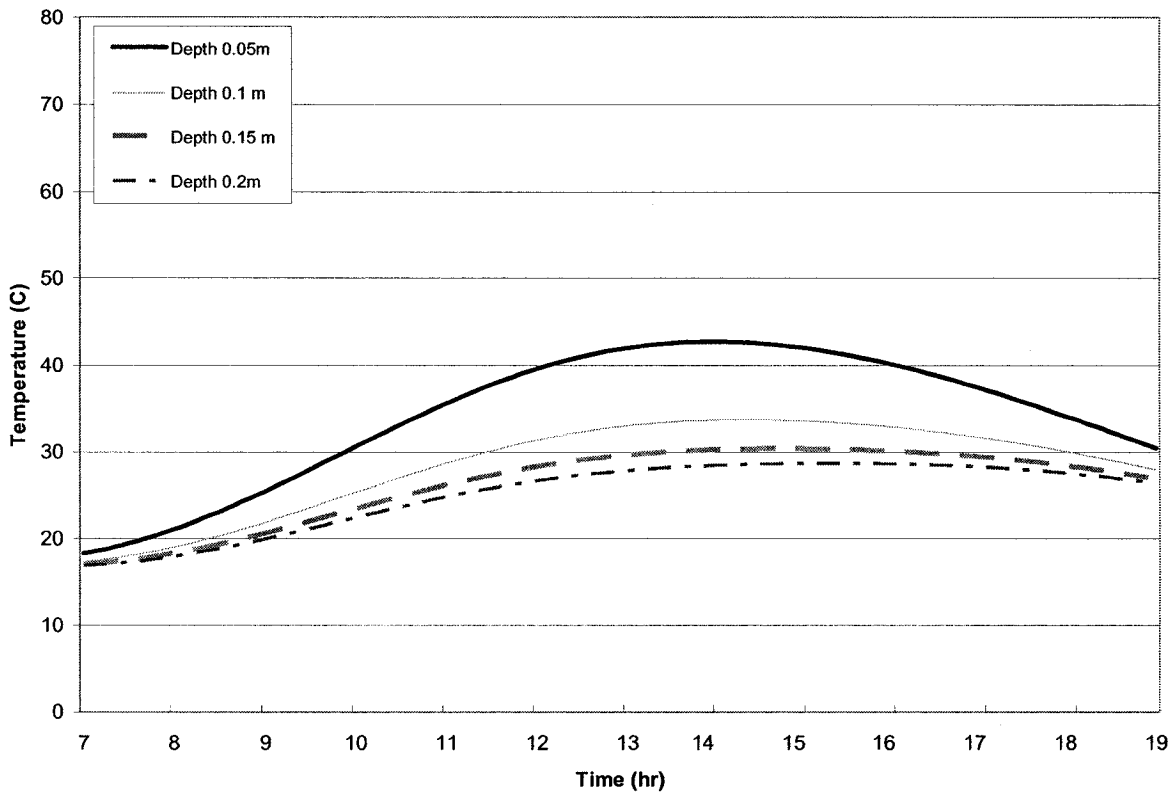

Figure 4.6: Simulated air outlet temperature vs. PV channel depth; S_{max}=915 W/m^2, V_{wind}=3.0 m/s, To_{max}=25°C, V_{air}=1.0m/s

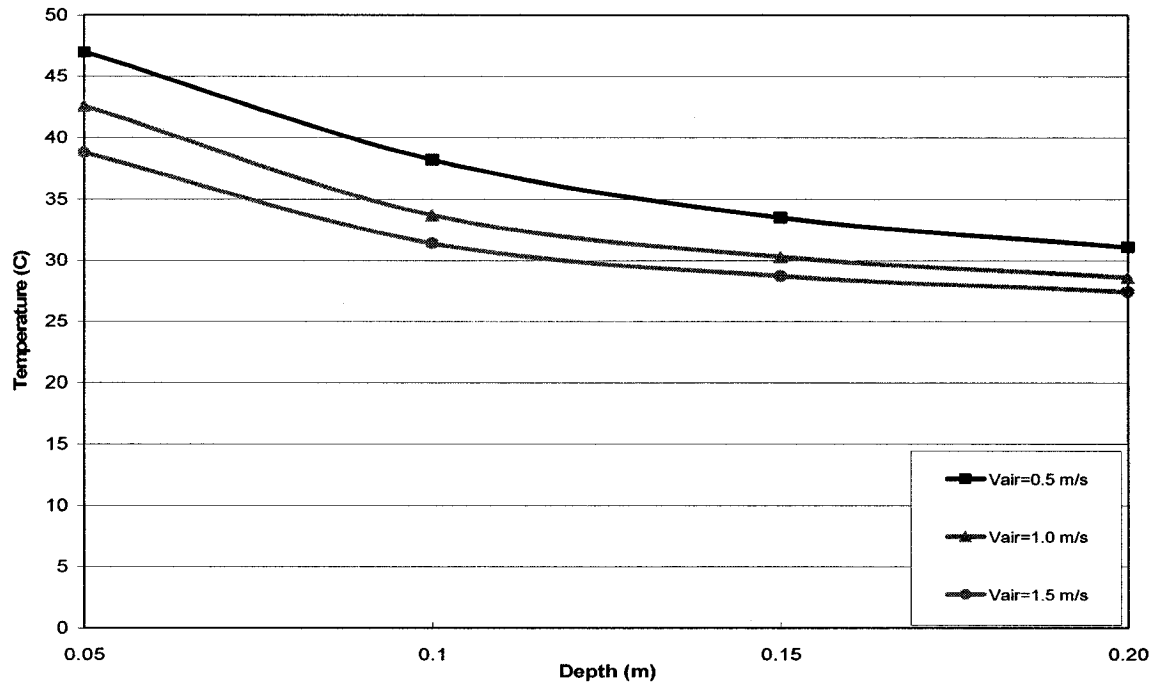

Figure 4.7: Simulated air outlet temperature vs. PV channel depth; S_{max}=915 W/m^2, V_{wind}=3.0m/s,To_{max}=25°C

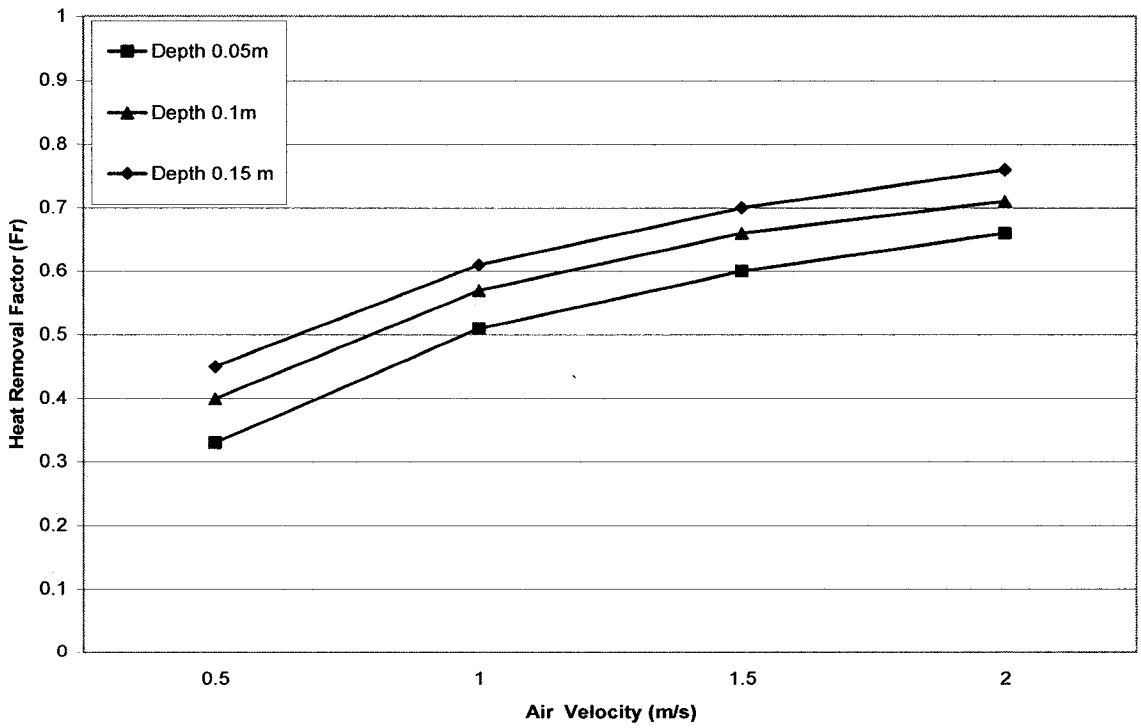

Figure 4.8: Simulated heat removal factor as a function of air speed in the PV cavity and PV cavity depth

4.4.3 *Air Outlet Temperature vs. Solar Radiation and Air Speeds in the PV cavity*

Figure 4.9 shows air outlet temperatures with various solar radiation levels and air flows. The air outlet temperature increases with higher levels of solar radiation as more solar energy is available to be converted into heat. As mentioned previously, it decreases with increasing air speeds. With air speeds from 0.5m/s to 2 m/s, air outlet temperature difference between those on sunny and cloudy days fluctuates from 15°C to 25°C. Air outlet temperature is lower with low outdoor temperatures than those obtained with higher ambient temperatures. These results can be used for developing fan control strategies to achieve desired air temperature at the outlet of the PV cavity.

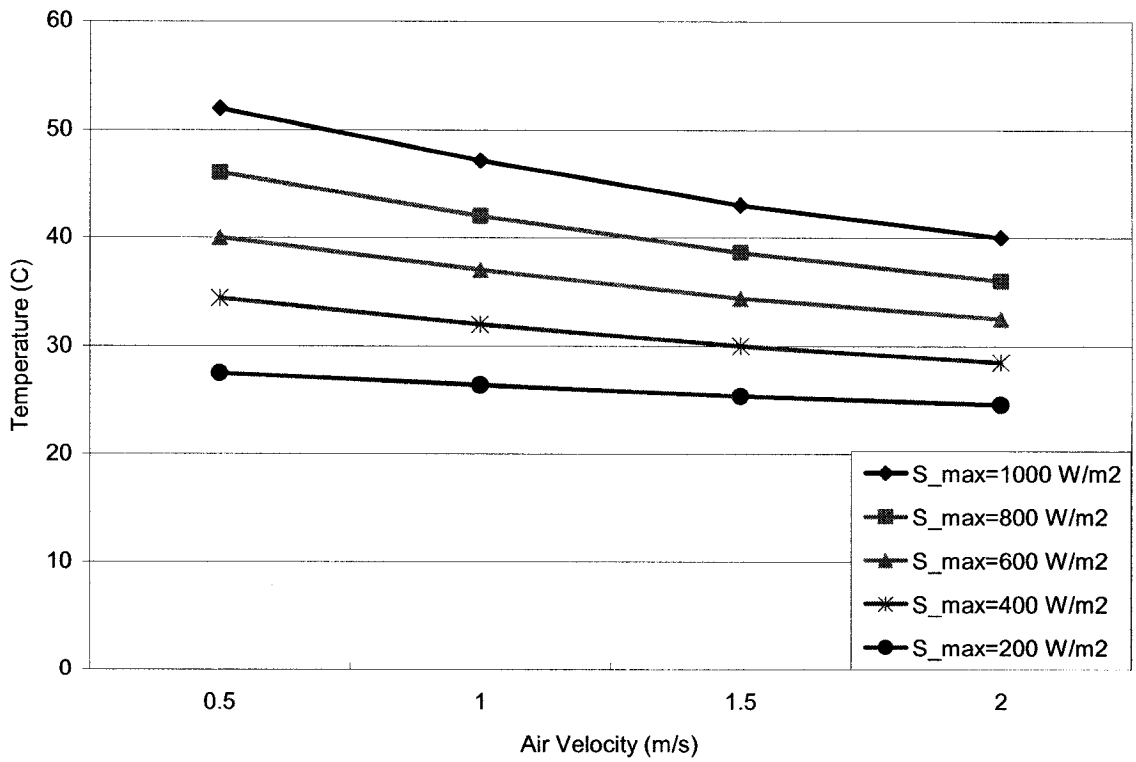

Figure 4.9: Simulated air outlet temperature increase vs. solar radiation and varying air speeds; V_{wind}=3.0 m/s, To_{max}=25°C

4.4.4 *Air Temperature Rise (To-Tin) vs. Solar Radiation, Air velocities and Outdoor Temperature*

Figure 4.10 presents air temperature of the flowing air as a function of incident solar radiation for different outdoor conditions and flow rates. Air temperature increases linearly with higher levels of solar irradiation. At both low and high irradiation levels, slightly higher temperature increase is achieved with lower outdoor temperatures. This is expected as higher temperature difference between ventilating air and surrounding walls of the PV channel is achieved resulting in higher heat exchange. Air temperature increase for air speed in the PV cavity is higher at 1.0 m/s than at 2.0 m/s due to higher air outlet temperatures. While air temperature rises at slope of 0.027 °C / W/m^2 for 1.0 m/s, for 2.0 m/s temperature increases at lower slope of 0.018 °C / W/m^2.

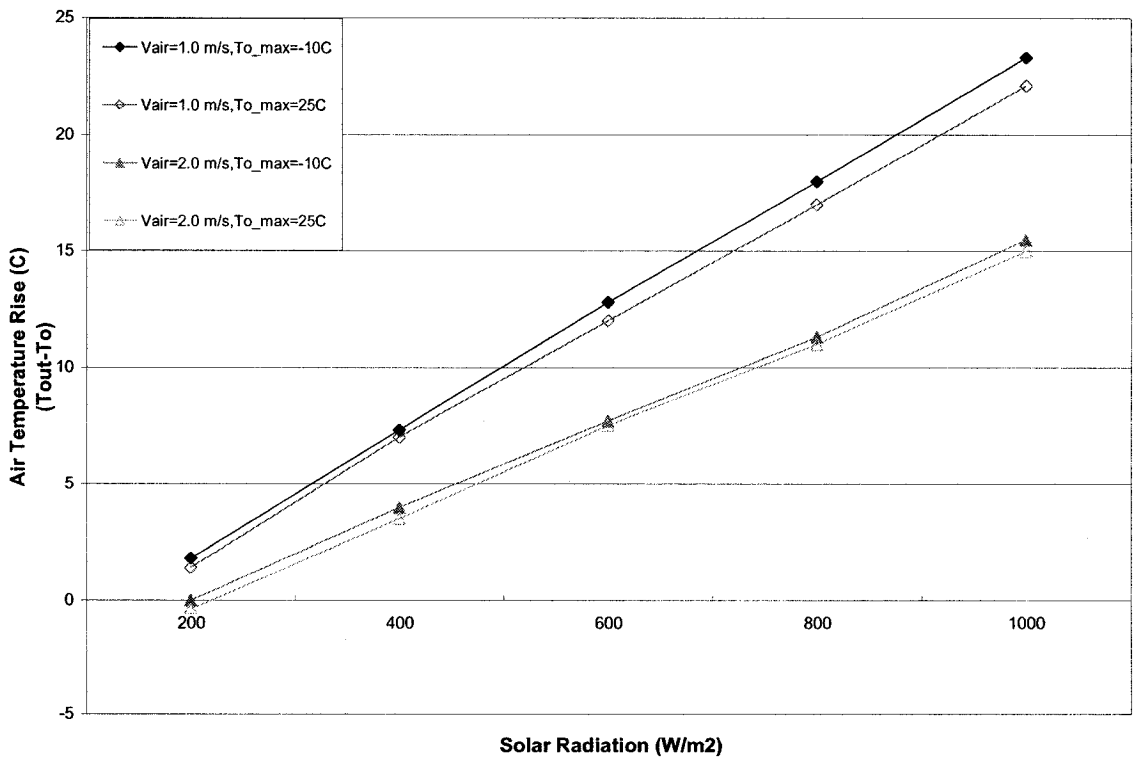

Figure 4.10: Simulated air temperature rise (To-Tin) vs solar Radiation, air speed and outdoor temperatures; V_{wind}=3.0 m/s

4.4.5 PV Temperature, Thermal and Electrical Efficiency vs. Varying Air Velocities and Outdoor Temperature

Figure 4.11 shows results with constant irradiation but varying velocity in the PV cavity and outdoor temperature. The PV surface temperature drops with increasing velocity. The temperature drops from 10°C to 15°C when velocity increases from 0.5m/s to 2.0 m/s, respectively. The higher temperature drop is observed for lower outdoor temperatures. For the same increase in air velocity, the PV cell efficiency increases by 3.3%. Again higher PV efficiencies are achieved with lower outdoor temperatures for 2% than those with higher outdoor temperature. Thermal efficiency significantly increases with increasing air speed in the cavity. Thermal efficiency up to 35% with ambient temperature of -10°C and up to 27% for ambient temperature of 25°C can be achieved. Air exiting temperatures of the PV cavity are decreasing in a linear manner for about 12°C with increasing air speed from 0.5 m/s to 2.0 m/s for both outdoor temperature scenarios. Although, outlet air temperature decreases with increasing velocity, thermal and electrical efficiency increase due to reduction of the heat losses to the outside.

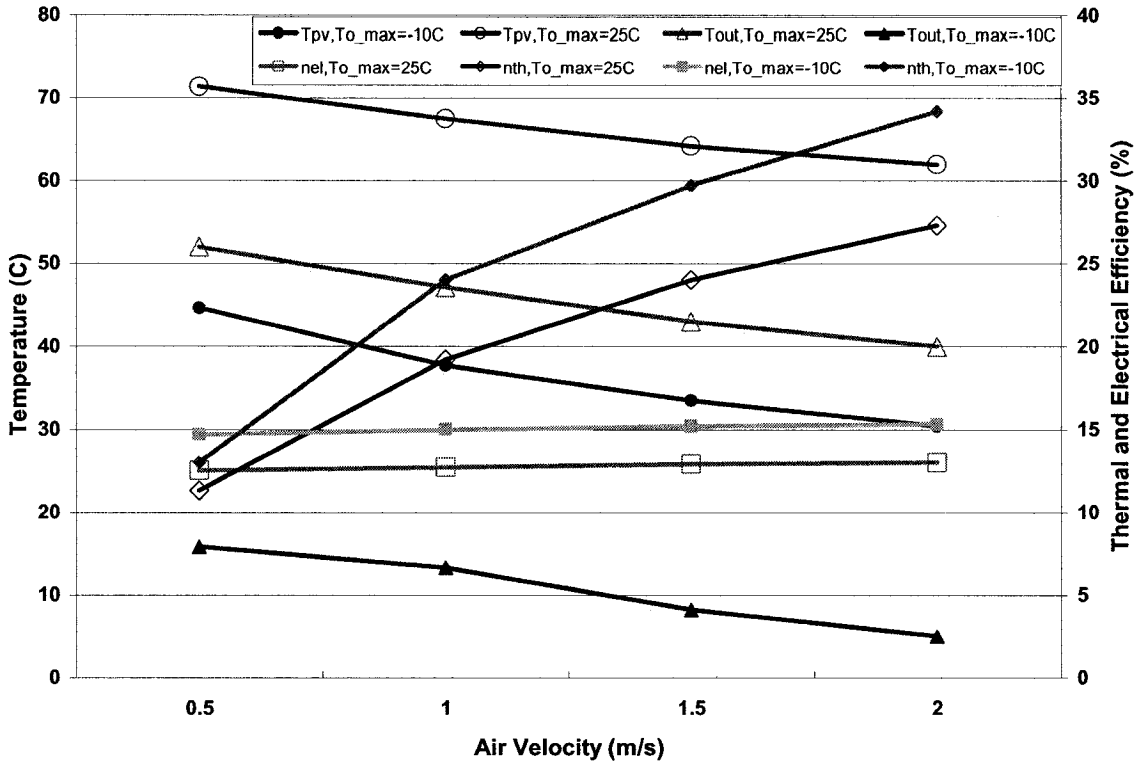

Figure 4.11: Simulated results as a function of varying air flow velocities and outdoor temperature; S_{max}=1000 W/m^2, V_{wind}= 3.0 m/s (n_{el}- electrical efficiency, n_{th}- thermal efficiency)

4.4.6 PV and Air Outlet Temperature, Thermal and Electrical Efficiency vs Varying Wind Speed

The PV surface and air outlet temperatures, thermo-electrical efficiencies of the BIPV/T roof as a function of wind speed are depicted in Figure 4.12. Charron (2004) concluded that CHTC found in literature were assumed to be constant for various wind speeds introducing an error in simulations. With increasing wind speed, the outdoor CHTC and top heat losses are increased; thus, PV surface and air outlet temperature are decreased.

With varying wind speed from 1m/s to 7m/s over 4.8 m long roof, the PV panel temperature drops for about 25°C and outlet air temperature drops for 15°C. For the same wind speed range, electrical efficiency increases from 12% to 13% and thermal efficiency decreases from 14% to 8%.

As can be seen, the wind speed has a strong impact on energy performance of the BIPV/T system and should be properly taken into consideration for analysis. The wind behaviour at the ground level is modeled as a turbulent boundary layer. Its properties are greatly influenced by terrain topography, roughness of the surfaces and height above the ground. The use of average daily wind speed obtained from a meteorological stations located at the airports can introduce a serious error in the energy analysis of the BIPV/T system. This is explained by the fact that wind anemometers are placed at the standard height of 10m above the ground at locations that provide an unobstructed wind approach over the ground of similar roughness. In contrast, in urban areas, heights and arrangements of the buildings create a topography that is significantly different than that around the airports.

Therefore, necessary corrections should be made to properly predict the wind velocity with respect to various surface roughness and height above the ground. The following power law correlation with appropriate exponents was found reasonable to predict the wind speed with acceptable accuracy (Hutcheon and Handegord, 1995):

$$\frac{V_Z}{V_g} = \left[\frac{Z}{Z_g}\right]^{\gamma} \tag{4.1}$$

Where, V_g is the mean gradient wind speed that corresponds to the free stream velocity at the edge of the boundary layer (m/s), Z_g is the gradient height above the ground at which ground roughness has no longer effect (m/s) V_z is wind speed (m/s) at any height *Z(m)* above the ground and γ is the mean speed exponent that varies from 0.1 for smooth surfaces to 0.4 for city centers.

For example, if the recorded average wind speed at Pierre Elliot Trudeau Airport in Montreal, Canada is 4 m/s and used for calculations, deceiving results for the BIPV/T system energy performance are obtained. Equation 4.1 should be employed for taking into account the wind effect properly. Additionally, selecting appropriate values for Z_g, γ for a sub-urban area and height of *e.g.* 5 m, a mean wind speed of 2.2 m/s should be used for BIPV/T roof energy analysis.

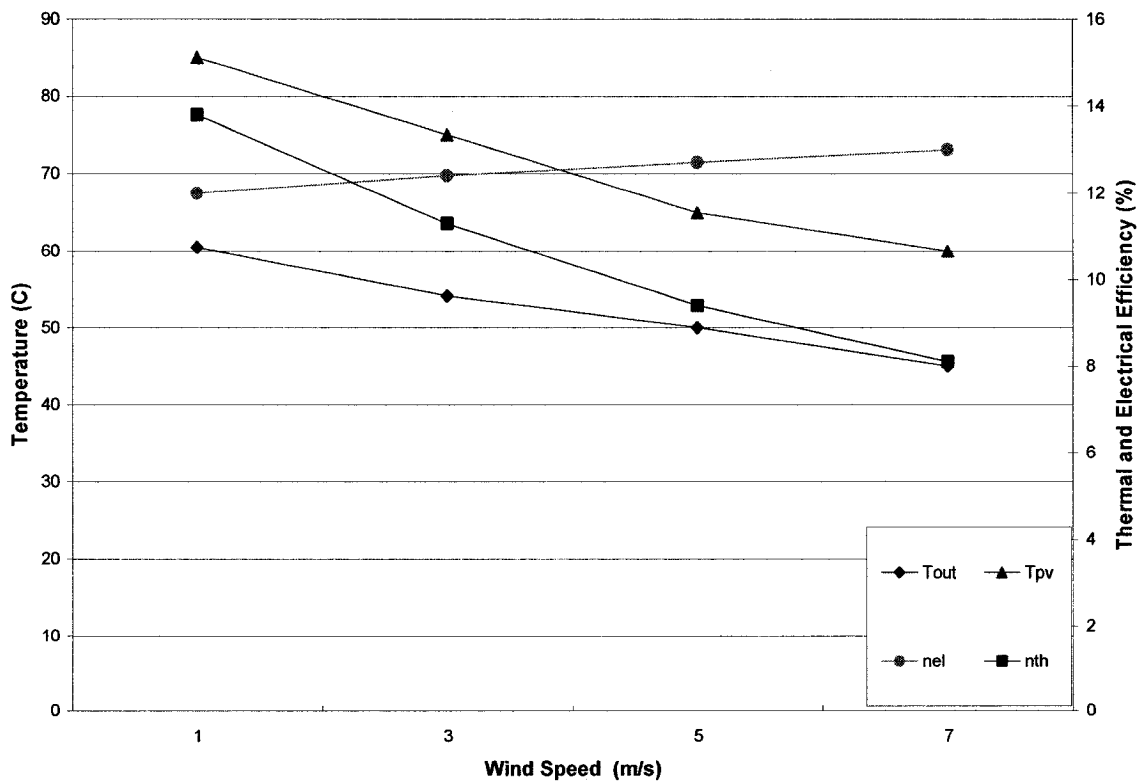

Figure 4.12: Simulated results with varying wind speed; S_{max}=1000 W/m^2, V_{air}=0.5 m/s, To_{max}=25°C

4.4.7 *PV and Air Outlet Temperature, Thermal and Electrical Efficiency vs Varying Outdoor Temperatures*

Figure 4.13 shows thermo-electrical performance of the BIPV/T roof with varying outdoor temperature used as an inlet to the BIPV/T system. Air temperature difference rise between outlet and inlet is almost constant at value of 25°C. PV surface temperature increase from 30°C to 70°C and air exiting temperature from 15°C to 50°C when maximum outdoor temperature varies from -10°C to 25°C, respectively. For the same range of outdoor temperatures, electrical efficiency drops from 15% to 12.5% and thermal efficiency drops from 14% to 11.7%.

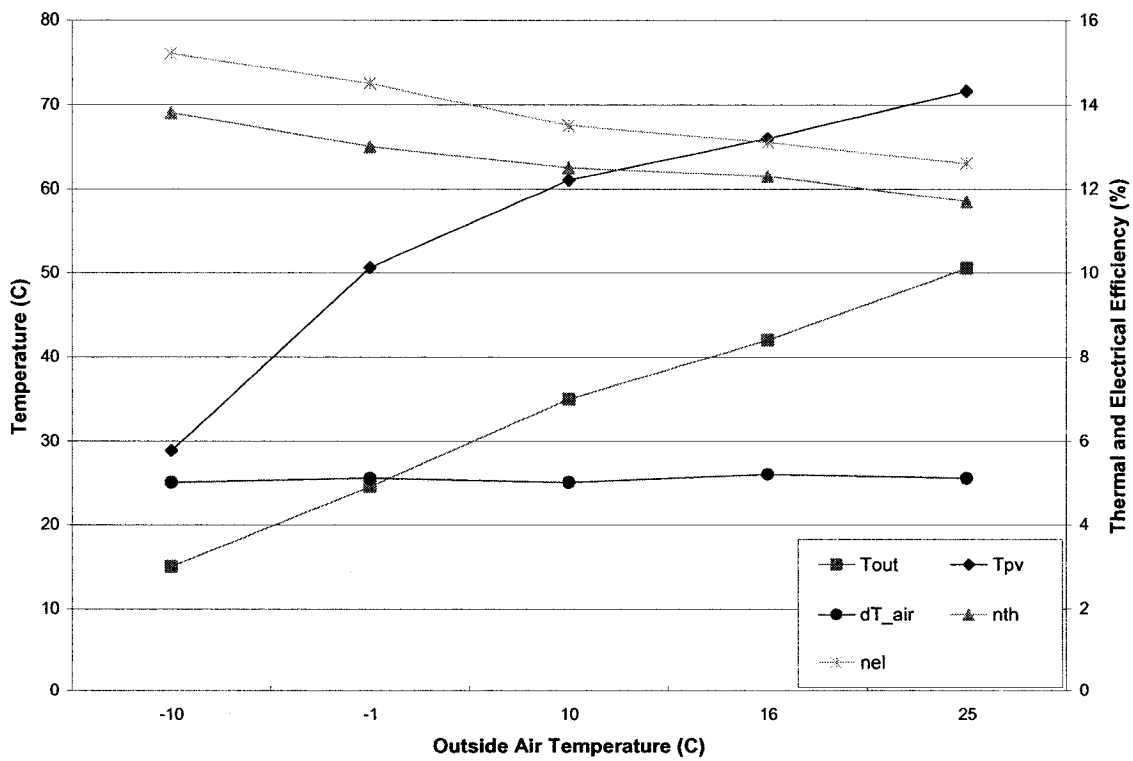

Figure 4.13: Results with varying outdoor temperature, S_{max}=1000 W/m^2, V_{air}=0.5 m/s, V_{wind}=3.0 m/s

4.4.8 *Collected Heat, Generated Electricity and Air Outlet Temperature as a Function of BIPV/T System to Total Roof Surface Ratio(A_{pv}/A_{roof})*

Results of recovered heat, generated electricity per day and maximum air outlet temperature for varying length (L_{pv}) and width (W_{pv}) of the PV roof and varying air speed for summer and winter scenario, are shown. The total roof area was kept constant.

Figures 4.14 and 4.15 present relationships between the unglazed BIPV/T system outputs and A_{pv}/A_{roof} ratio for summer with varying the air speed in the PV gap. In the case of varying A_{pv}, keeping constant L_{pv} but varying the W_{pv} of the BIPV/T roof, it was found that air outlet temperature remains constant and it is independent of W_{pv}. Air exit temperatures decrease by 4°C per 0.5 m /s air speed increase in the PV cavity. Collected heat and generated electricity rise in a linear fashion with increasing A_{pv}/A_{roof} ratio and are greater for higher values of air speed in the PV cavity. While collected heat with air speed in the cavity of 0.5 m/s is 0.65 kWh/ A_{pv}/A_{roof} , the recovered heat with air velocity in the cavity of 1.0 m/s is 1 kWh/ A_{pv}/A_{roof}. The generated electricity increases by 0.6 kWh/ A_{pv}/A_{roof} and it is slightly higher for the case with higher air speeds. In contrast, different results for air outlet temperature are obtained for changing the A_{pv}/A_{roof} ratio by varying the L_{pv} and keeping W_{pv} constant. Air outlet temperature rises reaching a maximum value of 10°C higher than that of constant L_{pv}. As expected, the amount of generated electricity is dependent on the total area of the PV panels and is the same for both contrasted cases with varying BIPV/T system geometry. The recovered heat by the BIPV/T system is less steep than those with constant length. While collected heat with an air speed in the cavity of 0.5 m/s is 0.4 kWh/ %, the recovered heat with air speed in the cavity of 1.0 m/s is 0.8 kWh/ A_{pv}/A_{roof}.

For a given increase in the A_{pv}/A_{roof} ratio, more heat is extracted for the case with increased W_{pv} than that for increased $L_{pv.}$ With an A_{pv}/A_{roof} ratio greater than 50%, collected heat with increasing W_{pv} is higher than that with constant W_{pv} as more air is transported in the PV cavity to remove the heat.

Figures 4.16-4.17 present similar results but for the winter scenario. The obtained values follow the same pattern but are lower than those for the summer scenario due to increased heat losses to the ambient and less available incident solar radiation. In the case with constant L_{pv} and an air speed of 0.5 m/s, it was found that 0.45 kWh of heat is collected per $A_{pv}/A_{roof.}$ For the case with an air speed of 1.0 m/s, it was found that 0.8 kWh of heat is collected per $A_{pv}/A_{roof.}$ With an air speed of 0.5 m/s, generated electricity increases at rate of 0.4 kWh/ A_{pv}/A_{roof} and is slightly higher than with an air speed of 1.0 m/s. Exiting air temperature of the PV cavity is constant regardless of A_{pv}/A_{roof} ratio with values 0f 4.5°C and 3°C for air speeds of 0.5 m/s and 1.0 m/s, respectively. In contrast, when varying $L_{pv,}$ the air outlet temperature can reach around 15°C and 10°C with air speeds of 0.5 m/s and 1.0 m/s. The amount of heat recovered increases at rate of 0.2 kWh/ A_{pv}/A_{roof} and 0.5 kWh/ A_{pv}/A_{roof} with air speeds of 0.5 m/s to 1.0 m/s, respectively. For all considered scenarios with A_{pv}/A_{roof} ratios higher than 25% system outputs are significantly increase linearly.

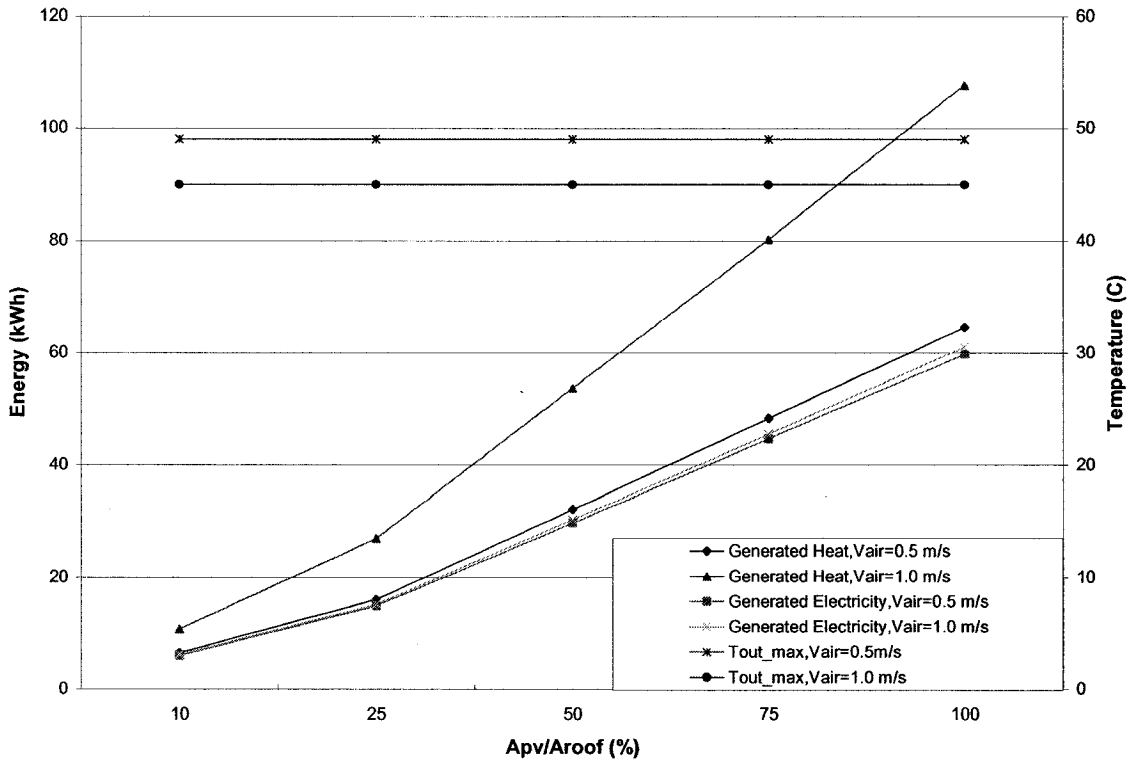

Figure 4.14: Simulated results with Lpv = const, Wpv≠const., Vair≠const, S_{max}=933W/m^2, To_{max}=21°C, V_{wind}= 3.0 m/s.

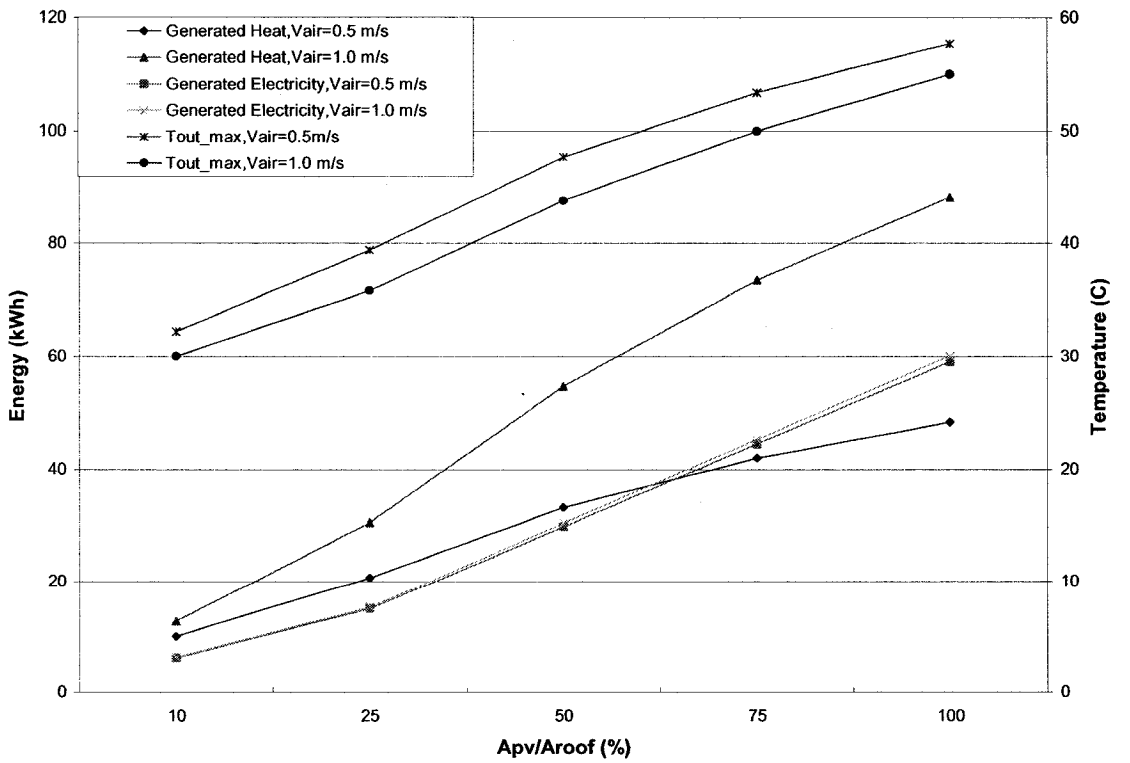

Figure 4.15: Simulated results with Lpv≠const, Wpv = const., Vair≠const., S_{max}=933 W/m^2, To_{max}=21°C, V_{wind} =3.0 m/s.

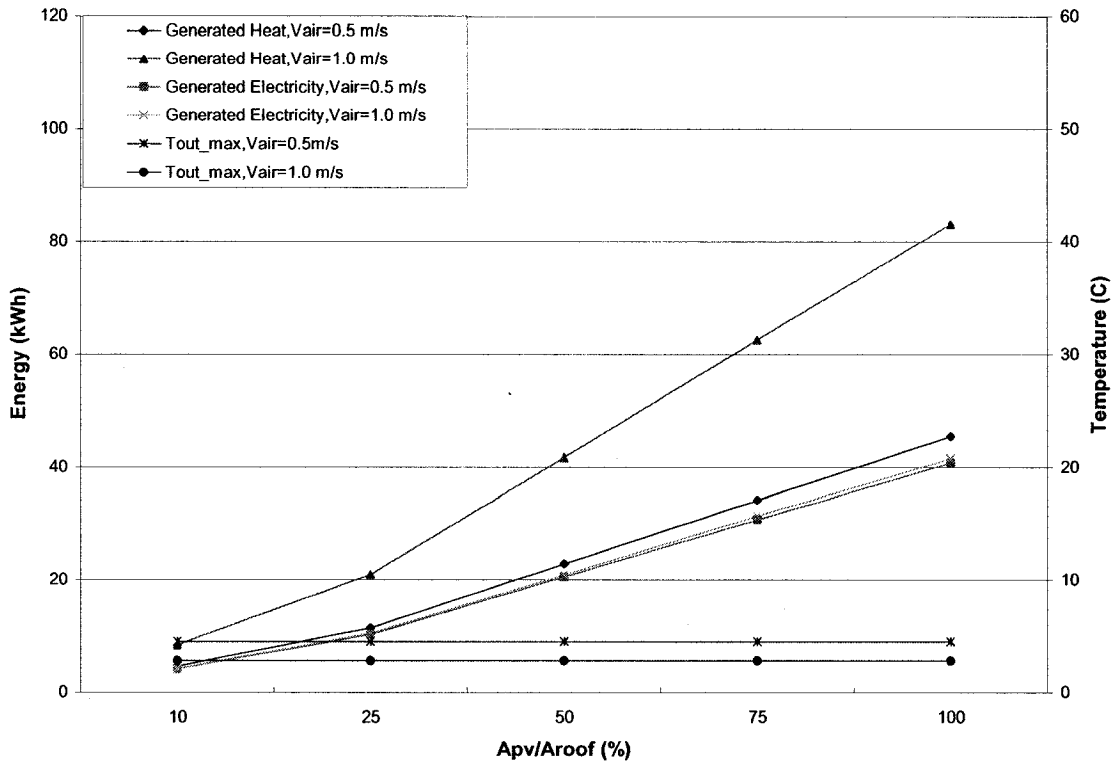

Figure 4.16: Simulated results with Lpv=const., Wpv≠const., Vair≠const., S_{max}=716W/m^2, To_{max}=-15°C, V_{wind} =3.0 m/s.

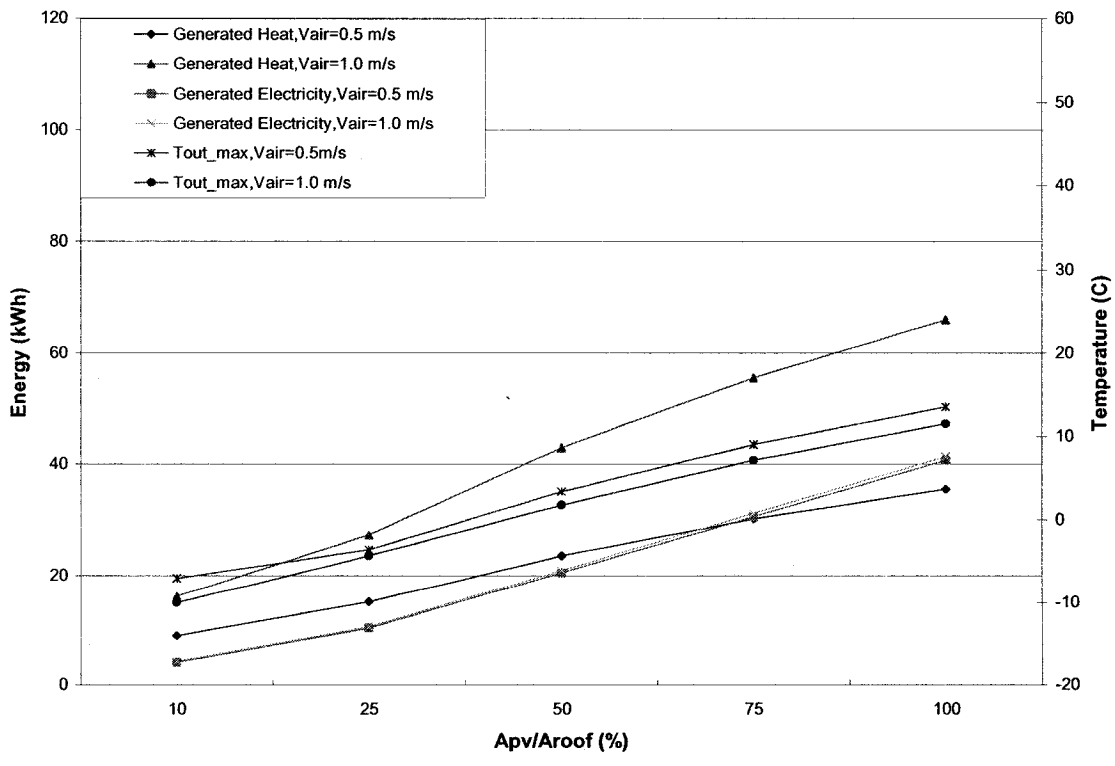

Figure 4.17: Results with Lpv≠const., Wpv=const., Vair≠const., S_{max}=716W/m^2, To_{max}=-15°C, V_{wind}= 3.0 m/s.

4.4.9 BIPV/T Roof Outputs as a Function of Length

Theoretical predictions of the unglazed BIPV/T roof performance with identical outdoor conditions and varying air speed in the PV cavity are presented by Figures 4.18. The results are obtained for steady state conditions and solar noon from equations 3.10 to 3.15 and present averaged values over the length and may be a source of discrepancy as opposed to a transient model. From results can be seen that effects of section size on temperature behaviour are significant. The temperature rise is asymptotic over the BIPV/T roof. Temperature rise is higher for air than that for the PV surface. The longer the PV roof is, the lower air temperature increase per 1m length is as less heat is transferred to ventilating air. In case of constant air flow of 1.0 m/s, temperature rise starts at about 6.5°C /m and ends at 3°C/m. This is expected as temperature difference is lower between the flowing air and surrounding surfaces, and thus a heat transfer is decreasing from the bottom to the top part of the BIPV/T roof. Both air and PV surface temperatures increase with length. Thermal efficiency is decreasing due to increased heat losses to ambient as the PV panel surface temperatures are also increased. Electrical efficiency is also decreasing due to increase of the PV panel temperatures with length. However, this decrease may be neglected as difference is about 0.4%.

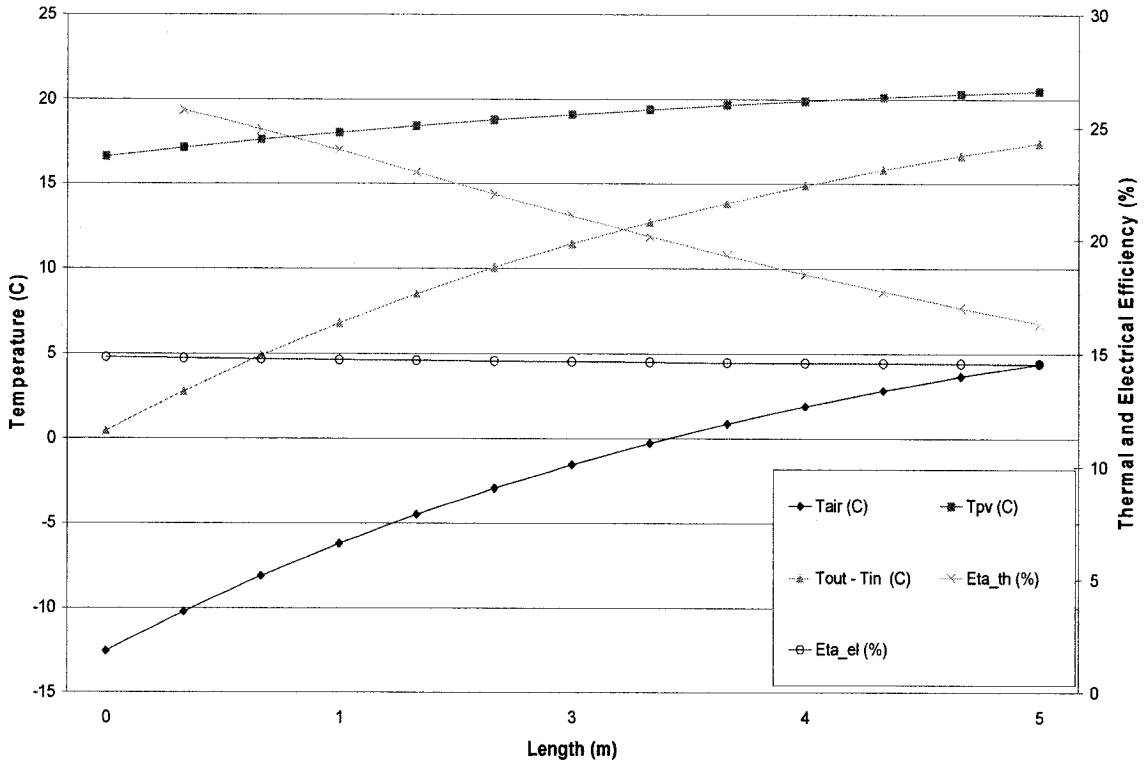

Figure 4.18: Simulated results as a function of length; S_{max}=1000 W/m^2, V_{air}=1.0 m/s, V_{wind} =2.2 m/s and To_{max}=-12°C

4.5 Solar Heat Supply to Thermal Rockbed Storage

The stored heat during the day can be useful for heating during the periods when zone temperature drops below set point temperature of 22°C. Investigations were performed on a design day in March with average wind speed of 2.2 m/s and mean ambient temperature of -2°C. The air speed in the PV cavity was set to 1.0 m/s. The BIPV/T systems of Configurations 1 and 3 were excluded from the analysis. A thermal rockbed storage is not beneficial for extreme winter conditions with unglazed BIPV/T open loop air system due to low air temperatures at the outlet of the PV gap. The BIPV/T system of Configuration 3 was also excluded from the analysis due to high temperatures

of the PV panels. High PV panel temperatures can affect the PV panel's durability. The air speed value that limits the PV panel temperature of the Configuration 3 on a day in March is presented later in this thesis. The energy interaction of BIPV/T system of Configuration 2 with thermal rockbed storage was investigated. The temperature distribution in the rockbed storage, decrease in heating load when stored heat in thermal storage is supplied to the zone and temperature increase in air zone temperature is presented. Moreover, correlations between needed rockbed volume to store recovered heat and BIPV/T roof area of Configuration 2 are determined. Major assumptions used in modeling thermal rockbed storage are given in Chapter 3.

4.5.1 Energy Interaction between BIPV/T Roof – Rockbed and Rockbed-Zone

Results from Figure 4.19 indicate the strong effect of the face velocity, rock size and rock diameter on air pressure drop across the rockbed storage. By increasing the face velocity calculated as air mass flow rate divided by rockbed frontal area and air density, the air pressure drop over the rockbed is increasing in exponential manner. Furthermore, small rocks produce high pressure drops. The smallest stone size should be at least larger than half the size of the largest (IEA, 2000). Finally, with higher values of rock porosity, the pressure drop is decreased over a rockbed for the same rock diameter. The optimum values for stone size, porosity and face velocity that could lead to the lowest fan energy consumption, will vary according to the system application. With parameters listed in Chapter 3 and face velocity of 0.1 m/s, the pressure drop across the 2 m high rockbed storage is about 42Pa.

Figure 4.20 shows the history of a temperature distribution in the rockbed thermal storage over 24 hour period with constant air flow rate in the PV cavity. Simulations were performed when no heat was stored at the beginning of the day, all collected heat was delivered to the storage and heat was extracted from the storage and delivered to the living space next day. The 6.6 m^3 rockbed is charged with recovered heat from the BIPV/T system of Configuration 2 when air temperature at the outlet from the PV gap is higher than initial temperature of the rockbed top layer. The initial temperature of the rockbed top layer is set to be equal to zone temperature of 20 °C. The rock temperature at the top starts to increase at about 11:00 hours, rises to 26°C at 14:00 and decreases to about 24°C at 16:00. The rockbed average temperature of 24°C at the top is rising to about 25°C about 0.4m from the top and declining to 21°C at the bottom.

This phenomenon is explained by the fact that heat is being collected at decreasing temperatures, cooling the upper zones in the rockbed storage and pushing the peak temperature downward. After 16:00 when fan is turned off, temperatures of the top layers in the rockbed are slightly decreasing and bottom layer temperatures are slightly increasing.

Figures 4.21 and 4.22 present decrease in heat load of the zone and increase in zone air temperature. Passive thermal response of the house was considered. With mass flow rate discharge of 0.2 kg/s, reduction in heating load is found to be 48.5 % and zone temperature increase is about 3°C.

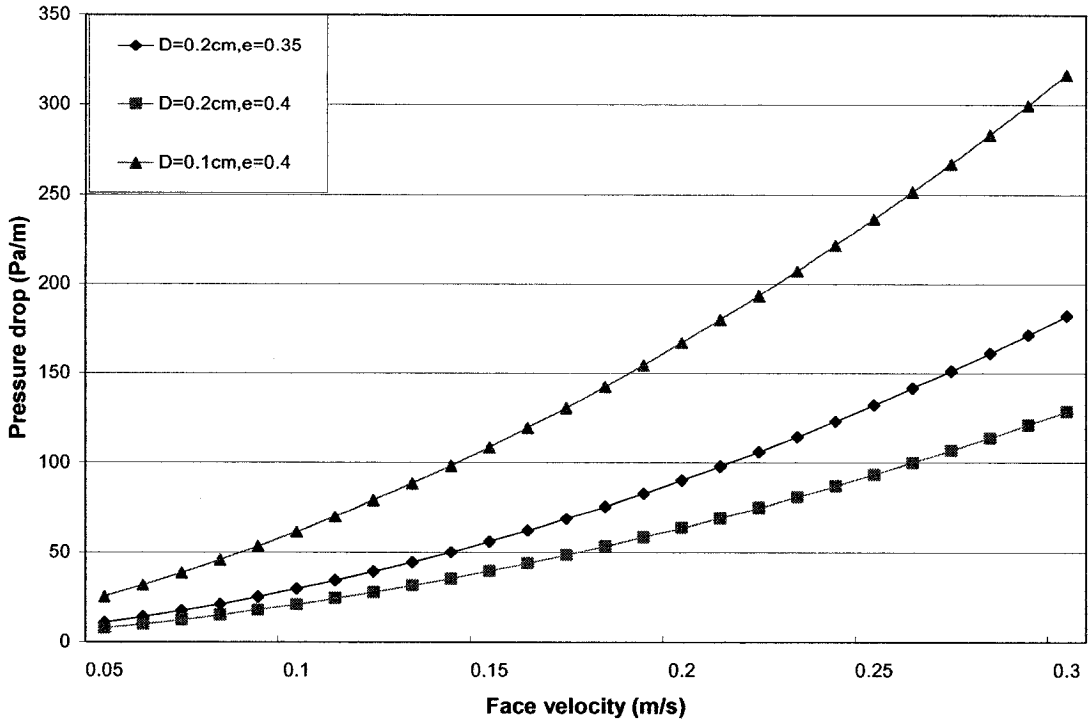

Figure 4.19: Unit pressure drop through the rockbed storage as a function of face velocity, rock porosity and diameter (D-rock diameter, e- rock porosity)

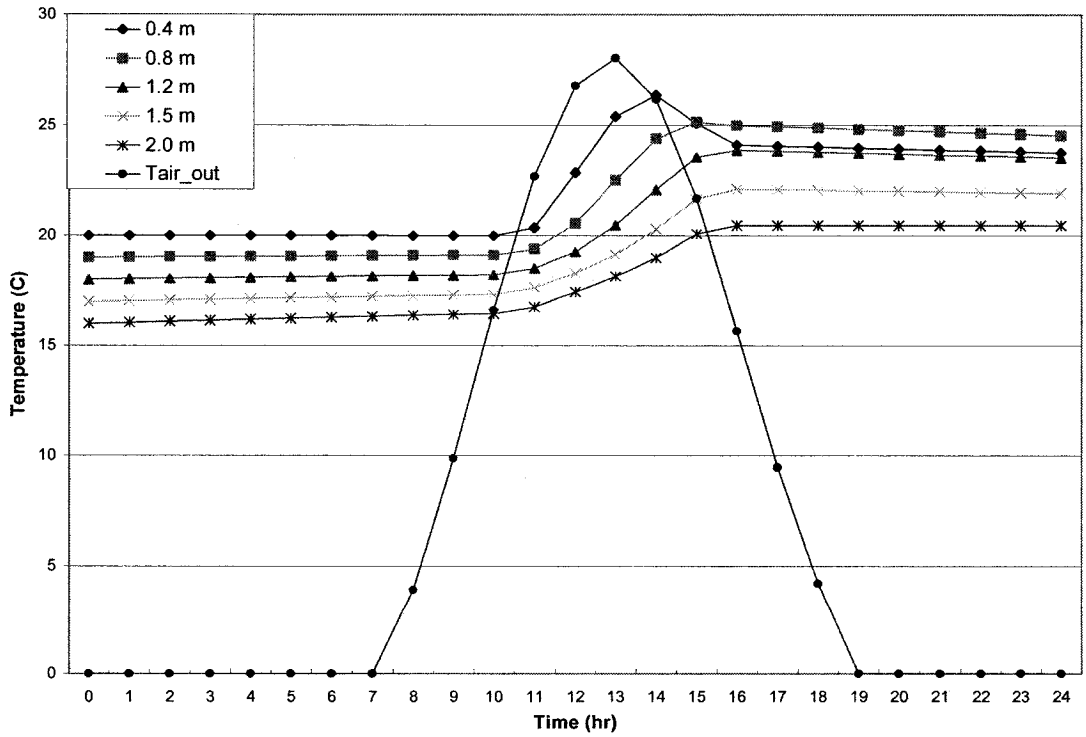

Figure 4.20: Temperature distribution in the rockbed storage, Configuration 2 with constant air flow rate through the PV cavity

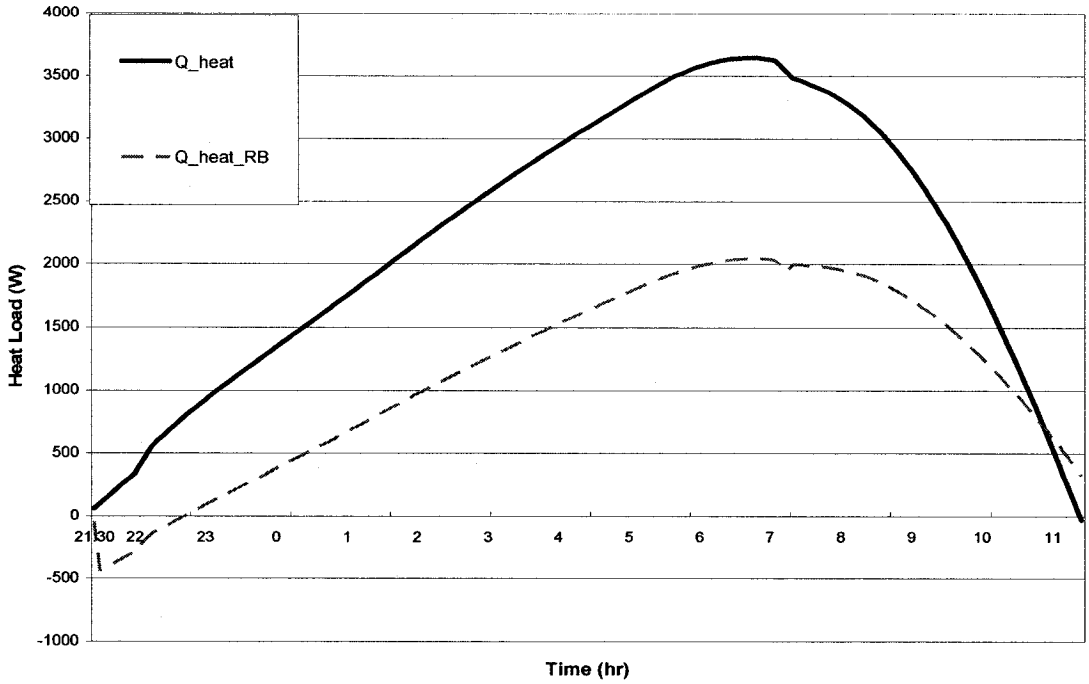

Figure 4.21: Heat load in the zone before and after heat supply from the rockbed

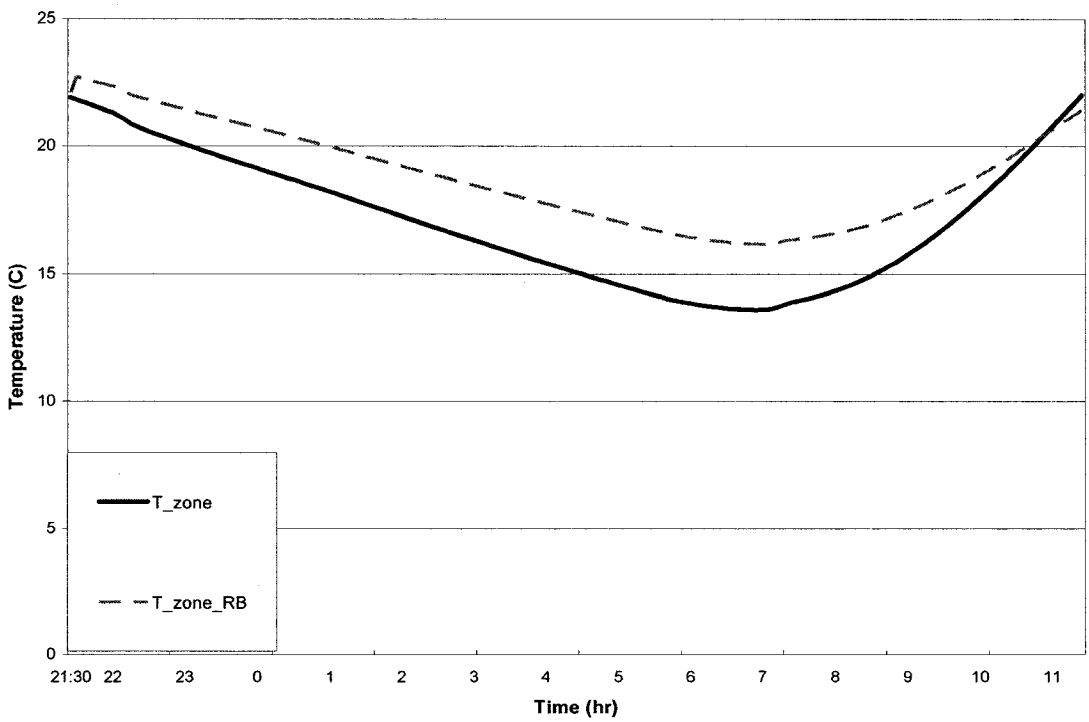

Figure 4.22: Air temperature in the zone before and after heat supply from the rockbed

4.5.2 *Volume of the Rockbed Thermal Storage as a Function of BIPV/T System Area*

Figure 4.23 shows linear relationship between thermal rockbed storage and unglazed BIPV/T-SAC system. A rectangular rockbed large enough for storage of all collected heat on a design day with maximum solar radiation was assumed with 23% thermal efficiency was assumed. Applying expressions 3.73-3.75 and using assumptions summarized in Chapter 3, the following correlations have been established for the months of October though March and depicted in Figure 4.23. For example, for a 65 m^2 BIPV/T system area of Configuration 2, the storage volume is found to be about 6 m^3 for October with constant rockbed height of 2m and cross section of the rockbed is about 1.75m x 1.75m.

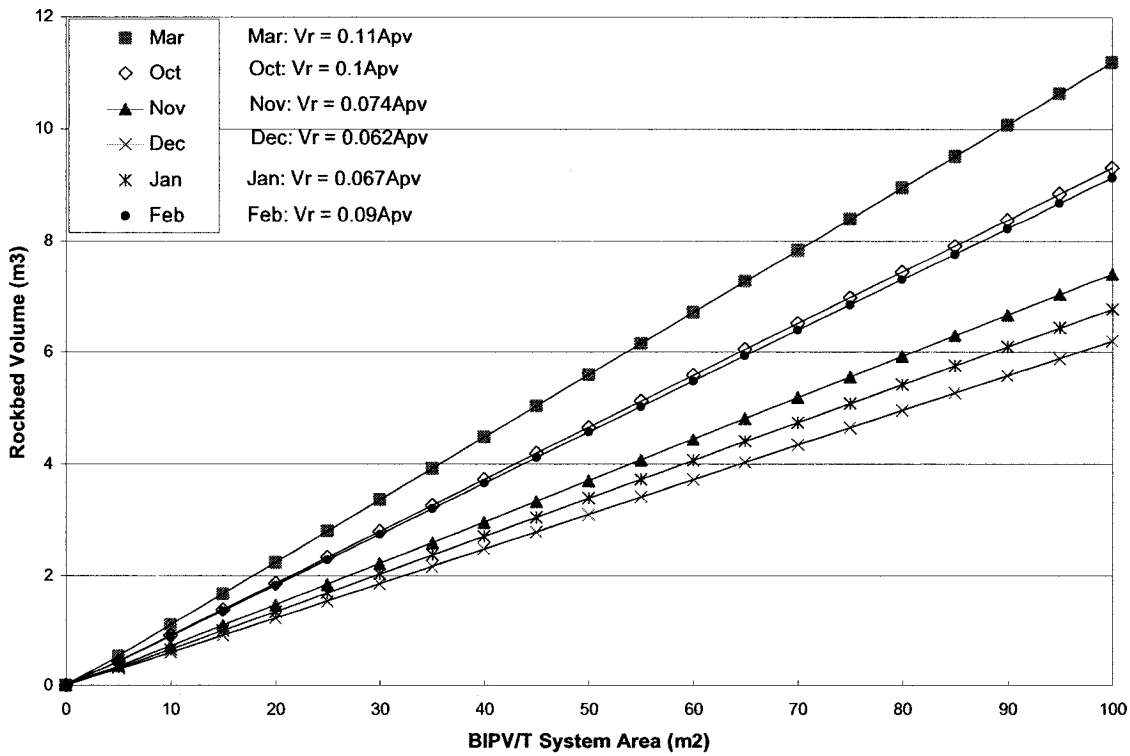

Figure 4.23: Volume of the rockbed as a function of the BIPV/T system area of the Configuration 2

4.6 BIPV/T System Interaction with Air to Water Heat Exchanger and Water Tank

In most climates a solar air system designed for space heating will have an excess heating capacity in the summer. The rate of extra heat depends upon BIPV/T roof configuration, control strategy, area, tilt angle and outdoor conditions. Moreover, effectiveness of an air- water heat exchanger and water tank size are the major factors in designing a solar system to operate in summer mode for heating domestic hot water (DHW). In this thesis, water temperature at the outlet of the air-water heat exchanger installed at the solar house is calculated and compared with that of experiments. Moreover, interaction of the glazed BIPV/T roof type (Configuration 3) with AWHE is also presented. Finally, time needed for heating 151 liters of water in the water tank installed in the solar house for both configurations is also calculated.

In summer, air - water heat exchanger is not bypassed as opposed to a winter operating mode. The air speed was measured to be 0.47 m/s at the inlet of the AWHE. Regarding the water side, water flow meter installed in the ¾" (19mm) copper pipe at the outlet of AWHE measured the water flow of 1.5GPM (0.1 L/s). Incident solar radiation was 985 W/m^2 and air temperature in the collecting duct was 53°C. Data were collected on September 8^{th}, 2006 between 13:00 and 16:40 hours. Experimental setup is explained in Chapter 3. Simulation and experimental data of the water temperature at the outlet of the AWHE are presented in Figure 4.24.

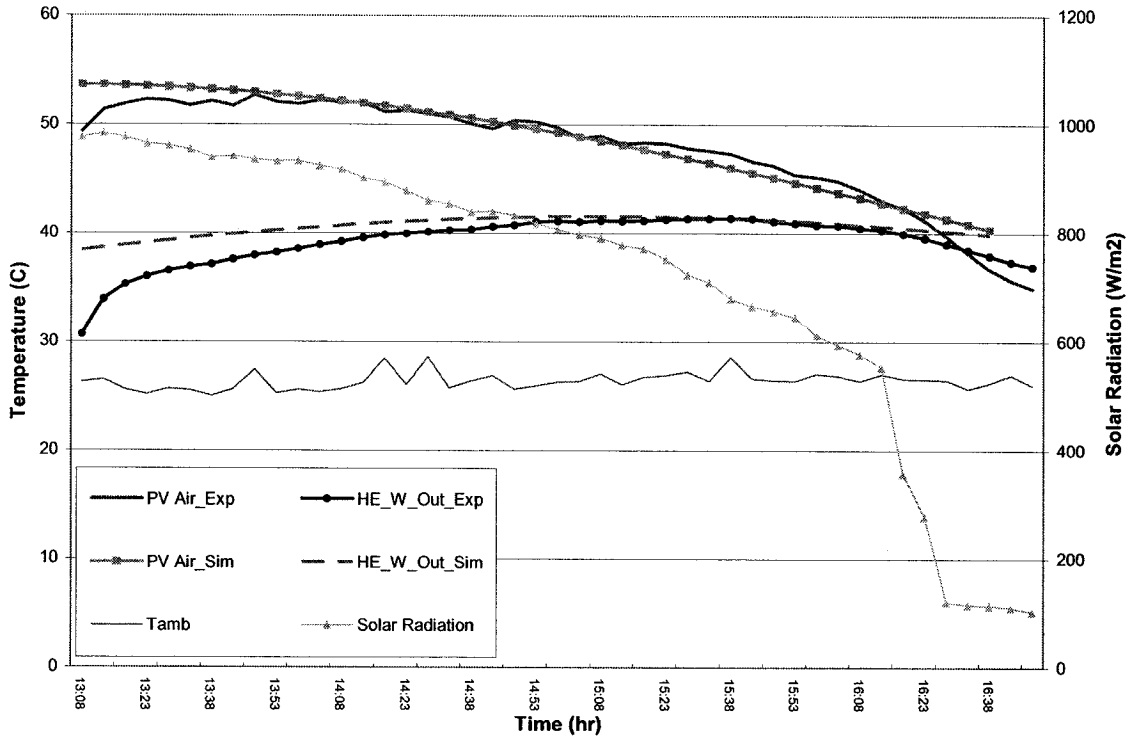

Figure 4.24: Experimental and simulation results of water temperature at the outlet of the AWHE; S_{max}=985 W/m^2, V_{air}=0.4 m/s, V_{wind}=2.8 m/s, To_{max}=26°C

From Figure 4.24 it can be concluded that maximum air temperature at the outlet of the BIPV/T roof is 53°C at 13:30 and drops afterwards as the sun goes down. Simulation results are in agreement with experimental results. Water temperature of 41°C is obtained at 15:40. Although for DHW purposes water temperature of 55°C-60°C is required, significant energy savings in auxiliary heating are achieved as less energy is needed to heat the water from 41°C to 60°C. Higher air and water temperatures can be expected during a typical hot summer days.

Interaction of the Configuration 3 BIPV/T roof with AWHE is presented by Figure 4.25. As can be seen a water temperature of 55°C at the outlet of the AWHE can be achieved.

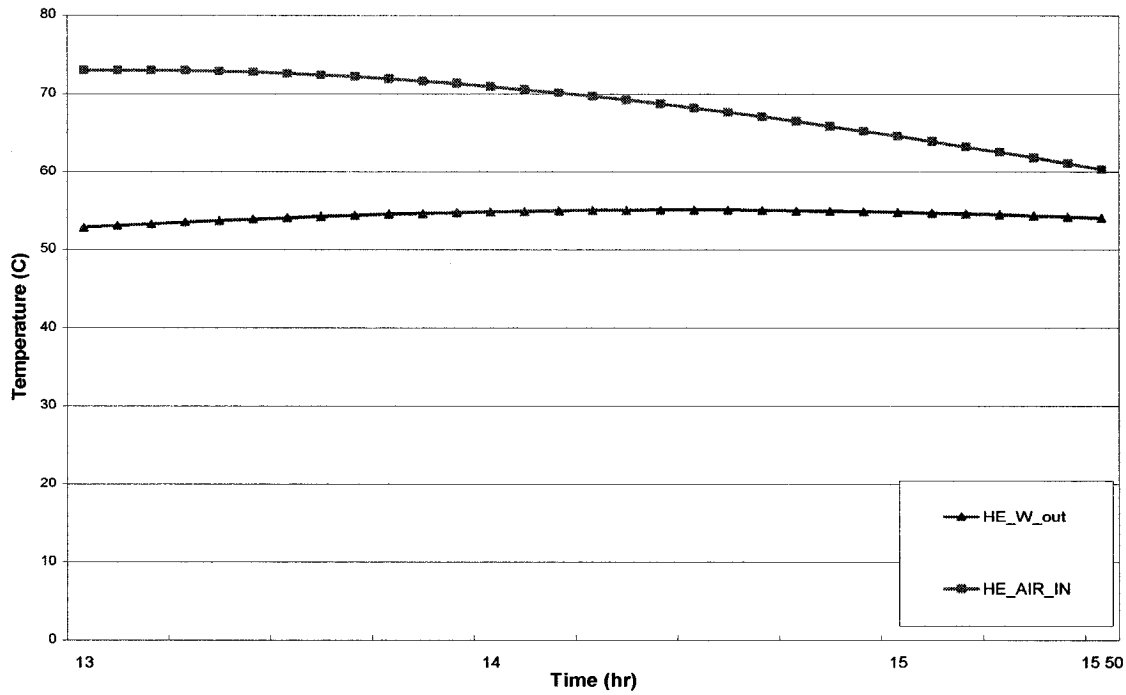

Figure 4.25: Simulation results of water temperature at the outlet of the AHWE with Configuration 3 BIPV/T system; S_{max}=900 W/m^2, V_{air}=0.4 m/s, V_{wind}=2.8 m/s, To_{max}=26°C

For practical purposes it is interesting to observe how much time is needed for heating the water in the water tank by recovered heat from the BIPV/T system. The initial temperature of the water in the tank was set to 12°C. Simulated output presented by Figure 4.26 illustrates that finding. Exponential water temperature rise is observed. It takes approximately 2 hours and 50 minutes to heat 151 liters of water from initial temperature of 12°C to 41°C for the unglazed BIPV/T roof (Configuration 1). For the same amount of time, temperature of the water in the water tank is heated up to 55°C with Configuration 3 BIPV/T system.

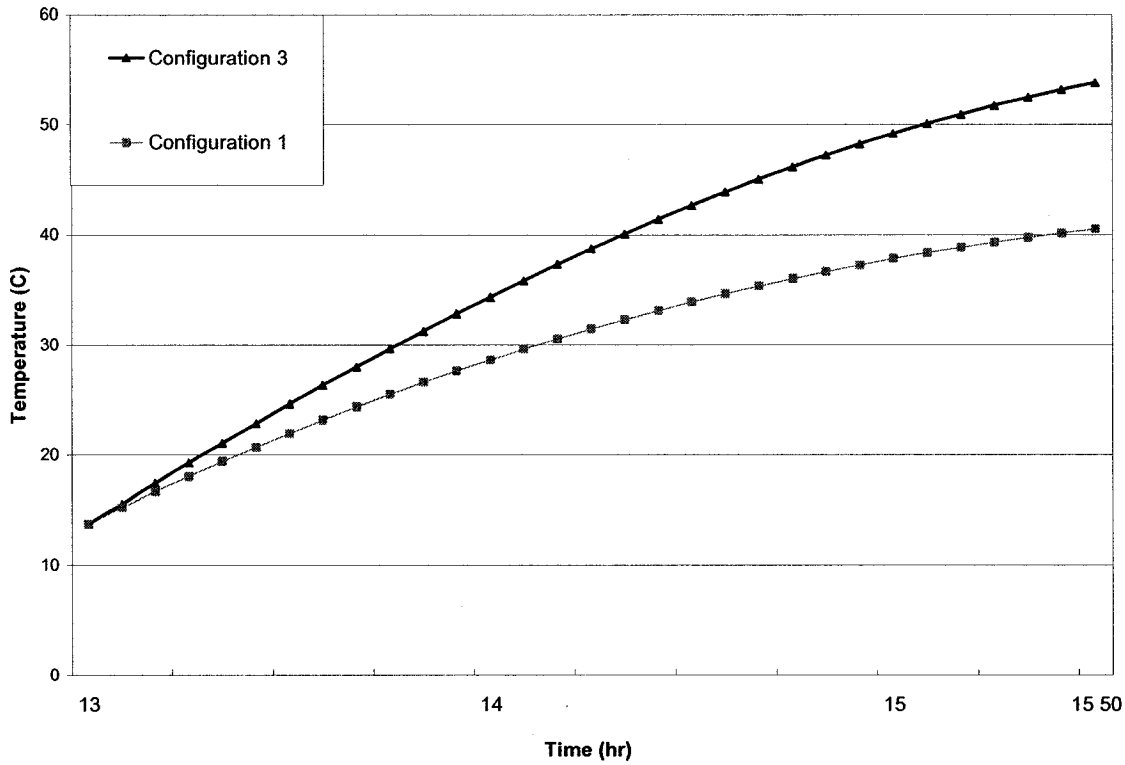

Figure 4.26: Simulated water temperature rise in the 151 liter water tank with Configurations 1 and 3 BIPV/T system

4.7 Expected Yearly Outputs for BIPV/T Roof Configurations

So far analyses have been focused on the open air loop unglazed BIPV/T roof energy performance under various ambient conditions where fan was operated from sunrise to sunset The yearly energy performance of the different BIPV/T roof Configurations 1 and 2 depicted in Figures 3.1 to 3.3, is presented and compared. Finally, the air velocity in the PV cavity that limits the PV panel temperature to 75°C of the Configuration 3 throughout the year is determined as very high PV temperatures lowers the PV panel durability.

Energy performance of the open air loop system with different BIPV/T roof configurations were analyzed throughout the year. A typical day in a month was selected according to Duffie and Beckman (1980) for simulations with a sunrise to sunset fan control strategy. While the wind speed was set to 2.2 m/s, the air speed in the PV cavity was set to 1.0 m/s Average outdoor temperatures are summarized in Table 4.4.

Table 4.4: Mean outdoor temperatures used in energy analysis of the various BIPV/T roof configurations for Montreal, Canada

	Jan	Feb	Mar	Apr	May	Jun	Jul	Aug	Sep	Oct	Nov	Dec
Outdoor Temp. (°C)	-10	-9	-2	6	13	18	21	20	15	9	2	-7

Figure 4.27 shows yearly collected heat and generated electricity by contrasted BIPV/T roof configurations. For Configuration 2, collected heat during the winter is up to 45% higher than that of Configuration 1. This is due to the fact that glazing cover reduces the top heat loss to the environment. In contrast, vertically added SAC has not yielded any significant increase in recovered heat during summer. This is explained by the fact that absorbed solar radiation of the glazed SAC depends on the physical optical properties of the glazed cover that varies with sun position over time. Generated electricity can be as high as 38.5 kWhr in summer and as low as 15.8 kWhr in winter due to the sun availability. Collected heat is generally much higher than generated electricity. This difference varies from 25% to 50% for Configuration 1 and from 50% to 65% for Configuration 2 throughout the year.

Figure 4.28 depicts both PV and air temperature variation throughout the year for above mentioned BIPV/T roof configurations. By adding 1.5m of vertical glazed SAC, temperature increase of the air at the outlet of the PV cavity is about 10°C in winter. Again, vertically added SAC has not yielded any significant increase in exiting air temperature in summer. Temperature of the PV panel for both configurations is lower than 75°C in summer. Thus, the durability of the PV panels is not in danger.

Table 4.5 summarizes the air velocities in the PV cavity that limit the temperature of the PV panel of the Configuration 3 below 75°C. While the highest value of 2.7 m/s is observed for July and August, the lowest is determined to be 1.1 m/s for March.

Table 4.5: Air speed in the PV gap that limits the glazed BIPV/T roof temperature below 75°C

	Mar	Apr	May	Jun	Jul	Aug	Sep	Oct
Air speed that limits PV panel temp. (m/s)	1.1	1.5	2.0	2.5	2.7	2.7	2.5	1.3
PV panel temp. with V_{air}=1 m/s (°C)	77	81	85	93	103	102	90	83

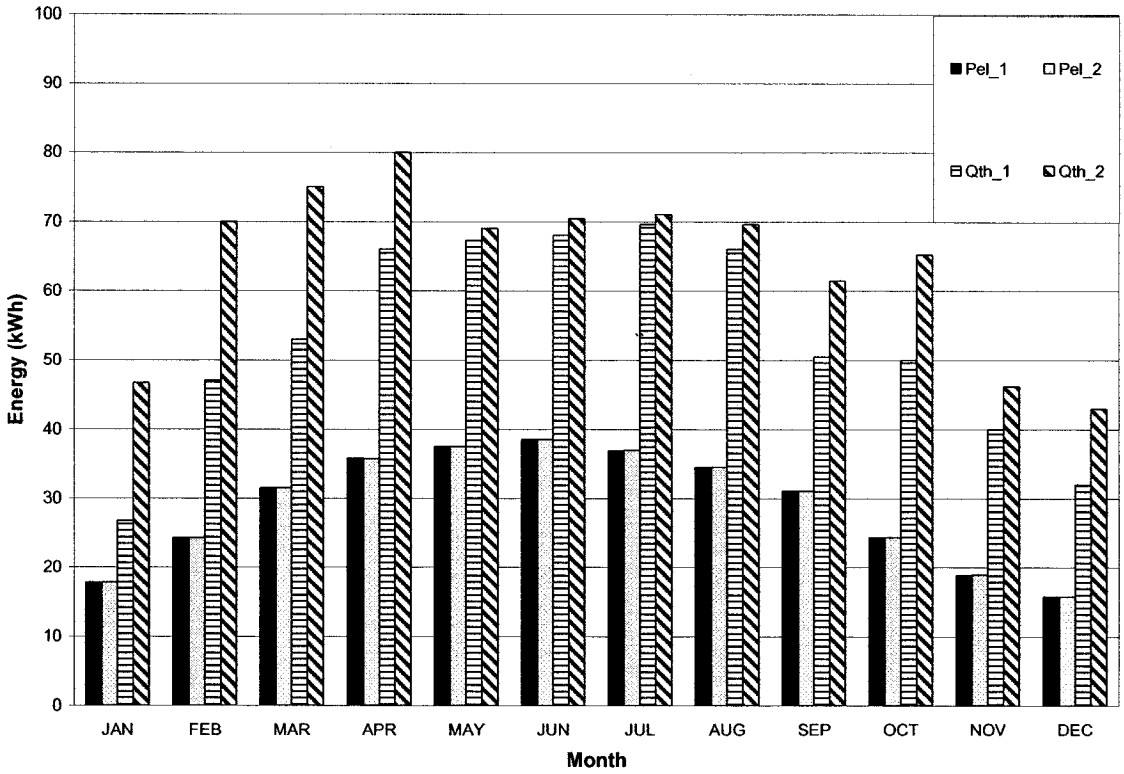

Figure 4.27: Daily collected heat and generated electricity by Configuration 1 and 2 BIPV/T roof

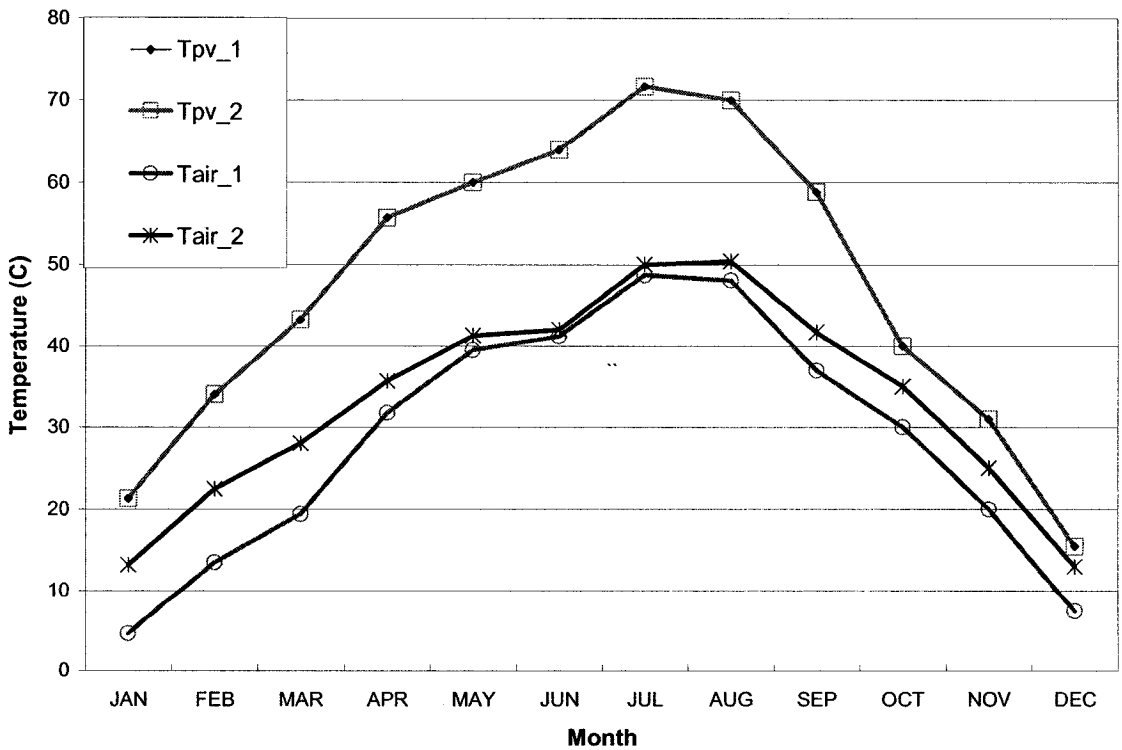

Figure 4.28: Daily PV surface and air outlet temperature of Configuration 1 and 2 BIPV/T roof

CHAPTER 5

CONCLUSIONS

5.1 Conclusions

This thesis has considered BIPV/T systems integrated into roof of residential houses, their integration with forced air heating systems and the utilization of the recovered heat. The following BIPV/T systems were considered in detail:

- Unglazed BIPV/T roof (Configuration 1)
- Unglazed BIPV/T roof connected to a glazed solar air collector (Configuration 2)
- Glazed BIPV/T roof (Configuration 3)
- Unglazed BIPV/T roof connected to a glazed solar air collector where air is passed behind the absorber and with a low-emissivity coating placed on a glass cover (Configuration 4)

Mathematical models were developed for all three systems and they were compared on a relative basis.

Thermographic analysis of the solar house was performed to investigate non-uniformities in the airflow beneath the BIPV/T roof. The first and half of the second column on the right side of the roof were excluded from the analysis as the air does not flow beneath that section of the BIPV/T roof and no heat can be recovered from that section of the roof.

A good agreement between the outputs of the presented BIPV/T roof model and experiments was obtained. An air temperature rise over 4.8m unglazed BIPV/T roof of around 25°C-30 °C can be achieved on a clear sunny day.

Ambient conditions such as solar radiation, outdoor air temperature and wind speed can significantly influence the energy performance of the unglazed BIPV/T system. By lowering the PV surface temperature, life durability of the PV panels can be extended. The air temperature in the PV gap could have a significant impact on heating/cooling loads in the zone. Dimensions and shape of the unglazed BIPV/T system as well as the PV cavity depth and air velocity in the PV cavity can have a significant effect on the unglazed BIPV/T system performance. Air speed in the PV cavity should be selected with respect to desired outlet temperatures, noise problems satisfying fresh air demands and fan energy consumption.For all considered scenarios with A_{pv}/A_{roof} ratios higher than 25% system, the outputs were significantly increased. Results for exiting air temperature of the PV cavity as a function of incident solar radiation levels and air speed in the PV cavity can be used for developing fan control strategies to achieve desired air outlet temperature of the PV cavity.

Thermal rockbed storage was not beneficial for extreme winter conditions with unglazed BIPV/T open loop air system configuration. Better temperature stratification in the rockbed storage has been achieved with Configuration 2 BIPV/T system. Moreover, while heating load has been reduced by 48.5 %, the air zone temperature increase has been determined to be about 3°C. The air pressure drop across the rockbed storage was found to depend upon face velocity, rock diameter and rock porosity.

The air-water heat exchanger component was modeled with acceptable accuracy as experimental results are in agreement with those of simulated. For the unglazed BIPV/T system, the water temperature of 41°C at the outlet of the air-water heat exchanger with thermal effectiveness of 0.8 can be achieved. Under the same conditions, the water temperature at the outlet of AWHE of 55°C can be obtained for glazed BIPV/T system. Although for DHW purposes water temperature of 60°C is required, significant energy savings in auxiliary heating can be achieved.

By adding 1.5m of vertical glazed SAC, temperature increase of the air at the outlet of the PV cavity was found to be about 10°C higher than unglazed BIPV/T system with air speed in the PV cavity of 1.0 m/s in winter. In summer, no significant increase in air outlet temperature has been noticed with Configuration 2 BIPV/T system. With passing the air behind the absorber of the SAC and putting low-emissivity coating on a glass cover, higher exiting air temperatures can be achieved compared with those of Configuration 2.

The air speed in the PV cavity that limits the PV panel temperature of the Configuration 3 roof type has been determined to vary from 1.1 m/s to 2.7 m/s throughout March to October. Recovered heat for the Configuration 2 roof is 35% higher than that of the Configuration 1. Again in summer, no significant increase in recovered heat between Configurations 1 and 2 has been noticed. Generated electricity can be 2.5 times higher in summer than that in winter.

5.2 Recommendations for Future Work

A BIPV/T roof is an advanced system with many interrelated parameters. Therefore, modeling such system and its interaction with HVAC components is a challenging task. Development of the solar-optimized houses as an integrated advanced technological system that approaches the net zero-energy target is the primary objective of the Solar Buildings Research Network (SBRN). This ambitious long-term project involves ten universities across Canada, several industrial companies and government energy agencies. This thesis is a part of the Project 1.1. *Integration of photovoltaic-thermal systems with facades, roofs and HVAC systems.* The following list of suggested recommendations for future work should contribute advancement in this area:

- Performance of the BIPV/T roof (Configuration 2) depicted in Figure 2.1 should be investigated under various fan control strategies throughout the year.
- Interaction of the Configurations 2 and 4 with AWHE component should be investigated as well as interaction of the Configuration 4 with rockbed storage.
- Energy performance of BIPV/T roof with polycrystalline and amorphous PV cells should be investigated.
- Performance of the closed air loop system with BIPV/T roof and its interaction with HVAC components should be investigated.
- To investigate the potential COP increase of the heat pump when using the preheated water or air by recovered heat from the BIPV/T roof as a heat source.
- Determination of the BIPV/T roof impact on the heating and cooling loads.
- Investigation of various fan control strategies to achieve the maximum BIPV/T system efficiency.

REFERENCES

Abbud I., Lof G., et al., (1995) Simulation of Solar Air Heating at Constant Temperature, *Solar Energy Vol. 54, No.2,* pp. 75-83

ASHRAE (2005) *ASHRAE Handbook – Fundamentals (SI)*, American Society of Heating, Refrigerating and Air-Conditioning Engineers, Inc., USA

ASHRAE (2000) *ASHRAE Handbook – HVAC Systems and Equipment (SI)*, American Society of Heating, Refrigerating and Air-Conditioning Engineers, Inc., USA

Athienitis A., Santamouris M., (2002) *Thermal Analysis and Design of Passive Solar Buildings*, James & James Ltd., London, UK

Athienitis A., (1998) *Building Thermal Analysis,* 2nd edition, MathCad electronic book, Mathsoft

Bazilian M., Prasad D., (2002) Modeling of a photovoltaic heat recovery system and its role in a design decision support tool for building professionals, *Renewable Energy 27*, pp. 57-68

Benemann J., et al., (2001) Building-Integrated PV Modules, *Solar Energy Materials & Solar Cells Vol. 67,* pp.345-354

Brinkworth B., Marshall R., and Ibrahim Z., (2000) A Validated Model of Naturally Ventilated PV Cladding, *Solar Energy Vol.69, No.1.* ,pp. 67-81

Candanedo, J., Pantic S., O' Neill B., Chen Y., (2006) *Research at the Concordia Solar Decathlon House,* poster presented at the SESCI/SBRN conference, Concordia University, Montreal, Canada

Chandra P., Willits D.,(1981) Pressure Drop and Heat Transfer Characteristics of Air-Rockbed Thermal Storage Systems, *Solar Energy Vol. 27, No.6*, pp. 547-553

Charron R., Athienitis A., (2006) Optimization of the performance of double-facades with integrated photovoltaic panels and motorized blinds, *Solar Energy Vol. 80, No.2,* pp. 482-491

Charron R., Athienitis A., and Beausoleil-Morrison I., (2005) Tools for the design of zero energy solar homes, *30th Annual Conference of the Solar Energy Society of Canada,* Vancouver August 2005

Charron R., (2004) *One and Two Dimensional Modeling of Ventilated Facades with Integrated Potovoltaics*, MASc Thesis, Concordia University, Montreal, Canada

Claessens J., DeHerde A., (2006) /Active Solar Heating and Photovoltaics/ http://erg.ucd.ie/mid_career/pdfs/tech_mod_5.pdf / Visited: November 21st, 2006

Clarke J., etal., (1996) / http://www.ibpsa.org/proceedings/BS1997/BS97_P214.pdf / Visited: December 8th, 2006

Costa M., et al., (2000) Optimal Design of Multi-Functional Ventilated Facades,

Crawley D., Hand J., et al., (2005) / Contrasting the capabilities of building energy performance simulation programs / www.eere.energy.gov / Visited: November 21st, 2006

DOE (2006) / http://www.eere.energy.gov/buildings/energyplus / Visited: November 24th, 2006

Duffie J., Beckman W., (1980) *Solar Engineering of Thermal Processes.* 2nd ed., John Wiley & Sons, New York, USA

Flir Systems (2006) / How Do Thermal Imaging Infrared Cameras Work / http://www.flirthermography.com/about/how_infrared_cameras.asp / Visited: July 18th, 2006

Gnielinski V., (1983) *Forced convection in ducts,* Hemisphere Publishing Corporation.

Guiavarch A., Peuportier B., (2006) Photovoltaic collectors efficiency according to their integration in buildings, *Solar Energy Vol. 80,* pp.65-77

Hausen S., (1943) *Darstellung des warmenberganges in rohren durch verallgemeinerte potenzbeiziehungen*, VDIZ 4, pp.91-98

Helden W., et al., (2004) PV Thermal Systems: PV Panels Supplying Renewable Electricity and Heat, *Progress in Photovoltaics: Research and Applications 12,* pp. 415-426

Hirata Y., Inasaka T., et al., (1998) Output variation of photovoltaic modules with environmental factors-II: Seasonal variation, *Solar Energy Vol. 61(3),* pp.169-178

Holman J., (1990) *Heat Transfer,* 7th edition, McGraw-Hill, USA

Howell J., / A Catalog of Radiation Heat Transfer Configuration Factors / http://www.me.utexas.edu/~howell/tablecon.html#C / visited: April 1st,2006.

Hughes, P.M., Klein, S.A., and Close, D., (1976) Packed Bed Thermal Storage Models for Solar Air Heating and Cooling Systems, *Journal of Heat Transfer*

Hutcheon N., Handegord G., (1995) *Building Science for a Cold Climate*, National Research Council of Canada

IEA (International Energy Agency), (2000) *Solar Air Systems – A Design Handbook*, Hastings R., Morck O., James & James Ltd. London, UK

Incropera F., DeWitt D., (1985) *Fundamentals of Heat and Mass transfer*, 2nd edition, John Wiley & Sons

Jones A., Underwood C., (2001) A Thermal Model for Photovoltaic Systems, *Solar Energy Vol. 70, No.4,* pp. 349-359

Kaushika N., Reddy K., (1999) Thermal design and field experiment of transparent honeycomb insulated integrated-collector-storage solar water heater, *Applied Thermal Engineering Vol. 19*, pp.145-161

Klein S., et al., (1976) A design procedure for solar heating systems, *Solar Energy Vol. 18,* pp. 113-127

Krauter S., et al., (1999) Combined Photovoltaic and Solar Thermal Systems for Façade Integration and Building Insulation, *Solar Energy Vol. 67*, pp.239-248.

Kreider J., Kreith F., (1981) *Solar Energy Handbook,* McGrow Hill Company, New York, USA

Kuang Y., Sumathy K., Wang R.Z., (2003) Study on a direct-expansion solar-assisted heat pump water heating system, *International Journal of Energy Research Vol. 27*, pp. 531-548

Liao L., (2005) *Numerical and Experimental Investigation of Building Integrated Photovoltaic Thermal System,* MASc Thesis, Concordia University, Montreal, Canada

Lin Q., Harrison S., (2003) Experimental study of natural convection in an asymmetrically heated inclined channel with radiation exchange, *Proceedings of HT200, ASME Summer Heat Transfer Conference,* July 21-23, 2003, Las Vegas, USA

McAdams W.H. (1954) *Heat Transmission, 3rd edition,* McGraw-Hill, New York, USA

McClellan T., Pedersen C., (2005) / Investigation of Outside Heat Balance Models for use in a Heat Balance Cooling Load Calculation Procedure www.bso.uiuc.edu/publications/outsidHB.pdf / visited: November 15th, 2005.

McQuiston F., Parker J., Spitler J., (2005) *Heating, Ventilating and Air Conditioning – Analysis and Design*, 6th Edition, John Wiley & Sons, Inc., USA

Mei L., Infield D., et al., (2003) Thermal modeling of a building with an integrated ventilated PV façade, *Energy and Buildings Vol.35, pp. 605-617*

Natural Resources Canada (2004) *Mainstreaming Building-Integrated Photovoltaics in Canada*, Natural Resources Canada, Canada

Natural Resources Canada (2002) *Photovoltaic Systems: A Buyer's Guide*, Natural Resources Canada, Canada

Ong K., (1995) Thermal Performance of Solar Air Heaters: Mathematical Model and Solution Procedure, *Solar Energy Vol. 55, No.2,* pp. 93-109

Ong K., Chow C., (2003) Performance of a solar chimney, S*olar Energy Vol. 74,* pp. 1-17

Pasini M., Athienitis A., (2006) Systems Design of the Canadian Solar Decathlon House, *ASHRAE Transactions Vol. 112, Part 2*

Saelens D., (2002) *Energy Performance Assessment of Single Storey Multiple-Skin Facades,* PhD Thesis, Katholieke Universiteit Leuven

Sagara K., Nakahara N., (1991) Thermal Performance and pressure drop of rock beds with large storage materials, *Solar Energy 47, No.3,* pp.157-163

Sharples S., Charlesworth P.S., (1998) Full-Scale Measurements of Wind-Induced Convective Heat Transfer from a Roof-Mounted Flat Plate Solar Collector, *Solar Energy Vol. 62, No.2,* pp.69-77

Sharples S., (1984) Full-scale Measurements of Convective Energy Losses from Exterior Building Surfaces, *Building Science 8,* pp. 259-267

Stec W., Paassen A.H.C., (2005) Symbiosis of the double skin façade with HVAC system, *Energy and Buildings Vol. 37,* pp. 461-469

Swinbank W. C., (1963) Longwave radiation from clear skies, *Q.J.R., Meteorol.Soc.89,*pp.339

Tang H., et al., (2001) A simulation study on the energy Performance of Photovoltaic Roofs, *ASHRAE Transactions Vol. 107 (2),* pp. 129-135

Tiwari G.N., (2002) *Solar Energy – Fundamentals, Design, Modeling and Applications* , Narosa Publishing House, New Delhi, India

TRNSYS 16 (2005), *TRNSYS help documentation*, included in the TRNSYS software

Yang H., et al., (2001) A simulation study on the energy performance of photovoltaic roofs, *ASHRAE Trans, 107(2)*: pp. 129-135

Yang H., et al., (2000) Simple approach to cooling load component calculation though PV walls, *Energy and Buildings Vol. 31,* pp. 285-290

Wang Y., et al., (2006) Influence of a building's integrated-photovoltaics on heating and cooling loads, *Applied Energy 83,* pp. 989-1003

Ward D., et al., (1977) Design of a Solar Heating and Cooling System for CSU Solar House II, *Solar Energy 19,* pp. 79-85

Wastmuff J.H., Charters W.W.S., Proctor D., (1977) *Solar and wind induced external coefficients solar collectors,* Int. Revue d'Hellio-technique 2, pp.56

Zondag H., De Vries D., et al., (2002) The Thermal and Electrical Yield of a PV-Thermal Collector, *Solar Energy Vol. 72., No. 2,* pp. 113-128

APPENDIX A: House Layout

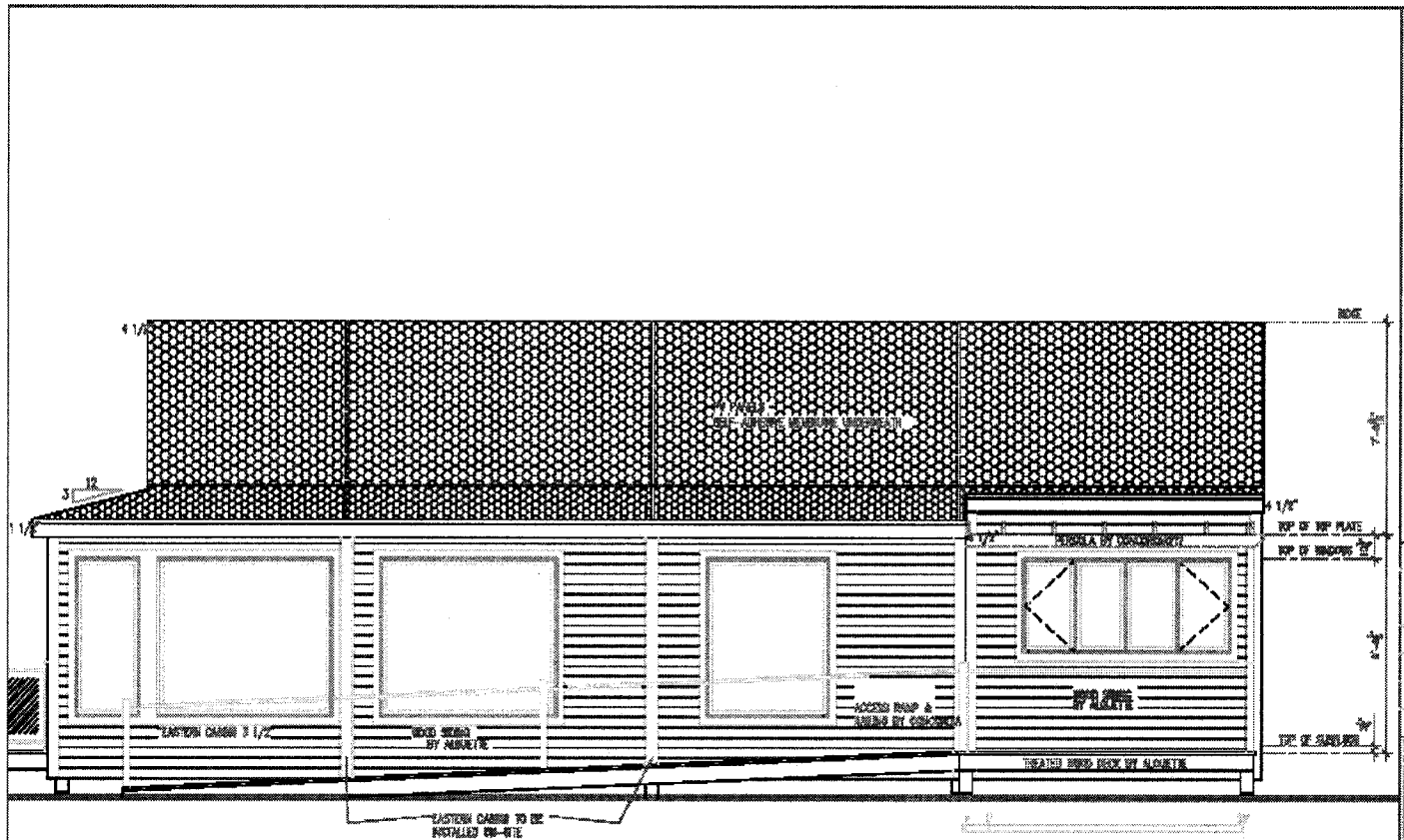

The Canadian Solar Decathlon Team

Concordia University | Université de Montréal

SOLAR DECATHLON 2005

SOUTH ELEVATION

AUGUST 2005

1/4" = 1'-0"

A-03

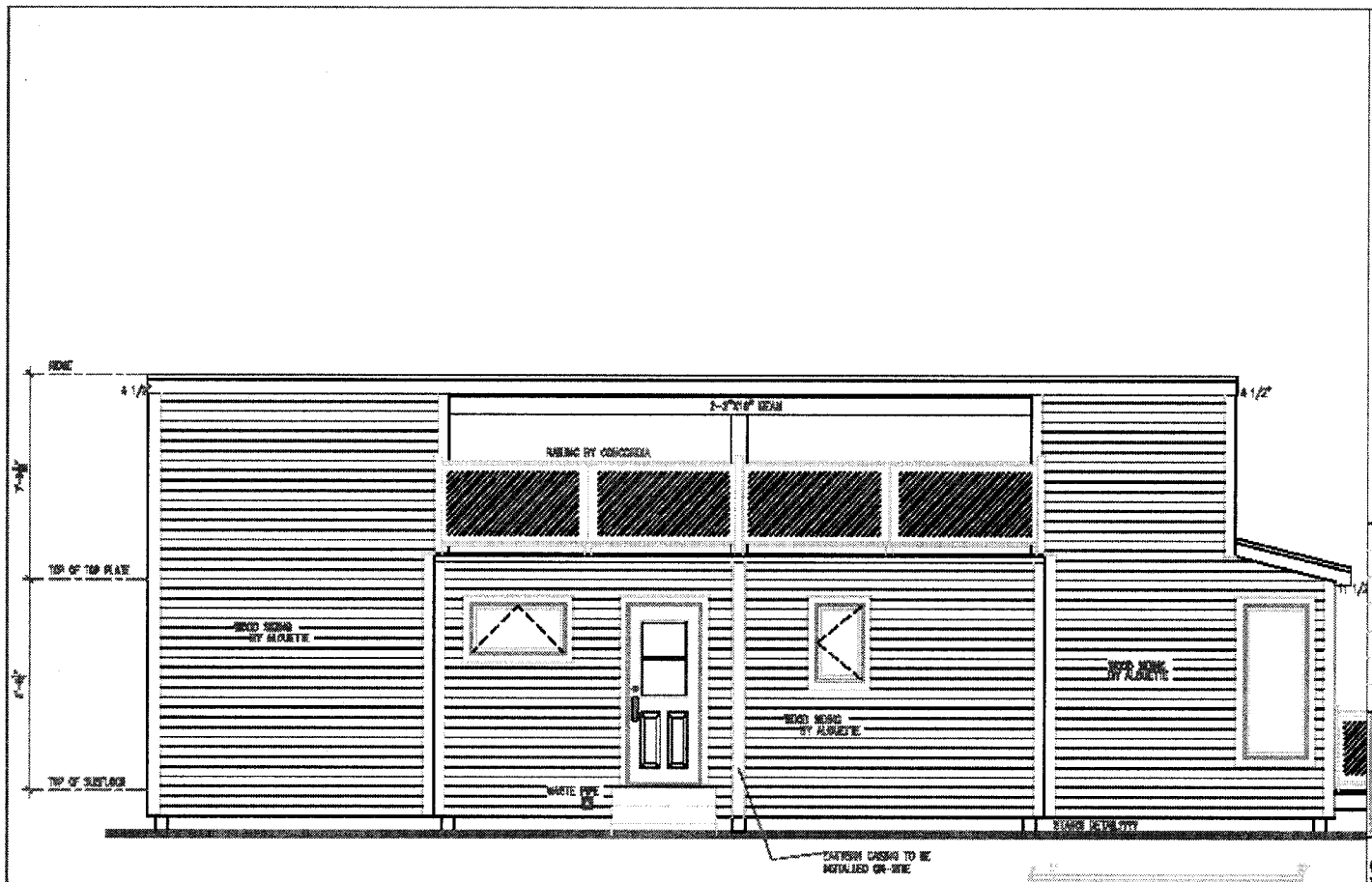

Concordia University
Université de Montréal

SOLAR DECATHLON 2005

NORTH ELEVATION

AUGUST 2005

1/4" = 1'-0"

A-03

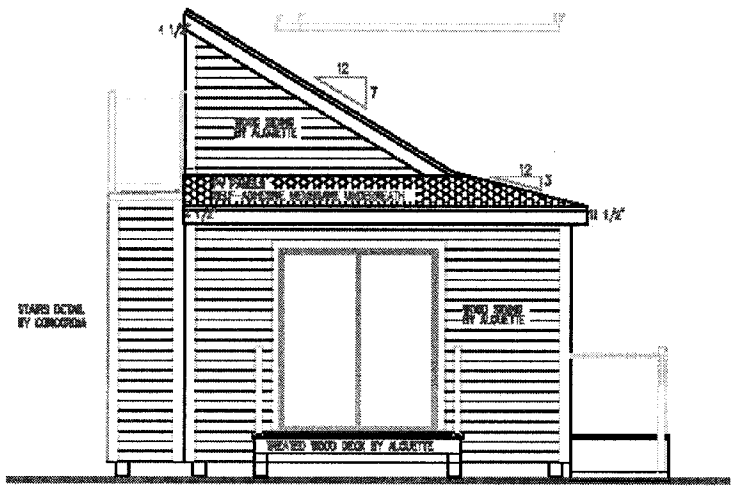

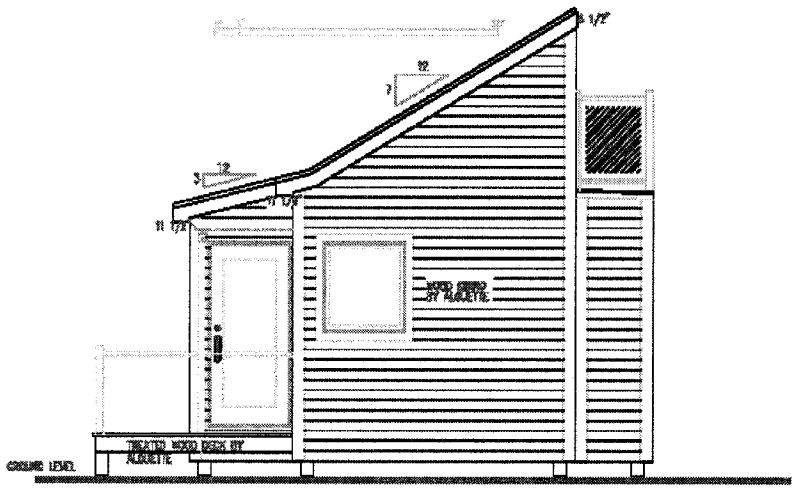

NOTES

1	AS-BUILT	AUGUST 2005
2	SHOP DWG	PRELIMINARY DESIGN
3	SHOP DWG	PRELIMINARY DESIGN
No.	Date	Revision

The Canadian Solar Decathlon Team

Concordia University | Université de Montréal

PROJECT
SOLAR DECATHLON 2005

DRAWING
EAST & WEST ELEVATIONS

DATE: AUGUST 2005	DRAWING NUMBER: A-07
SCALE: 1/4" = 1'-0"	

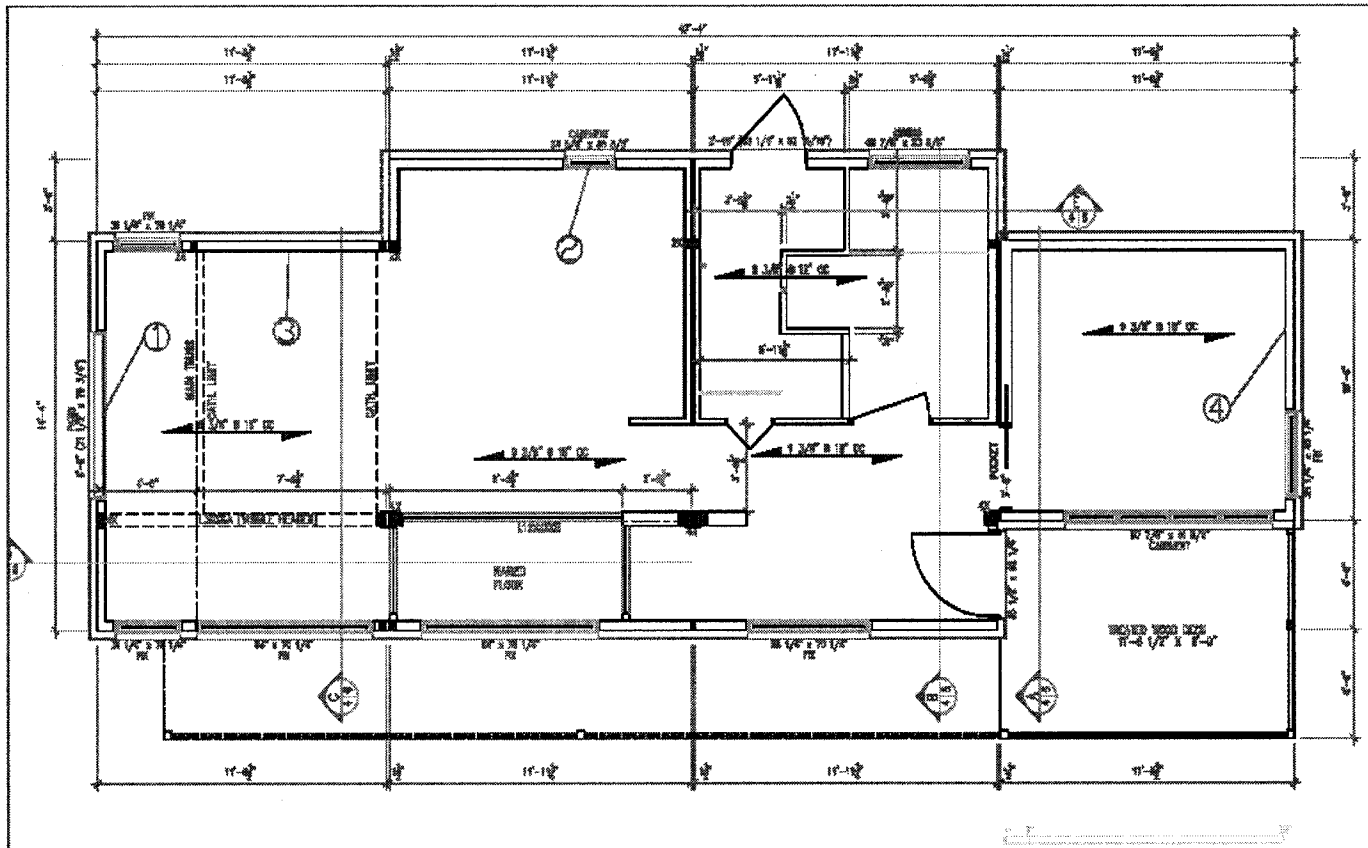

① SAFETY GLAZING USED FOR PATIO DOOR
② ALL GLAZINGS COMPLY WITH CC1.2 TO AVOID SAFETY GLAZING
③ ALL INTERIOR FINISHED COMPLY WITH CC1.1
④ 0.5" GYPSUM USED BECAUSE OF FOAM PLASTIC INSULATION IN WALLS AND CEILING

The Canadian Solar Decathlon Team

Concordia University | Université de Montréal

SOLAR DECATHLON 2005

CONSTRUCTION DETAILS

AUGUST 2005

1/4" = 1'-0"

S-02

APPENDIX B: Calculation of Solar Geometry, Incident Solar Radiation and Window Optical properties

SOLAR RADIATION

Wall/windows azimuth angles:

$\psi_1 := 0 \cdot deg$ South

$\psi_2 := 90 deg$ West

$\psi_3 := -90 deg$ East

$\psi_4 := 180 deg$ North

Wall absorptances: $\alpha s_{iw} := 0.9$

PV absorptance: $\alpha_{pv} := 0.9$

Location data: $L := 45.5 deg$ ..latitude $LNG := 74 deg$ ... longitude $LSM := 75 deg$ ... local sta meridian

$n := 17$ ..day number $\rho_g := 0.8$ ..ground reflectance

Solar geometry calculations

Time array: $it := 0, 1 .. 23$

$$ET(n) := \left[9.87 \sin\left(4 \cdot \pi \cdot \frac{n - 81}{364} \right) - 7.53 \cos\left[2 \cdot \pi \cdot \frac{(n - 81)}{364} \right] - 1.5 \sin\left(2 \cdot \pi \cdot \frac{n - 81}{364} \right) \right] \cdot min$$

Apparent solar time: $AST(it) := it \cdot hr + ET(n) + (LSM - LNG) \cdot \frac{hr}{15 deg}$

$s(it) := AST(it) - 12 hr$

Hour angle: $h_{it} := (AST(it) - 12 hr) \cdot \left(15 \frac{deg}{hr} \right)$

Declination angle $\delta := 23.45 deg \cdot \sin\left(360 \frac{284 + n}{365} \cdot deg \right)$

Solar altitude:

$$\alpha_{it} := \begin{cases} \operatorname{asin}\left[(\cos(L)) \cdot \cos(\delta) \cdot \cos(h_{it}) + (\sin(L)) \cdot \sin(\delta) \right] & \text{if } \operatorname{asin}\left[(\cos(L)) \cdot \cos(\delta) \cdot \cos(h_{it}) + (\sin(L)) \cdot \sin(\delta) \right] > 0 \cdot deg \\ 0 \cdot deg & \text{otherwise} \end{cases}$$

Sunset time:

$$t_s := \text{acos}\left(-\tan(L)\cdot\tan(\delta)\right)\cdot\frac{hr}{15deg}$$

Sunset time on the wall surface:

$$t_{ss} := \min\left[t_s, \left(\text{acos}\left(-\tan\left(L-\beta\right)\cdot\tan(\delta)\right)\right)\cdot\frac{hr}{15deg}\right]$$

Sunset time on the roof surface:

$$t_{ss\_roof\_1} := \min\left[t_s, \left(\text{acos}\left(-\tan\left(L-\beta_{roof\_1}\right)\cdot\tan(\delta)\right)\right)\cdot\frac{hr}{15deg}\right]$$

$$t_{ss\_roof\_2} := \min\left[t_s, \left(\text{acos}\left(-\tan\left(L-\beta_{roof\_2}\right)\cdot\tan(\delta)\right)\right)\cdot\frac{hr}{15deg}\right]$$

Solar azimuth:

$$\phi_{it} := \text{acos}\left(\frac{\sin(\alpha_{it})\cdot\sin(L)-\sin(\delta)}{\cos(\alpha_{it})\cdot\cos(L)}\right)\cdot\frac{h_{it}}{|h_{it}|}$$

Angle of incidence:

$$\cos\theta_{it,iw} := \cos(\alpha_{it})\cdot\cos\left(|\phi_{it}-\psi_{iw}|\right)\cdot\sin(\beta)+\sin(\alpha_{it})\cdot\cos(\beta)$$ ... windows and walls

$$\theta_{it,iw} := \text{acos}\left(\frac{\cos\theta_{it,iw}+|\cos\theta_{it,iw}|}{2}\right)$$

$$\cos\theta_{r1_{it}} := \cos(\alpha_{it})\cdot\cos\left(|\phi_{it}-\psi_1|\right)\cdot\sin\left(\beta_{roof\_1}\right)+\sin(\alpha_{it})\cdot\cos\left(\beta_{roof\_1}\right)$$

$$\theta_{r1_{it}} := \text{acos}\left(\frac{\cos\theta_{r1_{it}}+\left|\cos\theta_{r1_{it}}\right|}{2}\right)$$ ...Roof

$$\cos\theta_{r2_{it}} := \cos(\alpha_{it})\cdot\cos\left(|\phi_{it}-\psi_1|\right)\cdot\sin\left(\beta_{roof\_2}\right)+\sin(\alpha_{it})\cdot\cos\left(\beta_{roof\_2}\right)$$

$$\theta_{r2_{it}} := \text{acos}\left(\frac{\cos\theta_{r2_{it}}+\left|\cos\theta_{r2_{it}}\right|}{2}\right)$$

Calculate transmittance of atmosphere and glazing:

Beam atmospheric transmittance calculations: $Al := 0.035$ altitude (km)

Select summer or winter Option := "Winter"

$$r_o := \begin{cases} 0.97 \text{ if Option = "Summer"} \\ 1.03 \text{ otherwise} \end{cases} \qquad r_1 := \begin{cases} 0.99 \text{ if Option = "Summer"} \\ 1.01 \text{ otherwise} \end{cases}$$

$$r_k := \begin{cases} 1.02 \text{ if Option = "Summer"} \\ 1.0 \text{ otherwise} \end{cases}$$

$$a_o := r_o \cdot \left[0.4237 - 0.00821(6 - Al)^2\right] \qquad a_1 := r_1 \cdot \left[0.5055 + 0.00595(6.5 - Al)^2\right]$$

$$k := r_k \cdot \left[0.2711 + 0.01858(2.5 - Al)^2\right]$$

$$\tau b_{it} := if\left[\left(|s(it)| < |t_{ss}|\right), a_o + a_1 \cdot \exp\left(\frac{-k}{\sin(\alpha_{it})}\right), 0\right]$$

$$\tau rb1_{it} := if\left[\left(|s(it)| < |t_{ss\_roof\_1}|\right), a_o + a_1 \cdot \exp\left(\frac{-k}{\sin(\alpha_{it})}\right), 0\right]$$

$$\tau rb2_{it} := if\left[\left(|s(it)| < |t_{ss\_roof\_2}|\right), a_o + a_1 \cdot \exp\left(\frac{-k}{\sin(\alpha_{it})}\right), 0\right]$$

Determine now the glazing properties as a function of time interval j:

Glass properties:

$kL := 0.1$ ..extinction coeff.*glazing thickness

$n_g := 1.53$ ..refractive index

Angle of refraction and component reflectivity:

$$\theta'_{it,iw} := \operatorname{asin}\left(\frac{\sin(\theta_{it,iw})}{n_g}\right) \qquad r_{it,iw} := \frac{1}{2} \cdot \left[\left(\frac{\sin(\theta_{it,iw} - \theta'_{it,iw})}{\sin(\theta_{it,iw} + \theta'_{it,iw})}\right)^2 + \left(\frac{\tan(\theta_{it,iw} - \theta'_{it,iw})}{\tan(\theta_{it,iw} + \theta'_{it,iw})}\right)^2\right]$$

Beam transmittance, τ, reflectance, ρo, and absorptance, α, of glazing:

$$a_{it,iw} := \exp\left[-\frac{kL}{\sqrt{1 - \left(\frac{\sin(\theta_{it,iw})}{n_g}\right)^2}}\right] \qquad \tau_{it,iw} := \frac{\left(1 - r_{it,iw}\right)^2 \cdot a_{it,iw}}{1 - \left(r_{it,iw}\right)^2 \cdot \left(a_{it,iw}\right)^2}$$

$$\rho o_{it,iw} := r_{it,iw} + \frac{r_{it,iw}\cdot\left(1 - r_{it,iw}\right)^2\cdot\left(a_{it,iw}\right)^2}{1 - \left(r_{it,iw}\right)^2\cdot\left(a_{it,iw}\right)^2} \qquad \alpha_{s_{it,iw}} := 1 - \rho o_{it,iw} - \tau_{it,iw}$$

For double glazed windows:

$$\tau_{e_{it,iw}} := \frac{\left(\tau_{it,iw}\right)^2}{1 - \left(\rho o_{it,iw}\right)^2}$$

$$\alpha_{i_{it,iw}} := \alpha_{s_{it,iw}}\cdot\frac{\tau_{it,iw}}{1 - \left(\rho o_{it,iw}\right)^2} \qquad \alpha_{o_{it,iw}} := \alpha_{s_{it,iw}} + \alpha_{s_{it,iw}}\cdot\frac{\tau_{it,iw}\cdot\rho o_{it,iw}}{1 - \left(\rho o_{it,iw}\right)^2}$$

For glazed BIPV/T roof:

15 slope

$$kL_g := 0.1$$

$$\theta'_{rl_{it}} := \operatorname{asin}\left(\frac{\sin\left(\theta_{rl_{it}}\right)}{n_g}\right)$$

$$rl_{it} := \frac{1}{2}\cdot\left[\left(\frac{\sin\left(\theta_{rl_{it}} - \theta'_{rl_{it}}\right)}{\sin\left(\theta_{rl_{it}} + \theta'_{rl_{it}}\right)}\right)^2 + \left(\frac{\tan\left(\theta_{rl_{it}} - \theta'_{rl_{it}}\right)}{\tan\left(\theta_{rl_{it}} + \theta'_{rl_{it}}\right)}\right)^2\right]$$

$$a_{rl_{it}} := \exp\left[-\frac{kL_g}{\sqrt{1 - \left(\frac{\sin\left(\theta_{rl_{it}}\right)}{n_g}\right)^2}}\right]$$

$$\tau_{rl_{it}} := \frac{\left(1 - rl_{it}\right)^2\cdot a_{rl_{it}}}{1 - \left(rl_{it}\right)^2\cdot\left(a_{rl_{it}}\right)^2}$$

$$\rho_{rl_{it}} := rl_{it} + \frac{rl_{it}\cdot\left(1 - rl_{it}\right)^2\cdot\left(rl_{it}\right)^2}{1 - \left(rl_{it}\right)^2\cdot\left(a_{rl_{it}}\right)^2}$$

$$\alpha_{rl_{it}} := 1 - \rho_{rl_{it}} - \tau_{rl_{it}}$$

30 slope

$$kL_g := 0.1$$

$$\theta'_{r2_{it}} := \operatorname{asin}\left(\frac{\sin\left(\theta_{r2_{it}}\right)}{n_g}\right)$$

$$r2_{it} := \frac{1}{2}\cdot\left[\left(\frac{\sin\left(\theta_{r2_{it}} - \theta'_{r2_{it}}\right)}{\sin\left(\theta_{r2_{it}} + \theta'_{r2_{it}}\right)}\right)^2 + \left(\frac{\tan\left(\theta_{r2_{it}} - \theta'_{r2_{it}}\right)}{\tan\left(\theta_{r2_{it}} + \theta'_{r2_{it}}\right)}\right)^2\right]$$

$$a_{r2_{it}} := \exp\left[-\frac{kL_g}{\sqrt{1 - \left(\frac{\sin\left(\theta_{r2_{it}}\right)}{n_g}\right)^2}}\right]$$

$$\tau_{r2_{it}} := \frac{\left(1 - r2_{it}\right)^2\cdot a_{r2_{it}}}{1 - \left(r2_{it}\right)^2\cdot\left(a_{r2_{it}}\right)^2}$$

$$\rho_{r2_{it}} := r2_{it} + \frac{r2_{it}\cdot\left(1 - r2_{it}\right)^2\cdot\left(r2_{it}\right)^2}{1 - \left(r2_{it}\right)^2\cdot\left(a_{r2_{it}}\right)^2}$$

$$\alpha_{r2_{it}} := 1 - \rho_{r2_{it}} - \tau_{r2_{it}}$$

Incident solar radiation on exterior walls and transmitted by windows

Extraterrestrial normal solar radiation:

$$I_{on} := 1353\cdot\frac{watt}{m^2}\cdot\left(1 + 0.033\cdot\cos\left(360\cdot\frac{n}{365}\cdot deg\right)\right)$$

Determine beam solar radiation:

$$I_{b_{it,iw}} := \left(I_{on}\cdot\tau_{b_{it}}\cdot\cos\left(\theta_{it,iw}\right)\right)$$

..incident beam radiation on walls

$$I_{br1_{it}} := \left(I_{on}\cdot\tau_{rb1_{it}}\cdot\cos\left(\theta_{r1_{it}}\right)\right)$$

$$I_{br2_{it}} := \left(I_{on}\cdot\tau_{rb2_{it}}\cdot\cos\left(\theta_{r2_{it}}\right)\right)$$

Incident solar radiation on exterior walls and transmitted by windows

Extraterrestrial normal solar radiation: $I_{on} := 1353 \cdot \frac{watt}{m^2} \cdot \left(1 + 0.033 \cdot \cos\left(360 \cdot \frac{n}{365} \cdot deg \right) \right)$

Determine beam solar radiation: $I_{b_{it,iw}} := \left(I_{on} \cdot \tau_{b_{it}} \cdot \cos\left(\theta_{it,iw} \right) \right)$ ..incident beam radiation on

$I_{br1_{it}} := \left(I_{on} \cdot \tau_{rb1_{it}} \cdot \cos\left(\theta_{r1_{it}} \right) \right)$

$I_{br2_{it}} := \left(I_{on} \cdot \tau_{rb2_{it}} \cdot \cos\left(\theta_{r2_{it}} \right) \right)$

$G_{b_{it,iw}} := I_{b_{it,iw}} \cdot \tau_{e_{it,iw}}$ ..transmitted beam radiation

$\tau_{ed_{iw}} := \tau_{e_{7,1}}$ ..approximate value for diffuse transmittance (equal for all windows) equal to beam transmittance for θ=60deg $\theta_{7,1} = 59.379deg$

Incident instantaneous sky diffuse radiation on the walls,windows and roof

$$I_{ds_{it}} := I_{on} \cdot \sin\left(\alpha_{it}\right) \cdot \left(0.2710 - 0.2939 \tau_{b_{it}} \right) \cdot \frac{1 + \cos\left(\beta\right)}{2}$$

$$I_{dsr1_{it}} := I_{on} \cdot \sin\left(\alpha_{it}\right) \cdot \left(0.2710 - 0.2939 \tau_{rb1_{it}} \right) \cdot \frac{1 + \cos\left(\beta_{roof\_1}\right)}{2}$$

$$I_{dsr2_{it}} := I_{on} \cdot \sin\left(\alpha_{it}\right) \cdot \left(0.2710 - 0.2939 \tau_{rb2_{it}} \right) \cdot \frac{1 + \cos\left(\beta_{roof\_2}\right)}{2}$$

Incident instantaneous ground reflected radiation on the walls,windows and roof

$$I_{dg_{it}} := \left[I_{on} \cdot \sin\left(\alpha_{it}\right) \cdot \left(0.2710 - 0.2939 \tau_{b_{it}} + \tau_{b_{it}} \right) \right] \cdot \rho_g \cdot \frac{1 - \cos\left(\beta\right)}{2}$$

$$I_{dgr1_{it}} := \left[I_{on} \cdot \sin\left(\alpha_{it}\right) \cdot \left(0.2710 - 0.2939 \tau_{rb1_{it}} + \tau_{rb1_{it}} \right) \right] \cdot \rho_g \cdot \frac{1 - \cos\left(\beta_{roof\_1}\right)}{2}$$

$$I_{dgr2_{it}} := \left[I_{on} \cdot \sin\left(\alpha_{it}\right) \cdot \left(0.2710 - 0.2939 \tau_{rb2_{it}} + \tau_{rb2_{it}} \right) \right] \cdot \rho_g \cdot \frac{1 - \cos\left(\beta_{roof\_2}\right)}{2}$$

Total instantaneous solar irradiation incident on walls, windows and roof:

$I_{it,iw} := I_{b_{it,iw}} + I_{ds_{it}} + I_{dg_{it}}$ $I_{1_{it,7}} := I_{br1_{it}} + I_{dsr1_{it}} + I_{dgr1_{it}}$

$I_{2_{it,7}} := I_{br2_{it}} + I_{dsr2_{it}} + I_{dgr2_{it}}$

Transmited solar radiation through windows

$$Gd_{it,iw} := \tau ed_{iw} \cdot \left(Ids_{it} + Idg_{it} \right)$$ .. transmitted diffuse irradiation (instantaneous)

$$Gb_{it,iw} := Ib_{it,iw} \cdot \tau e_{it,iw}$$ ..beam transmitted solar radiation

$$G_{it,iw} := Gb_{it,iw} + Gd_{it,iw}$$ Total instantaneous solar radiation transmitted by windows:

$$Gt_{it} := \sum_{iw} G_{it,iw} \cdot Aw_{iw}$$ Total instantaneous solar radiation transmitted through all windows:

Solar radiation absorbed by room surfaces:

$$S_{it,si} := 0.3 \cdot Gt_{it} \cdot \frac{A_{si}}{\sum_{si} A_{si}}$$

Floor: $$S_{it,6} := 0.7 \cdot Gt_{it}$$

Roof: $$S1_{it,7} := \alpha r1_{it} \cdot I1_{it,7} \cdot Apv1$$

$$S1\_2_{it,7} := \alpha pv \cdot \tau r1_{it} \cdot I1_{it,7} \cdot Apv1$$

$$S2_{it,7} := \alpha r2_{it} \cdot I2_{it,7} \cdot \frac{Apv2}{2}$$

$$S2\_2_{it,7} := \alpha pv \cdot \tau r2_{it} \cdot I2_{it,7} \cdot \frac{Apv2}{2}$$

$$S3_{it,7} := \alpha pv \cdot I2_{it,7} \cdot Anpv$$

Total Incident Solar Radiation:

$$St1_{it,7} := I1_{it,7} \cdot Apv1$$

$$St2_{it,7} := I2_{it,7} \cdot \frac{Apv2}{2}$$

Absorbed solar radiation by exterior surfaces, outer and inner glazing

$$Sse_{it,iw} := \alpha si_{iw} \cdot I_{it,iw} \cdot A_{iw}$$ walls

$$Stao_{it,iw} := \left[\alpha o_{it,iw} \cdot Ib_{it,iw} + \alpha o_{8,iw} \cdot \left(Ids_{it} + Idg_{it} \right) \right] \cdot Aw_{iw} + \alpha i_{8,iw} \cdot 0.3 \cdot \left(Gt_{it} - G_{it,iw} \cdot Aw_{iw} \right)$$

$$Stai_{it,iw} := \left[\alpha i_{it,iw} \cdot Ib_{it,iw} + \alpha i_{8,iw} \cdot \left(Ids_{it} + Idg_{it} \right) \right] \cdot Aw_{iw} + \alpha o_{8,iw} \cdot 0.3 \cdot \left(Gt_{it} - G_{it,iw} \cdot Aw_{iw} \right)$$

APPENDIX C: Thermal Network

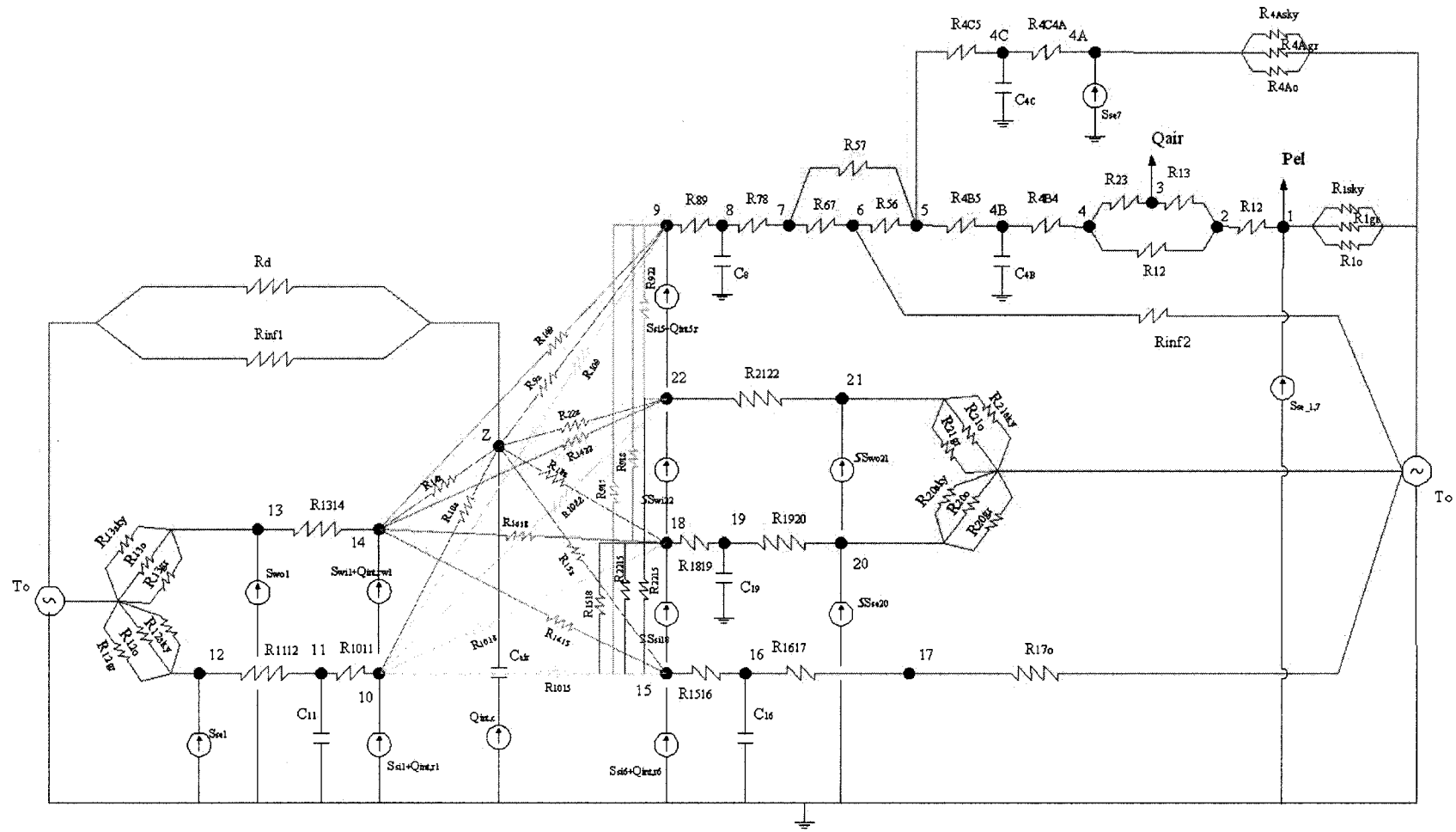

Figure C.1: Thermal network of Configuration 1

Legend

1 – Exterior surface of the PV panels

2 – Interior surface of the PV panels

3 – Mean air temperature in the PV cavity

4,4A – Exterior surface of the roof

4B, 4C - Thermal capacitance of the roof

5 - Interior surface of the roof

6 – Attic air

7 – Exterior surface of the ceiling

8 – Gypsum board

9 – Interior surface of the ceiling

10 – Interior surface of the south wall

11 – Gypsum board

12 – Exterior surface of the south wall

13 - Outer glazing of the south window

14 – Inner glazing of the south window

15 – Floor

16 – Concrete block

17 – Exterior floor surface

18 – Interior surface of the North, East, West wall

19 – Gypsum board

20 – Exterior surface of the North, East, West wall

21 - Outer glazing of the North, East, West window

22 - Inner glazing of the North, East, West window

Z – Zone air

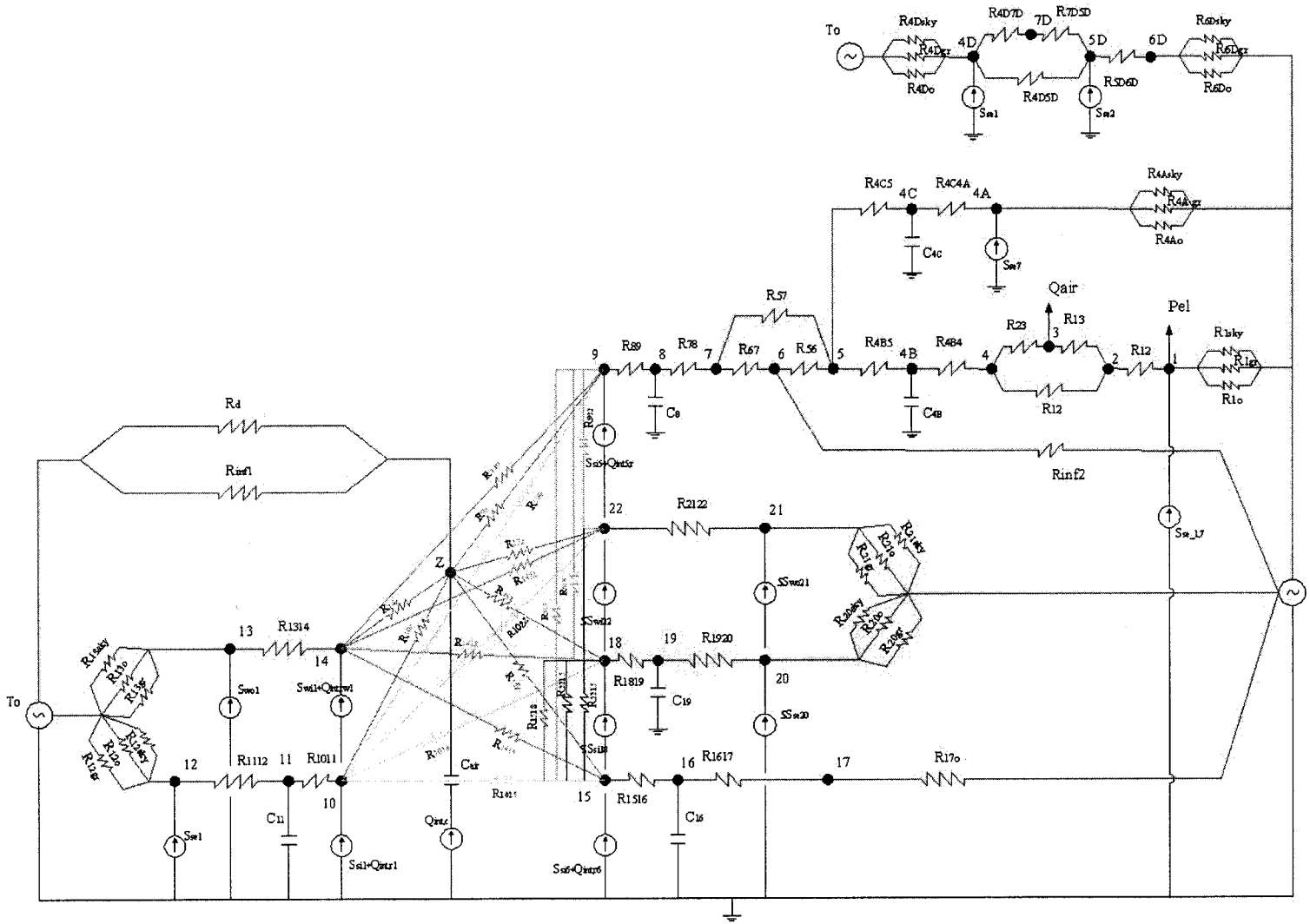

Figure C.2: Thermal network of Configuration 2

Legend

4D – Glass cover

5D – Absorber

6D – Back side of the absorber

7D – Mean air temperature

Description for other nodes is the same as those for Configuration 1.

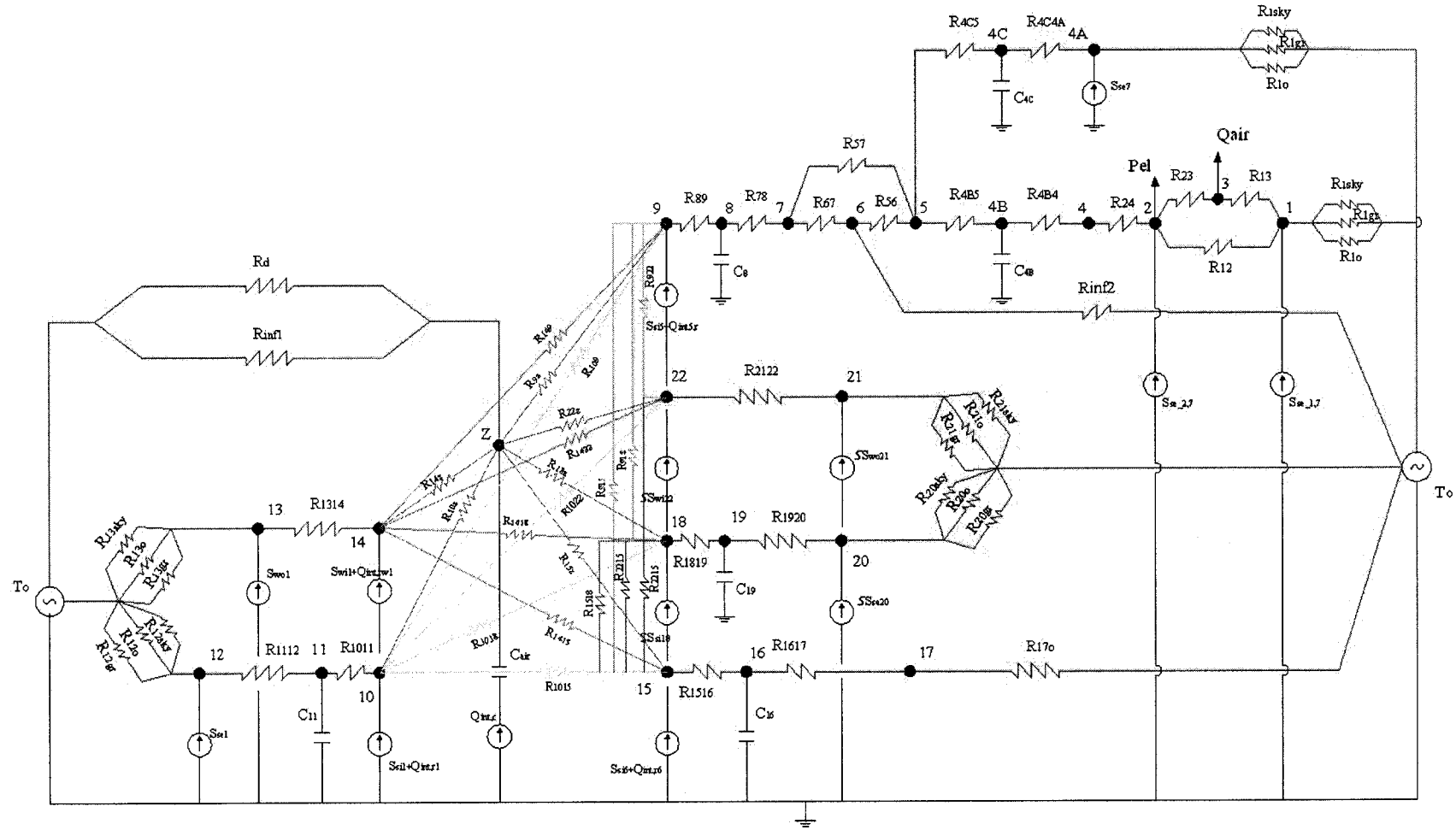

Figure C.3: Thermal network of Configuration 3

Legend

1 – Glass cover

2 – Exterior surface of the PV panels

3 – Mean air temperature in the PV cavity

4– Interior surface of the PV panels

4A, 4B - Thermal capacitance of the roof

5 - Interior surface of the roof

6 – Attic air

7 – Exterior surface of the ceiling

8 – Gypsum board

9 – Interior surface of the ceiling

10 – Interior surface of the south wall

11 – Gypsum board

12 – Exterior surface of the south wall

13 - Outer glazing of the south window

14 – Inner glazing of the south window

15 – Floor

16 – Concrete block

17 – Exterior floor surface

18 – Interior surface of the North, East, West wall

19 – Gypsum board

20 – Exterior surface of the North, East, West wall

21 - Outer glazing of the North, East, West window

22 - Inner glazing of the North, East, West window

Z – Zone air

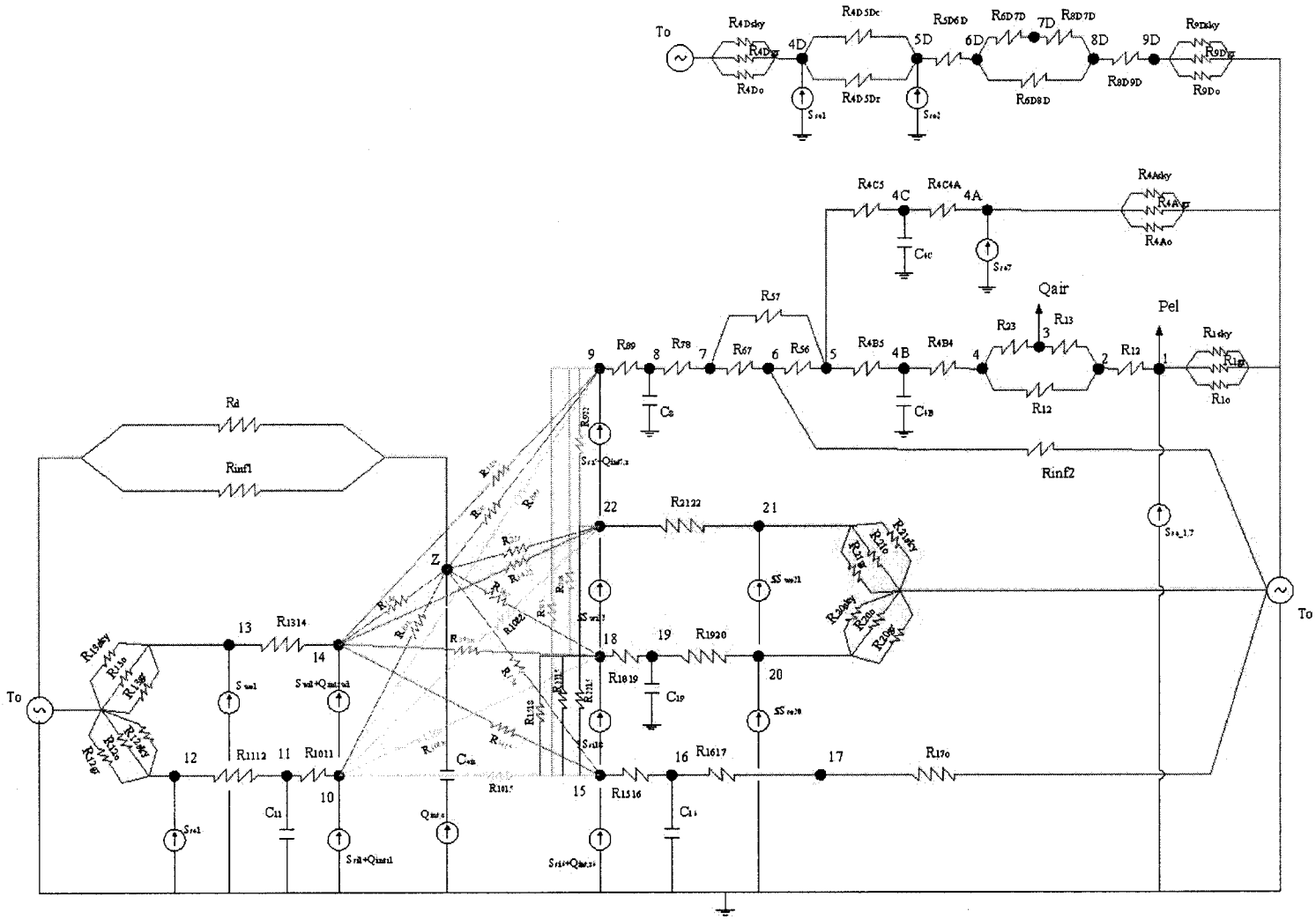

Figure C.4: Thermal network of Configuration 4

Legend

4D – Glass cover (with low-emissivity coating)

5D – Exterior side of the absorber

6D – Back side of the absorber

7D – Mean air temperature

8D – Exterior side of insulation

9D – Interior side of insulation

Description for other nodes is the same as those for Configuration 2.

APPENDIX D: Calculation of the View Factors

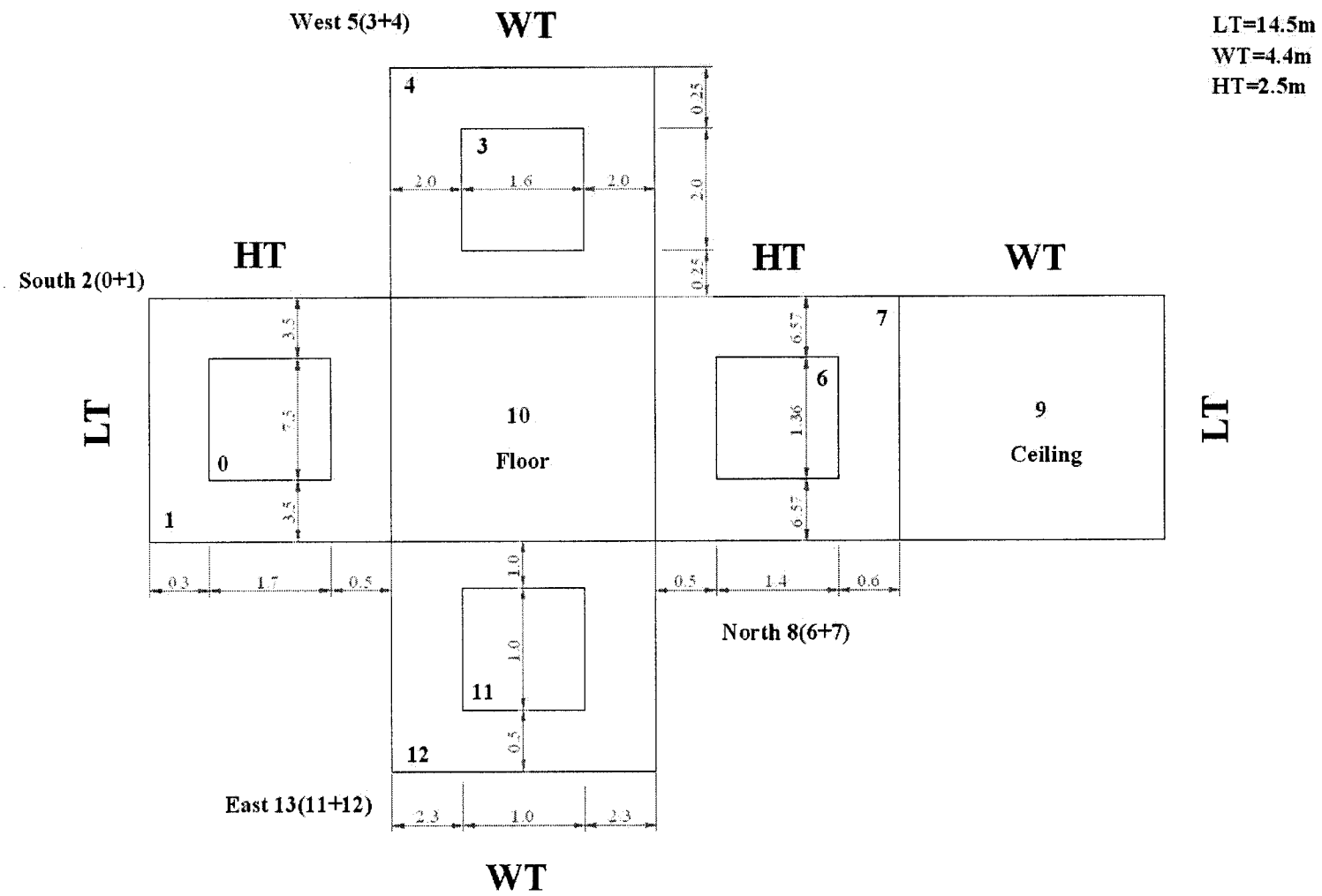

Figure D.1: Layout of the solar house interior

Zone dimensions:

$Hh := 2.5m$ ...height $Wh := 4.4m$ ... width $Lh := 14.5m$ ... length

$A_2 := Lh \cdot Hh$ $A_8 := A_2$ $A_5 := Wh \cdot Hh$ $A_{13} := A_5$ $A_{10} := Wh \cdot Lh$ $A_9 := A_{10}$

Windows:

$a_0 := 7.5m$ $b_0 := 1.7m$ $A_0 := a_0 \cdot b_0$

$a_3 := 1.6m$ $b_3 := 2.0m$ $A_3 := a_3 \cdot b_3$

$a_{11} := 1.0m$ $b_{11} := 1.0m$ $A_{11} := a_{11} \cdot b_{11}$

$a_6 := 1.4m$ $b_6 := 1.36m$ $A_6 := a_6 \cdot b_6$

Walls without windows:

$A_1 := A_2 - A_0$ $A_4 := A_5 - A_3$ $A_{12} := A_{13} - A_{11}$ $A_7 := A_8 - A_6$

Calculation of view factors between all surfaces Fij

The view factor between two identical opposed rectangles

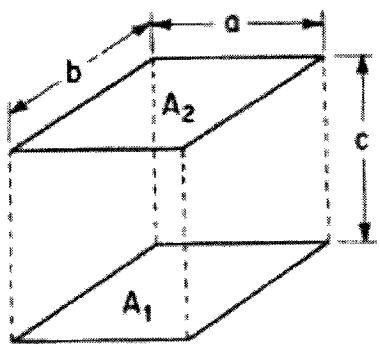

$$x = \frac{a}{c}$$

$$y = \frac{b}{c}$$

$$Fij(x,y) := \frac{2}{\pi \cdot x \cdot y} \cdot \left[\ln\left[\sqrt{\frac{\left(1+x^2\right)\cdot\left(1+y^2\right)}{1+x^2+y^2}} \right] + x\cdot\sqrt{1+y^2}\cdot\operatorname{atan}\left(\frac{x}{\sqrt{1+y^2}}\right) \ldots \right.$$
$$\left. + y\cdot\sqrt{1+x^2}\cdot\operatorname{atan}\left(\frac{y}{\sqrt{1+x^2}}\right) - x\cdot\operatorname{atan}(x) - y\cdot\operatorname{atan}(y) \right]$$

The view factor between surfaces at right angle

The view factor between surfaces at right angle

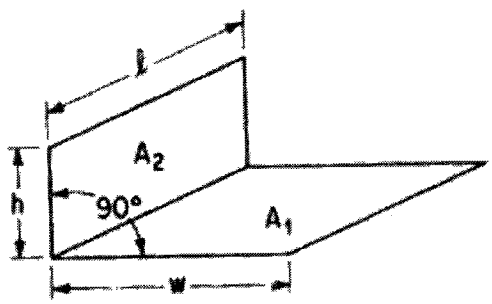

$$w = \frac{w1}{comm}$$

$$h = \frac{h2}{comm}$$

$$A\_a(h,w) := h^2 + w^2 \qquad B(w) := 1 + w^2 \qquad C(h) := 1 + h^2$$

$$D(h,w) := 1 + \left(h^2 + w^2\right) \qquad E(w) := w^2 \qquad G(h) := h^2$$

$$F12(w,h) := \frac{\left(w\cdot\operatorname{atan}\left(\frac{1.}{w}\right) + h\cdot\operatorname{atan}\left(\frac{1}{h}\right)\right) - \sqrt{A\_a(h,w)}\cdot\operatorname{atan}\left(\frac{1}{\sqrt{A\_a(h,w)}}\right) \ldots + 0.25\cdot\ln\left[\left(\frac{E(w)\cdot D(h,w)}{B(w)\cdot A\_a(h,w)}\right)^{E(w)}\cdot\left(\frac{G(h)\cdot D(h,w)}{C(h)\cdot A\_a(h,w)}\right)^{G(h)}\cdot\frac{B(w)\cdot C(h)}{D(h,w)}\right]}{\pi\cdot w}$$

VIEW FACTORS BETWEEN WEST AND EAST WALL

$a := Wh \qquad b := Hh \qquad c := Lh \qquad x := \frac{a}{c} \qquad y := \frac{b}{c}$

$F_{5,13} := Fij(x,y) \qquad F_{5,13} = 0.02 \qquad F_{13,5} := F_{5,13}$

VIEW FACTORS BETWEEN NORTH AND SOUTH WALL

$a := Hh \qquad b := Lh \qquad c := Wh \qquad x := \frac{a}{c} \qquad y := \frac{b}{c}$

$F_{2,8} := Fij(x,y) \qquad F_{2,8} = 0.162 \qquad F_{8,2} := F_{2,8}$

VIEW FACTORS BETWEEN FLOOR AND CEILING

$a := Wh \quad b := Lh \quad c := Hh \quad x := \frac{a}{c} \quad y := \frac{b}{c}$

$F_{9,10} := Fij(x,y) \quad F_{10,9} := F_{9,10}$

VIEW FACTORS BETWEEN FLOOR/CEILING AND NORTH/SOUTH WALL

$w1 := Wh \quad h2 := Hh \quad comm := Lh \quad w := \frac{w1}{comm} \quad h := \frac{h2}{comm}$

$F_{10,2} := F12(w,h) \quad F_{10,2} = 0.159 \quad F_{2,10} := \frac{F_{10,2}}{A_2} \cdot A_{10} \quad F_{2,10} = 0.357$

$F_{2,9} := F_{2,10} \quad F_{8,10} := F_{2,10} \quad F_{8,9} := F_{8,10} \quad F_{10,8} := F_{10,2} \quad F_{9,2} := \frac{A_2}{A_9} \cdot F_{2,9} \quad F_{9,2} := F_{9,8}$

VIEW FACTORS BETWEEN WEST/EAST AND NORTH/SOUTH WALL

$w1 := Lh \quad h2 := Wh \quad comm := Hh \quad w := \frac{w1}{comm} \quad h := \frac{h2}{comm}$

$F_{8,13} := F12(w,h) \quad F_{13,8} := A_8 \cdot \frac{F_{8,13}}{A_{13}} \quad F_{8,5} := F_{8,13} \quad F_{5,8} := F_{13,8} \quad F_{2,13} := F_{8,5}$

$F_{2,5} := F_{8,5} \quad F_{5,2} := F_{5,8} \quad F_{13,8} := F_{5,2} \quad F_{2,5} := F_{2,13} \quad F_{5,8} := F_{13,2} \quad F_{13,2} := F_{5,8}$

VIEW FACTORS BETWEEN WEST/EAST WALL AND FLOOR/CEILING

$w1 := Hh \quad h2 := Lh \quad comm := Wh \quad w := \frac{w1}{comm} \quad h := \frac{h2}{comm}$

$F_{5,9} := F12(w,h) \quad F_{5,10} := F_{5,9} \quad F_{9,5} := \frac{A_5}{A_9} \cdot F_{5,9} \quad F_{10,5} := \frac{A_5}{A_{10}} \cdot F_{5,10} \quad F_{10,13} := F_{10,5}$

$F_{13,10} := \frac{A_{10}}{A_{13}} \cdot F_{10,13} \quad F_{13,9} := F_{13,10} \quad F_{9,13} := \frac{A_{13}}{A_9} \cdot F_{13,9}$

SOUTH

View factor between south window-floor and window-ceiling

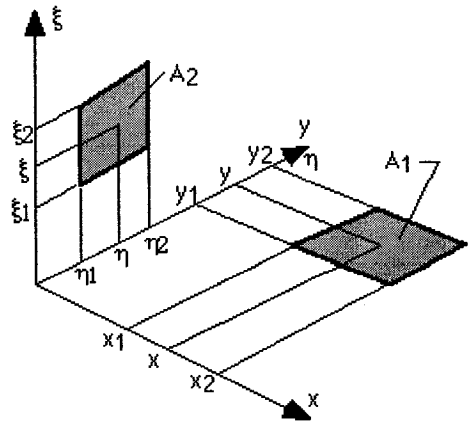

$x_1 := 0 \qquad x_2 := 5.6$

$y_1 := 0 \qquad y_2 := 14.5$

$\eta_1 := 3.5 \qquad \eta_2 := 11.($

$\zeta_1 := 0.5 \qquad \zeta_2 := 2.2$

$$G(1,i,k,j) := \frac{1}{2\cdot\pi}\cdot\left[\begin{array}{l}\left(y_j-\eta_k\right)\cdot\left[\left(x_i\right)^2+\left(\zeta_l\right)^2\right]^{0.5}\cdot\operatorname{atan}\left[\frac{y_j-\eta_k}{\left[\left(x_i\right)^2+\left(\zeta_l\right)^2\right]^{0.5}}\right]\ldots \\ +\ldots.-\frac{1}{4}\cdot\left[\left(x_i\right)^2+\left(\zeta_k\right)^2-\left(y_j-\eta_k\right)^2\right]\cdot\ln\left[\left(x_i\right)^2+\left(\zeta_l\right)^2+\left(y_j-\eta_k\right)^2\right]\end{array}\right]$$

$$F_{10,0} := \frac{1}{\left(x_2-x_1\right)\cdot\left(y_2-y_1\right)}\cdot\sum_{i=1}^{2}\sum_{j=1}^{2}\sum_{k=1}^{2}\sum_{l=1}^{2}\left[(-1)^{(i+j+k+l)}\cdot G(1,i,k,j)\right]$$

$$F_{0,10} := \frac{A_{10}}{A_0}\cdot F_{10,0} \qquad F_{0,9} := F_{0,10} \qquad F_{9,0} := F_{10,0}$$

$$F_{10,1} := F_{10,2} - F_{10,0} \qquad F_{1,10} := \frac{A_{10}}{A_1}\cdot F_{10,1} \qquad F_{1,9} := F_{1,10}$$

View factor between south window- west window

$x_1 := 2.0 \qquad x_2 := 3.6$

$y_1 := 0.25 \qquad y_2 := 2.25$

$\eta_1 := 0.5 \qquad \eta_2 := 2.2$

$\zeta_1 := 3.5 \qquad \zeta_2 := 11.0$

$$G(1,i,k,j) := \frac{1}{2\cdot\pi}\cdot\left[\begin{array}{l}\left(y_j-\eta_k\right)\cdot\left[\left(x_i\right)^2+\left(\zeta_l\right)^2\right]^{0.5}\cdot\operatorname{atan}\left[\dfrac{y_j-\eta_k}{\left[\left(x_i\right)^2+\left(\zeta_l\right)^2\right]^{0.5}}\right]\ldots \\ +\ldots.-\dfrac{1}{4}\cdot\left[\left(x_i\right)^2+\left(\zeta_k\right)^2-\left(y_j-\eta_k\right)^2\right]\cdot\ln\left[\left(x_i\right)^2+\left(\zeta_l\right)^2+\left(y_j-\eta_k\right)^2\right]\end{array}\right]$$

$$F_{3,0} := \frac{1}{\left(x_2-x_1\right)\cdot\left(y_2-y_1\right)}\cdot\sum_{i=1}^{2}\sum_{j=1}^{2}\sum_{k=1}^{2}\sum_{l=1}^{2}\left[(-1)^{(i+j+k+l)}\cdot G(1,i,k,j)\right]$$

$$F_{0,3} := \frac{A_3}{A_0}\cdot F_{3,0} \qquad F_{2,4} := F_{2,5}-F_{2,3} \qquad F_{4,2} := \frac{A_2}{A_4}\cdot F_{2,4}$$

View factor between south window- west wall

$x_1 := 0 \qquad x_2 := 5.6$

$y_1 := 0 \qquad y_2 := 2.5$

$\eta_1 := 0.5 \qquad \eta_2 := 2.2$

$\zeta_1 := 3.5 \qquad \zeta_2 := 11.0$

$$G(1,i,k,j) := \frac{1}{2\cdot\pi}\cdot\left[\begin{array}{l}\left(y_j-\eta_k\right)\cdot\left[\left(x_i\right)^2+\left(\zeta_l\right)^2\right]^{0.5}\cdot\operatorname{atan}\left[\dfrac{y_j-\eta_k}{\left[\left(x_i\right)^2+\left(\zeta_l\right)^2\right]^{0.5}}\right]\ldots \\ +\ldots.-\dfrac{1}{4}\cdot\left[\left(x_i\right)^2+\left(\zeta_k\right)^2-\left(y_j-\eta_k\right)^2\right]\cdot\ln\left[\left(x_i\right)^2+\left(\zeta_l\right)^2+\left(y_j-\eta_k\right)^2\right]\end{array}\right]$$

View factor between south window- north window

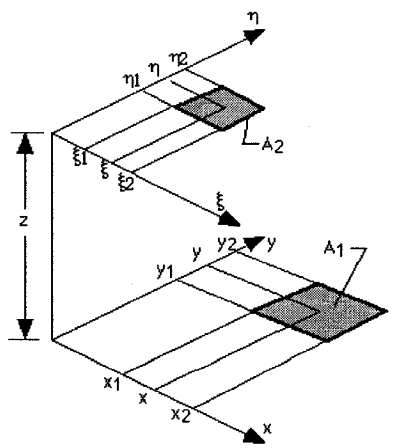

$x_1 := 0.5 \quad x_2 := 1.9$

$y_1 := 6.57 \quad y_2 := 7.93$

$\eta_1 := 3.5 \quad \eta_2 := 11.0$

$\zeta_1 := 0.5 \quad \zeta_2 := 2.2$

$z := 5.6$

$$G(l,i,k,j) := \frac{1}{2\cdot\pi}\cdot\left[\begin{array}{l}\left(y_j-\eta_k\right)\cdot\left[\left(x_i-\zeta_l\right)^2+z^2\right]^{0.5}\cdot\left[\operatorname{atan}\left[\frac{y_j-\eta_k}{\left[\left(x_i-\zeta_l\right)^2+z^2\right]^{0.5}}\right]+\left(x_i-\zeta_l\right)\cdot\left[\left(y_j-\eta_k\right)^2+z^2\right]^{0.5}\right]\ldots \\ +\ldots:\operatorname{atan}\left[\frac{x_i-\zeta_l}{\left[\left(y_j-\eta_k\right)^2+z^2\right]^{0.5}}\right]-\frac{z^2}{2}\cdot\ln\left[\left(x_i-\zeta_l\right)^2+\left(y_j-\eta_k\right)^2+z^2\right]\end{array}\right]$$

$$F_{6,0} := \frac{1}{\left(x_2-x_1\right)\cdot\left(y_2-y_1\right)}\cdot\sum_{i=1}^{2}\sum_{j=1}^{2}\sum_{k=1}^{2}\sum_{l=1}^{2}\left[(-1)^{(i+j+k+l)}\cdot G(l,i,k,j)\right] \qquad F_{0,6} := \frac{A_6}{A_0}\cdot F_{6,0}$$

$$F_{9,1} := F_{10,1}$$

View factor between south window- north wall

$x_1 := 0 \qquad x_2 := 2.5$

$y_1 := 0 \qquad y_2 := 14.5$

$\eta_1 := 3.5 \qquad \eta_2 := 11.0$

$\zeta_1 := 0.5 \qquad \zeta_2 := 2.2$

$z := 5.6$

$$G(l,i,k,j) := \frac{1}{2\cdot\pi}\cdot\left[\left[\left(y_j-\eta_k\right)\cdot\left[\left(x_i-\zeta_l\right)^2+z^2\right]^{0.5}\cdot\operatorname{atan}\left[\frac{y_j-\eta_k}{\left[\left(x_i-\zeta_l\right)^2+z^2\right]^{0.5}}\right]+\left(x_i-\zeta_l\right)\cdot\left[\left(y_j-\eta_k\right)^2+z^2\right]^{0.5}\right]\ldots\right.$$
$$\left.+\ldots\operatorname{atan}\left[\frac{x_i-\zeta_l}{\left[\left(y_j-\eta_k\right)^2+z^2\right]^{0.5}}\right]-\frac{z^2}{2}\cdot\ln\left[\left(x_i-\zeta_l\right)^2+\left(y_j-\eta_k\right)^2+z^2\right]\right]$$

$$F_{8,0} := \frac{1}{\left(x_2-x_1\right)\cdot\left(y_2-y_1\right)}\cdot\sum_{i=1}^{2}\sum_{j=1}^{2}\sum_{k=1}^{2}\sum_{l=1}^{2}\left[(-1)^{(i+j+k+l)}\cdot G(l,i,k,j)\right] \qquad F_{0,8} := \frac{A_8}{A_0}\cdot F_{8,0}$$

$$F_{0,7} := F_{0,8} - F_{0,6} \qquad F_{7,0} := \frac{A_0}{A_7}\cdot F_{0,7}$$

View factor between north window- south wall

$x_1 := 0.5 \qquad x_2 := 1.9$

$y_1 := 6.57 \qquad y_2 := 7.93$

$\eta_1 := 0 \qquad \eta_2 := 14.5$

$\zeta_1 := 0 \qquad \zeta_2 := 2.5$

$z := 5.6$

$$G(l,i,k,j) := \frac{1}{2\cdot\pi}\cdot\left[\left[\left(y_j-\eta_k\right)\cdot\left[\left(x_i-\zeta_l\right)^2+z^2\right]^{0.5}\cdot\operatorname{atan}\left[\frac{y_j-\eta_k}{\left[\left(x_i-\zeta_l\right)^2+z^2\right]^{0.5}}\right]+\left(x_i-\zeta_l\right)\cdot\left[\left(y_j-\eta_k\right)^2+z^2\right]^{0.5}\right]\ldots\right.$$
$$\left.+\ldots\cdot\operatorname{atan}\left[\frac{x_i-\zeta_l}{\left[\left(y_j-\eta_k\right)^2+z^2\right]^{0.5}}\right]-\frac{z^2}{2}\cdot\ln\left[\left(x_i-\zeta_l\right)^2+\left(y_j-\eta_k\right)^2+z^2\right]\right]$$

$$F_{6,2} := \frac{1}{\left(x_2-x_1\right)\cdot\left(y_2-y_1\right)}\cdot\sum_{i=1}^{2}\sum_{j=1}^{2}\sum_{k=1}^{2}\sum_{l=1}^{2}\left[(-1)^{(i+j+k+l)}\cdot G(l,i,k,j)\right] \qquad F_{2,6} := \frac{A_6}{A_2}\cdot F_{6,2}$$

$$F_{2,7} := F_{2,8} - F_{2,6} \qquad F_{7,2} := \frac{A_2}{A_7}\cdot F_{2,7} \qquad F_{8,1} := F_{8,2} - F_{8,0} \qquad F_{1,8} := \frac{A_8}{A_1}\cdot F_{8,1}$$

$$F_{1,6} := \frac{A_6}{A_1}\cdot F_{6,1} \qquad F_{1,7} := F_{1,8} - F_{1,6} \qquad F_{7,1} := \frac{A_1}{A_7}\cdot F_{1,7} \qquad F_{6,1} := F_{6,2} - F_{6,0}$$

WEST

View factor west window-floor/ceiling

$x_1 := 0 \qquad x_2 := 14.5$

$y_1 := 0 \qquad y_2 := 5.6$

$\eta_1 := 2.0 \qquad \eta_2 := 3.6$

$\zeta_1 := 0.25 \qquad \zeta_2 := 2.25$

$$G(l,i,k,j) := \frac{1}{2\cdot\pi}\cdot\left[\left[\left(y_j-\eta_k\right)\cdot\left[\left(x_i\right)^2+\left(\zeta_l\right)^2\right]^{0.5}\cdot\operatorname{atan}\left[\frac{y_j-\eta_k}{\left[\left(x_i\right)^2+\left(\zeta_l\right)^2\right]^{0.5}}\right]\right]\ldots\right.$$
$$\left.+\ldots-\frac{1}{4}\cdot\left[\left(x_i\right)^2+\left(\zeta_k\right)^2-\left(y_j-\eta_k\right)^2\right]\cdot\ln\left[\left(x_i\right)^2+\left(\zeta_l\right)^2+\left(y_j-\eta_k\right)^2\right]\right]$$

$$F_{10,3} := \frac{1}{\left(x_2-x_1\right)\cdot\left(y_2-y_1\right)}\cdot\sum_{i=1}^{2}\sum_{j=1}^{2}\sum_{k=1}^{2}\sum_{l=1}^{2}\left[(-1)^{(i+j+k+l)}\cdot G(l,i,k,j)\right]$$

$$F_{3,10} := \frac{A_{10}}{A_3} \cdot F_{10,3} \qquad F_{3,9} := F_{3,10} \qquad F_{9,3} := \frac{A_3}{A_9} \cdot F_{3,9}$$

View factor west window- north window

$x_1 := 6.57 \qquad x_2 := 7.93$

$y_1 := 0.5 \qquad y_2 := 1.9$

$\eta_1 := 0.25 \qquad \eta_2 := 2.25$

$\zeta_1 := 2.0 \qquad \zeta_2 := 3.6$

$$G(l,i,k,j) := \frac{1}{2\cdot\pi} \cdot \left[\begin{array}{l} \left[\left(y_j - \eta_k\right) \cdot \left[\left(x_i\right)^2 + \left(\zeta_l\right)^2 \right]^{0.5} \cdot \operatorname{atan}\left[\frac{y_j - \eta_k}{\left[\left(x_i\right)^2 + \left(\zeta_l\right)^2 \right]^{0.5}} \right] \right] \ldots \\ + \ldots - \frac{1}{4} \cdot \left[\left(x_i\right)^2 + \left(\zeta_k\right)^2 - \left(y_j - \eta_k\right)^2 \right] \cdot \ln\left[\left(x_i\right)^2 + \left(\zeta_l\right)^2 + \left(y_j - \eta_k\right)^2 \right] \end{array} \right]$$

$$F_{6,3} := \frac{1}{\left(x_2 - x_1\right)\cdot\left(y_2 - y_1\right)} \cdot \sum_{i=1}^{2} \sum_{j=1}^{2} \sum_{k=1}^{2} \sum_{l=1}^{2} \left[(-1)^{(i+j+k+l)} \cdot G(l,i,k,j) \right] \qquad F_{3,6} := \frac{A_6}{A_3} \cdot F_{6,3}$$

View factor west window- north wall

$x_1 := 0 \qquad x_2 := 14.5$

$y_1 := 0 \qquad y_2 := 2.5$

$\eta_1 := 0.25 \qquad \eta_2 := 2.25$

$\zeta_1 := 2.0 \qquad \zeta_2 := 3.6$

$$G(l,i,k,j) := \frac{1}{2\cdot\pi} \cdot \left[\begin{array}{l} \left[\left(y_j - \eta_k\right) \cdot \left[\left(x_i\right)^2 + \left(\zeta_l\right)^2 \right]^{0.5} \cdot \operatorname{atan}\left[\frac{y_j - \eta_k}{\left[\left(x_i\right)^2 + \left(\zeta_l\right)^2 \right]^{0.5}} \right] \right] \ldots \\ + \ldots . - \frac{1}{4} \cdot \left[\left(x_i\right)^2 + \left(\zeta_k\right)^2 - \left(y_j - \eta_k\right)^2 \right] \cdot \ln\left[\left(x_i\right)^2 + \left(\zeta_l\right)^2 + \left(y_j - \eta_k\right)^2 \right] \end{array} \right]$$

$$F_{8,3} := \frac{1}{(x_2 - x_1)\cdot(y_2 - y_1)} \cdot \sum_{i=1}^{2}\sum_{j=1}^{2}\sum_{k=1}^{2}\sum_{l=1}^{2}\left[(-1)^{(i+j+k+l)}\cdot G(l,i,k,j)\right] \qquad F_{3,8} := \frac{A_8}{A_3}\cdot F_{8,3}$$

$$F_{8,4} := F_{8,5} - F_{8,3} \quad F_{4,8} := \frac{A_8}{A_4}\cdot F_{8,4} \quad F_{3,7} := F_{3,8} - F_{3,6} \quad F_{7,3} := \frac{A_3}{A_7}\cdot F_{3,7}$$

View factor between west window- east window

$x_1 := 1.0 \quad x_2 := 2.0$

$y_1 := 2.3 \quad y_2 := 3.3$

$\eta_1 := 2.0 \quad \eta_2 := 3.6$

$\zeta_1 := 0.25 \quad \zeta_2 := 2.25$

$z := 14.5$

$$G(l,i,k,j) := \frac{1}{2\cdot\pi}\cdot\left[\left[\left(y_j - \eta_k\right)\cdot\left[\left(x_i - \zeta_l\right)^2 + z^2\right]^{0.5}\cdot\operatorname{atan}\left[\frac{y_j - \eta_k}{\left[\left(x_i - \zeta_l\right)^2 + z^2\right]^{0.5}}\right] + \left(x_i - \zeta_l\right)\cdot\left[\left(y_j - \eta_k\right)^2 + z^2\right]^{0.5}\right]\ldots\right.$$
$$\left. + \blacksquare\cdot\operatorname{atan}\left[\frac{x_i - \zeta_l}{\left[\left(y_j - \eta_k\right)^2 + z^2\right]^{0.5}}\right] - \frac{z^2}{2}\cdot\ln\left[\left(x_i - \zeta_l\right)^2 + \left(y_j - \eta_k\right)^2 + z^2\right]\right]$$

$$F_{11,3} := \frac{1}{(x_2 - x_1)\cdot(y_2 - y_1)} \cdot \sum_{i=1}^{2}\sum_{j=1}^{2}\sum_{k=1}^{2}\sum_{l=1}^{2}\left[(-1)^{(i+j+k+l)}\cdot G(l,i,k,j)\right] \qquad F_{3,11} := \frac{A_{11}}{A_3}\cdot F_{11,3}$$

View factor between west window- east wall

$x_1 := 0 \quad x_2 := 2.5 \quad z := 14.5$

$y_1 := 0 \quad y_2 := 5.6$

$\eta_1 := 2.0 \quad \eta_2 := 3.6$

$\zeta_1 := 0.25 \quad \zeta_2 := 2.25$

$$G(l,i,k,j) := \frac{1}{2\cdot\pi}\cdot\left[\begin{array}{l}\left[\left(y_j-\eta_k\right)\cdot\left[\left(x_i-\zeta_l\right)^2+z^2\right]^{0.5}\cdot\operatorname{atan}\left[\frac{y_j-\eta_k}{\left[\left(x_i-\zeta_l\right)^2+z^2\right]^{0.5}}\right]+\left(x_i-\zeta_l\right)\cdot\left[\left(y_j-\eta_k\right)^2+z^2\right]^{0.5}\right]\ldots \\ +\ldots.\operatorname{atan}\left[\frac{x_i-\zeta_l}{\left[\left(y_j-\eta_k\right)^2+z^2\right]^{0.5}}\right]-\frac{z^2}{2}\cdot\ln\left[\left(x_i-\zeta_l\right)^2+\left(y_j-\eta_k\right)^2+z^2\right]\end{array}\right]$$

$$F_{13,3} := \frac{1}{\left(x_2-x_1\right)\cdot\left(y_2-y_1\right)}\cdot\sum_{i=1}^{2}\sum_{j=1}^{2}\sum_{k=1}^{2}\sum_{l=1}^{2}\left[(-1)^{(i+j+k+l)}\cdot G(l,i,k,j)\right] \qquad F_{3,13} := \frac{A_{13}}{A_3}\cdot F_{13,3}$$

$$F_{3,12} := F_{3,13} - F_{3,11} \qquad F_{12,3} := \frac{A_3}{A_{12}}\cdot F_{3,12} \qquad F_{13,4} := F_{13,5} - F_{13,3} \qquad F_{4,13} := \frac{A_{13}}{A_4}\cdot F_{13,4}$$

View factor between west window- south wall

$$F_{3,2} := F_{3,8} \qquad F_{2,3} := \frac{A_3}{A_2}\cdot F_{3,2} \qquad F_{3,1} := F_{3,2} - F_{3,0} \qquad F_{1,3} := \frac{A_3}{A_1}\cdot F_{3,1} \qquad F_{1,4} := \frac{A_4}{A_1}\cdot F_{4,1}$$

EAST

View factor east window-floor/ceiling

$x_1 := 0 \qquad x_2 := 14.5$

$y_1 := 0 \qquad y_2 := 5.6$

$\eta_1 := 2.3 \qquad \eta_2 := 3.3$

$\zeta_1 := 1.0 \qquad \zeta_2 := 2.0$

$$G(l,i,k,j) := \frac{1}{2\cdot\pi}\cdot\left[\begin{array}{l}\left[\left(y_j-\eta_k\right)\cdot\left[\left(x_i\right)^2+\left(\zeta_l\right)^2\right]^{0.5}\cdot\operatorname{atan}\left[\frac{y_j-\eta_k}{\left[\left(x_i\right)^2+\left(\zeta_l\right)^2\right]^{0.5}}\right]\right]\ldots \\ +\ldots.-\frac{1}{4}\cdot\left[\left(x_i\right)^2+\left(\zeta_k\right)^2-\left(y_j-\eta_k\right)^2\right]\cdot\ln\left[\left(x_i\right)^2+\left(\zeta_l\right)^2+\left(y_j-\eta_k\right)^2\right]\end{array}\right]$$

$$F_{10,11} := \frac{1}{(x_2 - x_1)\cdot(y_2 - y_1)} \cdot \sum_{i=1}^{2}\sum_{j=1}^{2}\sum_{k=1}^{2}\sum_{l=1}^{2}\left[(-1)^{(i+j+k+l)}\cdot G(l,i,k,j)\right]$$

$$F_{11,9} := F_{11,10} \qquad F_{9,11} := \frac{A_{11}}{A_9}\cdot F_{11,9} \qquad F_{11,10} := \frac{A_{10}}{A_{11}}\cdot F_{10,11}$$

View factor east window-west wall

$x_1 := 1.0 \quad x_2 := 2.0$

$y_1 := 2.3 \quad y_2 := 3.3$

$\eta_1 := 0 \quad \eta_2 := 5.6$

$\zeta_1 := 0 \quad \zeta_2 := 2.5$

$z := 14.5$

$$G(l,i,k,j) := \frac{1}{2\cdot\pi}\cdot\left[\left[(y_j - \eta_k)\cdot\left[(x_i - \zeta_l)^2 + z^2\right]^{0.5}\cdot\operatorname{atan}\left[\frac{y_j - \eta_k}{\left[(x_i - \zeta_l)^2 + z^2\right]^{0.5}}\right] + (x_i - \zeta_l)\cdot\left[(y_j - \eta_k)^2 + z^2\right]^{0.5}\right]\ldots\right.$$
$$\left.+\ldots:\operatorname{atan}\left[\frac{x_i - \zeta_l}{\left[(y_j - \eta_k)^2 + z^2\right]^{0.5}}\right] - \frac{z^2}{2}\cdot\ln\left[(x_i - \zeta_l)^2 + (y_j - \eta_k)^2 + z^2\right]\right]$$

$$F_{11,5} := \frac{1}{(x_2 - x_1)\cdot(y_2 - y_1)} \cdot \sum_{i=1}^{2}\sum_{j=1}^{2}\sum_{k=1}^{2}\sum_{l=1}^{2}\left[(-1)^{(i+j+k+l)}\cdot G(l,i,k,j)\right] \qquad F_{5,11} := \frac{A_{11}}{A_5}\cdot F_{11,5}$$

$$F_{11,4} := F_{11,5} - F_{11,3} \qquad F_{4,11} := \frac{A_{11}}{A_4}\cdot F_{11,4} \qquad F_{5,12} := F_{5,13} - F_{5,11} \qquad F_{12,5} := \frac{A_5}{A_{12}}\cdot F_{5,12}$$

$$F_{12,4} := F_{12,5} - F_{12,3} \qquad F_{4,12} := \frac{A_{12}}{A_4}\cdot F_{12,4}$$

View factor east window-south wall

$x_1 := 0 \qquad x_2 := 14.5$

$y_1 := 0 \qquad y_2 := 2.5$

$\eta_1 := 1.0 \qquad \eta_2 := 2.0$

$\zeta_1 := 2.3 \qquad \zeta_2 := 3.3$

$$G(l,i,k,j) := \frac{1}{2\cdot\pi}\cdot\left[\begin{array}{l}\left[\left(y_j-\eta_k\right)\cdot\left[\left(x_i\right)^2+\left(\zeta_l\right)^2\right]^{0.5}\cdot\operatorname{atan}\left[\frac{y_j-\eta_k}{\left[\left(x_i\right)^2+\left(\zeta_l\right)^2\right]^{0.5}}\right]\right]\ldots \\ +\ldots.-\frac{1}{4}\cdot\left[\left(x_i\right)^2+\left(\zeta_k\right)^2-\left(y_j-\eta_k\right)^2\right]\cdot\ln\left[\left(x_i\right)^2+\left(\zeta_l\right)^2+\left(y_j-\eta_k\right)^2\right]\end{array}\right]$$

$$F_{2,11} := \frac{1}{\left(x_2-x_1\right)\cdot\left(y_2-y_1\right)}\cdot\sum_{i=1}^{2}\sum_{j=1}^{2}\sum_{k=1}^{2}\sum_{l=1}^{2}\left[(-1)^{(i+j+k+l)}\cdot G(l,i,k,j)\right] \qquad F_{11,2} := \frac{A_2}{A_{11}}\cdot F_{2,11}$$

$$F_{11,1} := F_{11,2} - F_{11,0} \qquad F_{1,11} := \frac{A_{11}}{A_1}\cdot F_{11,1}$$

View factor east window-north window

$x_1 := 2.3 \qquad x_2 := 3.3$

$y_1 := 1.0 \qquad y_2 := 2.0$

$\eta_1 := 0.5 \qquad \eta_2 := 1.9$

$\zeta_1 := 6.57 \qquad \zeta_2 := 7.93$

$$G(l,i,k,j) := \frac{1}{2\cdot\pi}\cdot\left[\begin{array}{l}\left[\left(y_j-\eta_k\right)\cdot\left[\left(x_i\right)^2+\left(\zeta_l\right)^2\right]^{0.5}\cdot\operatorname{atan}\left[\frac{y_j-\eta_k}{\left[\left(x_i\right)^2+\left(\zeta_l\right)^2\right]^{0.5}}\right]\right]\ldots \\ +\blacksquare-\frac{1}{4}\cdot\left[\left(x_i\right)^2+\left(\zeta_k\right)^2-\left(y_j-\eta_k\right)^2\right]\cdot\ln\left[\left(x_i\right)^2+\left(\zeta_l\right)^2+\left(y_j-\eta_k\right)^2\right]\end{array}\right]$$

$$F_{11,6} := \frac{1}{\left(x_2-x_1\right)\cdot\left(y_2-y_1\right)}\cdot\sum_{i=1}^{2}\sum_{j=1}^{2}\sum_{k=1}^{2}\sum_{l=1}^{2}\left[(-1)^{(i+j+k+l)}\cdot G(l,i,k,j)\right] \qquad F_{6,11} := \frac{A_{11}}{A_6}\cdot F_{11,6}$$

View factor east window-north wall

$$F_{11,8} := F_{11,2} \qquad F_{8,11} := \frac{A_{11}}{A_8} \cdot F_{11,8} \qquad F_{11,7} := F_{11,8} - F_{11,6} \qquad F_{7,11} := \frac{A_{11}}{A_7} \cdot F_{11,7}$$

$$F_{12,1} := F_{13,1} - F_{11,1} \qquad F_{1,12} := \frac{A_{12}}{A_1} \cdot F_{12,1} \qquad F_{12,2} := F_{12,0} + F_{12,1} \qquad F_{2,12} := \frac{A_{12}}{A_2} \cdot F_{12,2}$$

NORTH

View factor north window-floor/ceiling

$$x_1 := 0 \qquad x_2 := 5.6$$

$$y_1 := 0 \qquad y_2 := 14.5$$

$$\eta_1 := 0.5 \qquad \eta_2 := 1.9$$

$$\zeta_1 := 6.57 \qquad \zeta_2 := 7.93$$

$$G(l,i,k,j) := \frac{1}{2\cdot\pi} \cdot \left[\left[\left(y_j - \eta_k\right) \cdot \left[\left(x_i\right)^2 + \left(\zeta_l\right)^2 \right]^{0.5} \cdot \operatorname{atan}\left[\frac{y_j - \eta_k}{\left[\left(x_i\right)^2 + \left(\zeta_l\right)^2 \right]^{0.5}} \right] \right] \ldots \right.$$
$$\left. + \ldots . - \frac{1}{4} \cdot \left[\left(x_i\right)^2 + \left(\zeta_k\right)^2 - \left(y_j - \eta_k\right)^2 \right] \cdot \ln\left[\left(x_i\right)^2 + \left(\zeta_l\right)^2 + \left(y_j - \eta_k\right)^2 \right] \right]$$

$$F_{10,6} := \frac{1}{\left(x_2 - x_1\right)\cdot\left(y_2 - y_1\right)} \cdot \sum_{i=1}^{2} \sum_{j=1}^{2} \sum_{k=1}^{2} \sum_{l=1}^{2} \left[(-1)^{(i+j+k+l)} \cdot G(l,i,k,j) \right] \qquad F_{6,10} := \frac{A_{10}}{A_6} \cdot F_{10,6}$$

$$F_{6,9} := F_{6,10} \qquad F_{9,6} := \frac{A_6}{A_9} \cdot F_{6,9} \qquad F_{7,9} := F_{8,9} - F_{6,9} \qquad F_{9,7} := \frac{A_7}{A_9} \cdot F_{7,9} \qquad F_{7,10} := F_{7,9}$$

$$F_{10,7} := \frac{A_7}{A_{10}} \cdot F_{7,10}$$

View factor north window- south wall

$x_1 := 0.5 \quad x_2 := 1.9 \quad z := 5.6$

$y_1 := 6.57 \quad y_2 := 7.93$

$\eta_1 := 0 \quad \eta_2 := 14.5$

$\zeta_1 := 0 \quad \zeta_2 := 2.5$

$$G(l,i,k,j) := \frac{1}{2\cdot\pi}\cdot\left[\left[\left(y_j-\eta_k\right)\cdot\left[\left(x_i-\zeta_l\right)^2+z^2\right]^{0.5}\cdot\operatorname{atan}\left[\frac{y_j-\eta_k}{\left[\left(x_i-\zeta_l\right)^2+z^2\right]^{0.5}}\right]+\left(x_i-\zeta_l\right)\cdot\left[\left(y_j-\eta_k\right)^2+z^2\right]^{0.5}\right]\ldots\right.$$
$$\left.+\ldots.\operatorname{atan}\left[\frac{x_i-\zeta_l}{\left[\left(y_j-\eta_k\right)^2+z^2\right]^{0.5}}\right]-\frac{z^2}{2}\cdot\ln\left[\left(x_i-\zeta_l\right)^2+\left(y_j-\eta_k\right)^2+z^2\right]\right]$$

$$F_{6,2} := \frac{1}{\left(x_2-x_1\right)\cdot\left(y_2-y_1\right)}\cdot\sum_{i=1}^{2}\sum_{j=1}^{2}\sum_{k=1}^{2}\sum_{l=1}^{2}\left[(-1)^{(i+j+k+l)}\cdot G(l,i,k,j)\right] \qquad F_{2,6} := \frac{A_6}{A_2}\cdot F_{6,2}$$

$F_{6,1} := F_{6,2} - F_{6,0} \qquad F_{1,6} := \frac{A_6}{A_1}\cdot F_{6,1}$

View factor north window- east wall

$x_1 := 0 \quad x_2 := 5.6$

$y_1 := 0 \quad y_2 := 2.5$

$\eta_1 := 0.5 \quad \eta_2 := 1.9$

$\zeta_1 := 6.57 \quad \zeta_2 := 7.93$

$$G(l,i,k,j) := \frac{1}{2\cdot\pi}\cdot\left[\left[\left(y_j-\eta_k\right)\cdot\left[\left(x_i\right)^2+\left(\zeta_l\right)^2\right]^{0.5}\cdot\operatorname{atan}\left[\frac{y_j-\eta_k}{\left[\left(x_i\right)^2+\left(\zeta_l\right)^2\right]^{0.5}}\right]\right]\ldots\right.$$
$$\left.+\ldots.-\frac{1}{4}\cdot\left[\left(x_i\right)^2+\left(\zeta_k\right)^2-\left(y_j-\eta_k\right)^2\right]\cdot\ln\left[\left(x_i\right)^2+\left(\zeta_l\right)^2+\left(y_j-\eta_k\right)^2\right]\right]$$

$$F_{13,6} := \frac{1}{(x_2 - x_1)\cdot(y_2 - y_1)} \cdot \sum_{i=1}^{2} \sum_{j=1}^{2} \sum_{k=1}^{2} \sum_{l=1}^{2} \left[(-1)^{(i+j+k+l)} \cdot G(l,i,k,j) \right] \qquad F_{6,13} := \frac{A_{13}}{A_6} \cdot F_{13,6}$$

$$F_{13,7} := F_{13,8} - F_{13,6} \qquad F_{7,13} := \frac{A_{13}}{A_7} \cdot F_{13,7} \qquad F_{6,12} := F_{6,13} - F_{6,11} \qquad F_{12,6} := \frac{A_6}{A_{12}} \cdot F_{6,12}$$

$$F_{7,12} := F_{7,13} - F_{7,11} \qquad F_{12,7} := \frac{A_7}{A_{12}} \cdot F_{7,12} \qquad F_{12,8} := F_{12,7} + F_{12,6} \qquad F_{8,12} := \frac{A_{12}}{A_8} \cdot F_{12,8}$$

View factor north window- west wall

$$F_{6,5} := F_{6,13} \qquad F_{5,6} := \frac{A_6}{A_5} \cdot F_{6,5} \qquad F_{6,4} := F_{6,5} - F_{6,3} \qquad F_{4,6} := \frac{A_6}{A_4} \cdot F_{6,4}$$

$$F_{4,7} := F_{4,8} - F_{4,6} \qquad F_{7,4} := \frac{A_4}{A_7} \cdot F_{4,7} \qquad F_{7,5} := F_{7,4} + F_{7,3} \qquad F_{5,7} := \frac{A_7}{A_5} \cdot F_{7,5}$$

$$F_{9,12} := F_{9,13} - F_{9,11} \qquad F_{12,9} := \frac{A_9}{A_{12}} \cdot F_{9,12} \qquad F_{12,10} := F_{13,10} - F_{11,10}$$

$$F_{10,12} := \frac{A_{12}}{A_{10}} \cdot F_{12,10} \qquad F_{9,4} := F_{9,5} - F_{9,3} \qquad F_{4,9} := \frac{A_9}{A_4} \cdot F_{9,4}$$

$$F_{10,4} := F_{10,5} - F_{10,3} \qquad F_{4,10} := \frac{A_{10}}{A_4} \cdot F_{10,4} \qquad F_{12,9} := F_{12,10}$$

South

$Fv_{10\_18} := F_{1,7}$ $Fv_{10\_22} := F_{1,6}$ $Fv_{10\_23} := F_{1,4}$ $Fv_{10\_27} := F_{1,3}$ $Fv_{10\_28} := F_{1,1}$

$Fv_{14\_18} := F_{0,7}$ $Fv_{14\_22} := F_{0,6}$ $Fv_{14\_23} := F_{0,4}$ $Fv_{14\_27} := F_{0,3}$ $Fv_{14\_28} := F_{0,1}$

$Fv_{10\_31} := F_{1,11}$ $Fv_{10\_9} := F_{1,9}$ $Fv_{10\_15} := F_{1,10}$

$Fv_{14\_31} := F_{0,11}$ $Fv_{14\_9} := F_{0,9}$ $Fv_{14\_15} := F_{0,10}$

North

$Fv_{18\_10} := F_{7,1}$ $Fv_{18\_14} := F_{7,0}$ $Fv_{18\_23} := F_{7,4}$ $Fv_{18\_27} := F_{7,3}$ $Fv_{18\_28} := F_{7,12}$

$Fv_{22\_10} := F_{6,1}$ $Fv_{22\_14} := F_{6,0}$ $Fv_{22\_23} := F_{6,4}$ $Fv_{22\_27} := F_{6,3}$ $Fv_{22\_28} := F_{6,12}$

$Fv_{18\_31} := F_{7,11}$ $Fv_{18\_9} := F_{7,9}$ $Fv_{18\_15} := F_{7,10}$

$Fv_{22\_31} := F_{6,11}$ $Fv_{22\_9} := F_{6,9}$ $Fv_{22\_15} := F_{6,10}$

West

$Fv_{23\_10} := F_{4,1}$ $Fv_{23\_14} := F_{4,0}$ $Fv_{23\_18} := F_{4,7}$ $Fv_{23\_22} := F_{4,6}$ $Fv_{23\_28} := F_{4}$

$Fv_{27\_10} := F_{3,1}$ $Fv_{27\_14} := F_{3,0}$ $Fv_{27\_18} := F_{3,7}$ $Fv_{27\_22} := F_{3,6}$ $Fv_{27\_28} := F_{3}$

$Fv_{23\_31} := F_{4,11}$ $Fv_{23\_9} := F_{4,9}$ $Fv_{23\_15} := F_{4,10}$

$Fv_{27\_31} := F_{3,11}$ $Fv_{27\_9} := F_{3,9}$ $Fv_{27\_15} := F_{3,10}$

East

$Fv_{28\_10} := F_{12,1}$ $Fv_{28\_14} := F_{12,0}$ $Fv_{28\_18} := F_{12,7}$ $Fv_{28\_22} := F_{12,6}$ $Fv_{28\_23} := F_{12,4}$

$Fv_{31\_10} := F_{11,1}$ $Fv_{31\_14} := F_{11,0}$ $Fv_{31\_18} := F_{11,7}$ $Fv_{31\_22} := F_{11,6}$ $Fv_{31\_23} := F_{11,4}$

$Fv_{28\_27} := F_{12,3}$ $Fv_{28\_9} := F_{12,9}$ $Fv_{28\_15} := F_{12,10}$

$Fv_{31\_27} := F_{11,3}$ $Fv_{31\_9} := F_{11,9}$ $Fv_{31\_15} := F_{11,10}$

Ceiling

$Fv_{9\_10} := F_{9,1}$ $Fv_{9\_14} := F_{9,0}$ $Fv_{9\_18} := F_{9,7}$ $Fv_{9\_22} := F_{9,6}$ $Fv_{9\_23} := F_{9,4}$

$Fv_{9\_27} := F_{9,3}$ $Fv_{9\_28} := F_{9,12}$ $Fv_{9\_31} := F_{9,11}$ $Fv_{9\_15} := F_{9,10}$

Floor

$Fv_{15\_10} := F_{10,1}$ $Fv_{15\_14} := F_{10,0}$ $Fv_{15\_18} := F_{10,7}$ $Fv_{15\_22} := F_{10,6}$ $Fv_{15\_23} := F_{10,4}$

$Fv_{15\_27} := F_{10,3}$ $Fv_{15\_28} := F_{10,12}$ $Fv_{15\_31} := F_{10,11}$ $Fv_{15\_9} := F_{10,9}$

APPENDIX E: Simulation Model

Zone dimensions

$Hh := 2.5 \cdot m$ ...height $Lh := 14.5 \cdot m$ ... length $Wh := 4.4 \cdot m$ ... width

$Hc := 1.7m$ ... attic height

PV roof dimensions

$Lpv := 1.59m$ ...PV panel length

$Wpv := 0.79m$ ...PV panel width

$h_{pv} := 0.04m$ ... PV cavity height

$w_{pv1} := 6 \cdot Lpv - 2.4m$ $w_{pv1} = 7.14\,m$ ...PV cavity width@15 slope

$w_{pv2} := 7 \cdot Lpv - 2.4m$ $w_{pv2} = 8.73\,m$ ...PV cavity width@30 slope

$l_{pv1} := 2 \cdot Wpv$ $l_{pv1} = 1.58\,m$ ... PV cavity length@15 slope

$l_{pv2} := 4 \cdot Wpv$ $l_{pv2} = 3.16\,m$ ... PV cavity length@30 slope

$40 \cdot (Lpv \cdot Wpv) = 50.244\,m^2$ .... Total PV roof area

$A_{pv1} := 12 \cdot Lpv \cdot Wpv - 2 \cdot (1.5 \cdot Lpv \cdot Wpv)$ $A_{pv1} = 11.305\,m^2$

$A_{pv2} := 28 \cdot Lpv \cdot Wpv - 4 \cdot (1.5 \cdot Lpv \cdot Wpv)$ $A_{pv2} = 27.634\,m^2$

$A_{pv1} + A_{pv2} = 38.939\,m^2$ .... Total PV roof area used for calculations

Roof dimensions

$w_{roof1} := 10m$ ... Roof width@15 slope

$w_{roof2} := 14m$ .. Roof width@30 slope

$l_{roof1} := 1.6m$ ... Roof length@15 slope

$l_{roof2} := 4.1m$ ... Roof length@30 slope

$l_{roof1} \cdot w_{roof1} + l_{roof2} \cdot w_{roof2} = 73.4\,m^2$ ... Total roof area

$\beta_{roof\_1} := 15deg$

$\beta_{roof\_2} := 30deg$ ... roof angle

$\beta := 90deg$ .... walls

$\beta_{floor} := 0deg$ ... floor

Windows and door areas:

South: $A1 := 1.2m^2$ $A2 := 3.4m^2$ $A3 := 3.4m^2$ $A4 := 2.4m^2$ $A5 := 2.4m^2$

$Aw_1 := A1 + A2 + A3 + A4 + A5$ $Aw_1 = 12.8m^2$

West: $Aw_2 := 3.2m^2$

East: $Aw_3 := 1.0m^2$ $Ad_1 := 1.3m^2$

North: $A6 := 0.4m^2$ $A7 := 0.3m^2$ $A8 := 1.2m^2$ $Ad_2 := 1.3m^2$

$Aw_4 := A6 + A7 + A8$ $Aw_4 = 1.9m^2$

Wall net areas:

South: $A_1 := Lh \cdot Hh - Aw_1$

West: $A_2 := Wh \cdot Hh - Aw_2$

East: $A_3 := Wh \cdot Hh - (Aw_3 + Ad_1)$

North: $A_4 := Lh \cdot Hh - (Aw_4 + Ad_2)$

Ceiling: $A_5 := Wh \cdot Lh$

Floor: $A_6 := Wh \cdot Lh$

Roof: $A_7 := l_{roof1} \cdot w_{roof1} + l_{roof2} \cdot w_{roof2}$

Roof not covered with PV panels: $A_{npv} := A_7 - A_{pv1} - A_{pv2}$ $A_{npv} = 34.461m^2$

Infiltration conductance into the zone:

$Hi := 2.4 \cdot m$ ... internal height

$Vol1 := A_6 \cdot Hi$ .... volume of the zone $Vol2 := \frac{1}{2} \cdot Hc \cdot A_5$ ... volume of the attic

$ach := 0.5$ ... air changes per hour

$c_{air} := 1000 \frac{joule}{kg \cdot degC}$ ... specific heat capacity and density of air

$\rho_{air} := 1.2 \frac{kg}{m^3}$ ... density of air

$U_{infl} := \frac{ach \cdot Vol1}{3600sec} \cdot \rho_{air} \cdot c_{air}$ $U_{infl} = 25.52 \frac{W}{degC}$

$U_{inf2} := \frac{ach \cdot Vol2}{3600sec} \cdot \rho_{air} \cdot c_{air}$ $U_{inf2} = 9.038 \frac{W}{degC}$ ... Infiltration into the attic

$R_{infl} := \frac{1}{U_{infl}}$ $R_{inf2} := \frac{1}{U_{inf2}}$

$C_{air} := c_{air} \cdot Vol1 \cdot \rho_{air}$ $C_{air} = 1.837 \times 10^5 J$

THERMAL PROPERTIES OF THE BUILDING ENVELOPE

Doors

$R_d := 2 \frac{m^2 \cdot degC}{watt}$ $R_{door1} := \frac{R_d}{Ad_1}$ $R_{door2} := \frac{R_d}{Ad_2}$

South Wall:

gypsum board $L_1 := 0.013 \cdot m$ $\rho_1 := 800 \cdot \frac{kg}{m^3}$ $k_1 := 0.16 \cdot \frac{watt}{m \cdot degC}$ $c_1 := 750 \cdot \frac{joule}{kg \cdot degC}$

insulation $L_{ins1} := 0.13m$ $\rho_{ins} := 91.2 \cdot \frac{kg}{m^3}$ $k_{ins1} := 0.025 \cdot \frac{watt}{m \cdot degC}$

siding + sheathing $R_{sh1} := 0.37 \cdot m^2 \cdot \frac{degC}{watt}$

$R_g := \frac{L_1}{k_1}$ $R_{ins1} := \frac{L_{ins1}}{k_{ins1}}$ $\frac{L_1}{k_1} + \frac{L_{ins1}}{k_{ins1}} + R_{sh1} = 5.651 m^2 \frac{degC}{W}$

Other Walls:

All exterior walls are of the same construction: $ii := 1, 2..4$

$L_{ii} := L_1$ $k_{ii} := k_1$ $\rho_{ii} := \rho_1$ $c_{ii} := c_1$ $C_{ii} := \rho_{ii} \cdot c_{ii} \cdot A_{ii} \cdot L_{ii}$

$R_{gb_{ii}} := \frac{R_g}{A_{ii}}$ $R_{ins_{ii}} := \frac{R_{ins1}}{A_{ii}}$ $R_{sh_{ii}} := \frac{R_{sh1}}{A_{ii}}$

Ceiling:

gypsum board $L_5 := L_1$ $k_5 := k_1$ $c_5 := c_1$ $\rho_5 := \rho_1$

insulation $L_{ins5} := 0.18m$ $\rho_{ins} := 91.2\cdot\frac{kg}{m^3}$ $k_{ins5} := 0.020\cdot\frac{watt}{m\cdot degC}$

$R_{ins_5} := \frac{L_{ins5}}{k_{ins5}\cdot A_5}$ $Rgb_5 := \frac{R_g}{A_5}$ $\frac{L_{ins5}}{k_{ins5}} + R_g = 9.081 m^2\frac{degC}{W}$

Floor

Bricks $L_6 := 0.05m$ $k_6 := 1.7\cdot\frac{watt}{m\cdot degC}$ $\rho_6 := 1600\cdot\frac{kg}{m^3}$ $c_6 := 800\cdot\frac{joule}{kg\cdot degC}$

Insulation & plywood $L_{ins6} := 0.18m$ $k_{ins6} := 0.025\cdot\frac{watt}{m\cdot degC}$

$R_{c_6} := \frac{L_6}{k_6\cdot A_6}$ $R_{ins_6} := \frac{L_{ins6}}{k_{ins6}\cdot A_6}$ $\frac{L_6}{k_6} + \frac{L_{ins6}}{k_{ins6}} = 7.229 m^2\frac{degC}{W}$

Roof:

PV panels: $k_{pv} := 0.8\cdot\frac{watt}{m\cdot degC}$ $\rho_{pv} := 2500\cdot\frac{kg}{m^3}$ $L_{pv} := 0.019m$

Air gap: $L_{air} := 0.05m$ $c_{air} := 1000\cdot\frac{joule}{kg\cdot degC}$ $\rho_{air} := 1.2\cdot\frac{kg}{m^3}$ $k_{air} := 0.024\cdot\frac{watt}{m\cdot degC}$

Asphalt shingles: $R_s := 0.078\cdot\frac{m^2\cdot degC}{watt}$ $c_{roof} := 1700\cdot\frac{joule}{kg\cdot degC}$

Shingle Backer board+insulation $R_b := 6\cdot\frac{m^2\cdot degC}{watt}$ $\rho_{roof} := 800\cdot\frac{kg}{m^3}$

$R_{air} := \frac{L_{air}}{k_{air}\cdot A_7}$ $R_{ash} := \frac{R_s}{A_7}$ $R_{ins_7} := \frac{R_b}{A_7}$

$Vol3 := (A_{pv1} + A_{pv2})\cdot h_{roof}$ $Vol4 := A_{npv}\cdot h_{roof}$

$C_{4B} := c_{roof}\cdot Vol3\cdot\rho_{roof}$ $C_{4C} := c_{roof}\cdot Vol4\cdot\rho_{roof}$

Thermal capacitances:

$C_8 := c_5\cdot\rho_5\cdot A_5\cdot L_5$ $C_{11} := C_1$ $C_{16} := c_6\cdot\rho_6\cdot A_6\cdot L_6$ $C_{19} := \sum_{ii=2}^{4} C_{ii}$ $C_{4B} = 1.059\times 10^7 J$

$C_{4C} = 9.373\times 10^6 J$

Wall Resistances:

$$R_{1011} := \frac{R_{gb_1}}{2} \qquad R_{1819} := \sum_{ii=2}^{4} \frac{R_{gb_{ii}}}{2}$$

$$R_{1112} := \frac{R_{gb_1}}{2} + R_{ins_1} + R_{sh_1} \qquad R_{1920} := \sum_{ii=2}^{4} \left(\frac{R_{gb_{ii}}}{2} + R_{ins_{ii}} + R_{sh_{ii}} \right)$$

$$R_{78} := R_{ins_5} \qquad R_{1516} := R_{c_6} \qquad R_{4B4} := \frac{R_{ins_7} + R_{ash}}{2}$$

$$R_{89} := R_{gb_5} \qquad R_{1617} := R_{ins_6} \qquad R_{4B5} := R_{4B4}$$

$$TS1 := \left(\frac{C_{4B}}{\frac{1}{R_{4B4}} + \frac{1}{R_{4B5}}} \quad \frac{C_8}{\frac{1}{R_{89}} + \frac{1}{R_{78}}} \quad \frac{C_{11}}{\frac{1}{R_{1011}} + \frac{1}{R_{1112}}} \quad \frac{C_{16}}{\frac{1}{R_{1516}} + \frac{1}{R_{1617}}} \quad \frac{C_{19}}{\frac{1}{R_{1819}} + \frac{1}{R_{1920}}} \right)$$

$TS1 = \left(2.193 \times 10^5 \quad 628.08 \quad 314.597 \quad 1.875 \times 10^3 \quad 4.262 \times 10^3\right) s$ $\qquad \Delta t_{critical} := \min(TS1)$

$\Delta t_{critical} = 314.597 s$

$\Delta t := 300 sec$ ... simulation step (5min)

$NT := 86400 \frac{sec}{\Delta t} \cdot 5 \qquad NT = 1.44 \times 10^3$

$p := 0, 1 .. NT \qquad t_p := p \cdot \Delta t$ ..times at which simulation is to be performed. $\qquad n1 := 1, 2 .. 3$

OUTDOOR TEMPERATURE

$NTo := 24$ $\quad it := 0, 1 .. 23$ ...time index

$t_{it} := if(n > 92, it \cdot hr + 1hr, it \cdot hr - 1hr)$ Daylight Saving Time

$n := 0, 1 .. 3$ ...harmonics $\quad w_n := 2 \cdot \pi \cdot \frac{n}{24 \cdot hr}$ $\quad j := \sqrt{-1}$

$$Ton_n := \left(\sum_{it} To_{it} \cdot \frac{\exp(-j \cdot w_n \cdot t_{it})}{24} \right) \cdot degC$$ ...Fourier harmonic coefficients

$Ton_0 = -21.204 degC$ ... mean daily temperature

$Vw := 3.0 \ \frac{m}{sec}$ ... wind speed

$To_{it} :=$

−20.5
−21.6
−22.8
−23.6
−24.5
−24.8
−24.9
−25.3
−25.2
−24.7
−23.7
−22.3
−21.9
−21.1
−20
−19.1
−19.1
−19.5
−19.3
−19.9
−20.6
−21.5
−23

Absorbed Solar Energy

Reference:C:\Documents and Settings\s_pant\Desktop\Solar_Radiation_Glazing.mcd(R)

Outer glazing:

$$S1wo_{n,1} := \left(\sum_{it} S_{tao_{it,1}} \cdot \frac{\exp(-j \cdot w_n \cdot t_{it})}{24} \right)$$

$$S2wo_{n,2} := \left(\sum_{it} S_{tao_{it,2}} \cdot \frac{\exp(-j \cdot w_n \cdot t_{it})}{24} \right)$$

$$S3wo_{n,3} := \left(\sum_{it} S_{tao_{it,3}} \cdot \frac{\exp(-j \cdot w_n \cdot t_{it})}{24} \right)$$

$$S4wo_{n,4} := \left(\sum_{it} S_{tao_{it,4}} \cdot \frac{\exp(-j \cdot w_n \cdot t_{it})}{24} \right)$$

Inner glazing:

$$S1wi_{n,1} := \left(\sum_{it} S_{tai_{it,1}} \cdot \frac{\exp(-j \cdot w_n \cdot t_{it})}{24} \right)$$

$$S2wi_{n,2} := \left(\sum_{it} S_{tai_{it,2}} \cdot \frac{\exp(-j \cdot w_n \cdot t_{it})}{24} \right)$$

$$S3wi_{n,3} := \left(\sum_{it} S_{tai_{it,3}} \cdot \frac{\exp(-j \cdot w_n \cdot t_{it})}{24} \right)$$

$$S4wi_{n,4} := \left(\sum_{it} S_{tai_{it,4}} \cdot \frac{\exp(-j \cdot w_n \cdot t_{it})}{24} \right)$$

Exterior Walls:

$$S1se_{n,1} := \left(\sum_{it} Sse_{it,1} \cdot \frac{\exp\left(-j \cdot w_n \cdot t_{it}\right)}{24} \right)$$

$$S2se_{n,2} := \left(\sum_{it} Sse_{it,2} \cdot \frac{\exp\left(-j \cdot w_n \cdot t_{it}\right)}{24} \right)$$

$$S3se_{n,3} := \left(\sum_{it} Sse_{it,3} \cdot \frac{\exp\left(-j \cdot w_n \cdot t_{it}\right)}{24} \right)$$

$$S4se_{n,4} := \left(\sum_{it} Sse_{it,4} \cdot \frac{\exp\left(-j \cdot w_n \cdot t_{it}\right)}{24} \right)$$

Interior Walls:

$$S1si_{n,1} := \left(\sum_{it} S_{it,1} \cdot \frac{\exp\left(-j \cdot w_n \cdot t_{it}\right)}{24} \right)$$

$$S2si_{n,2} := \left(\sum_{it} S_{it,2} \cdot \frac{\exp\left(-j \cdot w_n \cdot t_{it}\right)}{24} \right)$$

$$S3si_{n,3} := \left(\sum_{it} S_{it,3} \cdot \frac{\exp\left(-j \cdot w_n \cdot t_{it}\right)}{24} \right)$$

$$S4si_{n,4} := \left(\sum_{it} S_{it,4} \cdot \frac{\exp\left(-j \cdot w_n \cdot t_{it}\right)}{24} \right)$$

Roof:

$$S7\_1_{n,7} := \left(\sum_{it} S1_{it,7} \cdot \frac{\exp\left(-j \cdot w_n \cdot t_{it}\right)}{24} \right)$$

$$S7\_2_{n,7} := \left(\sum_{it} S2_{it,7} \cdot \frac{\exp\left(-j \cdot w_n \cdot t_{it}\right)}{24} \right)$$

$$S7\_3_{n,7} := \left(\sum_{it} S3_{it,7} \cdot \frac{\exp\left(-j \cdot w_n \cdot t_{it}\right)}{24} \right)$$

Floor:

$$S6si_{n,6} := \left(\sum_{it} S_{it,6} \cdot \frac{\exp\left(-j \cdot w_n \cdot t_{it}\right)}{24} \right)$$

Ceiling:

$$S5si_{n,5} := \left(\sum_{it} S_{it,5} \cdot \frac{\exp\left(-j \cdot w_n \cdot t_{it}\right)}{24} \right)$$

Incident Solar Radiation

$$S_{t\_1_{n,7}} := \left(\sum_{it} St1_{it,7} \cdot \frac{\exp\left(-j \cdot w_n \cdot t_{it}\right)}{24} \right)$$

$$S_{t\_2_{n,7}} := \left(\sum_{it} St2_{it,7} \cdot \frac{\exp\left(-j \cdot w_n \cdot t_{it}\right)}{24} \right)$$

Generation time data for each time step (back to time domain)

Outside temperature

$$To_p := Ton_0 + 2\cdot\sum_{n1} Re\left[\left(Ton_{n1}\right)\cdot\exp\left(j\cdot w_{n1}\cdot t_p\right)\right]$$

$$Tsky_p := \left[\left(To_p + 273\right) - 6\right] - 273$$

$$Tgr_p := To_p$$

Outer glazing:

$$Swo1_p := if\left[\left[S1wo_{0,1} + 2\cdot\sum_{n1} Re\left[\left(S1wo_{n1,1}\right)\cdot\exp\left(j\cdot w_{n1}\cdot t_p\right)\right] > 0.0\,watt\right], S1wo_{0,1} + 2\cdot\sum_{n1} Re\left[\left(S1wo_{n1,1}\right)\cdot\exp\left(j\cdot w_{n1}\cdot t_p\right)\right], 0.0\,watt\right]$$

$$Swo2_p := if\left[\left[S2wo_{0,2} + 2\cdot\sum_{n1} Re\left[\left(S2wo_{n1,2}\right)\cdot\exp\left(j\cdot w_{n1}\cdot t_p\right)\right] > 0.0\,watt\right], S2wo_{0,2} + 2\cdot\sum_{n1} Re\left[\left(S2wo_{n1,2}\right)\cdot\exp\left(j\cdot w_{n1}\cdot t_p\right)\right], 0.0\,watt\right]$$

$$Swo3_p := if\left[\left[S3wo_{0,3} + 2\cdot\sum_{n1} Re\left[\left(S3wo_{n1,3}\right)\cdot\exp\left(j\cdot w_{n1}\cdot t_p\right)\right] > 0.0\,watt\right], S3wo_{0,3} + 2\cdot\sum_{n1} Re\left[\left(S3wo_{n1,3}\right)\cdot\exp\left(j\cdot w_{n1}\cdot t_p\right)\right], 0.0\,watt\right]$$

$$Swo4_p := if\left[\left[S4wo_{0,4} + 2\cdot\sum_{n1} Re\left[\left(S4wo_{n1,4}\right)\cdot\exp\left(j\cdot w_{n1}\cdot t_p\right)\right] > 0.0\,watt\right], S4wo_{0,4} + 2\cdot\sum_{n1} Re\left[\left(S4wo_{n1,4}\right)\cdot\exp\left(j\cdot w_{n1}\cdot t_p\right)\right], 0.0\,watt\right]$$

$$Swo21_p := Swo2_p + Swo3_p + Swo4_p$$

Inner glazing:

$$Swi1_p := if\left[\left[S1wi_{0,1} + 2\cdot\sum_{n1} Re\left[\left(S1wi_{n1,1}\right)\cdot\exp\left(j\cdot w_{n1}\cdot t_p\right)\right] > 0.0watt\right], S1wi_{0,1} + 2\cdot\sum_{n1} Re\left[\left(S1wi_{n1,1}\right)\cdot\exp\left(j\cdot w_{n1}\cdot t_p\right)\right], 0.0watt\right]$$

$$Swi2_p := if\left[\left[S2wi_{0,2} + 2\cdot\sum_{n1} Re\left[\left(S2wi_{n1,2}\right)\cdot\exp\left(j\cdot w_{n1}\cdot t_p\right)\right] > 0.0\,watt\right], S2wi_{0,2} + 2\cdot\sum_{n1} Re\left[\left(S2wi_{n1,2}\right)\cdot\exp\left(j\cdot w_{n1}\cdot t_p\right)\right], 0.0\,watt\right]$$

$$Swi3_p := if\left[\left[S3wi_{0,3} + 2\cdot\sum_{n1} Re\left[\left(S3wi_{n1,3}\right)\cdot\exp\left(j\cdot w_{n1}\cdot t_p\right)\right] > 0.0\,watt\right], S3wi_{0,3} + 2\cdot\sum_{n1} Re\left[\left(S3wi_{n1,3}\right)\cdot\exp\left(j\cdot w_{n1}\cdot t_p\right)\right], 0.0\,watt\right]$$

$$Swi4_p := if\left[\left[S4wi_{0,4} + 2\cdot\sum_{n1} Re\left[\left(S4wi_{n1,4}\right)\cdot\exp\left(j\cdot w_{n1}\cdot t_p\right)\right] > 0.0\,watt\right], S4wi_{0,4} + 2\cdot\sum_{n1} Re\left[\left(S4wi_{n1,4}\right)\cdot\exp\left(j\cdot w_{n1}\cdot t_p\right)\right], 0.0\,watt\right]$$

$$Swi22_p := Swi2_p + Swi3_p + Swi4_p$$

Exterior walls

$$Sse1_p := if\left[\left[S1se_{0,1} + 2\cdot\sum_{n1} Re\left[\left(S1se_{n1,1}\right)\cdot\exp\left(j\cdot w_{n1}\cdot t_p\right)\right] > 0.0\cdot watt\right], S1se_{0,1} + 2\cdot\sum_{n1} Re\left[\left(S1se_{n1,1}\right)\cdot\exp\left(j\cdot w_{n1}\cdot t_p\right)\right], 0.0\cdot watt\right]$$

$$Sse2_p := if\left[\left[S2se_{0,2} + 2\cdot\sum_{n1} Re\left[\left(S2se_{n1,2}\right)\cdot\exp\left(j\cdot w_{n1}\cdot t_p\right)\right] > 0.0watt\right], S2se_{0,2} + 2\cdot\sum_{n1} Re\left[\left(S2se_{n1,2}\right)\cdot\exp\left(j\cdot w_{n1}\cdot t_p\right)\right], 0.0watt\right]$$

$$Sse3_p := if\left[\left[S3se_{0,3} + 2\cdot\sum_{n1} Re\left[\left(S3se_{n1,3}\right)\cdot\exp\left(j\cdot w_{n1}\cdot t_p\right)\right] > 0.0watt\right], S3se_{0,3} + 2\cdot\sum_{n1} Re\left[\left(S3se_{n1,3}\right)\cdot\exp\left(j\cdot w_{n1}\cdot t_p\right)\right], 0.0watt\right]$$

$$Sse4_p := if\left[\left[S4se_{0,4} + 2\cdot\sum_{n1} Re\left[\left(S4se_{n1,4}\right)\cdot\exp\left(j\cdot w_{n1}\cdot t_p\right)\right] > 0.0watt\right], S4se_{0,4} + 2\cdot\sum_{n1} Re\left[\left(S4se_{n1,4}\right)\cdot\exp\left(j\cdot w_{n1}\cdot t_p\right)\right], 0.0watt\right]$$

$$Sse20_p := Sse2_p + Sse3_p + Sse4_p$$

Roof

$$Sse7\_1_p := if\left[\left(S7\_1_{0,7} + 2\cdot\sum_{n1} Re\left(S7\_1_{n1,7}\cdot\exp\left(j\cdot w_{n1}\cdot t_p\right)\right) > 0.0\cdot watt\right), S7\_1_{0,7} + 2\cdot\sum_{n1} Re\left[\left(S7\_1_{n1,7}\right)\cdot\exp\left(j\cdot w_{n1}\cdot t_p\right)\right], 0.0\cdot watt\right]$$

$$Sse7\_2_p := if\left[\left(S7\_2_{0,7} + 2\cdot\sum_{n1} Re\left(S7\_2_{n1,7}\cdot\exp\left(j\cdot w_{n1}\cdot t_p\right)\right) > 0.0\cdot watt\right), S7\_2_{0,7} + 2\cdot\sum_{n1} Re\left[\left(S7\_2_{n1,7}\right)\cdot\exp\left(j\cdot w_{n1}\cdot t_p\right)\right], 0.0\cdot watt\right]$$

$$Sse7\_3_p := if\left[\left(S7\_3_{0,7} + 2\cdot\sum_{n1} Re\left(S7\_3_{n1,7}\cdot\exp\left(j\cdot w_{n1}\cdot t_p\right)\right) > 0.0\cdot watt\right), S7\_3_{0,7} + 2\cdot\sum_{n1} Re\left[\left(S7\_3_{n1,7}\right)\cdot\exp\left(j\cdot w_{n1}\cdot t_p\right)\right], 0.0\cdot watt\right]$$

$$Sse7\_t1_p := if\left[\left(S_t\_1_{0,7} + 2\cdot\sum_{n1} Re\left(S_t\_1_{n1,7}\cdot\exp\left(j\cdot w_{n1}\cdot t_p\right)\right) > 0.0\cdot watt\right), S_t\_1_{0,7} + 2\cdot\sum_{n1} Re\left[\left(S_t\_1_{n1,7}\right)\cdot\exp\left(j\cdot w_{n1}\cdot t_p\right)\right], 0.0\cdot watt\right]$$

$$Sse7\_t2_p := if\left[\left(S_t\_2_{0,7} + 2\cdot\sum_{n1} Re\left(S_t\_2_{n1,7}\cdot\exp\left(j\cdot w_{n1}\cdot t_p\right)\right) > 0.0\cdot watt\right), S_t\_2_{0,7} + 2\cdot\sum_{n1} Re\left[\left(S_t\_2_{n1,7}\right)\cdot\exp\left(j\cdot w_{n1}\cdot t_p\right)\right], 0.0\cdot watt\right]$$

Interior walls

$$Ssi1_p := if\left[\left[S1si_{0,1} + 2\cdot\sum_{n1} Re\left[\left(S1si_{n1,1}\right)\cdot\exp\left(j\cdot w_{n1}\cdot t_p\right)\right] > 0.0watt\right], S1si_{0,1} + 2\cdot\sum_{n1} Re\left[\left(S1si_{n1,1}\right)\cdot\exp\left(j\cdot w_{n1}\cdot t_p\right)\right], 0.0watt\right]$$

$$Ssi2_p := if\left[\left[S2si_{0,2} + 2\cdot\sum_{n1} Re\left[\left(S2si_{n1,2}\right)\cdot\exp\left(j\cdot w_{n1}\cdot t_p\right)\right] > 0.0watt\right], S2si_{0,2} + 2\cdot\sum_{n1} Re\left[\left(S2si_{n1,2}\right)\cdot\exp\left(j\cdot w_{n1}\cdot t_p\right)\right], 0.0watt\right]$$

$$Ssi3_p := if\left[\left[S3si_{0,3} + 2\cdot\sum_{n1} Re\left[\left(S3si_{n1,3}\right)\cdot\exp\left(j\cdot w_{n1}\cdot t_p\right)\right] > 0.0watt\right], S3si_{0,3} + 2\cdot\sum_{n1} Re\left[\left(S3si_{n1,3}\right)\cdot\exp\left(j\cdot w_{n1}\cdot t_p\right)\right], 0.0watt\right]$$

$$Ssi4_p := if\left[\left[S4si_{0,4} + 2\cdot\sum_{n1} Re\left[\left(S4si_{n1,4}\right)\cdot\exp\left(j\cdot w_{n1}\cdot t_p\right)\right] > 0.0watt\right], S4si_{0,4} + 2\cdot\sum_{n1} Re\left[\left(S4si_{n1,4}\right)\cdot\exp\left(j\cdot w_{n1}\cdot t_p\right)\right], 0.0watt\right]$$

$$Ssi18_p := Ssi2_p + Ssi3_p + Ssi4_p$$

Ceiling:

$$Ssi5_p := if\left[\left[S5si_{0,5} + 2\cdot\sum_{n1} Re\left[\left(S5si_{n1,5}\right)\cdot\exp\left(j\cdot w_{n1}\cdot t_p\right)\right] > 0.0watt\right], S5si_{0,5} + 2\cdot\sum_{n1} Re\left[\left(S5si_{n1,5}\right)\cdot\exp\left(j\cdot w_{n1}\cdot t_p\right)\right], 0.0watt\right]$$

Floor

$$Ssi6_p := if\left[\left[S6si_{0,6} + 2\cdot\sum_{n1} Re\left[\left(S6si_{n1,6}\right)\cdot\exp\left(j\cdot w_{n1}\cdot t_p\right)\right] > 0.0watt\right], S6si_{0,6} + 2\cdot\sum_{n1} Re\left[\left(S6si_{n1,6}\right)\cdot\exp\left(j\cdot w_{n1}\cdot t_p\right)\right], 0.0watt\right]$$

Internal Gains

Radiative

$$Qrad_{int_p} := if\left(7hr < t_p < 22hr \vee 31hr < t_p < 46hr \vee 55hr < t_p < 70hr \vee 79hr < t_p < 94hr \vee 103hr < t_p < 118hr, 100\cdot watt, 0\cdot watt\right)$$

Convective

$$Qcav_{int_p} := if\left(7hr < t_p < 22hr \vee 31hr < t_p < 46hr \vee 55hr < t_p < 70hr \vee 79hr < t_p < 94hr \vee 103hr < t_p < 118hr, 30\cdot watt, 0\cdot watt\right)$$

$$Qrsi_{int_{p,si}} := Qrad_{int_p}\cdot\frac{A_{si}}{\sum_{si} A_{si}}$$

$$Qrw_{int_{p,iw}} := Qrad_{int_p}\cdot\frac{Aw_{iw}}{\sum_{iw} Aw_{iw}}$$

$$Qrsi18_{int_p} := Qrsi_{int_{p,2}} + Qrsi_{int_{p,3}} + Qrsi_{int_{p,4}}$$

$$Qrw22_{int_p} := Qrw_{int_{p,2}} + Qrw_{int_{p,3}} + Qrw_{int_{p,4}}$$

$$Qrsi_{int_{p,6}} := Qrad_{int_p}\cdot\frac{A_6}{\sum_{si} A_{si}}$$

Temperature Initial values:

$$\begin{pmatrix} T_{air\_out\_1_0} \\ T_{air\_out\_2_0} \\ T_{air\_out\_3_0} \\ T4A_0 \\ T4B\_1_0 \\ T4B\_2_0 \\ T4B\_3_0 \\ T4B_0 \\ T4C_0 \\ T5_0 \\ T6_0 \\ T7_0 \\ T8_0 \\ T9_0 \\ T10_0 \\ T11_0 \\ T12_0 \\ T13_0 \\ T14_0 \\ T15_0 \\ T16_0 \\ T17_0 \\ T18_0 \\ T19_0 \\ T20_0 \\ T21_0 \\ T22_0 \\ Tz_0 \\ Tr1_0 \\ Tr2_0 \\ Tr3_0 \\ Tr4_0 \\ Tr5_0 \end{pmatrix} := \begin{pmatrix} -11.5 \\ -7.8 \\ -4.8 \\ 0.3 \\ 1.5 \\ 1.9 \\ 13.2 \\ 14.2 \\ 14.5 \\ 14.8 \\ 15 \\ 16 \\ 17 \\ 18 \\ 19 \\ 19.1 \\ 19.2 \\ 19.3 \\ 19.4 \\ 19.5 \\ 19.6 \\ 19.7 \\ 19.8 \\ 18.1 \\ 18.2 \\ 18.5 \\ 18.7 \\ 16.1 \\ 16.2 \\ 16.3 \\ 16.4 \\ 16.8 \\ 17.3 \end{pmatrix} \text{degC}$$

$$Q_{heat_0} := 5000\text{W}$$

Calculation of convective heat transfer coefficients in the PV gap

SECTION 1

$V_{air1} := 0.55\frac{m}{sec}$ HE bypassed

$V_{air1_p} := if\left(90 < p < 198 \vee 378 < p < 486 \vee 667 < p < 774 \vee 954 < p < 1062 \vee 1242 < p < 1350, V_{air1}, 0\cdot\frac{m}{sec}\right)$

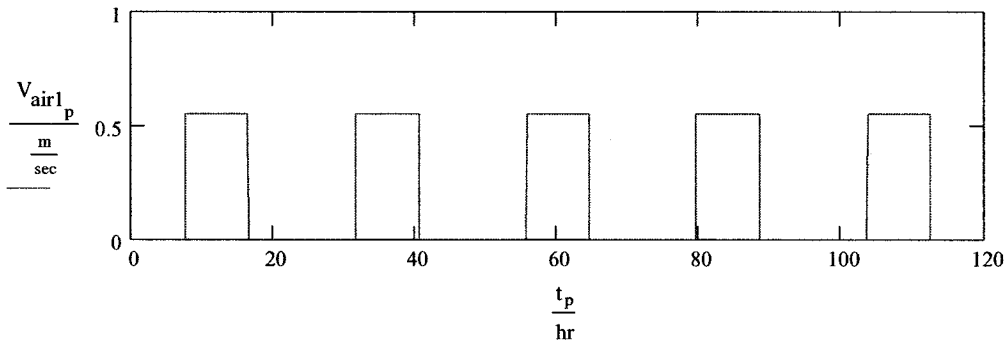

Thermal properties of the air

Assumed values:

$T1\_1_0 := -6.9degC$

$T2\_1_0 := -7.4degC$

$T3\_1_0 := -12.2degC$

$T4\_1_0 := -8.7degC$

Specific heat capacity of the air: $c_{p1} := \left[1.0057 + 0.000066\left(T3\_1_0 - 27\right)\right]\cdot 10^3\cdot\frac{joule}{kg\cdot degC}$ $c_{p1} = 1.003\times 10^3\ \frac{joule}{kg\cdot degC}$

Air density: $\rho_{air1} := \left[1.1774 - 0.00359\left(T3\_1_0 - 27\right)\right]\cdot\frac{kg}{m^3}$ $\rho_{air1} = 1.318\frac{kg}{m^3}$

Dynamic viscosity: $\mu_{air1} := \left[1.983 + 0.00184\left(T3\_1_0 - 27\right)\right]\cdot 10^{-5}\cdot\frac{kg}{m\cdot sec}$ $\mu_{air1} = 1.911\times 10^{-5}\ \frac{kg}{ms}$

$\mu_{w1} := \left[1.983 + 0.00184\left(\frac{T2\_1_0 + T4\_1_0}{2} - 27\right)\right]\cdot 10^{-5}\cdot\frac{kg}{m\cdot sec}$ $\mu_{w1} = 1.919\times 10^{-5}\ \frac{kg}{ms}$

Conductivity $k_{air1} := \left[0.02624 + 0.0000758\left(T3\_1_0 - 27\right)\right]\cdot\frac{watt}{m\cdot degC}$ $k_{air1} = 0.023\frac{watt}{m\cdot degC}$

Kynematic viscosity: $\nu_{air1} := \frac{\mu_{air1}}{\rho_{air1}}$ $\nu_{air1} = 1.45\times 10^{-5}\ \frac{m^2}{s}$

Thermal diffusivity: $a1 := \frac{k_{air1}}{c_{p1}\cdot\rho_{air1}}$ $a1 = 1.76\times 10^{-5}\ \frac{m^2}{s}$

Rayleigh Number: $Ra1 := \frac{g\cdot\left(T2\_1_0 - T4\_1_0\right)\cdot h_{pv}^{\ 3}}{a1\cdot\nu_{air1}\cdot\left(T3\_1_0 + 273\right)}$ $Ra1 = 1.226\times 10^{4}$

Prandtl's number $Pr1 := \frac{\nu_{air1}}{a1}$ $Pr1 = 0.824$

Hydraulic diameter: (for flat plates) $D_h := 2\cdot h_{pv}$ $D_h = 0.08m$

CONTROL STRATEGY

$m_{air_p} := \rho_{air1}\cdot V_{air1_p}\cdot\left(h_{pv}\cdot w_{pv1}\right)$

$m_{air_p} := if\left(90 < p < 198 \vee 378 < p < 486 \vee 667 < p < 774 \vee 954 < p < 1062 \vee 1242 < p < 1350, m_{air_p}, 10^{-5}\cdot\frac{kg}{sec}\right)$

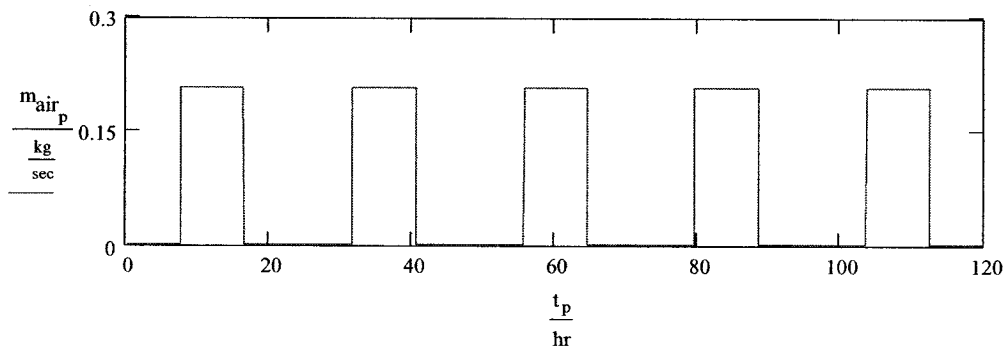

Reynold's number $Re1_p := \frac{V_{air1_p}\cdot D_h}{\nu_{air1}}$

$f1\_ := if\left[Re1\_ = 0, 0, \left(1.82\log\left(Re1\_\right) - 1.64\right)^{-2}\right]$ friction factor

$$Nu1_p := \begin{cases} 1.86\left(\frac{Re1_p \cdot Pr1 \cdot D_h}{l_{pv1}}\right)^{\frac{1}{3}} \cdot \left(\frac{\mu_{air1}}{\mu_{w1}}\right)^{0.14} & \text{if } \left(\frac{Re1_p \cdot Pr1 \cdot D_h}{l_{pv1}}\right)^{\frac{1}{3}} \cdot \left(\frac{\mu_{air1}}{\mu_{w1}}\right)^{0.14} \geq 2 \wedge 0.0044 < \left(\frac{\mu_{air1}}{\mu_{w1}}\right) < 9.75 \wedge 0.48 < Pr1 < 16700 \wedge 0.1 < Re1_p < 2300 \\ 7.54 & \text{if } \left(\frac{Re1_p \cdot Pr1 \cdot D_h}{l_{pv1}}\right)^{\frac{1}{3}} \cdot \left(\frac{\mu_{air1}}{\mu_{w1}}\right)^{0.14} < 2 \wedge 0.1 < Re1_p < 2300 \\ 0.116\left[\left(Re1_p\right)^{\frac{2}{3}} - 125\right] \cdot Pr1^{\frac{1}{3}} \cdot \left[1 + \left(\frac{D_h}{l_{pv1}}\right)^{\frac{2}{3}}\right] \cdot \left(\frac{\mu_{air1}}{\mu_{w1}}\right)^{0.14} & \text{if } 2300 < Re1_p < 6000 \\ \frac{\left(\frac{fl_p}{8}\right) \cdot \left(Re1_p - 1000\right) \cdot Pr1 \cdot \left[1 + \left(\frac{D_h}{l_{pv1}}\right)^{\frac{2}{3}}\right]}{1 + 12.7 \cdot \left(\frac{fl_p}{8}\right)^{0.5} \cdot \left(Pr1^{\frac{2}{3}} - 1\right)} & \text{if } 6000 < Re1_p < 1000000 \wedge 0 < \frac{D_h}{l_{pv1}} < 1 \wedge 0.6 < Pr1 < 2000 \\ \left[0.644 \cdot \left[\left(\frac{h_{pv}}{l_{roof1}}\right) \cdot Ra1 \cdot \sin\left(\beta_{roof\_1}\right)\right]^{0.25}\right] & \text{if } Re1_p \leq 0.1 \end{cases}$$

$$h_{c1_p} := \frac{Nu1_p \cdot k_{air1}}{D_h}$$

SECTION 2

Assumed:

$T1\_2_0 := -5.1degC$

$T2\_2_0 := -5.6degC$

$T3\_2_0 := -10.3degC$

$T4\_2_0 := -7.0degC$

Thermal properties of the air

Specific heat capacity of the air:

$$c_{p2} := \left[1.0057 + 0.000066\left(T3\_2_0 - 27\right)\right] \cdot 10^3 \cdot \frac{joule}{kg \cdot degC} \qquad c_{p2} = 1.003 \times 10^3 \frac{joule}{kg \cdot degC}$$

Air density:

$$\rho_{air2} := \left[1.1774 - 0.00359\left(T3\_2_0 - 27\right)\right] \cdot \frac{kg}{m^3} \qquad \rho_{air2} = 1.311 \frac{kg}{m^3}$$

Dynamic viscosity:

$$\mu_{air2} := \left[1.983 + 0.00184\left(T3\_2_0 - 27\right)\right] \cdot 10^{-5} \cdot \frac{kg}{m \cdot sec} \qquad \mu_{air2} = 1.914 \times 10^{-5} \frac{kg}{ms}$$

$$\mu_{w2} := \left[1.983 + 0.00184\left(\frac{T2\_2_0 + T4\_2_0}{2} - 27\right)\right] \cdot 10^{-5} \cdot \frac{kg}{m \cdot sec} \qquad \mu_{w2} = 1.922 \times 10^{-5} \frac{kg}{ms}$$

Conductivity

$$k_{air2} := \left[0.02624 + 0.0000758\left(T3\_2_0 - 27\right)\right] \cdot \frac{watt}{m \cdot degC} \qquad k_{air2} = 0.023 \frac{watt}{m \cdot degC}$$

Kynematic viscosity: $\nu_{air2} := \frac{\mu_{air2}}{\rho_{air2}}$ $\nu_{air2} = 1.46 \times 10^{-5} \frac{m^2}{s}$

Thermal diffusivity: $a2 := \frac{k_{air2}}{c_{p2} \cdot \rho_{air2}}$ $a2 = 1.78 \times 10^{-5} \frac{m^2}{s}$

Rayleigh Number: $Ra2 := \frac{g \cdot (T2\_2_0 - T4\_2_0) \cdot h_{pv}^{\ 3}}{a1 \cdot \nu_{air1} \cdot (T3\_2_0 + 273)}$ $Ra2 = 1.311 \times 10^4$

Prandtl's number $Pr2 := \frac{\nu_{air2}}{a2}$ $Pr2 = 0.82$

Hydraulic diameter: (for flat plates) $D_h := 2 \cdot h_{pv}$ $D_h = 0.08\,m$

$$V_{air2_p} := \frac{m_{air_p}}{(h_{pv} \cdot w_{pv2}) \cdot \rho_{air2}}$$

Reynold's number $Re2_p := \frac{V_{air2_p} \cdot D_h}{\nu_{air2}}$

$$f2_p := \text{if}\left[Re1_p = 0, 0, \left(1.82 \cdot \log\left(Re2_p\right) - 1.64\right)^{-2}\right]$$

$$Nu2_p := \begin{cases} 1.86 \left(\frac{Re2_p \cdot Pr2 \cdot D_h}{\frac{l_{pv2}}{2}} \right)^{\frac{1}{3}} \cdot \left(\frac{\mu_{air2}}{\mu_{w2}} \right)^{0.14} & \text{if } \left(\frac{Re2_p \cdot Pr2 \cdot D_h}{\frac{l_{pv2}}{2}} \right)^{\frac{1}{3}} \cdot \left(\frac{\mu_{air2}}{\mu_{w2}} \right)^{0.14} \geq 2 \wedge 0.0044 < \left(\frac{\mu_{air2}}{\mu_{w2}} \right) < 9.75 \wedge 0.48 < Pr2 < 16700 \wedge 0.1 < Re2_p < 23 \\ 7.54 \left(\frac{Re2_p \cdot Pr2 \cdot D_h}{\frac{l_{pv2}}{2}} \right)^{\frac{1}{3}} \cdot \left(\frac{\mu_{air2}}{\mu_{w2}} \right)^{0.14} & \text{if } < 2 \wedge 0.1 < Re2_p < 2300 \\ 0.116 \left[\left(Re2_p\right)^{\frac{2}{3}} - 125 \right] \cdot Pr2^{\frac{1}{3}} \cdot \left[1 + \left(\frac{D_h}{\frac{l_{pv2}}{2}} \right)^{\frac{2}{3}} \right] \cdot \left(\frac{\mu_{air2}}{\mu_{w2}} \right)^{0.14} & \text{if } 2300 < Re2_p < 6000 \\ \frac{\left(\frac{f2_p}{8} \right) \cdot \left(Re2_p - 1000\right) \cdot Pr2 \cdot \left[1 + \left(\frac{D_h}{\frac{l_{pv2}}{2}} \right)^{\frac{2}{3}} \right]}{1 + 12.7 \cdot \left(\frac{f2_p}{8} \right)^{0.5} \cdot \left(Pr2^{\frac{2}{3}} - 1 \right)} & \text{if } 6000 < Re2_p < 1000000 \wedge 0 < \frac{D_h}{\frac{l_{pv2}}{2}} < 1 \wedge 0.6 < Pr2 < 2000 \\ \left[0.644 \left[\left(\frac{h_{pv}}{\frac{l_{roof2}}{2}} \right) \cdot Ra2 \cdot \sin\left(\beta_{roof\_2}\right) \right] \right]^{0.25} & \text{if } Re1_p \leq 0.1 \end{cases}$$

$$h_{c2_p} := \frac{Nu2_p \cdot k_{air2}}{D_h}$$

Assumed:

$T1\_3_0 := -4.6\,degC$

$T2\_3_0 := -4.9\,degC$

$T3\_3_0 := -8.3\,degC$

$T4\_3_0 := -5.5\,degC$

Thermal properties of the air

Specific heat capacity of the air:

$$c_{p3} := \left[1.0057 + 0.000066\left(T3\_3_0 - 27\right)\right]\cdot 10^3 \cdot \frac{joule}{kg\cdot degC} \qquad c_{p3} = 1.003\times 10^3\ \frac{joule}{kg\cdot degC}$$

Air density:

$$\rho_{air3} := \left[1.1774 - 0.00359\left(T3\_3_0 - 27\right)\right]\cdot \frac{kg}{m^3} \qquad \rho_{air3} = 1.304\ \frac{kg}{m^3}$$

Dynamic viscosity:

$$\mu_{air3} := \left[1.983 + 0.00184\left(T3\_3_0 - 27\right)\right]\cdot 10^{-5}\cdot \frac{kg}{m\cdot sec} \qquad \mu_{air3} = 1.918\times 10^{-5}\ \frac{kg}{ms}$$

$$\mu_{w3} := \left[1.983 + 0.00184\left(\frac{T2\_3_0 + T4\_3_0}{2} - 27\right)\right]\cdot 10^{-5}\cdot \frac{kg}{m\cdot sec} \qquad \mu_{w3} = 1.924\times 10^{-5}\ \frac{kg}{ms}$$

Conductivity

$$k_{air3} := \left[0.02624 + 0.0000758\left(T3\_3_0 - 27\right)\right]\cdot \frac{watt}{m\cdot degC} \qquad k_{air3} = 0.024\ \frac{watt}{m\cdot degC}$$

Kynematic viscosity:

$$\nu_{air3} := \frac{\mu_{air3}}{\rho_{air3}} \qquad \nu_{air3} = 1.471\times 10^{-5}\ \frac{m^2}{s}$$

Thermal diffusivity:

$$a3 := \frac{k_{air3}}{c_{p3}\cdot \rho_{air3}} \qquad a3 = 1.801\times 10^{-5}\ \frac{m^2}{s}$$

Rayleigh Number:

$$Ra3 := \frac{g\cdot\left(T2\_3_0 - T4\_3_0\right)\cdot h_{pv}^{\ 3}}{a1\cdot \nu_{air1}\cdot\left(T3\_3_0 + 273\right)} \qquad Ra3 = 5.576\times 10^3$$

Prandtl's number

$$Pr3 := \frac{\nu_{air3}}{a3} \qquad Pr3 = 0.817$$

Hydraulic diameter: (for flat plates)

$$D_h := 2\cdot h_{pv} \qquad D_h = 0.08m$$

$$V_{air3_p} := \frac{m_{air_p}}{\left(h_{pv}\cdot w_{pv2}\right)\cdot \rho_{air3}}$$

Reynold's number

$$Re3_p := \frac{V_{air3_p}\cdot D_h}{\nu_{air3}}$$

$f3_p := if\left[Re1_p = 0, 0, \left(1.82\cdot \log\left(Re3_p\right) - 1.64\right)^{-2}\right]$ friction factor

1 1

$$h_{c3_p} := \frac{Nu3_p \cdot k_{air3}}{D_h}$$

Convective and Radiative Heat Transfer Coefficients -Initial Values

$\sigma := 5.6710^{-8} \cdot \frac{watt}{m^2 \cdot K^4}$ $\varepsilon := 0.9$

EXTERIOR CONVECTIVE HTC:

$$h_{1\_1o_0} := \left[\sqrt{\left(1.81\frac{\sqrt[3]{|T1\_1_0 - To_0|}}{1.382+\cos(\beta_{roof\_1})}\right)^2 + \left(2.38Vw^{0.89}\right)^2}\right]\cdot\frac{W}{m^2\cdot degC} + 4\cdot\sigma\cdot\varepsilon\cdot\left[\left(\frac{T1\_1_0 + To_0 + Tsky_0}{3} + 273\right)\cdot K\right]^3\cdot\frac{K}{degC}$$

$$h_{1\_2o_0} := \left[\sqrt{\left(1.81\frac{\sqrt[3]{|T1\_2_0 - To_0|}}{1.382+\cos(\beta_{roof\_2})}\right)^2 + \left(2.38Vw^{0.89}\right)^2}\right]\cdot\frac{W}{m^2\cdot degC} + 4\cdot\sigma\cdot\varepsilon\cdot\left[\left(\frac{T1\_2_0 + To_0 + Tsky_0}{3} + 273\right)\cdot K\right]^3\cdot\frac{K}{degC}$$

$$h_{1\_3o_0} := \left[\sqrt{\left(1.81\frac{\sqrt[3]{|T1\_3_0 - To_0|}}{1.382+\cos(\beta_{roof\_2})}\right)^2 + \left(2.38Vw^{0.89}\right)^2}\right]\cdot\frac{W}{m^2\cdot degC} + 4\cdot\sigma\cdot\varepsilon\cdot\left[\left(\frac{T1\_3_0 + To_0 + Tsky_0}{3} + 273\right)\cdot K\right]^3\cdot\frac{K}{degC}$$

$$h_{4A_0} := \left[\sqrt{\left(1.81\frac{\sqrt[3]{|T4A_0 - To_0|}}{1.382+\cos(\beta_{roof\_2})}\right)^2 + \left(2.38Vw^{0.89}\right)^2}\right]\cdot\frac{W}{m^2\cdot degC} + 4\cdot\sigma\cdot\varepsilon\cdot\left[\left(\frac{T4A_0 + To_0 + Tsky_0}{3} + 273\right)\cdot K\right]^3\cdot\frac{K}{degC}$$

$$h_{13o_0} := \left[\sqrt{\left(1.81\frac{\sqrt[3]{|T13_0 - To_0|}}{1.382+\cos(\beta)}\right)^2 + \left(2.38Vw^{0.89}\right)^2}\right]\frac{W}{m^2\cdot degC} + 4\cdot\sigma\cdot\varepsilon\cdot\left[\left(\frac{T13_0 + To_0 + Tsky_0}{3} + 273\right)\cdot K\right]^3\cdot\frac{K}{degC}$$

$$h_{21o_0} := \left[\sqrt{\left(1.81\frac{\sqrt[3]{|T21_0 - To_0|}}{1.382+\cos(\beta)}\right)^2 + \left(2.86Vw^{0.617}\right)^2}\right]\frac{W}{m^2\cdot degC} + 4\cdot\sigma\cdot\varepsilon\cdot\left[\left(\frac{T21_0 + To_0 + Tsky_0}{3} + 273\right)\cdot K\right]^3\cdot\frac{K}{degC}$$

$$h_{12o_0} := \left[1.81\frac{\sqrt[3]{|T12_0 - To_0|}}{1.382+\cos(\beta)} + 1.13\left[\sqrt{\left(1.81\frac{\sqrt[3]{|T12_0 - To_0|}}{1.382+\cos(\beta)}\right)^2 + \left(2.38Vw^{0.89}\right)^2} - 1.81\frac{\sqrt[3]{|T12_0 - To_0|}}{1.382+\cos(\beta)}\right]\right]\frac{watt}{m^2 degC} + 4\cdot\sigma\cdot\varepsilon\cdot\left[\left(\frac{T12_0 + To_0 + Tsky_0}{3} + 273\right)\cdot K\right]^3\cdot\frac{K}{degC}$$

$$h_{20o_0} := \left[1.81\frac{\sqrt[3]{|T20_0 - To_0|}}{1.382+\cos(\beta)} + 1.13\left[\sqrt{\left(1.81\frac{\sqrt[3]{|T20_0 - To_0|}}{1.382+\cos(\beta)}\right)^2 + \left(2.86Vw^{0.617}\right)^2} - 1.81\frac{\sqrt[3]{|T20_0 - To_0|}}{1.382+\cos(\beta)}\right]\right]\frac{watt}{m^2 degC} + 4\cdot\sigma\cdot\varepsilon\cdot\left[\left(\frac{T20_0 + To_0 + Tsky_0}{3} + 273\right)\cdot K\right]^3\cdot\frac{K}{degC}$$

INTERIOR CHTC

$$h10z_0 := 1.31\cdot\left(\left|T10_0 - Tz_0\right|\right)^{\frac{1}{3}}\cdot\frac{watt}{m^2 degC}$$

$$h14z_0 := 1.31\cdot\left(\left|T14_0 - Tz_0\right|\right)^{\frac{1}{3}}\cdot\frac{watt}{m^2 degC}$$

$$h18z_0 := 1.31\cdot\left(\left|T18_0 - Tz_0\right|\right)^{\frac{1}{3}}\cdot\frac{watt}{m^2 degC}$$

$$h22z_0 := 1.31\cdot\left(\left|T22_0 - Tz_0\right|\right)^{\frac{1}{3}}\cdot\frac{watt}{m^2 degC}$$

$$h56_0 := if\left[T5_0 > T6_0, 0.59\cdot\left(\frac{T5_0 - T6_0}{Lh\cdot m^{-1}}\right)^{0.25}\cdot\frac{watt}{m^2\cdot degC}, 1.52\cdot\left(T6_0 - T5_0\right)^{\frac{1}{3}}\cdot\frac{watt}{m^2 degC}\right]$$

$$h67_0 := if\left[T6_0 > T7_0, 0.59\cdot\left(\frac{T6_0 - T7_0}{Lh\cdot m^{-1}}\right)^{0.25}\cdot\frac{watt}{m^2\cdot degC}, 1.52\cdot\left(T7_0 - T6_0\right)^{\frac{1}{3}}\cdot\frac{watt}{m^2 degC}\right]$$

$$h9z_0 := if\left[T9_0 > Tz_0, 0.59\cdot\left(\frac{T9_0 - Tz_0}{Lh\cdot m^{-1}}\right)^{0.25}\cdot\frac{watt}{m^2\cdot degC}, 1.52\cdot\left(Tz_0 - T9_0\right)^{\frac{1}{3}}\cdot\frac{watt}{m^2 degC}\right]$$

$$h15z_0 := if\left[T15_0 > Tz_0, 1.52\cdot\left(T15_0 - Tz_0\right)^{\frac{1}{3}}\cdot\frac{watt}{m^2 degC}, 0.59\cdot\left(\frac{Tz_0 - T15_0}{Lh\cdot m^{-1}}\right)^{0.25}\cdot\frac{watt}{m^2\cdot degC}\right]$$

WINDOWS

$\varepsilon_1 := 0.9$ . . . emissivity of outer pane

$\varepsilon_{2e} := 0.1$ . . . emissivity of inner pane (low e)

$$\sigma := 5.67\cdot 10^{-8}\cdot\frac{watt}{m^2\cdot K^4}$$

$$h_{wc} := 2.0\cdot\frac{watt}{m^2 degC}$$

convective heat transfer coefficient for all windows
assumed value does not change much with deltaT

$$Tm0_{1314} := \left(273 + \frac{T13_0 + T14_0}{2}\right)K \qquad hr_{1314_0} := \frac{4\cdot\sigma\cdot Tm0_{1314}^{3}}{\left(\frac{1}{\varepsilon_1} + \frac{1}{\varepsilon_{2e}} - 1\right)}\frac{K}{degC}$$

$$Tm0_{2122} := \left(273 + \frac{T21_0 + T22_0}{2}\right)\cdot K \qquad hr_{2122_0} := \frac{4\cdot\sigma\cdot Tm0_{2122}^{3}}{\left(\frac{1}{\varepsilon_1} + \frac{1}{\varepsilon_{2e}} - 1\right)}\cdot\frac{K}{degC}$$

INTERIOR RADIATIVE HEAT TRANSFER COEFFICIENTS

Reference:C:\Documents and Settings\s_pant\Desktop\View_Factors.mcd(R)

South

$Fv_{10\_18} := F_{1,4} + F_{1,12} + F_{1,7}$ $Fv_{10\_9} := F_{1,9}$ $Fv_{10\_15} := F_{1,10}$ $Fv_{10\_22} := F_{1,3} + F_{1,11} + F_{1,6}$

$Fv_{14\_18} := F_{0,4} + F_{0,12} + F_{0,7}$ $Fv_{14\_9} := F_{0,9}$ $Fv_{14\_15} := F_{0,10}$ $Fv_{14\_22} := F_{0,3} + F_{0,11} + F_{0,6}$

Other surfaces (north,east,west)

$Fv_{18\_9} := F_{4,9} + F_{7,9} + F_{12,9}$ $Fv_{18\_10} := F_{4,1} + F_{7,1} + F_{12,1}$ $Fv_{18\_14} := F_{4,0} + F_{7,0} + F_{12,0}$

$Fv_{22\_9} := F_{3,9} + F_{6,9} + F_{11,9}$ $Fv_{22\_10} := F_{3,1} + F_{6,1} + F_{11,1}$ $Fv_{22\_14} := F_{3,0} + F_{6,0} + F_{11,0}$

$Fv_{18\_15} := F_{4,10} + F_{7,10} + F_{12,10}$ $Fv_{22\_15} := F_{3,10} + F_{6,10} + F_{11,10}$

Ceiling

$Fv_{9\_10} := F_{9,1}$ $Fv_{9\_14} := F_{9,0}$ $Fv_{9\_15} := F_{9,10}$ $Fv_{9\_18} := F_{9,4} + F_{9,7} + F_{9,12}$ $Fv_{9\_22} := F_{9,6} + F_{9,11} + F_{9,3}$

Floor

$Fv_{15\_10} := F_{10,1}$ $Fv_{15\_14} := F_{10,0}$ $Fv_{15\_18} := F_{10,4} + F_{10,7} + F_{10,12}$ $Fv_{15\_22} := F_{10,3} + F_{10,6} + F_{10,11}$ $Fv_{15\_9} := F_{10,9}$

PV cavity

$Fv_{2\_4} := 1$ $Fv_{4\_2} := 1$

Attic

$$Fv_{7\_5} := \frac{Wh + l_{roof} - Hc}{2 \cdot l_{roof}} \qquad Fv_{5\_7} := Fv_{7\_5}\frac{A_7}{A_5}$$

Initial values for interior heat transfer coefficients:

$\varepsilon_1 := 0.9$ $\varepsilon_2 := 0.9$

$F_\varepsilon := 0.9$

$$h_{109_0} := \sigma \cdot F_\varepsilon \cdot Fv_{10\_9} \cdot \left| \frac{\left[\left(T10_0 + 273\right)\cdot K\right]^4 - \left[\left(T9_0 + 273\right)\cdot K\right]^4}{T10_0 - T9_0} \right|$$

$$h_{149_0} := \sigma \cdot F_\varepsilon \cdot Fv_{14\_9} \cdot \left| \frac{\left[\left(T14_0 + 273\right)\cdot K\right]^4 - \left[\left(T9_0 + 273\right)\cdot K\right]^4}{T14_0 - T9_0} \right|$$

$$h_{1015_0} := \sigma \cdot F_\varepsilon \cdot Fv_{10\_15} \cdot \left| \frac{\left[\left(T10_0 + 273\right)\cdot K\right]^4 - \left[\left(T15_0 + 273\right)\cdot K\right]^4}{T10_0 - T15_0} \right|$$

$$h_{1415_0} := \sigma \cdot F_\varepsilon \cdot Fv_{14\_15} \cdot \left| \frac{\left[\left(T14_0 + 273\right)\cdot K\right]^4 - \left[\left(T15_0 + 273\right)\cdot K\right]^4}{T14_0 - T15_0} \right|$$

$$h_{1018_0} := \sigma \cdot F_\varepsilon \cdot Fv_{10\_18} \cdot \left| \frac{\left[\left(T10_0 + 273\right)\cdot K\right]^4 - \left[\left(T18_0 + 273\right)\cdot K\right]^4}{T10_0 - T18_0} \right|$$

$$h_{1418_0} := \sigma \cdot F_\varepsilon \cdot Fv_{14\_18} \cdot \left| \frac{\left[\left(T14_0 + 273\right)\cdot K\right]^4 - \left[\left(T18_0 + 273\right)\cdot K\right]^4}{T14_0 - T18_0} \right|$$

$$h_{1022_0} := \sigma \cdot F_\varepsilon \cdot Fv_{10\_22} \cdot \left| \frac{\left[\left(T10_0 + 273\right)\cdot K\right]^4 - \left[\left(T22_0 + 273\right)\cdot K\right]^4}{T10_0 - T22_0} \right|$$

$$h_{1422_0} := \sigma \cdot F_\varepsilon \cdot Fv_{14\_22} \cdot \left| \frac{\left[\left(T14_0 + 273\right)\cdot K\right]^4 - \left[\left(T22_0 + 273\right)\cdot K\right]^4}{T14_0 - T22_0} \right|$$

$$h_{189_0} := \sigma \cdot F_\varepsilon \cdot Fv_{18\_9} \cdot \left| \frac{\left[\left(T18_0 + 273\right)\cdot K\right]^4 - \left[\left(T9_0 + 273\right)\cdot K\right]^4}{T18_0 - T9_0} \right|$$

$$h_{1810_0} := \sigma \cdot F_\varepsilon \cdot Fv_{18\_10} \cdot \left| \frac{\left[\left(T18_0 + 273\right)\cdot K\right]^4 - \left[\left(T10_0 + 273\right)\cdot K\right]^4}{T18_0 - T10_0} \right|$$

$$h_{1814_0} := \sigma \cdot F_\varepsilon \cdot Fv_{18\_10} \cdot \left| \frac{\left[\left(T18_0 + 273\right)\cdot K\right]^4 - \left[\left(T14_0 + 273\right)\cdot K\right]^4}{T18_0 - T14_0} \right|$$

$$h_{1815_0} := \sigma \cdot F_\varepsilon \cdot Fv_{18\_15} \cdot \left| \frac{\left[\left(T18_0 + 273\right)\cdot K\right]^4 - \left[\left(T15_0 + 273\right)\cdot K\right]^4}{T18_0 - T15_0} \right|$$

$$h_{910_0} := \sigma \cdot F_\varepsilon \cdot Fv_{9\_10} \cdot \left| \frac{\left[\left(T9_0 + 273\right)\cdot K\right]^4 - \left[\left(T10_0 + 273\right)\cdot K\right]^4}{T9_0 - T10_0} \right|$$

$$h_{229_0} := \sigma \cdot F_\varepsilon \cdot Fv_{22\_9} \cdot \left| \frac{\left[\left(T22_0 + 273\right)K\right]^4 - \left[\left(T9_0 + 273\right)\cdot K\right]^4}{T22_0 - T9_0} \right|$$

$$h_{914_0} := \sigma \cdot F_\varepsilon \cdot Fv_{9\_14} \cdot \left| \frac{\left[\left(T9_0 + 273\right)\cdot K\right]^4 - \left[\left(T14_0 + 273\right)\cdot K\right]^4}{T9_0 - T14_0} \right|$$

$$h_{2210_0} := \sigma \cdot F_\varepsilon \cdot Fv_{22\_10} \cdot \left| \frac{\left[\left(T22_0 + 273\right)K\right]^4 - \left[\left(T10_0 + 273\right)\cdot K\right]^4}{T22_0 - T10_0} \right|$$

$$h_{915_0} := \sigma \cdot F_\varepsilon \cdot Fv_{9\_15} \cdot \left| \frac{\left[\left(T9_0 + 273\right)\cdot K\right]^4 - \left[\left(T15_0 + 273\right)\cdot K\right]^4}{T9_0 - T15_0} \right|$$

$$h_{2214_0} := \sigma \cdot F_\varepsilon \cdot Fv_{22\_14} \cdot \left| \frac{\left[\left(T22_0 + 273\right)K\right]^4 - \left[\left(T14_0 + 273\right)\cdot K\right]^4}{T22_0 - T14_0} \right|$$

$$h_{918_0} := \sigma \cdot F_\varepsilon \cdot Fv_{9\_18} \cdot \left| \frac{\left[\left(T9_0 + 273\right)\cdot K\right]^4 - \left[\left(T18_0 + 273\right)\cdot K\right]^4}{T9_0 - T18_0} \right|$$

$$h_{2215_0} := \sigma \cdot F_\varepsilon \cdot Fv_{22\_15} \cdot \left| \frac{\left[\left(T22_0 + 273\right)K\right]^4 - \left[\left(T15_0 + 273\right)\cdot K\right]^4}{T22_0 - T15_0} \right|$$

$$h_{922_0} := \sigma \cdot F_\varepsilon \cdot Fv_{9\_22} \cdot \left| \frac{\left[\left(T9_0 + 273\right)\cdot K\right]^4 - \left[\left(T22_0 + 273\right)\cdot K\right]^4}{T9_0 - T22_0} \right|$$

$$h_{159_0} := \sigma \cdot F_\varepsilon \cdot Fv_{15\_9} \cdot \left| \frac{\left[\left(T15_0 + 273\right)\cdot K\right]^4 - \left[\left(T9_0 + 273\right)\cdot K\right]^4}{T15_0 - T9_0} \right|$$

$$h_{1510_0} := \sigma \cdot F_\varepsilon \cdot Fv_{15\_10} \cdot \left| \frac{\left[\left(T15_0 + 273\right)\cdot K\right]^4 - \left[\left(T10_0 + 273\right)\cdot K\right]^4}{T15_0 - T10_0} \right|$$

$$h_{1514_0} := \sigma \cdot F_\varepsilon \cdot Fv_{15\_14} \cdot \left| \frac{\left[\left(T15_0 + 273\right)\cdot K\right]^4 - \left[\left(T14_0 + 273\right)\cdot K\right]^4}{T15_0 - T14_0} \right|$$

$$h_{1518_0} := \sigma \cdot F_\varepsilon \cdot Fv_{15\_18} \cdot \left| \frac{\left[\left(T15_0 + 273\right)\cdot K\right]^4 - \left[\left(T18_0 + 273\right)\cdot K\right]^4}{T15_0 - T18_0} \right|$$

$$h_{1522_0} := \sigma \cdot F_\varepsilon \cdot Fv_{15\_22} \cdot \left| \frac{\left[\left(T15_0 + 273\right)\cdot K\right]^4 - \left[\left(T22_0 + 273\right)\cdot K\right]^4}{T15_0 - T22_0} \right|$$

$$h_{57_0} := \sigma \cdot F_\varepsilon \cdot Fv_{5\_7} \cdot \left| \frac{\left[\left(T5_0 + 273\right)\cdot K\right]^4 - \left[\left(T7_0 + 273\right)\cdot K\right]^4}{T5_0 - T7_0} \right|$$

$$h_{75_0} := \sigma \cdot F_\varepsilon \cdot Fv_{7\_5} \cdot \left| \frac{\left[\left(T7_0 + 273\right)\cdot K\right]^4 - \left[\left(T5_0 + 273\right)\cdot K\right]^4}{T7_0 - T5_0} \right|$$

$$h_{24\_1_0} := \sigma \cdot F_\varepsilon \cdot Fv_{2\_4} \cdot \left| \frac{\left[\left(T2\_1_0 + 273\right)\cdot K\right]^4 - \left[\left(T4\_1_0 + 273\right)\cdot K\right]^4}{T2\_1_0 - T4\_1_0} \right| \qquad h_{42\_1_0} := h_{24\_1_0}$$

$$h_{24\_2_0} := \sigma \cdot F_\varepsilon \cdot Fv_{2\_4} \cdot \left| \frac{\left[\left(T2\_2_0 + 273\right)\cdot K\right]^4 - \left[\left(T4\_2_0 + 273\right)\cdot K\right]^4}{T2\_2_0 - T4\_2_0} \right| \qquad h_{42\_2_0} := h_{24\_2_0}$$

$$h_{24\_3_0} := \sigma \cdot F_\varepsilon \cdot Fv_{2\_4} \cdot \left| \frac{\left[\left(T2\_3_0 + 273\right)\cdot K\right]^4 - \left[\left(T4\_3_0 + 273\right)\cdot K\right]^4}{T2\_3_0 - T4\_3_0} \right| \qquad h_{42\_3_0} := h_{24\_3_0}$$

Thermal Resistances - Initial Values :

$$R_{1\_1eq_0} := \frac{1}{\left(h_{1\_1o_0}\right)\cdot A_{pv1}} \qquad R_{1\_2eq_0} := \frac{1}{\left(h_{1\_2o_0}\right)\cdot \frac{A_{pv2}}{2}} \qquad R_{1\_3eq_0} := \frac{1}{\left(h_{1\_3o_0}\right)\cdot \frac{A_{pv2}}{2}} \qquad R_{20eq_0} := \frac{1}{\left(h_{20o_0}\right)\cdot \sum_{si=2}^{4} A_{si}}$$

$$R_{4Aeq_0} := \frac{1}{\left(h_{4A_0}\right)\cdot A_{npv}} \qquad R_{12eq_0} := \frac{1}{\left(h_{12o_0}\right)\cdot A_1} \qquad R_{13eq_0} := \frac{1}{\left(h_{13o_0}\right)\cdot Aw_1} \qquad R_{21eq_0} := \frac{1}{\left(h_{21o_0}\right)\cdot \sum_{iw=2}^{4} A_{iw}}$$

$$R_{56_0} := \frac{1}{h_{56_0}\cdot A_7} \qquad R_{67_0} := \frac{1}{h_{67_0}\cdot A_5} \qquad R_{57_0} := \frac{1}{h_{57_0}\cdot A_7} \qquad R_{75_0} := \frac{1}{h_{75_0}\cdot A_5}$$

$$R_{910_0} := \frac{1}{h_{910_0}\cdot A_5} \qquad R_{914_0} := \frac{1}{h_{914_0}\cdot A_5} \qquad R_{915_0} := \frac{1}{h_{915_0}\cdot A_5} \qquad R_{918_0} := \frac{1}{h_{918_0}\cdot A_5}$$

$$R_{17o_0} := \frac{1}{h_{17o_0}\cdot A_6} \qquad R_{9z_0} := \frac{1}{h_{9z_0}\cdot A_5} \qquad R_{922_0} := \frac{1}{h_{922_0}\cdot A_5}$$

$$R_{24\_1_0} := \frac{1}{h_{24\_1_0}\cdot A_{pv1}} \qquad R_{24\_2_0} := \frac{1}{h_{24\_2_0}\cdot \frac{A_{pv2}}{2}} \qquad R_{24\_3_0} := \frac{1}{h_{24\_3_0}\cdot \frac{A_{pv2}}{2}}$$

$$R_{42\_1_0} := \frac{1}{h_{42\_1_0}\cdot A_{pv1}} \qquad R_{42\_2_0} := \frac{1}{h_{42\_2_0}\cdot \frac{A_{pv2}}{2}} \qquad R_{42\_3_0} := \frac{1}{h_{42\_3_0}\cdot \frac{A_{pv2}}{2}}$$

$$R_{10z_0} := \frac{1}{h_{10z_0}\cdot A_1} \qquad R_{14z_0} := \frac{1}{h_{14z_0}\cdot Aw_1} \qquad R_{15z_0} := \frac{1}{h_{15z_0}\cdot A_6}$$

$$R_{109_0} := \frac{1}{h_{109_0}\cdot A_1} \qquad R_{149_0} := \frac{1}{h_{149_0}\cdot Aw_1} \qquad R_{159_0} := \frac{1}{h_{159_0}\cdot A_6} \qquad R_{1510_0} := \frac{1}{h_{1510_0}\cdot A_6}$$

$$R_{1015_0} := \frac{1}{h_{1015_0}\cdot A_1} \qquad R_{1415_0} := \frac{1}{h_{1415_0}\cdot Aw_1} \qquad R_{1514_0} := \frac{1}{h_{1514_0}\cdot A_6}$$

$$R_{1018_0} := \frac{1}{h_{1018_0}\cdot A_1} \qquad R_{1418_0} := \frac{1}{h_{1418_0}\cdot Aw_1} \qquad R_{1518_0} := \frac{1}{h_{1518_0}\cdot A_6}$$

$$R_{1022_0} := \frac{1}{h_{1022_0}\cdot A_1} \qquad R_{1422_0} := \frac{1}{h_{1422_0}\cdot Aw_1} \qquad R_{1522_0} := \frac{1}{h_{1522_0}\cdot A_6}$$

$$R_{18z_0} := \frac{1}{h_{18z_0}\cdot \sum_{si=2}^{4} A_{si}} \qquad R_{22z_0} := \frac{1}{h_{22z_0}\cdot \sum_{iw=2}^{4} A_{iw}} \qquad R_{189_0} := \frac{1}{h_{189_0}\cdot \sum_{si=2}^{4} A_{si}} \qquad R_{229_0} := \frac{1}{h_{229_0}\cdot \sum_{iw=2}^{4} A_{iw}}$$

$$R_{1810_0} := \frac{1}{h_{1810_0} \cdot \sum_{si=2}^{4} A_{si}} \qquad R_{2210_0} := \frac{1}{h_{2210_0} \cdot \sum_{iw=2}^{4} A_{iw}} \qquad R_{2122_0} := \frac{1}{\left(h_{wc} + hr_{2122_0}\right) \cdot \sum_{iw=2}^{4} A_{iw}}$$

$$R_{1314_0} := \frac{1}{\left(h_{wc} + hr_{1314_0}\right) \cdot Aw_1} \qquad R_{1814_0} := \frac{1}{h_{1814_0} \cdot \sum_{si=2}^{4} A_{si}} \qquad R_{1815_0} := \frac{1}{h_{1815_0} \cdot \sum_{si=2}^{4} A_{si}}$$

$$R_{2214_0} := \frac{1}{h_{2214_0} \cdot \sum_{iw=2}^{4} A_{iw}} \qquad R_{2215_0} := \frac{1}{h_{2215_0} \cdot \sum_{iw=2}^{4} A_{iw}}$$

$$R_{23\_1_0} := \frac{1}{h_{c1_0} \cdot A_{pv1}} \qquad R_{43\_1_0} := \frac{1}{h_{c1_0} \cdot A_{pv1}} \qquad R_{12\_1} := \frac{L_{pv}}{k_{pv} \cdot A_{pv1}}$$

$$R_{23\_2_0} := \frac{1}{h_{c2_0} \cdot \frac{A_{pv2}}{2}} \qquad R_{43\_2_0} := \frac{1}{h_{c2_0} \cdot \frac{A_{pv2}}{2}} \qquad R_{12\_2} := \frac{L_{pv}}{k_{pv} \cdot \frac{A_{pv2}}{2}}$$

$$R_{23\_3_0} := \frac{1}{h_{c3_0} \cdot \frac{A_{pv2}}{2}} \qquad R_{43\_3_0} := \frac{1}{h_{c3_0} \cdot \frac{A_{pv2}}{2}} \qquad R_{12\_3} := \frac{L_{pv}}{k_{pv} \cdot \frac{A_{pv2}}{2}}$$

$$R_{4B4\_1} := \frac{\frac{R_s}{2}}{A_{pv1}} + \frac{\frac{R_b}{2}}{A_{pv1}} \qquad R_{4B4\_2} := \frac{\frac{R_s}{2}}{\frac{A_{pv2}}{2}} + \frac{\frac{R_b}{2}}{\frac{A_{pv2}}{2}} \qquad R_{4B4\_3} := R_{4B4\_2} \qquad R_{4C5} := \frac{\frac{R_s}{2}}{A_{npv}} + \frac{\frac{R_b}{2}}{A_{npv}}$$

$$R_{4B5\_1} := \frac{\frac{R_s}{2}}{A_{pv1}} + \frac{\frac{R_b}{2}}{A_{pv1}} \qquad R_{4B5\_2} := \frac{\frac{R_s}{2}}{\frac{A_{pv2}}{2}} + \frac{\frac{R_b}{2}}{\frac{A_{pv2}}{2}} \qquad R_{4B5\_3} := R_{4B5\_2} \qquad R_{4C4A} := \frac{\frac{R_s}{2}}{A_{npv}} + \frac{\frac{R_b}{2}}{A_{npv}}$$

$$P_{el\_1_0} := \left[0.142 - 0.000636\left(T1\_1_0 - 25 \cdot degC\right)\right] \cdot Sse7\_t1_0$$

$$P_{el\_2_0} := \left[0.142 - 0.000636\left(T1\_2_0 - 25 \cdot degC\right)\right] \cdot Sse7\_t2_0$$

$$P_{el\_3_0} := \left[0.142 - 0.000636\left(T1\_3_0 - 25 \cdot degC\right)\right] \cdot Sse7\_t2_0$$

Matrix of Configuration 1

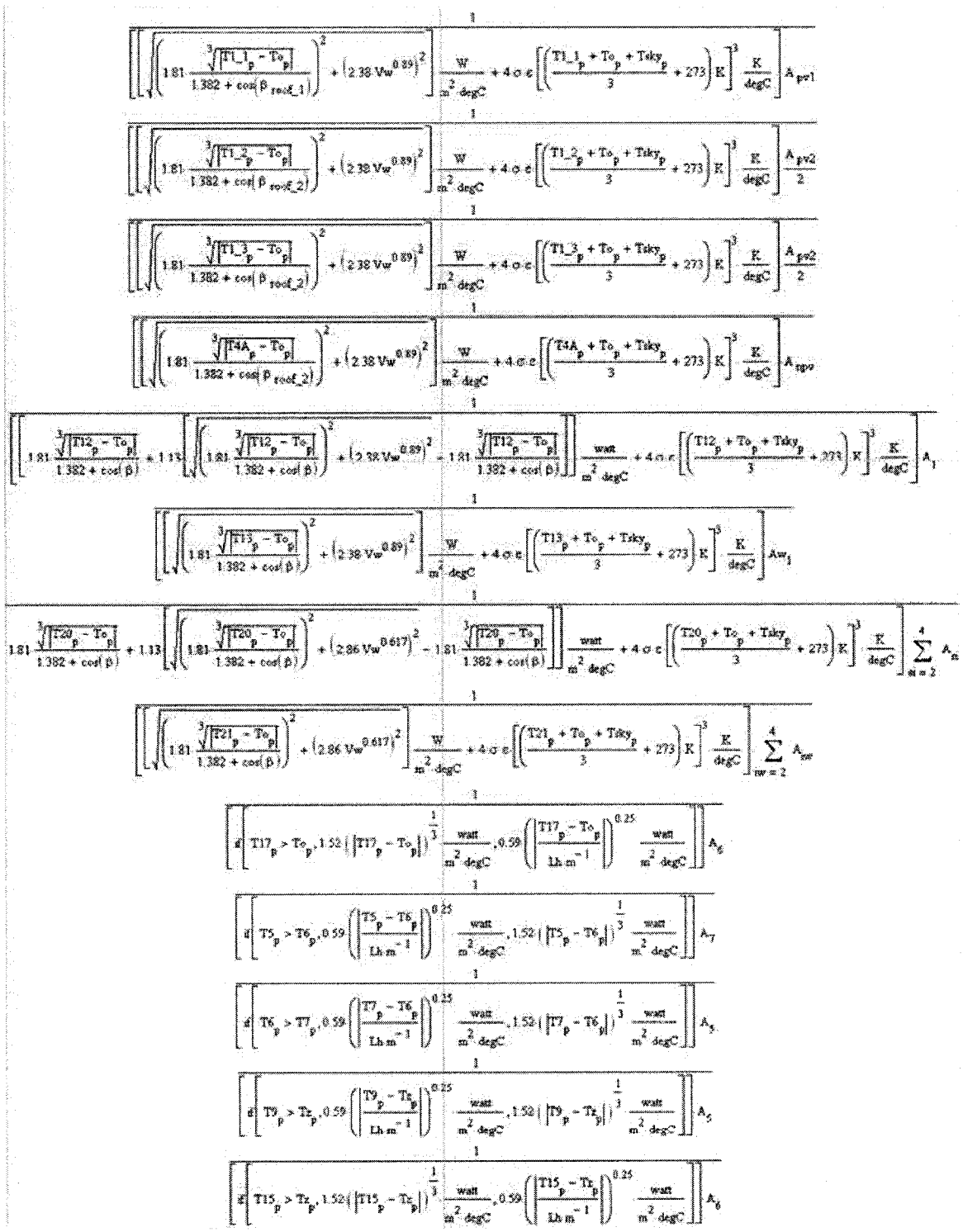

$$\frac{1}{\left[1.31\left(\left|T10_p - Tx_p\right|\right)^{\frac{1}{3}} \frac{watt}{m^2\ degC}\right] A_1}$$

$$\frac{1}{\left[1.31\left(\left|T14_p - Tx_p\right|\right)^{\frac{1}{3}} \frac{watt}{m^2\ degC}\right] Aw_1}$$

$$\frac{1}{\left[1.31\left(\left|T18_p - Tx_p\right|\right)^{\frac{1}{3}} \frac{watt}{m^2\ degC}\right] \sum_{as=2}^{4} A_{as}}$$

$$\frac{1}{\left[1.31\left(\left|T22_p - Tx_p\right|\right)^{\frac{1}{3}} \frac{watt}{m^2\ degC}\right] \sum_{aw=2}^{4} A_{aw}}$$

$$\frac{1}{\left[h_{wc} + \frac{4\,\sigma\left[\left(273 + \frac{T13_p + T14_p}{2}\right) K\right]^3}{\left(\frac{1}{\varepsilon_1} + \frac{1}{\varepsilon_{2e}} - 1\right)} \frac{K}{degC}\right] Aw_1}$$

$$\frac{1}{\left[h_{wc} + \frac{4\,\sigma\left[\left(273 + \frac{T21_p + T22_p}{2}\right) K\right]^3}{\left(\frac{1}{\varepsilon_1} + \frac{1}{\varepsilon_{2e}} - 1\right)} \frac{K}{degC}\right] \sum_{aw=2}^{4} A_{aw}}$$

$$\frac{1}{\left[\sigma F_\varepsilon Fv_{2\_4}\left[\frac{\left[\left(T2\_1_p + 273\right) K\right]^4 - \left[\left(T4\_1_p + 273\right) K\right]^4}{T2\_1_p - T4\_1_p}\right]\right] A_{pw1}}$$

$$\frac{1}{\left[\sigma F_\varepsilon Fv_{2\_4}\left[\frac{\left[\left(T4\_1_p + 273\right) K\right]^4 - \left[\left(T2\_1_p + 273\right) K\right]^4}{T4\_1_p - T2\_1_p}\right]\right] A_{pw1}}$$

$$\frac{1}{\left[\sigma F_\varepsilon Fv_{2\_4}\left[\frac{\left[\left(T2\_2_p + 273\right) K\right]^4 - \left[\left(T4\_2_p + 273\right) K\right]^4}{T2\_2_p - T4\_2_p}\right]\right] \frac{A_{pw2}}{2}}$$

$$\frac{1}{\left[\sigma F_\varepsilon Fv_{2\_4}\left[\frac{\left[\left(T4\_2_p + 273\right) K\right]^4 - \left[\left(T2\_2_p + 273\right) K\right]^4}{T4\_2_p - T2\_2_p}\right]\right] \frac{A_{pw2}}{2}}$$

$$\frac{1}{\left[\sigma F_\varepsilon Fv_{2\_4}\left[\frac{\left[\left(T2\_3_p + 273\right) K\right]^4 - \left[\left(T4\_3_p + 273\right) K\right]^4}{T2\_3_p - T4\_3_p}\right]\right] \frac{A_{pw2}}{2}}$$

$$\frac{1}{\left[\sigma F_\varepsilon Fv_{2\_4}\left[\frac{\left[\left(T4\_3_p + 273\right) K\right]^4 - \left[\left(T2\_3_p + 273\right) K\right]^4}{T4\_3_p - T2\_3_p}\right]\right] \frac{A_{pw2}}{2}}$$

$$\frac{1}{\left[\sigma F_\varepsilon Fv_{5\_7}\left[\frac{\left[\left(T5_p + 273\right) K\right]^4 - \left[\left(T7_p + 273\right) K\right]^4}{T5_p - T7_p}\right]\right] A_5}$$

$$\begin{pmatrix} R_{1\_1eq_{p+1}} \\ R_{1\_2eq_{p+1}} \\ R_{1\_3eq_{p+1}} \\ R_{4Aeq_{p+1}} \\ R_{12eq_{p+1}} \\ R_{13eq_{p+1}} \\ R_{20eq_{p+1}} \\ R_{21eq_{p+1}} \\ R_{17o_{p+1}} \\ R_{56_{p+1}} \\ R_{67_{p+1}} \\ R_{9z_{p+1}} \\ R_{15z_{p+1}} \\ R_{10z_{p+1}} \\ R_{14z_{p+1}} \\ R_{+\infty} \end{pmatrix}$$

$$\begin{pmatrix} \frac{1}{\left[\sigma \cdot F_{e} \cdot Fv_{7\_5}\left[\frac{\left[(T7_p + 273)\cdot K\right]^4 - \left[(T5_p + 273)\cdot K\right]^4}{T7_p - T5_p}\right] A_7\right]} \\ \frac{1}{\left[\sigma \cdot F_{e} \cdot Fv_{9\_10}\left[\frac{\left[(T9_p + 273)\cdot K\right]^4 - \left[(T10_p + 273)\cdot K\right]^4}{T9_p - T10_p}\right] A_5\right]} \\ \frac{1}{\left[\sigma \cdot F_{e} \cdot Fv_{9\_14}\left[\frac{\left[(T9_p + 273)\cdot K\right]^4 - \left[(T14_p + 273)\cdot K\right]^4}{T9_p - T14_p}\right] A_5\right]} \\ \frac{1}{\left[\sigma \cdot F_{e} \cdot Fv_{9\_15}\left[\frac{\left[(T9_p + 273)\cdot K\right]^4 - \left[(T15_p + 273)\cdot K\right]^4}{T9_p - T15_p}\right] A_5\right]} \\ \frac{1}{\left[\sigma \cdot F_{e} \cdot Fv_{9\_18}\left[\frac{\left[(T9_p + 273)\cdot K\right]^4 - \left[(T18_p + 273)\cdot K\right]^4}{T9_p - T18_p}\right] A_5\right]} \\ \frac{1}{\left[\sigma \cdot F_{e} \cdot Fv_{9\_22}\left[\frac{\left[(T9_p + 273)\cdot K\right]^4 - \left[(T22_p + 273)\cdot K\right]^4}{T9_p - T22_p}\right] A_5\right]} \\ \frac{1}{\left[\sigma \cdot F_{e} \cdot Fv_{10\_9}\left[\frac{\left[(T10_p + 273)\cdot K\right]^4 - \left[(T9_p + 273)\cdot K\right]^4}{T10_p - T9_p}\right] A_1\right]} \\ \frac{1}{\left[\sigma \cdot F_{e} \cdot Fv_{10\_15}\left[\frac{\left[(T10_p + 273)\cdot K\right]^4 - \left[(T15_p + 273)\cdot K\right]^4}{T10_p - T15_p}\right] A_1\right]} \\ \frac{1}{\left[\sigma \cdot F_{e} \cdot Fv_{10\_18}\left[\frac{\left[(T10_p + 273)\cdot K\right]^4 - \left[(T18_p + 273)\cdot K\right]^4}{T10_p - T18_p}\right] A_1\right]} \\ \frac{1}{\left[\sigma \cdot F_{e} \cdot Fv_{10\_22}\left[\frac{\left[(T10_p + 273)\cdot K\right]^4 - \left[(T22_p + 273)\cdot K\right]^4}{T10_p - T22_p}\right] A_1\right]} \\ \frac{1}{\left[\sigma \cdot F_{e} \cdot Fv_{14\_9}\left[\frac{\left[(T14_p + 273)\cdot K\right]^4 - \left[(T9_p + 273)\cdot K\right]^4}{T14_p - T9_p}\right] Aw_1\right]} \\ \frac{1}{\left[\sigma \cdot F_{e} \cdot Fv_{14\_15}\left[\frac{\left[(T14_p + 273)\cdot K\right]^4 - \left[(T15_p + 273)\cdot K\right]^4}{T14_p - T15_p}\right] Aw_1\right]} \\ \frac{1}{\left[\sigma \cdot F_{e} \cdot Fv_{14\_18}\left[\frac{\left[(T14_p + 273)\cdot K\right]^4 - \left[(T18_p + 273)\cdot K\right]^4}{T14_p - T18_p}\right] Aw_1\right]} \\ \frac{1}{\sigma \cdot F_{e} \cdot Fv_{14\_22}\left[\frac{\left[(T14_p + 273)\cdot K\right]^4 - \left[(T22_p + 273)\cdot K\right]^4}{T14_p - T22_p}\right] Aw_1} \end{pmatrix}$$

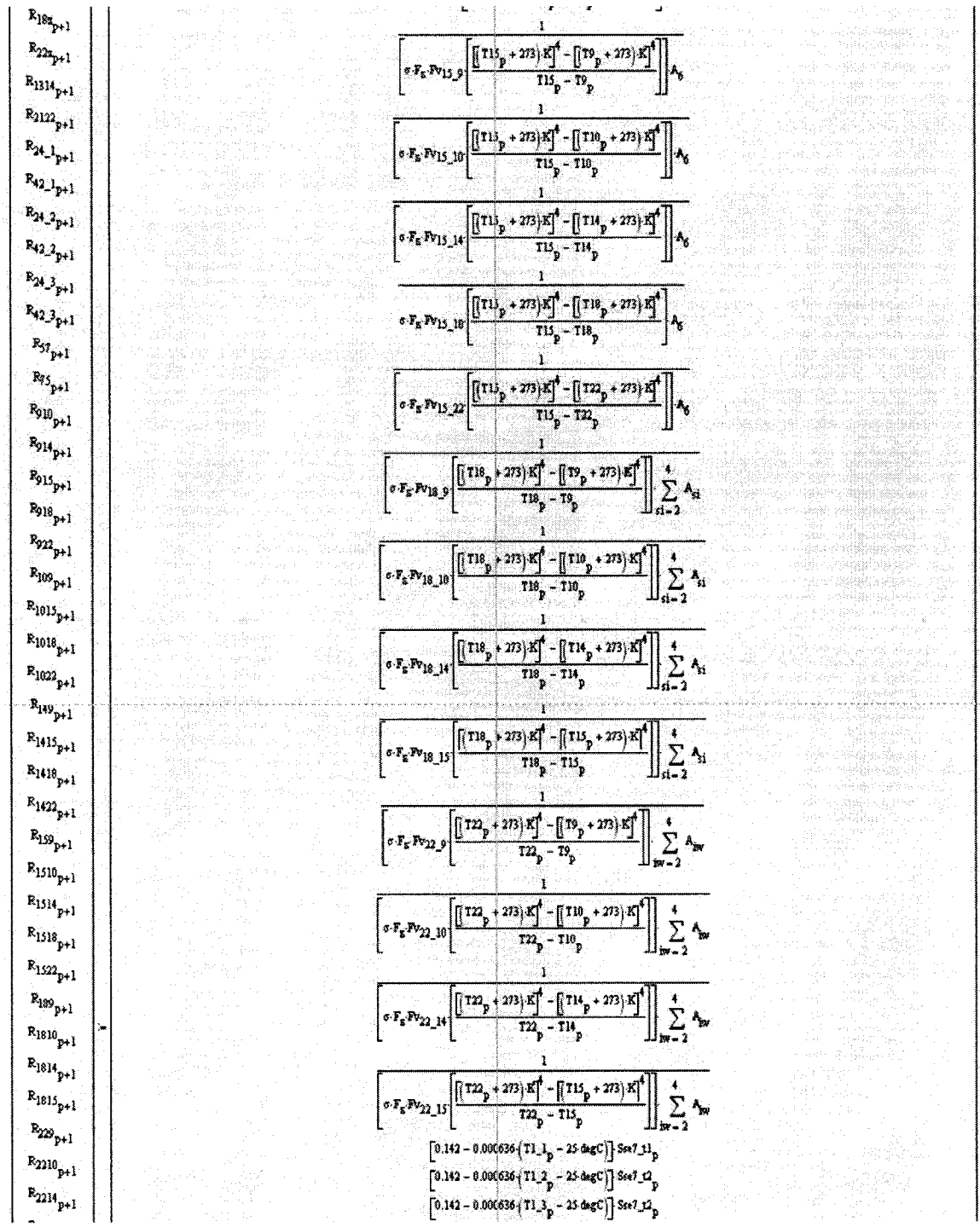

$K_{2215_{p+1}}$

$$\frac{\frac{To_p}{R_{1\_1eq_p}} + \left(Sse7\_1_p - P_{el\_1_p}\right) + \frac{T2\_1_p}{R_{12\_1}}}{\frac{1}{R_{1\_1eq_p}} + \frac{1}{R_{12\_1}}}$$

$P_{el\_1_{p+1}}$

$P_{el\_2_{p+1}}$

$$\frac{\frac{T1\_1_p}{R_{12\_1}} + \frac{T3\_1_p}{\frac{1}{h_{c1_p} \cdot A_{pv1}}} + \frac{T4\_1_p}{R_{24\_1_p}}}{\frac{1}{R_{12\_1}} + \frac{1}{\frac{1}{h_{c1_p} \cdot A_{pv1}}} + \frac{1}{R_{24\_1_p}}}$$

$P_{el\_3_{p+1}}$

$T1\_1_{p+1}$

$T2\_1_{p+1}$

$$\left[1 - e^{\frac{-\left(h_{c1_p} + h_{c1_p}\right)\left(A_{pv1}\right)}{m_{air_p} \cdot c_{p1}}}\right]\left[\frac{To_0 - \frac{\left(h_{c1_p} T2\_1_p + h_{c1_p} T4\_1_p\right)}{\left(h_{c1_p} + h_{c1_p}\right)}}{\frac{\left(h_{c1_p} + h_{c1_p}\right)\left(A_{pv1}\right)}{m_{air_p} \cdot c_{p1}}}\right] + \frac{h_{c1_p} T2\_1_p + h_{c1_p} T4\_1_p}{\left(h_{c1_p} + h_{c1_p}\right)}$$

$T3\_1_{p+1}$

$T_{air\_out\_1_{p+1}}$

$$\left[1 - e^{\frac{-\left(h_{c1_p} + h_{c1_p}\right) A_{pv1}}{m_{air_p} \cdot c_{p1}}}\right]\frac{h_{c1_p} T2\_1_p + h_{c1_p} T4\_1_p}{h_{c1_p} + h_{c1_p}} + \left[e^{\frac{-\left(h_{c1_p} + h_{c1_p}\right) A_{pv1}}{m_{air_p} \cdot c_{p1}}}\right] To_0$$

$T4\_1_{p+1}$

$T1\_2_{p+1}$

$$\frac{\frac{T3\_1_p}{\frac{1}{h_{c1_p} \cdot A_{pv1}}} + \frac{T2\_1_p}{R_{42\_1_p}} + \frac{T4B\_1_p}{R_{4B4\_1}}}{\frac{1}{\frac{1}{h_{c1_p} \cdot A_{pv1}}} + \frac{1}{R_{42\_1_p}} + \frac{1}{R_{4B4\_1}}}$$

$T2\_2_{p+1}$

$T3\_2_{p+1}$

$T_{air\_out\_2_{p+1}}$

$T4\_2_{p+1}$

$T1\_3_{p+1}$

$$\frac{\frac{To_p}{R_{1\_2eq_p}} + \left(Sse7\_2_p - P_{el\_2_p}\right) + \frac{T2\_2_p}{R_{12\_2}}}{\frac{1}{R_{1\_2eq_p}} + \frac{1}{R_{12\_2}}}$$

$T2\_3_{p+1}$

$T3\_3_{p+1}$

$T_{air\_out\_3_{p+1}}$

$T4\_3_{p+1}$

$T4A_{p+1}$

$$\frac{\frac{T1\_2_p}{R_{12\_2}} + \frac{T3\_2_p}{\frac{1}{h_{c2_p} \frac{A_{pv2}}{2}}} + \frac{T4\_2_p}{R_{24\_2_p}}}{\frac{1}{R_{12\_2}} + \frac{1}{\frac{1}{h_{c2_p} \frac{A_{pv2}}{2}}} + \frac{1}{R_{24\_2_p}}}$$

$T5_{p+1}$

$T4B\_1_{p+1}$

$T4B\_2_{p+1}$

$T4B\_3_{p+1}$

$T4B_{p+1}$

$T4C_{p+1}$

$T6_{p+1}$

$T7_{p+1}$

$T8_{p+1}$

$T9_{p+1}$

$T10_{p+1}$

$$\left[1 - e^{\frac{-\left(h_{c2_p} + h_{c2_p}\right)\frac{A_{pv2}}{2}}{m_{air_p} \cdot c_{p2}}}\right]\left[\frac{T_{air\_out\_1_p} - \frac{\left(h_{c2_p} T2\_2_p + h_{c2_p} T4\_2_p\right)}{\left(h_{c2_p} + h_{c2_p}\right)}}{\frac{\left(h_{c2_p} + h_{c2_p}\right)\frac{A_{pv2}}{2}}{m_{air_p} \cdot c_{p2}}}\right] + \frac{h_{c2_p} T2\_2_p + h_{c2_p} T4\_2_p}{\left(h_{c2_p} + h_{c2_p}\right)}$$

$T11_{p+1}$

$T12_{p+1}$

$T13_{p+1}$

$T14_{p+1}$

$T15_{p+1}$

$T16_{p+1}$

$T17_{p+1}$

$T18_{p+1}$

$T19_{p+1}$

$$\left[1 - e^{\frac{-\left(h_{c2_p} + h_{c2_p}\right)\frac{A_{pv2}}{2}}{m_{air_p} \cdot c_{p2}}}\right]\frac{h_{c2_p} T2\_2_p + h_{c2_p} T4\_2_p}{h_{c2_p} + h_{c2_p}} + \left[e^{\frac{-\left(h_{c2_p} + h_{c2_p}\right)\frac{A_{pv2}}{2}}{m_{air_p} \cdot c_{p2}}}\right] T_{air\_out\_1_p}$$

$$\begin{pmatrix} T19_{p+1} \\ T20_{p+1} \\ T21_{p+1} \\ T22_{p+1} \\ Tx_{p+1} \\ Q_{p+1} \end{pmatrix}$$

$$\frac{\dfrac{T3\_2_p}{\dfrac{1}{h_{c2_p}\cdot\dfrac{A_{pv2}}{2}}} + \dfrac{T2\_2_p}{R_{42\_2_p}} + \dfrac{T4B\_2_p}{R_{4B4\_2}}}{\dfrac{1}{\dfrac{1}{h_{c2_p}\cdot\dfrac{A_{pv2}}{2}}} + \dfrac{1}{R_{42\_2_p}} + \dfrac{1}{R_{4B4\_2}}}$$

$$\frac{\dfrac{To_p}{R_{1\_3eq_p}} + \left(Sse7\_2_p - P_{el\_3_p}\right) + \dfrac{T2\_3_p}{R_{12\_3}}}{\dfrac{1}{R_{1\_3eq_p}} + \dfrac{1}{R_{12\_3}}}$$

$$\frac{\dfrac{T1\_3_p}{R_{12\_3}} + \dfrac{T3\_3_p}{\dfrac{1}{h_{c3_p}\cdot\dfrac{A_{pv2}}{2}}} + \dfrac{T4\_3_p}{R_{24\_3_p}}}{\dfrac{1}{R_{12\_3}} + \dfrac{1}{\dfrac{1}{h_{c3_p}\cdot\dfrac{A_{pv2}}{2}}} + \dfrac{1}{R_{24\_3_p}}}$$

$$\left[1 - e^{\frac{-\left(h_{c3_p}+h_{c3_p}\right)\cdot\frac{A_{pv2}}{2}}{m_{air_p}\cdot c_{p3}}}\right]\left[\frac{T_{air\_out\_2_p} - \dfrac{\left(h_{c3_p}\cdot T2\_3_p + h_{c3_p}\cdot T4\_3_p\right)}{\left(h_{c3_p}+h_{c3_p}\right)}}{\dfrac{\left(h_{c3_p}+h_{c3_p}\right)\cdot\dfrac{A_{pv2}}{2}}{m_{air_p}\cdot c_{p3}}}\right] + \frac{h_{c3_p}\cdot T2\_3_p + h_{c3_p}\cdot T4\_3_p}{\left(h_{c3_p}+h_{c3_p}\right)}$$

$$\left[1 - e^{\frac{-\left(h_{c3_p}+h_{c3_p}\right)\cdot\frac{A_{pv2}}{2}}{m_{air_p}\cdot c_{p3}}}\right]\frac{h_{c3_p}\cdot T2\_3_p + h_{c3_p}\cdot T4\_3_p}{h_{c3_p}+h_{c3_p}} + \left[e^{\frac{-\left(h_{c3_p}+h_{c3_p}\right)\cdot\frac{A_{pv2}}{2}}{m_{air_p}\cdot c_{p3}}}\right]T_{air\_out\_2_p}$$

$$\frac{\dfrac{T3\_3_p}{\dfrac{1}{h_{c3_p}\cdot\dfrac{A_{pv2}}{2}}} + \dfrac{T2\_3_p}{R_{42\_3_p}} + \dfrac{T4B\_3_p}{R_{4B4\_3}}}{\dfrac{1}{\dfrac{1}{h_{c3_p}\cdot\dfrac{A_{pv2}}{2}}} + \dfrac{1}{R_{42\_3_p}} + \dfrac{1}{R_{4B4\_3}}}$$

$$\frac{\dfrac{To_p}{R_{4Aeq_p}} + Sse7\_3_p + \dfrac{T4C_p}{R_{4C4A}}}{\dfrac{1}{R_{4Aeq_p}} + \dfrac{1}{R_{4C4A}}}$$

$$\frac{\dfrac{T4B_p}{R_{4B5}} + \dfrac{T6_p}{R_{56_p}} + \dfrac{T7_p}{R_{57_p}} + \dfrac{T4C_p}{R_{4C5}}}{\dfrac{1}{R_{4B5}} + \dfrac{1}{R_{56_p}} + \dfrac{1}{R_{57_p}} + \dfrac{1}{R_{4C5}}}$$

$$\frac{\Delta t}{\dfrac{C_{4B}}{3}}\left(\frac{T4\_1_p - T4B\_1_p}{R_{4B4\_1}} + \frac{T5_p - T4B\_1_p}{R_{4B5\_1}}\right) + T4B\_1_p$$

$$\frac{\Delta t}{\frac{C_{4B}}{3}}\left(\frac{T4\_1_p - T4B\_1_p}{R_{4B4\_1}} + \frac{T5_p - T4B\_1_p}{R_{4B5\_1}}\right) + T4B\_1_p$$

$$\frac{\Delta t}{\frac{C_{4B}}{3}}\left(\frac{T4\_2_p - T4B\_2_p}{R_{4B4\_2}} + \frac{T5_p - T4B\_2_p}{R_{4B5\_2}}\right) + T4B\_2_p$$

$$\frac{\Delta t}{\frac{C_{4B}}{3}}\left(\frac{T4\_3_p - T4B\_3_p}{R_{4B4\_3}} + \frac{T5_p - T4B\_3_p}{R_{4B5\_3}}\right) + T4B\_3_p$$

$$\frac{T4B\_1_p + T4B\_2_p + T4B\_3_p}{3}$$

$$\frac{\Delta t}{C_{4C}}\left(\frac{T4A_p - T4C_p}{R_{4C4A}} + \frac{T5_p - T4C_p}{R_{4C5}}\right) + T4C_p$$

$$\frac{\frac{T5_p}{R_{56_p}} + \frac{T7_p}{R_{67_p}} + \frac{To_p}{R_{mf2}}}{\frac{1}{R_{56_p}} + \frac{1}{R_{67_p}} + \frac{1}{R_{mf2}}}$$

$$\frac{\frac{T5_p}{R_{75_p}} + \frac{T6_p}{R_{67_p}} + \frac{T8_p}{R_{78}}}{\frac{1}{R_{75_p}} + \frac{1}{R_{67_p}} + \frac{1}{R_{78}}}$$

$$\frac{\Delta t}{C_8}\left(\frac{T7_p - T8_p}{R_{78}} + \frac{T9_p - T8_p}{R_{89}}\right) + T8_p$$

$$\frac{\frac{T8_p}{R_{89}} + \left(Sn5_p + Qrn_{mt_{p,5}}\right) + \frac{Tz_p}{R_{9z_p}} + \frac{T10_p}{R_{910_p}} + \frac{T14_p}{R_{914_p}} + \frac{T18_p}{R_{918_p}} + \frac{T22_p}{R_{922_p}} + \frac{T15_p}{R_{915_p}}}{\frac{1}{R_{89}} + \frac{1}{R_{9z_p}} + \frac{1}{R_{910_p}} + \frac{1}{R_{914_p}} + \frac{1}{R_{918_p}} + \frac{1}{R_{922_p}} + \frac{1}{R_{915_p}}}$$

$$\frac{\frac{T11_p}{R_{1011}} + \left(Sn1_p + Qrn_{mt_{p,1}}\right) + \frac{Tz_p}{R_{10z_p}} + \frac{T15_p}{R_{1015_p}} + \frac{T18_p}{R_{1018_p}} + \frac{T22_p}{R_{1022_p}} + \frac{T9_p}{R_{109_p}}}{\frac{1}{R_{1011}} + \frac{1}{R_{10z_p}} + \frac{1}{R_{1015_p}} + \frac{1}{R_{1018_p}} + \frac{1}{R_{1022_p}} + \frac{1}{R_{109_p}}}$$

$$\frac{\Delta t}{C_{11}}\left(\frac{T10_p - T11_p}{R_{1011}} + \frac{T12_p - T11_p}{R_{1112}}\right) + T11_p$$

$$\frac{\frac{T11_p}{R_{1112}} + Sn1_p + \frac{To_p}{R_{12eq_p}}}{\frac{1}{R_{1112}} + \frac{1}{R_{12eq_p}}}$$

$$\frac{\frac{T14_p}{R_{1314_p}} + Sw1_p + \frac{To_p}{R_{13eq_p}}}{\frac{1}{R_{1314_p}} + \frac{1}{R_{13eq_p}}}$$

$$\frac{\frac{T13_p}{R_{1314_p}} + \left(Sw1_p + Qrw_{mt_{p,1}}\right) + \frac{Tz_p}{R_{14z_p}} + \frac{T15_p}{R_{1415_p}} + \frac{T22_p}{R_{1422_p}} + \frac{T9_p}{R_{149_p}} + \frac{T18_p}{R_{1418_p}}}{\frac{1}{R_{1314_p}} + \frac{1}{R_{14z_p}} + \frac{1}{R_{1415_p}} + \frac{1}{R_{1422_p}} + \frac{1}{R_{149_p}} + \frac{1}{R_{1418_p}}}$$

$$\frac{\frac{T13_p}{R_{1314_p}} + \left(Swil_F + Qrw_{int_{p,1}}\right) + \frac{Tz_p}{R_{14z_p}} + \frac{T15_p}{R_{1415_p}} + \frac{T22_F}{R_{1422_p}} + \frac{T9_p}{R_{149_p}} + \frac{T18_F}{R_{1418_p}}}{\frac{1}{R_{1314_F}} + \frac{1}{R_{14z_p}} + \frac{1}{R_{1415_p}} + \frac{1}{R_{1422_p}} + \frac{1}{R_{149_p}} + \frac{1}{R_{1418_p}}}$$

$$\frac{\frac{T10_p}{R_{1510_p}} + \frac{T9_p}{R_{159_p}} + \frac{Tz_p}{R_{15z_p}} + \frac{T14_p}{R_{1514_p}} + \frac{T16_p}{R_{1516}} + \frac{T18_F}{R_{1518_p}} + \frac{T22_p}{R_{1522_p}} + \left(Ssi6_p + Qrsi_{int_{p,6}}\right)}{\frac{1}{R_{1510_p}} + \frac{1}{R_{15z_p}} + \frac{1}{R_{1514_p}} + \frac{1}{R_{1516}} + \frac{1}{R_{1518_p}} + \frac{1}{R_{1522_p}} + \frac{1}{R_{159_p}}}$$

$$\frac{\Delta t}{C_{16}}\left(\frac{T17_p - T16_p}{R_{1617}} + \frac{T15_p - T16_p}{R_{1516}}\right) + T16_p$$

$$\frac{\frac{To_p}{R_{17o_p}} + \frac{T16_p}{R_{1617}}}{\frac{1}{R_{17o_p}} + \frac{1}{R_{1617}}}$$

$$\frac{\frac{T10_p}{R_{1810_F}} + \frac{T15_p}{R_{1815_p}} + \frac{T9_p}{R_{189_p}} + \frac{Tz_p}{R_{18z_p}} + \frac{T14_p}{R_{1814_p}} + \frac{T19_F}{R_{1819}} + Ssi8_p + Qrsi8_{int_p}}{\frac{1}{R_{1810_p}} + \frac{1}{R_{18z_p}} + \frac{1}{R_{1814_p}} + \frac{1}{R_{1819}} + \frac{1}{R_{1815_p}} + \frac{1}{R_{189_p}}}$$

$$\frac{\Delta t}{C_{19}}\left(\frac{T18_p - T19_p}{R_{1819}} + \frac{T20_p - T19_p}{R_{1920}}\right) + T19_p$$

$$\frac{\frac{T19_p}{R_{1920}} + \frac{To_p}{R_{20eq_p}} + Swi20_p}{\frac{1}{R_{1920}} + \frac{1}{R_{20eq_p}}}$$

$$\frac{\frac{T22_p}{R_{2122_p}} + \frac{To_p}{R_{21eq_p}} + Swo21_p}{\frac{1}{R_{2122_F}} + \frac{1}{R_{21eq_p}}}$$

$$\frac{\frac{Tz_F}{R_{22z_p}} + \frac{T15_p}{R_{2215_F}} + \frac{T21_p}{R_{2122_p}} + \frac{T10_p}{R_{2210_p}} + \frac{T9_p}{R_{229_p}} + \frac{T14_F}{R_{2214_p}} + Swi22_p + Qrw22_{int_p}}{\frac{1}{R_{22z_p}} + \frac{1}{R_{2215_F}} + \frac{1}{R_{2122_F}} + \frac{1}{R_{2210_p}} + \frac{1}{R_{2214_p}} + \frac{1}{R_{229_p}}}$$

$$\frac{\Delta t}{C_{air}}\left(\frac{T9_F - Tz_p}{R_{9z_p}} + \frac{T22_p - Tz_p}{R_{22z_p}} + \frac{T18_p - Tz_p}{R_{18z_p}} + \frac{T15_p - Tz_p}{R_{15z_p}} + \frac{T14_p - Tz_p}{R_{14z_p}} + \frac{T10_p - Tz_p}{R_{10z_p}} + \frac{To_p - Tz_p}{R_{infl}} + \frac{To_p - Tz_p}{R_{door1}} + \frac{To_p - Tz_p}{R_{door2}} + Qrev_{air_p}\right) + Tz_p$$

$$\frac{Tsp - T9_p}{R_{9z_p}} + \frac{Tsp - T22_p}{R_{22z_p}} + \frac{Tsp - T18_F}{R_{18z_p}} + \frac{Tsp - T15_F}{R_{15z_p}} + \frac{Tsp - T14_p}{R_{14z_p}} + \frac{Tsp - T10_p}{R_{10z_p}} + \frac{Tsp - To_F}{R_{infl}} + \frac{Tsp - To_p}{R_{door1}} + \frac{Tsp - To_p}{R_{door2}} - Qrev_{air_p}$$

Matrix of Configuration 2

$$\left[\left[\sqrt{\left(1.81\cdot\frac{\sqrt[3]{\left|T1\_1_p - To_p\right|}}{1.382+\cos(\beta_{roof\_1})}\right)^2+\left(2.38\cdot Vw^{0.89}\right)^2}\right]\cdot\frac{W}{m^2\cdot degC}+4\cdot\sigma\cdot\varepsilon\cdot\left[\left(\frac{T1\_1_p+To_p+Tsky_p}{3}+273\right)\cdot K\right]^3\cdot\frac{K}{degC}\right]\cdot A_{pv1}$$

$$\left[\left[\sqrt{\left(1.81\cdot\frac{\sqrt[3]{\left|T1\_2_p - To_p\right|}}{1.382+\cos(\beta_{roof\_2})}\right)^2+\left(2.38\cdot Vw^{0.89}\right)^2}\right]\cdot\frac{W}{m^2\cdot degC}+4\cdot\sigma\cdot\varepsilon\cdot\left[\left(\frac{T1\_2_p+To_p+Tsky_p}{3}+273\right)\cdot K\right]^3\cdot\frac{K}{degC}\right]\cdot\frac{A_{pv2}}{2}$$

$$\left[\left[\sqrt{\left(1.81\cdot\frac{\sqrt[3]{\left|T1\_3_p - To_p\right|}}{1.382+\cos(\beta_{roof\_2})}\right)^2+\left(2.38\cdot Vw^{0.89}\right)^2}\right]\cdot\frac{W}{m^2\cdot degC}+4\cdot\sigma\cdot\varepsilon\cdot\left[\left(\frac{T1\_3_p+To_p+Tsky_p}{3}+273\right)\cdot K\right]^3\cdot\frac{K}{degC}\right]\cdot\frac{A_{pv2}}{2}$$

$$\left[\left[\sqrt{\left(1.81\cdot\frac{\sqrt[3]{\left|T4A_p - To_p\right|}}{1.382+\cos(\beta_{roof\_2})}\right)^2+\left(2.38\cdot Vw^{0.89}\right)^2}\right]\cdot\frac{W}{m^2\cdot degC}+4\cdot\sigma\cdot\varepsilon\cdot\left[\left(\frac{T4A_p+To_p+Tsky_p}{3}+273\right)\cdot K\right]^3\cdot\frac{K}{degC}\right]\cdot A_{upv}$$

$$\left[\left[\sqrt{\left(1.81\cdot\frac{\sqrt[3]{\left|T4D_p - To_p\right|}}{1.382+\cos(\beta)}\right)^2+\left(2.38\cdot Vw^{0.89}\right)^2}\right]\cdot\frac{W}{m^2\cdot degC}+4\cdot\sigma\cdot\varepsilon\cdot\left[\left(\frac{T4D_p+To_p+Tsky_p}{3}+273\right)\cdot K\right]^3\cdot\frac{K}{degC}\right]\cdot A_{sat}$$

$$\left[\left[\sqrt{\left(1.81\cdot\frac{\sqrt[3]{\left|T6D_p - To_p\right|}}{1.382+\cos(\beta)}\right)^2+\left(2.86\cdot Vw^{0.617}\right)^2}\right]\cdot\frac{W}{m^2\cdot degC}+4\cdot\sigma\cdot\varepsilon\cdot\left[\left(\frac{T6D_p+To_p+Tsky_p}{3}+273\right)\cdot K\right]^3\cdot\frac{K}{degC}\right]\cdot A_{sat}$$

$$\left[\left[1.81\cdot\frac{\sqrt[3]{\left|T12_p - To_p\right|}}{1.382+\cos(\beta)}+1.13\left[\sqrt{\left(1.81\cdot\frac{\sqrt[3]{\left|T12_p - To_p\right|}}{1.382+\cos(\beta)}\right)^2+\left(2.38\cdot Vw^{0.89}\right)^2}-1.81\cdot\frac{\sqrt[3]{\left|T12_p - To_p\right|}}{1.382+\cos(\beta)}\right]\right]\cdot\frac{watt}{m^2\cdot degC}+4\cdot\sigma\cdot\varepsilon\cdot\left[\left(\frac{T12_p+To_p+Tsky_p}{3}+273\right)\cdot K\right]^3\cdot\frac{K}{degC}\right]\cdot A_1$$

$$\left[\left[\sqrt{\left(1.81\cdot\frac{\sqrt[3]{\left|T13_p - To_p\right|}}{1.382+\cos(\beta)}\right)^2+\left(2.38\cdot Vw^{0.89}\right)^2}\right]\cdot\frac{W}{m^2\cdot degC}+4\cdot\sigma\cdot\varepsilon\cdot\left[\left(\frac{T13_p+To_p+Tsky_p}{3}+273\right)\cdot K\right]^3\cdot\frac{K}{degC}\right]\cdot Aw_1$$

$$\left[\left[1.81\cdot\frac{\sqrt[3]{\left|T20_p - To_p\right|}}{1.382+\cos(\beta)}+1.13\left[\sqrt{\left(1.81\cdot\frac{\sqrt[3]{\left|T20_p - To_p\right|}}{1.382+\cos(\beta)}\right)^2+\left(2.86\cdot Vw^{0.617}\right)^2}-1.81\cdot\frac{\sqrt[3]{\left|T20_p - To_p\right|}}{1.382+\cos(\beta)}\right]\right]\cdot\frac{watt}{m^2\cdot degC}+4\cdot\sigma\cdot\varepsilon\cdot\left[\left(\frac{T20_p+To_p+Tsky_p}{3}+273\right)\cdot K\right]^3\cdot\frac{K}{degC}\right]\cdot\sum_{m=2}^{4}A_m$$

$$\left[\left[\sqrt{\left(1.81\cdot\frac{\sqrt[3]{\left|T21_p - To_p\right|}}{1.382+\cos(\beta)}\right)^2+\left(2.86\cdot Vw^{0.617}\right)^2}\right]\cdot\frac{W}{m^2\cdot degC}+4\cdot\sigma\cdot\varepsilon\cdot\left[\left(\frac{T21_p+To_p+Tsky_p}{3}+273\right)\cdot K\right]^3\cdot\frac{K}{degC}\right]\cdot\sum_{ww=2}^{4}A_{ww}$$

$$\left[if\left[T17_p > To_p, 1.52\left(\left|T17_p - To_p\right|\right)^{\frac{1}{3}}\cdot\frac{watt}{m^2\cdot degC}, 0.59\left(\left|\frac{T17_p - To_p}{Lh\cdot m^{-1}}\right|\right)^{0.25}\cdot\frac{watt}{m^2\cdot degC}\right]\right]\cdot A_6$$

$$\left[if\left[T5_p > T6_p, 0.59\left(\left|\frac{T5_p - T6_p}{Lh\cdot m^{-1}}\right|\right)^{0.25}\cdot\frac{watt}{m^2\cdot degC}, 1.52\left(\left|T5_p - T6_p\right|\right)^{\frac{1}{2}}\cdot\frac{watt}{m^2\cdot degC}\right]\right]\cdot A_7$$

$$\frac{1}{\left[\text{if}\left[T6_p > T7_p, 0.59\left(\left|\frac{T7_p - T6_p}{Lh \cdot m^{-1}}\right|\right)^{0.25} \frac{watt}{m^2 \cdot degC}, 1.52\left(\left|T7_p - T6_p\right|\right)^{\frac{1}{3}} \cdot \frac{watt}{m^2 \cdot degC}\right]\right] \cdot A_5}$$

$$\frac{1}{\left[\text{if}\left[T9_p > Tz_p, 0.59\left(\left|\frac{T9_p - Tz_p}{Lh \cdot m^{-1}}\right|\right)^{0.25} \frac{watt}{m^2 \cdot degC}, 1.52\left(\left|T9_p - Tz_p\right|\right)^{\frac{1}{3}} \cdot \frac{watt}{m^2 \cdot degC}\right]\right] \cdot A_5}$$

$$\frac{1}{\left[\text{if}\left[T15_p > Tz_p, 1.52\left(\left|T15_p - Tz_p\right|\right)^{\frac{1}{3}} \cdot \frac{watt}{m^2 \cdot degC}, 0.59\left(\left|\frac{T15_p - Tz_p}{Lh \cdot m^{-1}}\right|\right)^{0.25} \cdot \frac{watt}{m^2 \cdot degC}\right]\right] \cdot A_6}$$

$$\frac{1}{\left[1.31\left(\left|T10_p - Tz_p\right|\right)^{\frac{1}{3}} \cdot \frac{watt}{m^2 \cdot degC}\right] \cdot A_1}$$

$$\frac{1}{\left[1.31\left(\left|T14_p - Tz_p\right|\right)^{\frac{1}{3}} \cdot \frac{watt}{m^2 \cdot degC}\right] \cdot Aw_1}$$

$$\frac{1}{\left[1.31\left(\left|T18_p - Tz_p\right|\right)^{\frac{1}{3}} \cdot \frac{watt}{m^2 \cdot degC}\right] \sum_{si=2}^{4} A_{si}}$$

$$\frac{1}{\left[1.31\left(\left|T22_p - Tz_p\right|\right)^{\frac{1}{3}} \cdot \frac{watt}{m^2 \cdot degC}\right] \sum_{sw=2}^{4} A_{sw}}$$

$$\frac{1}{\left[h_{wc} + \frac{4 \cdot \sigma \cdot \left[\left(273 + \frac{T13_p + T14_p}{2}\right) K\right]^3}{\left(\frac{1}{\varepsilon_1} + \frac{1}{\varepsilon_{2e}} - 1\right)} \frac{K}{degC}\right] \cdot Aw_1}$$

$$\frac{1}{\left[h_{wc} + \frac{4 \cdot \sigma \cdot \left[\left(273 + \frac{T21_p + T22_p}{2}\right) K\right]^3}{\left(\frac{1}{\varepsilon_1} + \frac{1}{\varepsilon_{2e}} - 1\right)} \frac{K}{degC}\right] \sum_{sw=2}^{4} A_{sw}}$$

$$\frac{1}{\left[\sigma \cdot F_\varepsilon \cdot Fv_{2\_4}\left[\frac{\left[\left(T2\_1_p + 273\right) K\right]^4 - \left[\left(T4\_1_p + 273\right) \cdot K\right]^4}{T2\_1_p - T4\_1_p}\right]\right] \cdot A_{pv1}}$$

$$\frac{1}{\left[\sigma \cdot F_\varepsilon \cdot Fv_{2\_4}\left[\frac{\left[\left(T4\_1_p + 273\right) K\right]^4 - \left[\left(T2\_1_p + 273\right) \cdot K\right]^4}{T4\_1_p - T2\_1_p}\right]\right] \cdot A_{pv1}}$$

$$\frac{1}{\left[\sigma \cdot F_\varepsilon \cdot Fv_{2\_4}\left[\frac{\left[\left(T2\_2_p + 273\right) K\right]^4 - \left[\left(T4\_2_p + 273\right) \cdot K\right]^4}{T2\_2_p - T4\_2_p}\right]\right] \frac{A_{pv2}}{2}}$$

$$\begin{pmatrix} R_{1\_1eq_{p+1}} \\ R_{1\_2eq_{p+1}} \\ R_{1\_3eq_{p+1}} \\ R_{4Aeq_{p+1}} \\ R_{4Deq_{p+1}} \\ R_{6Deq_{p+1}} \\ R_{12eq} \end{pmatrix}$$

$$\frac{1}{\left[\sigma \cdot F_{\varepsilon} \cdot Fv_{2\_4}\left[\frac{\left[\left(T4\_2_p + 273\right)\cdot K\right]^4 - \left[\left(T2\_2_p + 273\right)\cdot K\right]^4}{T4\_2_p - T2\_2_p}\right]\right] \cdot \frac{A_{pv2}}{2}}$$

$$\frac{1}{\left[\sigma \cdot F_{\varepsilon} \cdot Fv_{2\_4}\left[\frac{\left[\left(T2\_3_p + 273\right)\cdot K\right]^4 - \left[\left(T4\_3_p + 273\right)\cdot K\right]^4}{T2\_3_p - T4\_3_p}\right]\right] \cdot \frac{A_{pv2}}{2}}$$

$$\frac{1}{\left[\sigma \cdot F_{\varepsilon} \cdot Fv_{2\_4}\left[\frac{\left[\left(T4\_3_p + 273\right)\cdot K\right]^4 - \left[\left(T2\_3_p + 273\right)\cdot K\right]^4}{T4\_3_p - T2\_3_p}\right]\right] \cdot \frac{A_{pv2}}{2}}$$

$$\frac{1}{\left[\sigma \cdot F_{\varepsilon} \cdot Fv_{5\_7}\left[\frac{\left[\left(T5_p + 273\right)\cdot K\right]^4 - \left[\left(T7_p + 273\right)\cdot K\right]^4}{T5_p - T7_p}\right]\right] \cdot A_5}$$

$$\frac{1}{\left[\sigma \cdot F_{\varepsilon} \cdot Fv_{7\_5}\left[\frac{\left[\left(T7_p + 273\right)\cdot K\right]^4 - \left[\left(T5_p + 273\right)\cdot K\right]^4}{T7_p - T5_p}\right]\right] \cdot A_7}$$

$$\frac{1}{\left[\sigma \cdot F_{\varepsilon} \cdot Fv_{9\_10}\left[\frac{\left[\left(T9_p + 273\right)\cdot K\right]^4 - \left[\left(T10_p + 273\right)\cdot K\right]^4}{T9_p - T10_p}\right]\right] \cdot A_5}$$

$$\frac{1}{\left[\sigma \cdot F_{\varepsilon} \cdot Fv_{9\_14}\left[\frac{\left[\left(T9_p + 273\right)\cdot K\right]^4 - \left[\left(T14_p + 273\right)\cdot K\right]^4}{T9_p - T14_p}\right]\right] \cdot A_5}$$

$$\frac{1}{\left[\sigma \cdot F_{\varepsilon} \cdot Fv_{9\_15}\left[\frac{\left[\left(T9_p + 273\right)\cdot K\right]^4 - \left[\left(T15_p + 273\right)\cdot K\right]^4}{T9_p - T15_p}\right]\right] \cdot A_5}$$

$$\frac{1}{\left[\sigma \cdot F_{\varepsilon} \cdot Fv_{9\_18}\left[\frac{\left[\left(T9_p + 273\right)\cdot K\right]^4 - \left[\left(T18_p + 273\right)\cdot K\right]^4}{T9_p - T18_p}\right]\right] \cdot A_5}$$

$$\frac{1}{\left[\sigma \cdot F_{\varepsilon} \cdot Fv_{10\_9}\left[\frac{\left[\left(T10_p + 273\right)\cdot K\right]^4 - \left[\left(T9_p + 273\right)\cdot K\right]^4}{T10_p - T9_p}\right]\right] \cdot A_1}$$

$$\frac{1}{\left[\sigma \cdot F_{\varepsilon} \cdot Fv_{10\_15}\left[\frac{\left[\left(T10_p + 273\right)\cdot K\right]^4 - \left[\left(T15_p + 273\right)\cdot K\right]^4}{T10_p - T15_p}\right]\right] \cdot A_1}$$

$$\frac{1}{\left[\sigma \cdot F_{\varepsilon} \cdot Fv_{10\_22}\left[\frac{\left[\left(T10_p + 273\right)\cdot K\right]^4 - \left[\left(T22_p + 273\right)\cdot K\right]^4}{T10_p - T22_p}\right]\right] \cdot A_1}$$

$$\frac{1}{\left[\sigma \cdot F_{\varepsilon} \cdot Fv_{14\_9}\left[\frac{\left[\left(T14_p + 273\right)\cdot K\right]^4 - \left[\left(T9_p + 273\right)\cdot K\right]^4}{T14_p - T9_p}\right]\right] \cdot Aw_1}$$

$$\frac{1}{\left[\sigma \cdot F_{\varepsilon} \cdot Fv_{14\_15}\left[\frac{\left[\left(T14_p + 273\right)\cdot K\right]^4 - \left[\left(T15_p + 273\right)\cdot K\right]^4}{T14_p - T15_p}\right]\right] \cdot Aw_1}$$

$$R_{13eq_{p+1}} \quad \frac{1}{\left[\sigma \cdot F_g \cdot Fv_{14\_18}\left[\frac{\left[\left(T14_p + 273\right)\cdot K\right]^4 - \left[\left(T18_p + 273\right)\cdot K\right]^4}{T14_p - T18_p}\right]\right] \cdot Aw_1}$$

$$R_{20eq_{p+1}} \quad \frac{1}{\left[\sigma \cdot F_g \cdot Fv_{14\_22}\left[\frac{\left[\left(T14_p + 273\right)\cdot K\right]^4 - \left[\left(T22_p + 273\right)\cdot K\right]^4}{T14_p - T22_p}\right]\right] \cdot Aw_1}$$

$$R_{21eq_{p+1}} \quad \frac{1}{\left[\sigma \cdot F_g \cdot Fv_{15\_9}\left[\frac{\left[\left(T15_p + 273\right)\cdot K\right]^4 - \left[\left(T9_p + 273\right)\cdot K\right]^4}{T15_p - T9_p}\right]\right] A_6}$$

$$R_{17o_{p+1}} \quad \frac{1}{\left[\sigma \cdot F_g \cdot Fv_{15\_10}\left[\frac{\left[\left(T15_p + 273\right)\cdot K\right]^4 - \left[\left(T10_p + 273\right)\cdot K\right]^4}{T15_p - T10_p}\right]\right] A_6}$$

$$R_{55_{p+1}} \quad \frac{1}{\left[\sigma \cdot F_g \cdot Fv_{15\_14}\left[\frac{\left[\left(T15_p + 273\right)\cdot K\right]^4 - \left[\left(T14_p + 273\right)\cdot K\right]^4}{T15_p - T14_p}\right]\right] A_6}$$

$$R_{67_{p+1}} \quad \frac{1}{\left[\sigma \cdot F_g \cdot Fv_{18\_10}\left[\frac{\left[\left(T18_p + 273\right)\cdot K\right]^4 - \left[\left(T10_p + 273\right)\cdot K\right]^4}{T18_p - T10_p}\right]\right] \sum_{si=2}^{4} A_{si}}$$

$$R_{9x_{p+1}} \quad \frac{1}{\left[\sigma \cdot F_g \cdot Fv_{18\_14}\left[\frac{\left[\left(T18_p + 273\right)\cdot K\right]^4 - \left[\left(T14_p + 273\right)\cdot K\right]^4}{T18_p - T14_p}\right]\right] \sum_{si=2}^{4} A_{si}}$$

$$R_{15z_{p+1}} \quad \frac{1}{\left[\sigma \cdot F_g \cdot Fv_{22\_10}\left[\frac{\left[\left(T22_p + 273\right)\cdot K\right]^4 - \left[\left(T10_p + 273\right)\cdot K\right]^4}{T22_p - T10_p}\right]\right] \sum_{sw=2}^{4} A_{sw}}$$

$$R_{10z_{p+1}} \quad \frac{1}{\left[\sigma \cdot F_g \cdot Fv_{22\_14}\left[\frac{\left[\left(T22_p + 273\right)\cdot K\right]^4 - \left[\left(T14_p + 273\right)\cdot K\right]^4}{T22_p - T14_p}\right]\right] \sum_{sw=2}^{4} A_{sw}}$$

$$R_{14z_{p+1}} \quad \frac{1}{\left[\sigma \cdot F_g \cdot Fv_{4D\_5D}\left[\frac{\left[\left(T4D_p + 273\right)\cdot K\right]^4 - \left[\left(T5D_p + 273\right)\cdot K\right]^4}{T4D_p - T5D_p}\right]\right] A_{sw}}$$

$$R_{18z_{p+1}} \quad \frac{1}{\left[\sigma \cdot F_g \cdot Fv_{5D\_4D}\left[\frac{\left[\left(T5D_p + 273\right)\cdot K\right]^4 - \left[\left(T4D_p + 273\right)\cdot K\right]^4}{T5D_p - T4D_p}\right]\right] A_{sw}}$$

$$R_{22z_{p+1}} \quad \left[0.142 - 0.000636\cdot\left(T1\_1_p - 25\cdot degC\right)\right] Sre7\_1_p$$

$$R_{1314_{p+1}} \quad \left[0.142 - 0.000636\cdot\left(T1\_2_p - 25\cdot degC\right)\right] Sre7\_2_p$$

$$R_{2122_{p+1}} \quad \left[0.142 - 0.000636\cdot\left(T1\_3_p - 25\cdot degC\right)\right] Sre7\_3_p$$

$$R_{24\_1_{p+1}} \quad \frac{\frac{To_p}{R_{1\_1eq_p}} + \left(Sre7\_1_p - P_{el\_1_p}\right) + \frac{T2\_1_p}{R_{12\_1}}}{\frac{1}{R_{1\_1eq_0}} + \frac{1}{R_{12\_1}}}$$

$$R_{42\_1_{p+1}}$$

$$R_{24\_2_{p+1}}$$

$$R_{42\_2_{p+1}}$$

$$R_{24\_3_{p+1}}$$

$$R_{42\_3_{p+1}}$$

$$R_{57_{p+1}}$$

$$R_{95_{p+1}}$$

$$R_{910_{p+1}}$$

$$R_{914_{p+1}}$$

$$R_{915_{p+1}}$$

$$R_{918_{p+1}}$$

$$R_{189_{p+1}}$$

$$R_{1015_{p+1}}$$

$$R_{1022_{p+1}}$$

$$R_{149_{p+1}}$$

$$R_{1415_{p+1}}$$

$$R_{1418_{p+1}}$$

$$R_{1422_{p+1}}$$

$$R_{139_{p+1}}$$

$R_{1510_{p+1}}$

$R_{1514_{p+1}}$

$R_{1810_{p+1}}$

$R_{1814_{p+1}}$

$R_{2210_{p+1}}$

$R_{2214_{p+1}}$

$R_{4D5D_{p+1}}$

$R_{5D4D_{p+1}}$

$P_{el\_1_{p+1}}$

$P_{el\_2_{p+1}}$

$P_{el\_3_{p+1}}$

$T1\_1_{p+1}$

$T2\_1_{p+1}$

$T3\_1_{p+1}$

$T_{air\_out\_1_{p+1}}$

$T4\_1_{p+1}$

$T1\_2_{p+1}$

$T2\_2_{p+1}$

$T3\_2_{p+1}$

$T_{air\_out\_2_{p+1}}$

$T4\_2_{p+1}$

$T1\_3_{p+1}$

$T2\_3_{p+1}$

$T3\_3_{p+1}$

$T_{air\_out\_3_{p+1}}$

$T4\_3_{p+1}$

$T4A_{p+1}$

$T5_{p+1}$

$T4B\_1_{p+1}$

$T4B\_2_{p+1}$

$T4B\_3_{p+1}$

$T4B_{p+1}$

$T4C_{p+1}$

$T4D_{p+1}$

$T7D_{p+1}$

$=$

$$\frac{\frac{T1\_1_p}{R_{12\_1}} + \frac{T3\_1_p}{\frac{1}{h_{c1_p} \cdot A_{pv1}}} + \frac{T4\_1_p}{R_{24\_1_p}}}{\frac{1}{R_{12\_1}} + \frac{1}{\frac{1}{h_{c1_p} \cdot A_{pv1}}} + \frac{1}{R_{24\_1_p}}}$$

$$\left[1 - e^{\frac{-\left(h_{c1_F} + h_{c1_p}\right) \cdot A_{pv1}}{m_{air_p} \cdot c_{p1}}}\right] \left[\frac{To_{fl} - \frac{\left(h_{c1_p} \cdot T2\_1_p + h_{c1_p} \cdot T4\_1_p\right)}{\left(h_{c1_p} + h_{c1_p}\right)}}{\frac{\left(h_{c1_F} + h_{c1_p}\right) \cdot A_{pv1}}{m_{air_p} \cdot c_{p1}}}\right] + \frac{h_{c1_p} \cdot T2\_1_p + h_{c1_p} \cdot T4\_1_p}{\left(h_{c1_p} + h_{c1_p}\right)}$$

$$\left[1 - e^{\frac{-\left(h_{c1_p} + h_{c1_p}\right) \cdot A_{pv1}}{m_{air_p} \cdot c_{p1}}}\right] \frac{h_{c1_p} \cdot T2\_1_p + h_{c1_p} \cdot T4\_1_p}{h_{c1_p} + h_{c1_p}} + \left[e^{\frac{-\left(h_{c1_p} + h_{c1_p}\right) \cdot A_{pv1}}{m_{air_p} \cdot c_{p1}}}\right] To_{fl}$$

$$\frac{\frac{T3\_1_F}{\frac{1}{h_{c1_F} \cdot A_{pv1}}} + \frac{T2\_1_p}{R_{42\_1_p}} + \frac{T4B\_1_p}{R_{4B4\_1}}}{\frac{1}{\frac{1}{h_{c1_F} \cdot A_{pv1}}} + \frac{1}{R_{42\_1_p}} + \frac{1}{R_{4B4\_1}}}$$

$$\frac{\frac{To_p}{R_{1\_2eq_p}} + \left(Ssc7\_2_p - P_{el\_2_p}\right) + \frac{T2\_2_p}{R_{12\_2}}}{\frac{1}{R_{1\_2eq_p}} + \frac{1}{R_{12\_2}}}$$

$$\frac{\frac{T1\_2_p}{R_{12\_2}} + \frac{T3\_2_p}{\frac{1}{h_{c2_p} \cdot \frac{A_{pv2}}{2}}} + \frac{T4\_2_p}{R_{24\_2_p}}}{\frac{1}{R_{12\_2}} + \frac{1}{\frac{1}{h_{c2_p} \cdot \frac{A_{pv2}}{2}}} + \frac{1}{R_{24\_2_p}}}$$

$$\left[1 - e^{\frac{-\left(h_{c2_p} + h_{c2_p}\right) \cdot \frac{A_{pv2}}{2}}{m_{air_p} \cdot c_{p2}}}\right] \left[\frac{T_{air\_out\_1_p} - \frac{\left(h_{c2_p} \cdot T2\_2_p + h_{c2_p} \cdot T4\_2_p\right)}{\left(h_{c2_p} + h_{c2_p}\right)}}{\frac{\left(h_{c2_p} + h_{c2_p}\right) \cdot \frac{A_{pv2}}{2}}{m_{air_p} \cdot c_{p2}}}\right] + \frac{h_{c2_p} \cdot T2\_2_p + h_{c2_p} \cdot T4\_2_p}{\left(h_{c2_p} + h_{c2_p}\right)}$$

$$\left[1 - e^{\frac{-\left(h_{c2_p} + h_{c2_p}\right) \cdot \frac{A_{pv2}}{2}}{m_{air_p} \cdot c_{p2}}}\right] \frac{h_{c2_p} \cdot T2\_2_p + h_{c2_p} \cdot T4\_2_p}{h_{c2_p} + h_{c2_p}} + \left[e^{\frac{-\left(h_{c2_p} + h_{c2_p}\right) \cdot \frac{A_{pv2}}{2}}{m_{air_p} \cdot c_{p2}}}\right] T_{air\_out\_1_p}$$

$$
\begin{pmatrix}
T_{air\_out\_4_{p+1}} \\
T5D_{p+1} \\
T6D_{p+1} \\
T6_{p+1} \\
T7_{p+1} \\
T8_{p+1} \\
T9_{p+1} \\
T10_{p+1} \\
T11_{p+1} \\
T12_{p+1} \\
T13_{p+1} \\
T14_{p+1} \\
T15_{p+1} \\
T16_{p+1} \\
T17_{p+1} \\
T18_{p+1} \\
T19_{p+1} \\
T20_{p+1} \\
T21_{p+1} \\
T22_{p+1} \\
Tr_{p+1} \\
Q_{p+1}
\end{pmatrix}
\begin{pmatrix}
\dfrac{\dfrac{T3\_2_p}{\frac{1}{h_{c2_p}\frac{A_{pv2}}{2}}} + \dfrac{T2\_2_p}{R_{42\_2_p}} + \dfrac{T4B\_2_p}{R_{4B4\_2}}}{\dfrac{1}{\frac{1}{h_{c2_p}\frac{A_{pv2}}{2}}} + \dfrac{1}{R_{42\_2_p}} + \dfrac{1}{R_{4B4\_2}}} \\
\dfrac{\dfrac{To_p}{R_{1\_3eq_p}} + \left(Sse7\_2_p - P_{el\_3_p}\right) + \dfrac{T2\_3_p}{R_{12\_3}}}{\dfrac{1}{R_{1\_3eq_p}} + \dfrac{1}{R_{12\_3}}} \\
\dfrac{\dfrac{T1\_3_p}{R_{12\_3}} + \dfrac{T3\_3_p}{\frac{1}{h_{c3_p}\frac{A_{pv2}}{2}}} + \dfrac{T4\_3_p}{R_{24\_3_p}}}{\dfrac{1}{R_{12\_3}} + \dfrac{1}{\frac{1}{h_{c3_p}\frac{A_{pv2}}{2}}} + \dfrac{1}{R_{24\_3_p}}} \\
\left[1 - e^{\frac{-\left(h_{c3_p}+h_{c3_p}\right)\frac{A_{pv2}}{2}}{m_{air_p} c_{p3}}}\right]\left[\dfrac{T_{air\_out\_2_p} - \dfrac{\left(h_{c3_p} T2\_3_p + h_{c3_p} T4\_3_p\right)}{\left(h_{c3_p}+h_{c3_p}\right)}}{\frac{\left(h_{c3_p}+h_{c3_p}\right)\frac{A_{pv2}}{2}}{m_{air_p} c_{p3}}}\right] + \dfrac{h_{c3_p} T2\_3_p + h_{c3_p} T4\\_3}{\left(h_{c3_p}+h_{c3_p}\right)} \\
\left[1 - e^{\frac{-\left(h_{c3_p}+h_{c3_p}\right)\frac{A_{pv2}}{2}}{m_{air_p} c_{p3}}}\right]\dfrac{h_{c3_p} T2\_3_p + h_{c3_p} T4\_3_p}{h_{c3_p}+h_{c3_p}} + \left[e^{\frac{-\left(h_{c3_p}+h_{c3_p}\right)\frac{A_{pv2}}{2}}{m_{air_p} c_{p3}}}\right] T_{air\_out\_2_p} \\
\dfrac{\dfrac{T3\_3_p}{\frac{1}{h_{c3_p}\frac{A_{pv2}}{2}}} + \dfrac{T2\_3_p}{R_{42\_3_p}} + \dfrac{T4B\_3_p}{R_{4B4\_3}}}{\dfrac{1}{\frac{1}{h_{c3_p}\frac{A_{pv2}}{2}}} + \dfrac{1}{R_{42\_3_p}} + \dfrac{1}{R_{4B4\_3}}} \\
\dfrac{\dfrac{To_p}{R_{4Aeq_p}} + Sse7\_3_p + \dfrac{T4C_p}{R_{4C4A}}}{\dfrac{1}{R_{4Aeq_p}} + \dfrac{1}{R_{4C4A}}} \\
\dfrac{\dfrac{T4B_p}{R_{4E5}} + \dfrac{T6_p}{R_{56_p}} + \dfrac{T7_p}{R_{57_p}} + \dfrac{T4C_p}{R_{4C5}}}{\dfrac{1}{R_{4E5}} + \dfrac{1}{R_{56_p}} + \dfrac{1}{R_{57_p}} + \dfrac{1}{R_{4C5}}}
\end{pmatrix}
$$

$$\frac{\Delta t}{\frac{C_{4B}}{3}}\left(\frac{T4\_1_p - T4B\_1_p}{R_{4B4\_1}} + \frac{T5_p - T4B\_1_p}{R_{4B5\_1}}\right) + T4B\_1_p$$

$$\frac{\Delta t}{\frac{C_{4B}}{3}}\left(\frac{T4\_2_p - T4B\_2_p}{R_{4B4\_2}} + \frac{T5_p - T4B\_2_p}{R_{4B5\_2}}\right) + T4B\_2_p$$

$$\frac{\Delta t}{\frac{C_{4B}}{3}}\left(\frac{T4\_3_p - T4B\_3_p}{R_{4B4\_3}} + \frac{T5_p - T4B\_3_p}{R_{4B5\_3}}\right) + T4B\_3_p$$

$$\frac{T4B\_1_p + T4B\_2_p + T4B\_3_p}{3}$$

$$\frac{\Delta t}{C_{4C}}\left(\frac{T4A_p - T4C_p}{R_{4C4A}} + \frac{T5_p - T4C_p}{R_{4C5}}\right) + T4C_p$$

$$\frac{\frac{To_p}{R_{4Aeq_p}} + \frac{T7D_p}{\frac{1}{h_{c4_p} \cdot A_{sac}}} + \frac{T5D_p}{R_{4D5D_p}} + Sse4D_p}{\frac{1}{R_{4Aeq_p}} + \frac{1}{\frac{1}{h_{c4_p} \cdot A_{sac}}} + \frac{1}{R_{4D5D_p}}}$$

$$\left[1 - e^{\frac{-\left(h_{c4_p} + h_{c4_p}\right) \cdot A_{sac}}{m_{air_p} \cdot c_{p4}}}\right]\left[T_{air\_out\_3_p} - \frac{\left(h_{c4_p} \cdot T4D_p + h_{c4_p} \cdot T5D_p\right)}{\left(h_{c4_p} + h_{c4_p}\right)}\right] \Bigg/ \frac{\left(h_{c4_p} + h_{c4_p}\right) \cdot A_{sac}}{m_{air_p} \cdot c_{p4}} + \frac{h_{c4_p} \cdot T4D_p + h_{c4_p} \cdot T5D_p}{\left(h_{c4_p} + h_{c4_p}\right)}$$

$$\left[1 - e^{\frac{-\left(h_{c4_p} + h_{c4_p}\right) \cdot A_{sac}}{m_{air_p} \cdot c_{p4}}}\right]\frac{h_{c4_p} \cdot T4D_p + h_{c4_p} \cdot T5D_p}{h_{c4_p} + h_{c4_p}} + \left[e^{\frac{-\left(h_{c4_p} + h_{c4_p}\right) \cdot A_{sac}}{m_{air_p} \cdot c_{p4}}}\right] T_{air\_out\_3_p}$$

$$\frac{\frac{T4D_p}{R_{5D4D_p}} + \frac{T7D_p}{\frac{1}{h_{c4_p} \cdot A_{sac}}} + \frac{T6D_p}{R_{5D6D}} + Sse5D_p}{\frac{1}{R_{5D4D_p}} + \frac{1}{\frac{1}{h_{c4_p} \cdot A_{sac}}} + \frac{1}{R_{5D6D}}}$$

$$\frac{\frac{T5D_p}{R_{5D6D}} + \frac{To_p}{R_{4Aeq_p}}}{\frac{1}{R_{5D6D}} + \frac{1}{R_{4Aeq_p}}}$$

$$\frac{\frac{T5_p}{R_{56_p}} + \frac{T7_p}{R_{67_p}} + \frac{To_p}{R_{inf2}}}{\frac{1}{R_{56_p}} + \frac{1}{R_{67_p}} + \frac{1}{R_{inf2}}}$$

$$\frac{\frac{T5_p}{R_{75_p}} + \frac{T6_p}{R_{67_p}} + \frac{T8_p}{R_{78}}}{\frac{1}{R_{75_p}} + \frac{1}{R_{67_p}} + \frac{1}{R_{78}}}$$

$$\frac{\Delta t}{C_8}\left(\frac{T7_p - T8_p}{R_{78}} + \frac{T9_p - T8_p}{R_{89}}\right) + T8_p$$

$$\frac{\frac{T8_p}{R_{89}} + \left(Ssi5_p + Qrsi_{int_{p,5}}\right) + \frac{Tz_p}{R_{9z_p}} + \frac{T10_p}{R_{910_p}} + \frac{T14_p}{R_{914_p}} + \frac{T18_p}{R_{918_p}} + \frac{T15_p}{R_{915_p}}}{\frac{1}{R_{89}} + \frac{1}{R_{9z_p}} + \frac{1}{R_{910_p}} + \frac{1}{R_{914_p}} + \frac{1}{R_{918_p}} + \frac{1}{R_{915_p}}}$$

$$\frac{\frac{T11_p}{R_{1011}} + \left(Ssi1_p + Qrsi_{int_{p,1}}\right) + \frac{Tz_p}{R_{10z_p}} + \frac{T15_p}{R_{1015_p}} + \frac{T22_p}{R_{1022_p}} + \frac{T9_p}{R_{109_p}}}{\frac{1}{R_{1011}} + \frac{1}{R_{10z_p}} + \frac{1}{R_{1015_p}} + \frac{1}{R_{1022_p}} + \frac{1}{R_{109_p}}}$$

$$\frac{\Delta t}{C_{11}}\left(\frac{T10_p - T11_p}{R_{1011}} + \frac{T12_p - T11_p}{R_{1112}}\right) + T11_p$$

$$\frac{\frac{T11_p}{R_{1112}} + Ssi1_p + \frac{To_p}{R_{12eq_p}}}{\frac{1}{R_{1112}} + \frac{1}{R_{12eq_p}}}$$

$$\frac{\frac{T14_p}{R_{1314_p}} + Swo1_p + \frac{To_p}{R_{13eq_p}}}{\frac{1}{R_{1314_p}} + \frac{1}{R_{13eq_p}}}$$

$$\frac{\frac{T13_p}{R_{1314_p}} + \left(Swi1_p + Qrw_{int_{p,1}}\right) + \frac{Tz_p}{R_{14z_p}} + \frac{T15_p}{R_{1415_p}} + \frac{T22_p}{R_{1422_p}} + \frac{T9_p}{R_{149_p}} + \frac{T18_p}{R_{1418_p}}}{\frac{1}{R_{1314_p}} + \frac{1}{R_{14z_p}} + \frac{1}{R_{1415_p}} + \frac{1}{R_{1422_p}} + \frac{1}{R_{149_p}} + \frac{1}{R_{1418_p}}}$$

$$\frac{\frac{T10_p}{R_{1510_p}} + \frac{T9_p}{R_{159_p}} + \frac{Tz_p}{R_{15z_p}} + \frac{T14_p}{R_{1514_p}} + \frac{T16_p}{R_{1516}} + \left(Ssi6_p + Qrsi_{int_{p,6}}\right)}{\frac{1}{R_{1510_p}} + \frac{1}{R_{15z_p}} + \frac{1}{R_{1514_p}} + \frac{1}{R_{1516}} + \frac{1}{R_{159_p}}}$$

$$\frac{\Delta t}{C_{16}}\left(\frac{T17_p - T16_p}{R_{1617}} + \frac{T15_p - T16_p}{R_{1516}}\right) + T16_p$$

$$\frac{\frac{To_p}{R_{17o_p}} + \frac{T16_p}{R_{1617}}}{\frac{1}{R_{17o_p}} + \frac{1}{R_{1617}}}$$

$$\frac{\frac{T10_p}{R_{1810_p}} + \frac{Tz_p}{R_{18z_p}} + \frac{T14_p}{R_{1814_p}} + \frac{T19_p}{R_{1819}} + Ssi8_p + Qrsi8_{int_p}}{\frac{1}{R_{1810_p}} + \frac{1}{R_{18z_p}} + \frac{1}{R_{1814_p}} + \frac{1}{R_{1819}}}$$

$$\frac{\Delta t}{C_{19}}\left(\frac{T18_p - T19_p}{R_{1819}} + \frac{T20_p - T19_p}{R_{1920}}\right) + T19_p$$

$$
\left[
\begin{array}{c}
\dfrac{\dfrac{T19_p}{R_{1920}} + \dfrac{To_p}{R_{20eq_p}} + Sse20_p}{\dfrac{1}{R_{1920}} + \dfrac{1}{R_{20eq_p}}} \\[2ex]
\dfrac{\dfrac{T22_p}{R_{2122_p}} + \dfrac{To_p}{R_{21eq_p}} + Swo21_p}{\dfrac{1}{R_{2122_p}} + \dfrac{1}{R_{21eq_p}}} \\[2ex]
\dfrac{\dfrac{Tz_p}{R_{22z_p}} + \dfrac{T21_p}{R_{2122_p}} + \dfrac{T10_p}{R_{2210_p}} + \dfrac{T14_p}{R_{2214_p}} + Swi22_p + Qrw22_{int_p}}{\dfrac{1}{R_{22z_p}} + \dfrac{1}{R_{2122_p}} + \dfrac{1}{R_{2210_p}} + \dfrac{1}{R_{2214_p}}} \\[2ex]
\dfrac{\Delta t}{C_{air}} \left(\dfrac{T9_p - Tz_p}{R_{9z_p}} + \dfrac{T22_p - Tz_p}{R_{22z_p}} + \dfrac{T18_p - Tz_p}{R_{18z_p}} + \dfrac{T15_p - Tz_p}{R_{15z_p}} + \dfrac{T14_p - Tz_p}{R_{14z_p}} + \dfrac{T10_p - Tz_p}{R_{10z_p}} + \dfrac{To_p - Tz_p}{R_{infl}} + \dfrac{To_p - Tz_p}{R_{door1}} + \dfrac{To_p - Tz_p}{R_{door2}} + Qcav_{int_p} + Qrb_p \right) + Tz_p \\[2ex]
\dfrac{Tsp - T9_p}{R_{9z_p}} + \dfrac{Tsp - T22_p}{R_{22z_p}} + \dfrac{Tsp - T18_p}{R_{18z_p}} + \dfrac{Tsp - T15_p}{R_{15z_p}} + \dfrac{Tsp - T14_p}{R_{14z_p}} + \dfrac{Tsp - T10_p}{R_{10z_p}} + \dfrac{Tsp - To_p}{R_{infl}} + \dfrac{Tsp - To_p}{R_{door1}} + \dfrac{Tsp - To_p}{R_{door2}} - Qcav_{int_p} - Qrb_p
\end{array}
\right]
$$

Matrix of Configuration 3

$$\frac{1}{\left[\sqrt{\left(1.81\cdot\frac{\sqrt[3]{\left|T1\_1_p - To_p\right|}}{1.382+\cos(\beta_{roof\_1})}\right)^2+\left(2.38\cdot Vw^{0.89}\right)^2}\right]\cdot\frac{W}{m^2\cdot degC}+4\cdot\sigma\cdot\varepsilon\cdot\left[\left(\frac{T1\_1_p+To_p+Tsky_p}{3}+273\right)\cdot K\right]^3\cdot\frac{K}{degC}\cdot A_{pv1}}$$

$$\frac{1}{\left[\sqrt{\left(1.81\cdot\frac{\sqrt[3]{\left|T1\_2_p - To_p\right|}}{1.382+\cos(\beta_{roof\_1})}\right)^2+\left(2.38\cdot Vw^{0.89}\right)^2}\right]\cdot\frac{W}{m^2\cdot degC}+4\cdot\sigma\cdot\varepsilon\cdot\left[\left(\frac{T1\_2_p+To_p+Tsky_p}{3}+273\right)\cdot K\right]^3\cdot\frac{K}{degC}\cdot\frac{A_{pv2}}{2}}$$

$$\frac{1}{\left[\sqrt{\left(1.81\cdot\frac{\sqrt[3]{\left|T1\_3_p - To_p\right|}}{1.382+\cos(\beta_{roof\_2})}\right)^2+\left(2.38\cdot Vw^{0.89}\right)^2}\right]\cdot\frac{W}{m^2\cdot degC}+4\cdot\sigma\cdot\varepsilon\cdot\left[\left(\frac{T1\_3_p+To_p+Tsky_p}{3}+273\right)\cdot K\right]^3\cdot\frac{K}{degC}\cdot\frac{A_{pv2}}{2}}$$

$$\frac{1}{\left[\sqrt{\left(1.81\cdot\frac{\sqrt[3]{\left|T4A_p - To_p\right|}}{1.382+\cos(\beta_{roof\_2})}\right)^2+\left(2.38\cdot Vw^{0.89}\right)^2}\right]\cdot\frac{W}{m^2\cdot degC}+4\cdot\sigma\cdot\varepsilon\cdot\left[\left(\frac{T4A_p+To_p+Tsky_p}{3}+273\right)\cdot K\right]^3\cdot\frac{K}{degC}\cdot A_{npv}}$$

$$\frac{1}{\left[1.81\cdot\frac{\sqrt[3]{\left|T12_p - To_p\right|}}{1.382+\cos(\beta)}+1.13\cdot\left[\sqrt{\left(1.81\cdot\frac{\sqrt[3]{\left|T12_p - To_p\right|}}{1.382+\cos(\beta)}\right)^2+\left(2.38\cdot Vw^{0.89}\right)^2}-1.81\cdot\frac{\sqrt[3]{\left|T12_p - To_p\right|}}{1.382+\cos(\beta)}\right]\right]\cdot\frac{watt}{m^2\cdot degC}+4\cdot\sigma\cdot\varepsilon\cdot\left[\left(\frac{T12_p+To_p+Tsky_p}{3}+273\right)\cdot K\right]^3\cdot\frac{K}{degC}\cdot A_1}$$

$$\frac{1}{\left[\sqrt{\left(1.81\cdot\frac{\sqrt[3]{\left|T13_p - To_p\right|}}{1.382+\cos(\beta)}\right)^2+\left(2.38\cdot Vw^{0.89}\right)^2}\right]\cdot\frac{W}{m^2\cdot degC}+4\cdot\sigma\cdot\varepsilon\cdot\left[\left(\frac{T13_p+To_p+Tsky_p}{3}+273\right)\cdot K\right]^3\cdot\frac{K}{degC}\cdot Aw_1}$$

$$\frac{1}{1.81\cdot\frac{\sqrt[3]{\left|T20_p - To_p\right|}}{1.382+\cos(\beta)}+1.13\cdot\left[\sqrt{\left(1.81\cdot\frac{\sqrt[3]{\left|T20_p - To_p\right|}}{1.382+\cos(\beta)}\right)^2+\left(2.86\cdot Vw^{0.617}\right)^2}-1.81\cdot\frac{\sqrt[3]{\left|T20_p - To_p\right|}}{1.382+\cos(\beta)}\right]\cdot\frac{watt}{m^2\cdot degC}+4\cdot\sigma\cdot\varepsilon\cdot\left[\left(\frac{T20_p+To_p+Tsky_p}{3}+273\right)\cdot K\right]^3\cdot\frac{K}{degC}\cdot\sum_{si=2}^{6}A_{si}}$$

$$\frac{1}{\left[\sqrt{\left(1.81\cdot\frac{\sqrt[3]{\left|T21_p - To_p\right|}}{1.382+\cos(\beta)}\right)^2+\left(2.86\cdot Vw^{0.617}\right)^2}\right]\cdot\frac{W}{m^2\cdot degC}+4\cdot\sigma\cdot\varepsilon\cdot\left[\left(\frac{T21_p+To_p+Tsky_p}{3}+273\right)\cdot K\right]^3\cdot\frac{K}{degC}\cdot\sum_{iw=2}^{4}A_{iw}}$$

$$\frac{1}{\left[if\left[T17_p>To_p,1.52\cdot\left|T17_p-To_p\right|^{\frac{1}{3}}\cdot\frac{watt}{m^2\cdot degC},0.59\cdot\left(\frac{T17_p-To_p}{Lh\cdot m^{-1}}\right)^{0.25}\cdot\frac{watt}{m^2\cdot degC}\right]\right]\cdot A_g}$$

$$\frac{1}{\left[if\left[T5_p>T6_p,0.59\cdot\left(\frac{T5_p-T6_p}{Lh\cdot m^{-1}}\right)^{0.25}\cdot\frac{watt}{m^2\cdot degC},1.52\cdot\left|T5_p-T6_p\right|^{\frac{1}{3}}\cdot\frac{watt}{m^2\cdot degC}\right]\right]\cdot A_7}$$

$$\frac{1}{\left[if\left[T6_p>T7_p,0.59\cdot\left(\frac{T7_p-T6_p}{Lh\cdot m^{-1}}\right)^{0.25}\cdot\frac{watt}{m^2\cdot degC},1.52\cdot\left|T7_p-T6_p\right|^{\frac{1}{3}}\cdot\frac{watt}{m^2\cdot degC}\right]\right]\cdot A_5}$$

$$\frac{1}{\left[if\left[T9_p>Tz_p,0.59\cdot\left(\frac{T9_p-Tz_p}{Lh\cdot m^{-1}}\right)^{0.25}\cdot\frac{watt}{m^2\cdot degC},1.52\cdot\left|T9_p-Tz_p\right|^{\frac{1}{3}}\cdot\frac{watt}{m^2\cdot degC}\right]\right]\cdot A_5}$$

$$\frac{1}{\left[if\left[T15_p > Tz_p, 1.52\left(\left| T15_p - Tz_p \right| \right)^{\frac{1}{3}} \cdot \frac{watt}{m^2 \cdot degC}, 0.59 \left(\left| \frac{T15_p - Tz_p}{Lh \cdot m^{-1}} \right| \right)^{0.25} \cdot \frac{watt}{m^2 \cdot degC} \right] \cdot A_f \right]}$$

$$\frac{1}{\left[1.31 \left(\left| T10_p - Tz_p \right| \right)^{\frac{1}{3}} \cdot \frac{watt}{m^2 \cdot degC} \right] A_1}$$

$$\frac{1}{\left[1.31 \left(\left| T14_p - Tz_p \right| \right)^{\frac{1}{3}} \cdot \frac{watt}{m^2 \cdot degC} \right] \cdot Aw_1}$$

$$\frac{1}{\left[1.31 \cdot \left(\left| T18_p - Tz_p \right| \right)^{\frac{1}{3}} \cdot \frac{watt}{m^2 \cdot degC} \right] \sum_{si=2}^{4} A_{si}}$$

$$\frac{1}{\left[1.31 \left(\left| T22_p - Tz_p \right| \right)^{\frac{1}{3}} \frac{watt}{m^2 \cdot degC} \right] \sum_{iw=2}^{4} A_{iw}}$$

$$\frac{1}{\left[h_{wr} + \frac{4 \cdot \sigma \cdot \left[\left(273 + \frac{T13_p + T14_p}{2} \right) K \right]^3}{\left(\frac{1}{\varepsilon_1} + \frac{1}{\varepsilon_{2e}} - 1 \right)} \cdot \frac{K}{degC} \right] Aw_1}$$

$$\frac{1}{\left[h_{wr} + \frac{4 \cdot \sigma \cdot \left[\left(273 + \frac{T21_p + T22_p}{2} \right) K \right]^3}{\left(\frac{1}{\varepsilon_1} + \frac{1}{\varepsilon_{2e}} - 1 \right)} \cdot \frac{K}{degC} \right] \cdot \sum_{iw=2}^{4} A_{iw}}$$

$$\frac{1}{\left[\sigma \cdot F_\varepsilon \cdot Fv_{2\_4} \left[\frac{\left[(T2\_1_p + 273) \cdot K \right]^4 - \left[(T1\_1_p + 273) \cdot K \right]^4}{T2\_1_p - T1\_1_p} \right] A_{pv1} \right]}$$

$$\frac{1}{\left[\sigma \cdot F_\varepsilon \cdot Fv_{2\_4} \left[\frac{\left[(T1\_1_p + 273) \cdot K \right]^4 - \left[(T2\_1_p + 273) \cdot K \right]^4}{T1\_1_p - T2\_1_p} \right] A_{pv1} \right]}$$

$$\frac{1}{\left[\sigma \cdot F_\varepsilon \cdot Fv_{2\_4} \left[\frac{\left[(T2\_2_p + 273) \cdot K \right]^4 - \left[(T1\_2_p + 273) \cdot K \right]^4}{T2\_2_p - T1\_2_p} \right] \frac{A_{pv2}}{2} \right]}$$

$$\frac{1}{\left[\sigma \cdot F_\varepsilon \cdot Fv_{2\_4} \left[\frac{\left[(T1\_2_p + 273) \cdot K \right]^4 - \left[(T2\_2_p + 273) \cdot K \right]^4}{T1\_2_p - T2\_2_p} \right] \frac{A_{pv2}}{2} \right]}$$

$$\frac{1}{\left[\sigma \cdot F_\varepsilon \cdot Fv_{2\_4} \left[\frac{\left[(T2\_3_p + 273) \cdot K \right]^4 - \left[(T1\_3_p + 273) \cdot K \right]^4}{T2\_3_p - T1\_3_p} \right] \frac{A_{pv2}}{3} \right]}$$

$$\frac{1}{\left[\sigma \cdot F_\varepsilon \cdot Fv_{2\_4} \left[\frac{\left[(T1\_3_p + 273) \cdot K \right]^4 - \left[(T2\_3_p + 273) \cdot K \right]^4}{T1\_3_p - T2\_3_p} \right] \frac{A_{pv2}}{2} \right]}$$

$$B_{1\_1eq_{p+1}}$$

$$R_{1\_2eq_{p+1}}$$

$$R_{1\_3eq_{p+1}}$$

$$R_{4Aeq_{p+1}}$$

$$R_{12eq_{p+1}}$$

$$R_{13eq_{p+1}}$$

$$R_{20eq_{p+1}}$$

$$R_{21eq_{p+1}}$$

$$R_{17o_{p+1}}$$

$$R_{56_{p+1}}$$

$$B_{67_{p+1}}$$

$$R_{9g_{p+1}}$$

$$R_{15z_{p+1}}$$

$$R_{10z_{p+1}}$$

$$R_{14z_{p+1}}$$

$$R_{18z_{p+1}}$$

$$R_{22z_{p+1}}$$

$$R_{1314_{p+1}}$$

$$R_{2122_{p+1}}$$

$$R_{12\_1_{p+1}}$$

$$R_{21\_1_{p+1}}$$

$$\frac{1}{\left[\sigma \cdot F_g \cdot Fv_{5\_7}\left[\frac{\left[(T5_p + 273)\cdot K\right]^4 - \left[(T7_p + 273)\cdot K\right]^4}{T5_p - T7_p}\right]\right]} \cdot A_5$$

$$\frac{1}{\left[\sigma \cdot F_g \cdot Fv_{7\_5}\left[\frac{\left[(T7_p + 273)\cdot K\right]^4 - \left[(T5_p + 273)\cdot K\right]^4}{T7_p - T5_p}\right]\right]} \cdot A_7$$

$$\frac{1}{\left[\sigma \cdot F_g \cdot Fv_{9\_10}\left[\frac{\left[(T9_p + 273)\cdot K\right]^4 - \left[(T10_p + 273)\cdot K\right]^4}{T9_p - T10_p}\right]\right]} \cdot A_5$$

$$\frac{1}{\left[\sigma \cdot F_g \cdot Fv_{9\_14}\left[\frac{\left[(T9_p + 273)\cdot K\right]^4 - \left[(T14_p + 273)\cdot K\right]^4}{T9_p - T14_p}\right]\right]} \cdot A_5$$

$$\frac{1}{\left[\sigma \cdot F_g \cdot Fv_{9\_15}\left[\frac{\left[(T9_p + 273)\cdot K\right]^4 - \left[(T15_p + 273)\cdot K\right]^4}{T9_p - T15_p}\right]\right]} \cdot A_5$$

$$\frac{1}{\left[\sigma \cdot F_g \cdot Fv_{9\_18}\left[\frac{\left[(T9_p + 273)\cdot K\right]^4 - \left[(T18_p + 273)\cdot K\right]^4}{T9_p - T18_p}\right]\right]} \cdot A_5$$

$$\frac{1}{\left[\sigma \cdot F_g \cdot Fv_{9\_22}\left[\frac{\left[(T9_p + 273)\cdot K\right]^4 - \left[(T22_p + 273)\cdot K\right]^4}{T9_p - T22_p}\right]\right]} \cdot A_5$$

$$\frac{1}{\left[\sigma \cdot F_g \cdot Fv_{10\_9}\left[\frac{\left[(T10_p + 273)\cdot K\right]^4 - \left[(T9_p + 273)\cdot K\right]^4}{T10_p - T9_p}\right]\right]} \cdot A_1$$

$$\frac{1}{\left[\sigma \cdot F_g \cdot Fv_{10\_15}\left[\frac{\left[(T10_p + 273)\cdot K\right]^4 - \left[(T15_p + 273)\cdot K\right]^4}{T10_p - T15_p}\right]\right]} \cdot A_1$$

$$\frac{1}{\left[\sigma \cdot F_g \cdot Fv_{10\_18}\left[\frac{\left[(T10_p + 273)\cdot K\right]^4 - \left[(T18_p + 273)\cdot K\right]^4}{T10_p - T18_p}\right]\right]} \cdot A_1$$

$$\frac{1}{\left[\sigma \cdot F_g \cdot Fv_{10\_22}\left[\frac{\left[(T10_p + 273)\cdot K\right]^4 - \left[(T22_p + 273)\cdot K\right]^4}{T10_p - T22_p}\right]\right]} \cdot A_1$$

$$\frac{1}{\left[\sigma \cdot F_g \cdot Fv_{14\_9}\left[\frac{\left[(T14_p + 273)\cdot K\right]^4 - \left[(T9_p + 273)\cdot K\right]^4}{T14_p - T9_p}\right]\right]} \cdot Aw_1$$

$$\frac{1}{\left[\sigma \cdot F_g \cdot Fv_{14\_15}\left[\frac{\left[(T14_p + 273)\cdot K\right]^4 - \left[(T15_p + 273)\cdot K\right]^4}{T14_p - T15_p}\right]\right]} \cdot Aw_1$$

$$\frac{1}{\left[\sigma \cdot F_g \cdot Fv_{14\_18}\left[\frac{\left[(T14_p + 273)\cdot K\right]^4 - \left[(T18_p + 273)\cdot K\right]^4}{T14_p - T18_p}\right]\right]} \cdot Aw_1$$

$$R_{21\_2_{p+1}}$$

$$R_{12\_3_{p+1}}$$

$$R_{21\_3_{p+1}}$$

$$R_{57_{p+1}}$$

$$R_{75_{p+1}}$$

$$R_{910_{p+1}}$$

$$R_{914_{p+1}}$$

$$R_{915_{p+1}}$$

$$R_{918_{p+1}}$$

$$R_{922_{p+1}}$$

$$R_{109_{p+1}}$$

$$R_{1015_{p+1}}$$

$$R_{1018_{p+1}}$$

$$R_{1022_{p+1}}$$

$$R_{149_{p+1}}$$

$$R_{1415_{p+1}}$$

$$R_{1418_{p+1}}$$

$$R_{1422_{p+1}}$$

$$R_{159_{p+1}}$$

$$R_{1510_{p+1}}$$

$$R_{1514_{p+1}}$$

$$R_{1518_{p+1}}$$

$$R_{1522_{p+1}}$$

$$R_{189_{p+1}}$$

$$R_{1810_{p+1}}$$

$$R_{1814_{p+1}}$$

$$R_{1815_{p+1}}$$

$$R_{229_{p+1}}$$

$$R_{2210_{p+1}}$$

$$R_{2214_{p+1}}$$

$$R_{2215_{p+1}}$$

$$P_{el\_1_{p+1}}$$

$$P_{el\_2_{p+1}}$$

$$P_{el\_3_{p+1}}$$

$$T1\_1_{p+1}$$

$$T2\_1_{p+1}$$

$$=$$

$$\frac{1}{\sigma \cdot F_e \cdot Fv_{14\_22}\left[\frac{\left[\left(T14_p + 273\right)\cdot K\right]^4 - \left[\left(T22_p + 273\right)\cdot K\right]^4}{T14_p - T22_p}\right] Aw_1}$$

$$\frac{1}{\left[\sigma \cdot F_e \cdot Fv_{15\_9}\left[\frac{\left[\left(T15_p + 273\right)\cdot K\right]^4 - \left[\left(T9_p + 273\right)\cdot K\right]^4}{T15_p - T9_p}\right]\right] A_6}$$

$$\frac{1}{\left[\sigma \cdot F_e \cdot Fv_{15\_10}\left[\frac{\left[\left(T15_p + 273\right)\cdot K\right]^4 - \left[\left(T10_p + 273\right)\cdot K\right]^4}{T15_p - T10_p}\right]\right] A_6}$$

$$\frac{1}{\left[\sigma \cdot F_e \cdot Fv_{15\_14}\left[\frac{\left[\left(T15_p + 273\right)\cdot K\right]^4 - \left[\left(T14_p + 273\right)\cdot K\right]^4}{T15_p - T14_p}\right]\right] A_6}$$

$$\frac{1}{\left[\sigma \cdot F_e \cdot Fv_{15\_18}\left[\frac{\left[\left(T15_p + 273\right)\cdot K\right]^4 - \left[\left(T18_p + 273\right)\cdot K\right]^4}{T15_p - T18_p}\right]\right] A_6}$$

$$\frac{1}{\left[\sigma \cdot F_e \cdot Fv_{15\_22}\left[\frac{\left[\left(T15_p + 273\right)\cdot K\right]^4 - \left[\left(T22_p + 273\right)\cdot K\right]^4}{T15_p - T22_p}\right]\right] A_6}$$

$$\frac{1}{\left[\sigma \cdot F_e \cdot Fv_{18\_9}\left[\frac{\left[\left(T18_p + 273\right)\cdot K\right]^4 - \left[\left(T9_p + 273\right)\cdot K\right]^4}{T18_p - T9_p}\right]\right] \sum_{si=2}^{4} A_{si}}$$

$$\frac{1}{\left[\sigma \cdot F_e \cdot Fv_{18\_10}\left[\frac{\left[\left(T18_p + 273\right)\cdot K\right]^4 - \left[\left(T10_p + 273\right)\cdot K\right]^4}{T18_p - T10_p}\right]\right] \sum_{si=2}^{4} A_{si}}$$

$$\frac{1}{\left[\sigma \cdot F_e \cdot Fv_{18\_14}\left[\frac{\left[\left(T18_p + 273\right)\cdot K\right]^4 - \left[\left(T14_p + 273\right)\cdot K\right]^4}{T18_p - T14_p}\right]\right] \sum_{si=2}^{4} A_{si}}$$

$$\frac{1}{\left[\sigma \cdot F_e \cdot Fv_{18\_15}\left[\frac{\left[\left(T18_p + 273\right)\cdot K\right]^4 - \left[\left(T15_p + 273\right)\cdot K\right]^4}{T18_p - T15_p}\right]\right] \sum_{si=2}^{4} A_{si}}$$

$$\frac{1}{\left[\sigma \cdot F_e \cdot Fv_{22\_9}\left[\frac{\left[\left(T22_p + 273\right)\cdot K\right]^4 - \left[\left(T9_p + 273\right)\cdot K\right]^4}{T22_p - T9_p}\right]\right] \sum_{sw=2}^{4} A_{sw}}$$

$$\frac{1}{\left[\sigma \cdot F_e \cdot Fv_{22\_10}\left[\frac{\left[\left(T22_p + 273\right)\cdot K\right]^4 - \left[\left(T10_p + 273\right)\cdot K\right]^4}{T22_p - T10_p}\right]\right] \sum_{sw=2}^{4} A_{sw}}$$

$$\frac{1}{\left[\sigma \cdot F_e \cdot Fv_{22\_14}\left[\frac{\left[\left(T22_p + 273\right)\cdot K\right]^4 - \left[\left(T14_p + 273\right)\cdot K\right]^4}{T22_p - T14_p}\right]\right] \sum_{sw=2}^{4} A_{sw}}$$

$$\frac{1}{\left[\sigma \cdot F_e \cdot Fv_{22\_15}\left[\frac{\left[\left(T22_p + 273\right)\cdot K\right]^4 - \left[\left(T15_p + 273\right)\cdot K\right]^4}{T22 - T15}\right]\right] \sum^{4} A_{sw}}$$

$$T_{air\_out\_1_{p+1}} = \left[0.142 - 0.000636\left(T2\_1_p - 25\,degC\right)\right] Sse7\_t1_p$$

$$T4\_1_{p+1} = \left[0.142 - 0.000636\left(T2\_2_p - 25\,degC\right)\right] Sse7\_t2_p$$

$$T1\_2_{p+1} = \left[0.142 - 0.000636\left(T2\_3_p - 25\,degC\right)\right] Sse7\_t2_p$$

$$T2\_2_{p+1} = \frac{\frac{T3\_1_p}{R_{13\_1}} + Sse7\_1_p + \frac{T2\_1_p}{R_{12\_1_p}} + \frac{To_p}{R_{1\_1eq_p}}}{\frac{1}{R_{1\_1eq_p}} + \frac{1}{R_{12\_1_p}} + \frac{1}{R_{13\_1}}}$$

$$T3\_2_{p+1} = \frac{\frac{T1\_1_p}{R_{12\_1_p}} + \frac{T3\_1_p}{R_{23\_1}} + \frac{T4\_1_p}{R_{24\_1}} + \left(Sse7\_12_p - P_{el\_1_p}\right)}{\frac{1}{R_{12\_1_p}} + \frac{1}{R_{23\_1}} + \frac{1}{R_{24\_1}}}$$

$$T_{air\_out\_2_{p+1}} = \left[1 - e^{\frac{-\left(h_{c1}+h_{c1}\right)\left(A_{pv1}\right)}{m_{air}\,c_{p1}}}\right]\left[\frac{To_0 - \frac{\left(h_{c1}\,T1\_1_p + h_{c1}\,T2\_1_p\right)}{\left(h_{c1}+h_{c1}\right)}}{\frac{\left(h_{c1}+h_{c1}\right)\left(A_{pv1}\right)}{m_{air}\,c_{p1}}}\right] + \frac{h_{c1}\,T2\_1_p + h_{c1}\,T1\_1_p}{\left(h_{c1}+h_{c1}\right)}$$

$$T4\_2_{p+1} = \left[1 - e^{\frac{-\left(h_{c1}+h_{c1}\right)\left(A_{pv1}\right)}{m_{air}\,c_{p1}}}\right]\frac{h_{c1}\,T2\_1_p + h_{c1}\,T1\_1_p}{h_{c1}+h_{c1}} + \left[e^{\frac{-\left(h_{c1}+h_{c1}\right)\left(A_{pv1}\right)}{m_{air}\,c_{p1}}}\right]To_0$$

$$T1\_3_{p+1} = \frac{\frac{T2\_1_p}{R_{24\_1}} + \frac{T4B_p}{R_{4B4\_1}}}{\frac{1}{R_{24\_1}} + \frac{1}{R_{4B4\_1}}}$$

$$T2\_3_{p+1} = \frac{\frac{T3\_2_p}{R_{13\_2}} + Sse7\_2_p + \frac{T2\_2_p}{R_{12\_2_p}} + \frac{To_p}{R_{1\_2eq_p}}}{\frac{1}{R_{1\_2eq_p}} + \frac{1}{R_{12\_2_p}} + \frac{1}{R_{13\_2}}}$$

$$T3\_3_{p+1} = \frac{\frac{T1\_2_p}{R_{12\_2_p}} + \frac{T3\_2_p}{R_{23\_2}} + \frac{T4\_2_p}{R_{24\_2}} + \left(Sse7\_22_p - P_{el\_2_p}\right)}{\frac{1}{R_{12\_2_p}} + \frac{1}{R_{23\_2}} + \frac{1}{R_{24\_2}}}$$

$$T_{air\_out\_3_{p+1}} = \left[1 - e^{\frac{-\left(h_{c2}+h_{c2}\right)\frac{A_{pv2}}{2}}{m_{air}\,c_{p2}}}\right]\left[\frac{T_{air\_out\_1_p} - \frac{\left(h_{c2}\,T2\_2_p + h_{c2}\,T1\_2_p\right)}{\left(h_{c2}+h_{c2}\right)}}{\frac{\left(h_{c2}+h_{c2}\right)\cdot\frac{A_{pv2}}{2}}{m_{air}\,c_{p2}}}\right] + \frac{h_{c2}\,T2\_2_p + h_{c2}\,T1\_2_p}{\left(h_{c2}+h_{c2}\right)}$$

$$T4\_3_{p+1} = \left[1 - e^{\frac{-\left(h_{c2}+h_{c2}\right)\cdot\frac{A_{pv2}}{2}}{m_{air}\,c_{p2}}}\right]\frac{h_{c2}\,T2\_2_p + h_{c2}\,T1\_2_p}{h_{c2}+h_{c2}} + \left[e^{\frac{-\left(h_{c2}+h_{c2}\right)\frac{A_{pv2}}{2}}{m_{air}\,c_{p2}}}\right]T_{air\_out\_1_p}$$

$$T4_{p+1} = \frac{\frac{T2\_2_p}{R_{24\_2}} + \frac{T4B_p}{R_{4B4\_2}}}{\frac{1}{R_{24\_2}} + \frac{1}{R_{4B4\_2}}}$$

$$T4A_{p+1} = \frac{\frac{T3\_3_p}{R_{13\_3}} + Sse7\_2_p + \frac{T2\_3_p}{R_{12\_3_p}} + \frac{To_p}{R_{1\_3eq_p}}}{\frac{1}{R_{1\_3eq_p}} + \frac{1}{R_{12\_3_p}} + \frac{1}{R_{13\_3}}}$$

$T5_{p+1}$

$T4B_{p+1}$

$T4C_{p+1}$

$T6_{p+1}$

$T7_{p+1}$

$T8_{p+1}$

$T9_{p+1}$

$T10_{p+1}$

$T11_{p+1}$

$T12_{p+1}$

$T13_{p+1}$

$T14_{p+1}$

$T15_{p+1}$

$T16_{p+1}$

$T17_{p+1}$

$T18_{p+1}$

$T19_{p+1}$

$T20_{p+1}$

$T21_{p+1}$

$T22_{p+1}$

Ts_{p+1}

Q_{heat_p}

$$\frac{\frac{T3\_3_p}{R_{13\_3}} + Sse7\_2_p + \frac{T2\_3_p}{R_{12\_3_p}} + \frac{To_p}{R_{1\_3eq_p}}}{\frac{1}{R_{1\_3eq_p}} + \frac{1}{R_{12\_3_p}} + \frac{1}{R_{13\_3}}}$$

$$\frac{\frac{T1\_3_p}{R_{12\_3_p}} + \frac{T3\_3_p}{R_{23\_3}} + \frac{T4\_3_p}{R_{24\_3}} + \left(Sse7\_22_p - P_{el\_3_p}\right)}{\frac{1}{R_{12\_3_p}} + \frac{1}{R_{23\_3}} + \frac{1}{R_{24\_3}}}$$

$$\left[1 - e^{\frac{-\left(h_{c3}+h_{c3}\right)\cdot\frac{A_{pv2}}{2}}{m_{air}\cdot c_{p3}}}\right]\left[T_{air\_out\_2_p} - \frac{\left(h_{c3}\cdot T2\_3_p + h_{c3}\cdot T1\_3_p\right)}{\left(h_{c3}+h_{c3}\right)}\right]\cdot\frac{\left(h_{c3}+h_{c3}\right)\cdot\frac{A_{pv2}}{2}}{m_{air}\cdot c_{p3}} + \frac{h_{c3}\cdot T2\_3_p + h_{c3}\cdot T1\_3_p}{\left(h_{c3}+h_{c3}\right)}$$

$$\left[1 - e^{\frac{-\left(h_{c3}+h_{c3}\right)\cdot\frac{A_{pv2}}{2}}{m_{air}\cdot c_{p3}}}\right]\frac{h_{c3}\cdot T2\_3_p + h_{c3}\cdot T1\_3_p}{h_{c3}+h_{c3}} + \left[e^{\frac{-\left(h_{c3}+h_{c3}\right)\cdot\frac{A_{pv2}}{2}}{m_{air}\cdot c_{p3}}}\right]T_{air\_out\_2_p}$$

$$\frac{\frac{T2\_3_p}{R_{24\_3}} + \frac{T4B_p}{R_{4B4\_3}}}{\frac{1}{R_{24\_3}} + \frac{1}{R_{4B4\_3}}}$$

$$\frac{T2\_1_p + T2\_2_p + T2\_3_p}{3}$$

$$\frac{\frac{To_p}{R_{4Aeq_p}} + Sse7\_3_p + \frac{T4C_p}{R_{4C4A}}}{\frac{1}{R_{4Aeq_p}} + \frac{1}{R_{4C4A}}}$$

$$\frac{\frac{T4B_p}{R_{4B5}} + \frac{T6_p}{R_{56_p}} + \frac{T7_p}{R_{57_p}} + \frac{T4C_p}{R_{4C5}}}{\frac{1}{R_{4B5}} + \frac{1}{R_{56_p}} + \frac{1}{R_{57_p}} + \frac{1}{R_{4C5}}}$$

$$\frac{\Delta t}{C_{4B}}\left(\frac{T4_p - T4B_p}{R_{4B5}} + \frac{T5_p - T4B_p}{R_{4B5}}\right) + T4B_p$$

$$\frac{\Delta t}{C_{4C}}\left(\frac{T4A_p - T4C_p}{R_{4C4A}} + \frac{T5_p - T4C_p}{R_{4C5}}\right) + T4C_p$$

$$\frac{\frac{T5_p}{R_{56_p}} + \frac{T7_p}{R_{67_p}} + \frac{To_p}{R_{inf2}}}{\frac{1}{R_{56_p}} + \frac{1}{R_{67_p}} + \frac{1}{R_{inf2}}}$$

$$\frac{\frac{T5_p}{R_{75_p}} + \frac{T6_p}{R_{67_p}} + \frac{T8_p}{R_{78}}}{\frac{1}{R_{75_p}} + \frac{1}{R_{67_p}} + \frac{1}{R_{78}}}$$

$$\frac{\Delta t}{C_8}\left(\frac{T7_p - T8_p}{R_{78}} + \frac{T9_p - T8_p}{R_{89}}\right) + T8_p$$

$$\frac{\frac{T8_p}{R_{89}} + \left(Ssi5_p + Qrsi_{int_{p,5}}\right) + \frac{Tz_p}{R_{9z_p}} + \frac{T10_p}{R_{910_p}} + \frac{T14_p}{R_{914_p}} + \frac{T18_p}{R_{918_p}} + \frac{T22_p}{R_{922_p}} + \frac{T15_p}{R_{915_p}}}{\frac{1}{R_{89}} + \frac{1}{R_{9z_p}} + \frac{1}{R_{910_p}} + \frac{1}{R_{914_p}} + \frac{1}{R_{918_p}} + \frac{1}{R_{922_p}} + \frac{1}{R_{915_p}}}$$

$$\frac{\frac{T11_p}{R_{1011}} + \left(Ssi1_p + Qrsi_{int_{p,1}}\right) + \frac{Tz_p}{R_{10z_p}} + \frac{T15_p}{R_{1015_p}} + \frac{T18_p}{R_{1018_p}} + \frac{T22_p}{R_{1022_p}} + \frac{T9_p}{R_{109_p}}}{\frac{1}{R_{1011}} + \frac{1}{R_{10z_p}} + \frac{1}{R_{1015_p}} + \frac{1}{R_{1018_p}} + \frac{1}{R_{1022_p}} + \frac{1}{R_{109_p}}}$$

$$\frac{\Delta t}{C_{11}}\left(\frac{T10_p - T11_p}{R_{1011}} + \frac{T12_p - T11_p}{R_{1112}}\right) + T11_p$$

$$\frac{\frac{T11_p}{R_{1112}} + Ssi1_p + \frac{To_p}{R_{12eq_p}}}{\frac{1}{R_{1112}} + \frac{1}{R_{12eq_p}}}$$

$$\frac{\frac{T14_p}{R_{1314_p}} + Swo1_p + \frac{To_p}{R_{13eq_p}}}{\frac{1}{R_{1314_p}} + \frac{1}{R_{13eq_p}}}$$

$$\frac{\frac{T13_p}{R_{1314_p}} + \left(Swi1_p + Qrw_{int_{p,1}}\right) + \frac{Tz_p}{R_{14z_p}} + \frac{T15_p}{R_{1415_p}} + \frac{T22_p}{R_{1422_p}} + \frac{T9_p}{R_{149_p}} + \frac{T18_p}{R_{1418_p}}}{\frac{1}{R_{1314_p}} + \frac{1}{R_{14z_p}} + \frac{1}{R_{1415_p}} + \frac{1}{R_{1422_p}} + \frac{1}{R_{149_p}} + \frac{1}{R_{1418_p}}}$$

$$\frac{\frac{T10_p}{R_{1510_p}} + \frac{T9_p}{R_{159_p}} + \frac{Tz_p}{R_{15z_p}} + \frac{T14_p}{R_{1514_p}} + \frac{T16_p}{R_{1516}} + \frac{T18_p}{R_{1518_p}} + \frac{T22_p}{R_{1522_p}} + \left(Ssi6_p + Qrsi_{int_{p,6}}\right)}{\frac{1}{R_{1510_p}} + \frac{1}{R_{15z_p}} + \frac{1}{R_{1514_p}} + \frac{1}{R_{1516}} + \frac{1}{R_{1518_p}} + \frac{1}{R_{1522_p}} + \frac{1}{R_{159_p}}}$$

$$\frac{\Delta t}{C_{16}}\left(\frac{T17_p - T16_p}{R_{1617}} + \frac{T15_p - T16_p}{R_{1516}}\right) + T16_p$$

$$\frac{\frac{To_p}{R_{17o_p}} + \frac{T16_p}{R_{1617}}}{\frac{1}{R_{17o_p}} + \frac{1}{R_{1617}}}$$

$$\frac{\frac{T10_p}{R_{1810_p}} + \frac{T15_p}{R_{1815_p}} + \frac{T9_p}{R_{189_p}} + \frac{Tz_p}{R_{18z_p}} + \frac{T14_p}{R_{1814_p}} + \frac{T19_p}{R_{1819}} + Ssi8_p + Qrsi8_{int_p}}{\frac{1}{R_{1810_p}} + \frac{1}{R_{18z_p}} + \frac{1}{R_{1814_p}} + \frac{1}{R_{1819}} + \frac{1}{R_{1815_p}} + \frac{1}{R_{189_p}}}$$

$$\frac{\Delta t}{C_{19}}\left(\frac{T18_p - T19_p}{R_{1819}} + \frac{T20_p - T19_p}{R_{1920}}\right) + T19_p$$

$$\left[\begin{array}{c}
\dfrac{\dfrac{T19_p}{R_{1920}}+\dfrac{To_p}{R_{20eq_p}}+Sw20_p}{\dfrac{1}{R_{1920}}+\dfrac{1}{R_{20eq_p}}} \\
\dfrac{\dfrac{T22_p}{R_{2122_p}}+\dfrac{To_p}{R_{21eq_p}}+Swo21_p}{\dfrac{1}{R_{2122_p}}+\dfrac{1}{R_{21eq_p}}} \\
\dfrac{\dfrac{Tz_p}{R_{22z_p}}+\dfrac{T15_p}{R_{2215_p}}+\dfrac{T21_p}{R_{2122_p}}+\dfrac{T10_p}{R_{2210_p}}+\dfrac{T9_p}{R_{229_p}}+\dfrac{T14_p}{R_{2214_p}}+Swi22_p+Qrw22_{int_p}}{\dfrac{1}{R_{22z_p}}+\dfrac{1}{R_{2215_p}}+\dfrac{1}{R_{2122_p}}+\dfrac{1}{R_{2210_p}}+\dfrac{1}{R_{2214_p}}+\dfrac{1}{R_{229_p}}} \\
\dfrac{\Delta t}{C_{air}}\left(\dfrac{T9_p-Tz_p}{R_{9z_p}}+\dfrac{T22_p-Tz_p}{R_{22z_p}}+\dfrac{T18_p-Tz_p}{R_{18z_p}}+\dfrac{T15_p-Tz_p}{R_{15z_p}}+\dfrac{T14_p-Tz_p}{R_{14z_p}}+\dfrac{T10_p-Tz_p}{R_{10z_p}}+\dfrac{To_p-Tz_p}{R_{infl}}+\dfrac{To_p-Tz_p}{R_{door1}}+\dfrac{To_p-Tz_p}{R_{door2}}+Qcev_{wi_p}\right)+Tz_p \\
\dfrac{Tep-T9_p}{R_{9z_p}}+\dfrac{Tep-T22_p}{R_{22z_p}}+\dfrac{Tep-T18_p}{R_{18z_p}}+\dfrac{Tep-T15_p}{R_{15z_p}}+\dfrac{Tep-T14_p}{R_{14z_p}}+\dfrac{Tep-T10_p}{R_{10z_p}}+\dfrac{Tep-To_p}{R_{infl}}+\dfrac{Tep-To_p}{R_{door1}}+\dfrac{Tep-To_p}{R_{door2}}-Qcev_{int_p}
\end{array}\right]$$

Matrix of Configuration 4 (equations for SAC only)

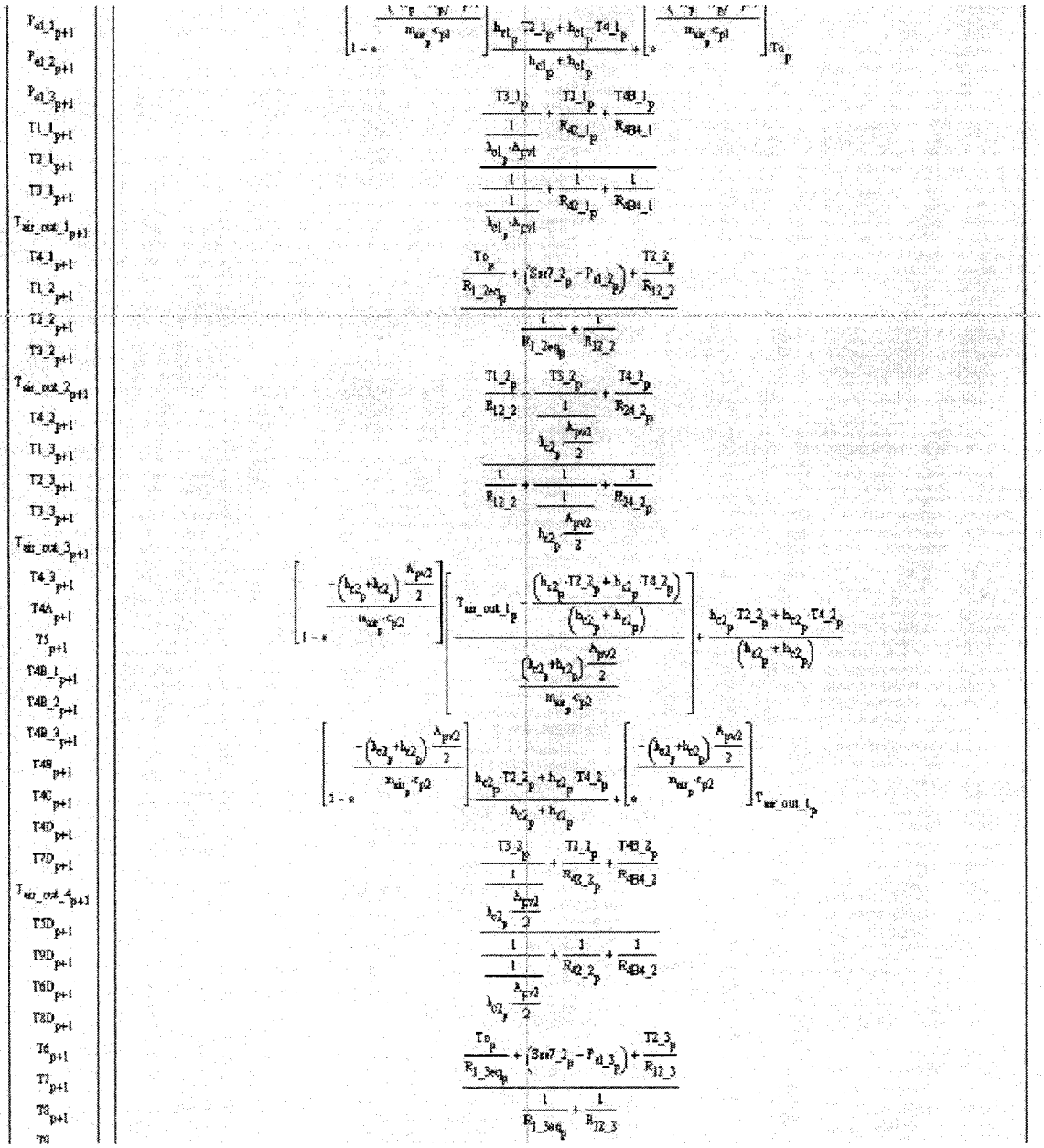

$$\frac{\frac{T5D_p}{R_{4D5D_p}} + \frac{To_p}{R_{4Deq_p}} + Sse4D_p}{\frac{1}{R_{4D5D_p}} + \frac{1}{R_{4Deq_p}}}$$

$$\left[1 - e^{\frac{-\left(h_{c4_p} + h_{c4_p}\right) \cdot A_{sac}}{m_{air_p} \cdot c_{p4}}}\right] \left[\frac{T_{air\_out\_3_p} - \frac{\left(h_{c4_p} \cdot T4D_p + h_{c4_p} \cdot T5D_p\right)}{\left(h_{c4_p} + h_{c4_p}\right)}}{\frac{\left(h_{c4_p} + h_{c4_p}\right) \cdot A_{sac}}{m_{air_p} \cdot c_{p4}}}\right] + \frac{h_{c4_p} \cdot T4D_p + h_{c4_p} \cdot T5D_p}{\left(h_{c4_p} + h_{c4_p}\right)}$$

$$\left[1 - e^{\frac{-\left(h_{c4_p} + h_{c4_p}\right) \cdot A_{sac}}{m_{air_p} \cdot c_{p4}}}\right] \frac{h_{c4_p} \cdot T4D_p + h_{c4_p} \cdot T5D_p}{h_{c4_p} + h_{c4_p}} + \left[e^{\frac{-\left(h_{c4_p} + h_{c4_p}\right) \cdot A_{sac}}{m_{air_p} \cdot c_{p4}}}\right] T_{air\_out\_3_p}$$

$$\frac{\frac{T4D_p}{R_{4D5D_p}} + \frac{T6D_p}{R_{5D6D}} + Sse5D_p}{\frac{1}{R_{4D5D_p}} + \frac{1}{R_{5D6D}}}$$

$$\frac{\frac{T8D_p}{R_{8D9D}} + \frac{To_p}{R_{9Deq_p}}}{\frac{1}{R_{8D9D}} + \frac{1}{R_{9Deq_p}}}$$

$$\frac{\frac{T5D_p}{R_{5D6D}} + \frac{T7D_p}{\frac{1}{h_{c4_p} \cdot A_{sac}}} + \frac{T8D_p}{R_{6D8D_p}}}{\frac{1}{R_{5D6D}} + \frac{1}{\frac{1}{h_{c4_p} \cdot A_{sac}}} + \frac{1}{R_{6D8D_p}}}$$

$$\frac{\frac{T6D_p}{R_{6D8D_p}} + \frac{T7D_p}{\frac{1}{h_{c4_p} \cdot A_{sac}}} + \frac{T9D_p}{R_{8D9D}}}{\frac{1}{R_{6D8D_p}} + \frac{1}{\frac{1}{h_{c4_p} \cdot A_{sac}}} + \frac{1}{R_{8D9D}}}$$

Energy Balance

$St := \max(Sse7\_t1) + \max(Sse7\_t2) + \max(Sse7\_t2)$

$St = 33.492kW$

$Qair := \max(m_{air}) \cdot c_{p1} \cdot \left(\max(T_{air\_out\_3}) - To_{1314}\right)$

$Qair = 8.342kW$

$Refl := \left(1 - \alpha_{pv}\right) \cdot St$

$Refl = 3.349kW$

$Power := \max(P_{el\_1}) + \max(P_{el\_2}) + \max(P_{el\_3})$

$Power = 4.833kW$

$$Qtop\_loss := \left[\max\left(\frac{1}{R_{1\_1eq}}\right) \cdot \left(\max\left(T1\_1 - To_{1314}\right)\right) + \max\left(\frac{1}{R_{1\_2eq}}\right) \cdot \left(\max\left(T1\_2 - To_{1314}\right)\right)\right] \ldots + \max\left(\frac{1}{R_{1\_3eq}}\right) \cdot \left(\max\left(T1\_3 - To_{1314}\right)\right)$$

$Qtop\_loss = 18.467kW$

$$Qback\_loss := \frac{\max(T4\_1) - T4B\_1_{1309}}{R_{4B4\_1}} + \frac{\max(T4\_2) - T4B\_2_{1309}}{R_{4B4\_2}} + \frac{\max(T4\_3) - T4B\_3_{1309}}{R_{4B4\_3}}$$

$Qback\_loss = 0.197kW$

$IN := St$

$OUT := Qair + Refl + Power + Qtop\_loss + Qback\_loss$

$IN = 33.492kW$

$$\left|\frac{IN - OUT}{IN}\right| = 5.066\%$$

$OUT = 35.188kW$

Results – Configuration 1

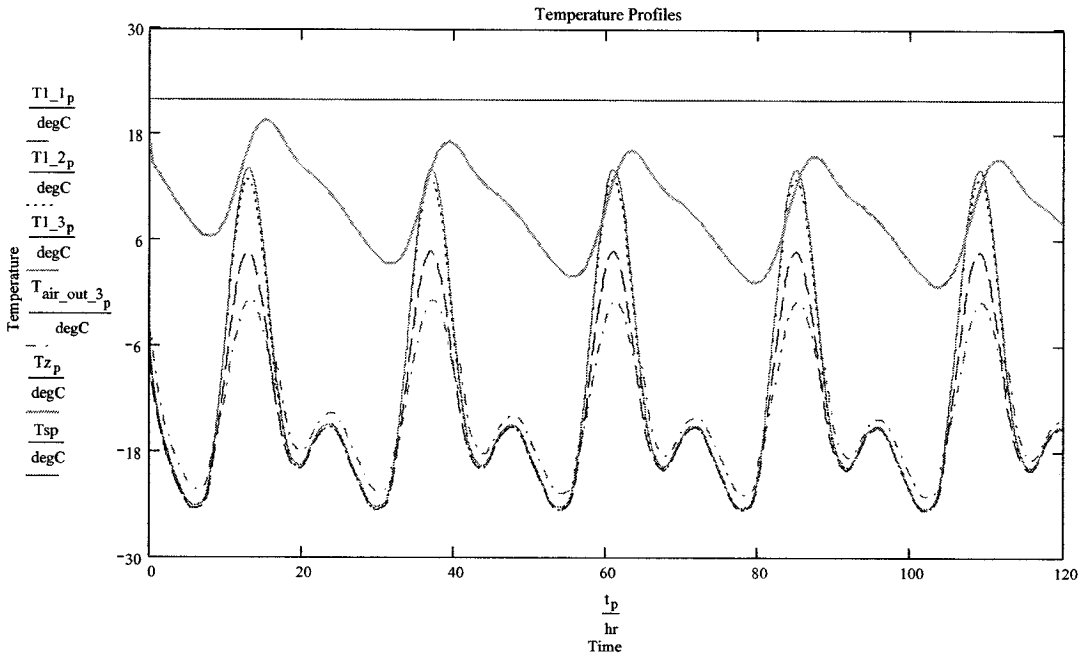

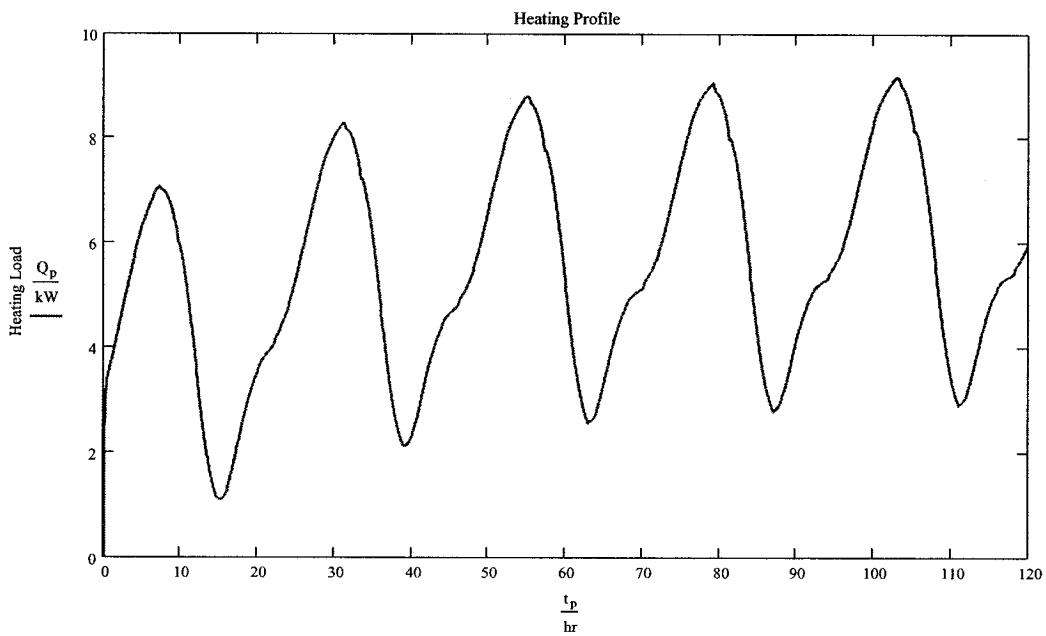

Thermal and electrical efficiency

$$\eta_{th\_1} := \frac{m_{air\_davg} \cdot c_{p1} \cdot \left(T_{air\_out\_1\_davg} - Ton_0\right)}{Sse7\_t1\_davg} \qquad \eta_{th\_1} = 41.303\%$$

$$\eta_{th\_2} := \frac{m_{air\_davg} \cdot c_{p2} \cdot \left(T_{air\_out\_2\_davg} - T_{air\_out\_1\_davg}\right)}{Sse7\_t2\_davg} \qquad \eta_{th\_2} = 11.169\%$$

$$\eta_{th\_3} := \frac{m_{air\_davg} \cdot c_{p3} \cdot \left(T_{air\_out\_3\_davg} - T_{air\_out\_2\_davg}\right)}{Sse7\_t2\_davg} \qquad \eta_{th\_3} = 9.196\%$$

$$\eta_{th\_avg} := \frac{m_{air\_davg} \cdot c_{p3} \cdot \left(T_{air\_out\_3\_davg} - Ton_0\right)}{Sse7\_t1\_davg + 2Sse7\_t2\_davg} \qquad \eta_{th\_avg} = 17.821\%$$

$$\eta_{el\_1} := 0.142 - 0.000636(T1\_1\_davg - 25 \cdot degC) \qquad \eta_{el\_1} = 16.134\%$$

$$\eta_{el\_2} := 0.142 - 0.000636(T1\_2\_davg - 25 \cdot degC) \qquad \eta_{el\_2} = 15.81\%$$

$$\eta_{el\_3} := 0.142 - 0.000636(T1\_3\_davg - 25 \cdot degC) \qquad \eta_{el\_3} = 15.768\%$$

$$\eta_{el} := \frac{\eta_{el\_1} + \eta_{el\_2} + \eta_{el\_3}}{3} \qquad \eta_{el} = 15.904\%$$

Daily Solar Radiation

$$Sse7\_t1\_daily := \sum_{p=1242}^{1350} Sse7\_t1_p \cdot \Delta t \qquad Sse7\_t1\_daily = 35.677 kW \cdot hr$$

$$Sse7\_t2\_daily := \sum_{p=1242}^{1350} Sse7\_t2_p \cdot \Delta t \qquad Sse7\_t2\_daily = 54.871 kW \cdot hr$$

$$Sse7\_1\_daytime := \sum_{p=1242}^{1350} Sse7\_1_p \cdot \Delta t \qquad Sse7\_1\_daytime = 32.109 kW \cdot hr$$

$$Sse7\_2\_daytime := \sum_{p=1242}^{1350} Sse7\_2_p \cdot \Delta t \qquad Sse7\_2\_daytime = 49.384 kW \cdot hr$$

Total available solar radiation

$Sse7\_t1\_daily + 2 \cdot Sse7\_t2\_daily = 145.418 kW \cdot hr$

Solar Radiation When Collecting

$Sse7\_1\_daytime + 2 \cdot Sse7\_2\_daytime = 130.877 kW \cdot hr$

Heat Generated:

$Q_{u\_collected} := \eta_{th\_1} \cdot Sse7\_t1\_daily + \eta_{th\_2} \cdot Sse7\_t2\_daily + \eta_{th\_3} \cdot Sse7\_t2\_daily$

$Q_{u\_collected} = 25.91 kW \cdot hr$

Electricity Generated:

$P_{el} := \eta_{el\_1} \cdot Sse7\_t1\_daily + \eta_{el\_2} \cdot Sse7\_t2\_daily + \eta_{el\_3} \cdot Sse7\_t2\_daily$

$P_{el} = 23.083 kW \cdot hr$

Heating Load:

$$Q_{heat\_avg} := \sum_{p=1152}^{1440} Q_p \cdot \Delta t \qquad Q_{heat\_avg} = 148.109 kW \cdot hr$$

APPENDIX F: HVAC Components

AIR TO WATER HEAT EXCHANGER

AIR SIDE

$T_{hi_p} := T_{air\_out\_3_p}$

$A_{HE\_air} := 0.3m^2$

$V_{HE\_air\_avg} := 0.47 \cdot \frac{m}{sec}$

WATER SIDE

$T_{ci_p} := Tci_p$

$Q_w := 1.5 \cdot \frac{gal}{min}$

$\rho_{HE\_load} := 995 \frac{kg}{m^3}$

$c_{pHE\_load} := 4175 \frac{joule}{kg \cdot degC}$

$A_{HE\_w} := \frac{\pi}{4} \cdot (0.019m)^2$

$V_{HE\_water} := \frac{Q_w}{A_{HE\_w}}$

$V_{HE\_water} = 0.334 \frac{m}{s}$

$mc\_load := \rho_{HE\_load} \cdot V_{HE\_water} \cdot A_{HE\_w} \cdot c_{pHE\_load}$

$mc\_source := \rho_{air} \cdot V_{HE\_air\_avg} \cdot A_{HE\_air} \cdot c_{p3}$

$mc\_min := min(mc\_load, mc\_source)$

Effectiveness of the heat exchanger: $\varepsilon_{HE} := 0.1, 0.2 .. 1$

$$T_{c\_out}(\varepsilon_{HE}, p) := \frac{\varepsilon_{HE} \cdot (T_{hi_p} - T_{ci_p}) \cdot mc\_min}{mc\ load} + T_{ci_p} \qquad Q_{HE}(\varepsilon_{HE}, p) := \varepsilon_{HE} \cdot mc\_min \cdot (T_{hi_p} - T_{ci_p})$$

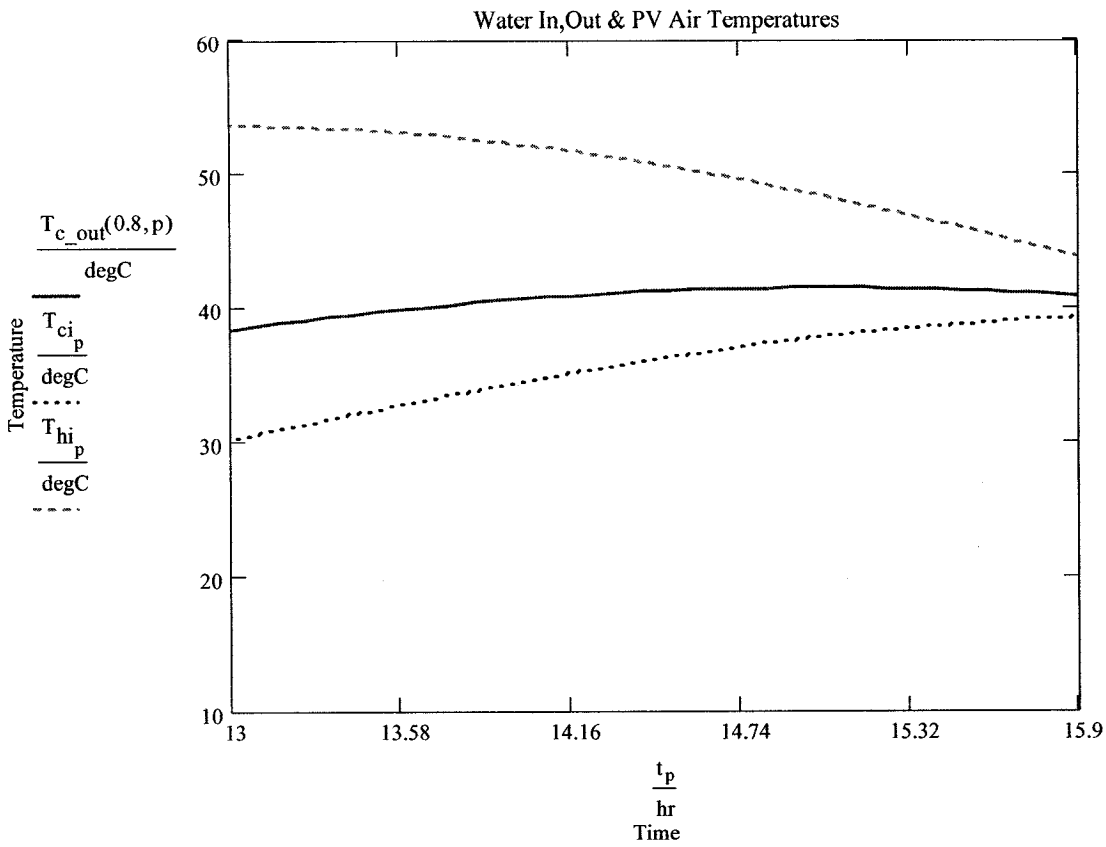
Water In,Out & PV Air Temperatures
60
50
40
30
20
10
13
13.58
14.16
14.74
15.32
15.9
Temperature
$T_{c\_out}(0.8,p)$ degC
T_{ci_p} degC
T_{hi_p} degC
t_p hr
Time

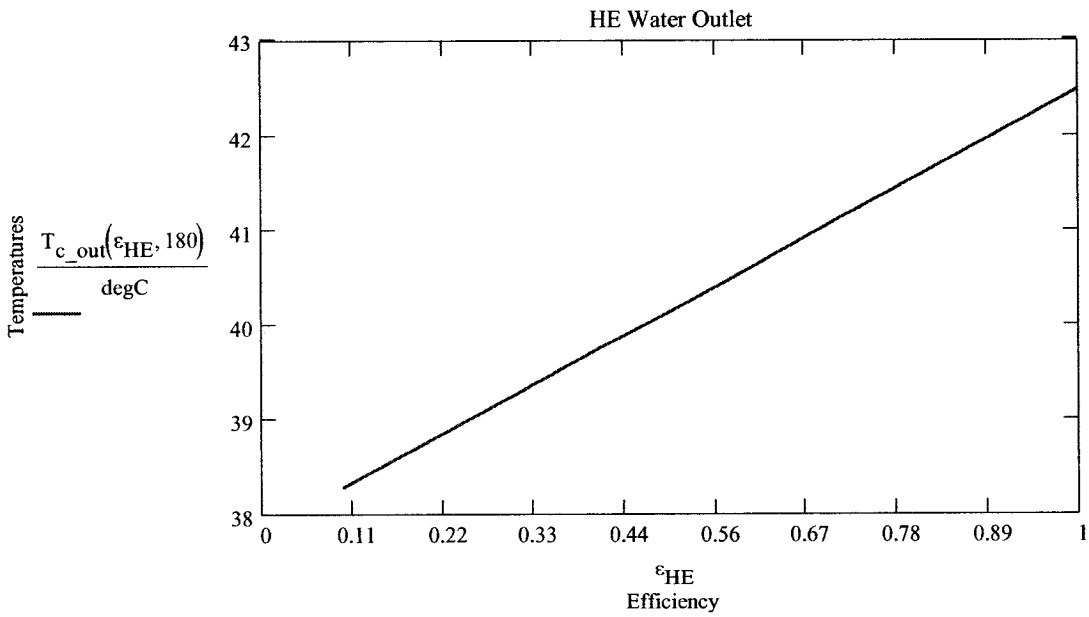
HE Water Outlet
43
42
41
40
39
38
0
0.11
0.22
0.33
0.44
0.56
0.67
0.78
0.89
1
Temperatures
$T_{c\_out}(\varepsilon_{HE}, 180)$ degC
ε_{HE}
Efficiency

ROCKBED

Sizing the rockbed

Rock size: $D_e := 20 \cdot 10^{-3} \cdot m$

Rockbed porosity:
(0.33<e< 0.46) $\varepsilon := 0.4$

Bulk density: $ro_r := 1533 \frac{kg}{m^3}$

Rock conductivity: $k_r := 0.125 \frac{watt}{m \cdot degC}$

Rock speific heat: $c_r := 0.88 \cdot 10^3 \cdot \frac{joule}{kg \cdot degC}$

Change in rockbed temperture: $\Delta T := 30 degC$

Height of the rockbed:
(vertical airflow) $h_r := 2m$

Days of thermal storage energy required: $n := 1$

Storage capacity: $C_{storage} := Q_{u\_collected} \cdot n$ $C_{storage} = 7.416 \times 10^4 watt \cdot hr$

Rockbed volume: $V_r := \frac{C_{storage}}{c_r \cdot ro_r \cdot \Delta T}$ $V_r = 6.596 m^3$

Face area: $A_f := \frac{V_r}{h_r}$ $A_f = 3.298 m^2$

(square cross-section) $a_r := \sqrt{A_f}$ $a_r = 1.816 m$

Final dimensions: $a_r = 1.8 m$ (Square cross-section)

$h_r = 2 m$

Temperature distribution

$P := 2\cdot(h_r + a_r)$ $P = 7.632m$

$Ur := 1.8\frac{watt}{m^2 degC}$

$\Delta x := \frac{h_r}{5}$ $C1_r := ro_r \cdot c_r \cdot \Delta x \cdot A_f$ $C2_r := C1_r$ $C3_r := C1_r$ $C4_r := C1_r$ $C5_r := C1_r$

$Rr_{12} := \frac{\Delta x}{k_r \cdot A_f}$ $Rr_{23} := Rr_{12}$ $Rr_{34} := Rr_{12}$ $Rr_{45} := Rr_{12}$ $Rr_5 := \frac{Rr_{12}}{2}$ $Rr_1 := Rr_5$

$T_a := 20degC$ $T_{in_p} := T_{air\_out\_4_p}$

$$TS2 := \left(\frac{C1_r}{\frac{1}{Rr_1} + \frac{1}{Rr_{12}}} \quad \frac{C2_r}{\frac{1}{Rr_{12}} + \frac{1}{Rr_{23}}} \quad \frac{C3_r}{\frac{1}{Rr_{23}} + \frac{1}{Rr_{34}}} \quad \frac{C4_r}{\frac{1}{Rr_{34}} + \frac{1}{Rr_{45}}} \quad \frac{C5_r}{\frac{1}{Rr_{45}} + \frac{1}{Rr_5}} \right)$$

$TS2 = (5.756\times 10^5 \quad 8.634\times 10^5 \quad 8.634\times 10^5 \quad 8.634\times 10^5 \quad 5.756\times 10^5)\,s$

$\Delta t1 := 300sec$

$$m_{air_p} := if\left[(74 < p < 214 \vee 362 < p < 502 \vee 650 < p < 790 \vee 938 < p < 1078 \vee 1226 < p < 1366) \cdot \left(T_{air\_out\_4_p} > Tr1_0\right), m_{air_p}, 0\cdot\frac{kg}{sec}\right]$$

CHARGING

$$\begin{pmatrix} Tr1_{p+1} \\ Tr2_{p+1} \\ Tr3_{p+1} \\ Tr4_{p+1} \\ Tr5_{p+1} \end{pmatrix} := \begin{bmatrix} \frac{\Delta t1}{C1_r}\cdot\left[m_{air_p}\cdot c_{p1}\cdot\left(T_{in_p} - Tr1_p\right)\right] - \frac{\Delta t1}{C1_r}\cdot Ur\cdot P\cdot\Delta x\cdot\left(Tr1_p - T_a\right) + \frac{\Delta t1}{C1_r}\cdot\left(\frac{Tr2_p - Tr1_p}{Rr_{12}}\right) + Tr1_p \\ \frac{\Delta t1}{C2_r}\cdot\left[m_{air_p}\cdot c_{p1}\cdot\left(Tr1_p - Tr2_p\right)\right] - \frac{\Delta t1}{C2_r}\cdot Ur\cdot P\cdot\Delta x\cdot\left(Tr2_p - T_a\right) + \frac{\Delta t1}{C2_r}\cdot\left(\frac{Tr1_p - Tr2_p}{Rr_{12}} + \frac{Tr3_p - Tr2_p}{Rr_{23}}\right) + Tr2_p \\ \frac{\Delta t1}{C3_r}\cdot\left[m_{air_p}\cdot c_{p1}\cdot\left(Tr2_p - Tr3_p\right)\right] - \frac{\Delta t1}{C3_r}\cdot Ur\cdot P\cdot\Delta x\cdot\left(Tr3_p - T_a\right) + \frac{\Delta t1}{C3_r}\cdot\left(\frac{Tr2_p - Tr3_p}{Rr_{23}} + \frac{Tr4_p - Tr3_p}{Rr_{34}}\right) + Tr3_p \\ \frac{\Delta t1}{C4_r}\cdot\left[m_{air_p}\cdot c_{p1}\cdot\left(Tr3_p - Tr4_p\right)\right] - \frac{\Delta t1}{C4_r}\cdot Ur\cdot P\cdot\Delta x\cdot\left(Tr4_p - T_a\right) + \frac{\Delta t1}{C4_r}\cdot\left(\frac{Tr3_p - Tr4_p}{Rr_{34}} + \frac{Tr5_p - Tr4_p}{Rr_{45}}\right) + Tr4_p \\ \frac{\Delta t1}{C5_r}\cdot\left[m_{air_p}\cdot c_{p1}\cdot\left(Tr4_p - Tr5_p\right)\right] - \frac{\Delta t1}{C5_r}\cdot Ur\cdot P\cdot\Delta x\cdot\left(Tr5_p - T_a\right) + \frac{\Delta t1}{C5_r}\cdot\left(\frac{Tr4_p - Tr5_p}{Rr_{45}}\right) + Tr5_p \end{bmatrix}$$

DISCHARGING

$$Tr1_0 := \frac{\sum_{p=180}^{288} Tr1_p}{108} \qquad Tr2_0 := \frac{\sum_{p=180}^{288} Tr2_p}{108} \qquad Tr3_0 := \frac{\sum_{p=180}^{288} Tr3_p}{108} \qquad Tr4_0 := \frac{\sum_{p=180}^{288} Tr4_p}{108} \qquad Tr5_0 := \frac{\sum_{p=180}^{288} Tr5_p}{108}$$

$$T_{in_p} := Tz_p \qquad m_{air} := 0.2\frac{kg}{sec}$$

$$m_{air\_2_p} := if\left[(288 < p < 425)\cdot\left(Tz_p < Tsp\right), m_{air}, 0\cdot\frac{kg}{sec}\right]$$

$$\begin{pmatrix} Tr5_{p+1} \\ Tr4_{p+1} \\ Tr3_{p+1} \\ Tr2_{p+1} \\ Tr1_{p+1} \end{pmatrix} := \begin{bmatrix} \frac{\Delta t1}{C5_r}\cdot\left[m_{air\_2_p}\cdot c_{p1}\cdot\left(T_{in_p} - Tr5_p\right)\right] - \frac{\Delta t1}{C5_r}\cdot Ur\cdot P\cdot\Delta x\cdot\left(Tr5_p - T_a\right) + \frac{\Delta t1}{C5_r}\cdot\left(\frac{Tr4_p - Tr5_p}{Rr_{45}}\right) + Tr5_p \\ \frac{\Delta t1}{C4_r}\cdot\left[m_{air\_2_p}\cdot c_{p1}\cdot\left(Tr5_p - Tr4_p\right)\right] - \frac{\Delta t1}{C4_r}\cdot Ur\cdot P\cdot\Delta x\cdot\left(Tr4_p - T_a\right) + \frac{\Delta t1}{C4_r}\cdot\left(\frac{Tr3_p - Tr4_p}{Rr_{34}} + \frac{Tr5_p - Tr4_p}{Rr_{45}}\right) + Tr4_p \\ \frac{\Delta t1}{C3_r}\cdot\left[m_{air\_2_p}\cdot c_{p1}\cdot\left(Tr4_p - Tr3_p\right)\right] - \frac{\Delta t1}{C3_r}\cdot Ur\cdot P\cdot\Delta x\cdot\left(Tr3_p - T_a\right) + \frac{\Delta t1}{C3_r}\cdot\left(\frac{Tr2_p - Tr3_p}{Rr_{23}} + \frac{Tr4_p - Tr3_p}{Rr_{34}}\right) + Tr3_p \\ \frac{\Delta t1}{C2_r}\cdot\left[m_{air\_2_p}\cdot c_{p1}\cdot\left(Tr3_p - Tr2_p\right)\right] - \frac{\Delta t1}{C2_r}\cdot Ur\cdot P\cdot\Delta x\cdot\left(Tr2_p - T_a\right) + \frac{\Delta t1}{C2_r}\cdot\left(\frac{Tr1_p - Tr2_p}{Rr_{12}} + \frac{Tr3_p - Tr2_p}{Rr_{23}}\right) + Tr2_p \\ \frac{\Delta t1}{C1_r}\cdot\left[m_{air\_2_p}\cdot c_{p1}\cdot\left(Tr2_p - Tr1_p\right)\right] - \frac{\Delta t1}{C1_r}\cdot Ur\cdot P\cdot\Delta x\cdot\left(Tr5_p - T_a\right) + \frac{\Delta t1}{C1_r}\cdot\left(\frac{Tr2_p - Tr1_p}{Rr_{12}}\right) + Tr1_p \end{bmatrix}$$

$$Qrb_p := m_{air\_2_p}\cdot c_{p1}\cdot\left(Tr1_p - Tz_p\right)$$

APPENDIX G: Technical Details of BP 4175 Solar Panel

(www.bp.com)

bp solar

BP 4175

175 Watt Photovoltaic Module

High-efficiency photovoltaic module using silicon nitride monocrystalline silicon cells.

Performance

Rated power (P_{max})	175W
Power tolerance	± 5%
Nominal voltage	24V
Limited Warranty[1]	25 years

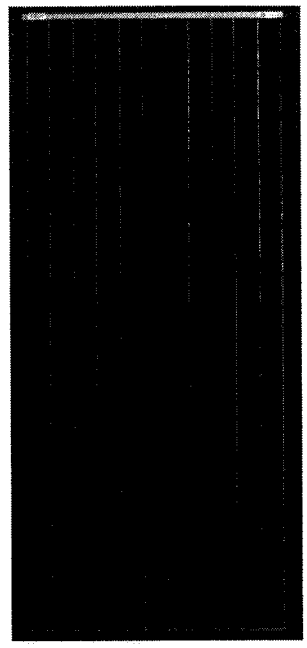

Configuration

BP 4175B Framed module with output cables and polarized Multicontact (MC) connectors

Electrical Characteristics[2]	BP 4175
Maximum power (P_{max})[3]	175W
Voltage at Pmax (V_{mp})	35.7V
Current at Pmax (I_{mp})	4.9A
Warranted minimum P_{max}	166.5W
Short-circuit current (I_{sc})	5.4A
Open-circuit voltage (V_{oc})	44.0V
Temperature coefficient of I_{sc}	(0.065±0.015)%/ °C
Temperature coefficient of V_{oc}	-(160±10)mV/°C
Temperature coefficient of power	-(0.5±0.05)%/ °C
NOCT (Air 20°C, Sun 0.8kW/m², wind 1m/s)	47±2°C
Maximum series fuse rating	15A (S, L)
Maximum system voltage	600V (U.S. NEC & IEC 61215 rating)

Mechanical Characteristics

Dimensions	Length: 1595mm (62.8") Width: 790mm (31.1") Depth: 50mm (1.97")
Weight	15.4 kg (34.0 pounds)
Solar Cells	72 cells (125mm x 125mm) in a 6x12 matrix connected in series
Output Cables	RHW AWG# 12 (3.3mm) cable with polarized weatherproof DC rated Multicontact connectors; asymmetrical lengths - 1250mm (-) and 800mm (+)
Diodes	***IntegraBus***™ technology includes Schottky by-pass diodes integrated into the printed circuit board bus
Construction	Front: High-transmission 3mm (1/8th inch) tempered glass; Back: Tedlar; Encapsulant: EVA
Frame	Bronze anodized aluminum alloy type 6063T6 Universal frame

1. Module Warranty: 25-year limited warranty of 80% power output; 12-year limited warranty of 90% power output; 5-year limited warranty of materials and workmanship. See your local representative for full terms of these warranties.
2. These data represent the performance of typical BP 4175 products, and are based on measurements made in accordance with ASTM E1036 corrected to SRC (STC.)
3. During the stabilization process that occurs during the first few months of deployment, module power may decrease by up to 3% from typical P_{max}.

3034-v2 09/04